Environmental Degradation Processes within Aqueous Solutions

A DISSERTATION
SUBMITTED TO THE FACULTY OF THE GRADUATE SCHOOL
OF THE UNIVERSITY OF MINNESOTA
BY

Matthew Lee Grandbois

IN PARTIAL FULFILLMENT OF THE REQUIREMENTS
FOR THE DEGREE OF
DOCTOR OF PHILOSOPHY

Advisor: Kristopher McNeill

May 2010

Acknowledgement

I would like to thank the following people for their contributions to the work described in this thesis:

Dr. Douglas Latch for his contribution to the development of the reaction-diffusion model of singlet oxygen production within microheterogeneous systems in Chapter 2.

Dr. Tamar Kohn and Dr. Kara Nelson for their collaboration on the photoinactivation of MS2 within dissolved organic matter solutions in Chapter 3.

Dr. Zhibo Li, Dr. Marc Hillmyer, Dr. Timothy Lodge, and Chun Liu for their collaboration on the photoproduction of singlet oxygen within aqueous block copolymer micelle solutions in Chapter 4.

I would also like to thank the following people for their help and support during my graduate school career:

Dr. Kris McNeill for helping me grow from a synthetic chemist into an environmental scientist and for always supporting me, no matter which continent I was on at the time.

The members of the McNeill research group for their invaluable talents, advice, and friendship for which I will always be grateful.

Kris Murphy and Dr. Matthew Meyer for their advice and friendship during our graduate school careers.

Dr. Letitia Yao for her help and experience in the NMR Lab.

Dr. Dana Reed and Sean Murray for their experience in the Mass Spec Lab.

Dedication

To my wife and my family, for their patience and unending support.

Table of Contents

List of Tables

List of Schemes and Figures

List of Symbols and Abbreviations

α	:	Extinction coefficient or absorbance coefficient
$^1\Delta_g$	:	Lowest singlet excited electronic state of molecular oxygen
δ	:	Chemical shift
Δ	:	Change
ε	:	Molar absorptivity
Φ	:	Quantum yield
η	:	Viscosity
λ	:	Wavelength
μ	:	Ionic strength
ρ	:	Density
$^3\Sigma_g$	:	Triplet ground electronic state of molecular oxygen
$^1\Sigma_g$	:	Singlet excited electronic state of molecular oxygen
μL	:	Microliter
μs	:	Microsecond
[S]	:	Concentration of a species
a	:	area
A	:	Absorbance
AIBN	:	Azobisisobutyronitrile
ALHA	:	Aldrich humic acid
Ar	:	Aryl

b	:	Path length
BPA	:	2-Biphenylcarboxylic acid
BZC	:	3,4-Benzocoumarin
$\bullet Br_2^-$	:	Bromide radical anion
$\bullet CH_3$	:	Methyl radical
C	:	Carbon
C_{aq}	:	Contribution of singlet oxygen within the bulk aqueous phase
$CBrCl_3$	:	Bromo-trichloromethane
C_{DOM}	:	Contribution of singlet oxygen within dissolved organic matter phase
CD_3OD	:	Deuterated methanol
$CDCl_3$	:	Deuterated chloroform
CEVS	:	Controlled environment vitrification system
CF	:	Correction factor
CF_3	:	Trifluoromethyl
CH_2Cl_2	:	Dichloromethane
CH_4	:	Methane
Cl	:	Chloro
cm	:	Centimeter
Cryo-TEM	:	Cyrogenic transmission electron microscopy
CTAB	:	Cetyl trimethylammonium bromide
d	:	Doublet
D	:	Diffusivity

D_2O	:	Deuterium oxide
DABCO	:	Diazobicyclo[2.2.2]octane
DLS	:	Dynamic light scattering
DNA	:	Deoxyribonucleic acid
DOC	:	Dissolved organic carbon
^{1}DOM	:	Ground singlet electronic state of dissolved organic matter
^{1}DOM*	:	Excited singlet electronic state of dissolved organic matter
^{3}DOM*	:	Excited triplet electronic state of dissolved organic matter
[DOM]	:	Concentration of dissolved organic matter
DOM	:	Dissolved organic matter
eq.	:	Equation or Equivalent
ESR	:	Electron spin resonance
f_{aq}	:	Fraction within the aqueous phase
f_{DOM}	:	Fraction within the organic phase
$Fe(OH)^{2+}$	:	Iron hydroxide complex
Fe^{3+}	:	Trivalent iron
Fe_{TOT}	:	Total amount of iron
FFA	:	Furfuryl alcohol
FFF	:	Flow field-flow fractionation
FLHA	:	Fluka humic acid
fM	:	Femtomolar
FT-IR	:	Fourier-transform infrared spectroscopy

g	:	Gram
h	:	Planck’s constant or hours
H	:	Hydrogen
H•	:	Hydrogen radical
H^+	:	Hydrogen cation
HCl	:	Hydrochloric acid
Hg	:	Mercury
HO	:	Hydroxyl
HOO•	:	Hydroperoxyl radical
H_2O	:	Water
H_2O_2	:	Hydrogen peroxide
HP-SEC	:	High performance size exclusion chromatography
$\langle I_\lambda \rangle_z$	:	Mean light intensity
I	:	Light intensity
ICT	:	Intramolecular charge transfer
IHSS	:	International Humic Substance Society
I_0	:	Initial light intensity
IR	:	Infrared
ISC	:	Intersystem crossing
kcal	:	Kilocalories
k_{+diff}	:	Back-diffusion rate constant
k_{-diff}	:	Forward-diffusion rate constant

$k_{^1O_2}$	:	Dissolved organic matter-normalized singlet oxygen formation rate constant
k_{abs}	:	Absorption rate constant
$k_{abs,thick}$	:	Thick layer absorbance rate constant
$k_{abs,thin}$	:	Thin layer absorbance rate constant
k_{aq}	:	Aqueous phase inactivation rate constant
k_b	:	Boltzmann constant
kDa	:	Kilodaltons
k_{DOM}	:	Dissolved organic matter phase inactivation rate constant
keV	:	Kilo-electron volt
k_f	:	Formation rate constant
$k_{f,DOM}$	:	Interior dissolved organic matter singlet oxygen formation rate constant
KIE	:	Kinetic isotope effect
k_{MIC}	:	Deactivation rate constant of singlet oxygen by micelle interior
$k_{MS2\text{-}1O2}$	:	Inactivation rate constant of MS2 by singlet oxygen
k_{obs}	:	Observed rate constant
k_{obs}(blank)	:	Observed rate constant in a blank solution
k_{rxn}	:	Reaction rate constant
k_{solv}	:	Solvent deactivation rate constant
$k_{f,tot}$	:	Bulk solution singlet oxygen formation rate constant
K_{OM}	:	Organic matter – water partition coefficient
K_{MIC}	:	Micelle – water partition coefficient

k_{sens}	:	Sensitization rate constant
k_q	:	Quenching rate constant
l	:	Length
L	:	Liter
M	:	Molar
m.p.	:	Melting point
m/z	:	Mass to charge ratio
Me	:	Methyl
MeO	:	Methoxy
mg	:	Milligram
Mg^{2+}	:	Magnesium cation
MgCl	:	Magnesium chloride
MHz	:	Megahertz
mL	:	Milliliter
mm	:	Millimeter
mM	:	Millimolar
M^{n+} and M^{n+1}	:	Transition metal cation
mol	:	Mole
MS	:	Mass spectroscopy
MW	:	Molecular weight
n	:	number
N or ^{15}N	:	Nitrogen

N_A	:	Avogadro's number
Na^+	:	Sodium cation
NaCl	:	Sodium chloride
$NaHCO_3$	:	Sodium bicarbonate
$NaNO_2$	:	Sodium nitrite
NaOH	:	Sodium hydroxide
Na_2SO_4	:	Sodium sulfate
NADH	:	Nicotinamide adenine dinucleotide dehydrogenase
nm	:	Nanometer
NMe_2	:	Dimethylamino
NMR	:	Nuclear magnetic resonance
N_s	:	Surfactant packing parameter
N_3^-	:	Azide anion
NO_2^-	:	Nitrite anion
NO_3^-	:	Nitrate anion
NO•	:	Nitric oxide radical
NO_2•	:	Nitric dioxide radical
$^1O_2$	:	Singlet oxygen
$[^1O_2]_{app}$	:	Apparent singlet oxygen concentration
$[^1O_2]_{aq}$	:	Aqueous steady-state singlet oxygen concentration
$[^1O_2]_{DOM}$	:	Interior dissolved organic matter micelle singlet oxygen concentration
$[^1O_2]_{ss}$	:	Steady-State singlet oxygen concentration

O	:	Oxygen
O_2	:	Ground state molecular oxygen
O_2^-	:	Superoxide anion
O_3	:	Ozone
•OH	:	Hydroxyl radical
^-OH	:	Hydroxide anion
-O-CH_3	:	Methoxy
P	:	Probability
PCS	:	Photon correlation spectroscopy
PDI	:	Polydispersity index
PEE	:	Poly(ethylethylene)
PEO	:	Poly(ethylene oxide)
PEP	:	Poly(ethylene-*alt*-propylene)
PFU	:	Plaque forming units
pH	:	Potential of hydrogen
PLFA	:	Pony Lake fulvic acid
pM	:	Picomolar
ppm	:	Parts per million
PPRI	:	Photochemically produced reactive intermediates
Q	:	Quencher
r	:	Radius
R	:	Ratio or Rate

RNA	:	Ribonucleic acid
RO_2•	:	Organoperoxyl radical
ROS	:	Reactive oxygen species
s	:	Seconds or Singlet
S	:	Sulfur or Sensitivity
S_λ	:	Wavelength specific screening factor
S_0	:	Ground singlet electronic state
S_1	:	First excited singlet electronic state
SEC	:	Size exclusion chromatography
SDS	:	Sodium dodecyl sulfate
SRFA	:	Suwannee River fulvic acid
SRHA	:	Suwannee River humic acid
t	:	Time or Triplet
T	:	Temperature
TBAF	:	*tert*-Butylammonium fluoride
TBS	:	*tert*-Butyl dimethyl silyl
^{t}Bu	:	*tert*-Butyl
TEM	:	Transmission electron microscopy
THF	:	Tetrahydrofuran
TiO_2	:	Titanium dioxide
TPMA	:	2-[1-(3-*tert*-butyldimethylsiloxy)phenyl)-1-methoxymethylene]-tricyclo[3.3.1.1]decane

TPMA•DOM	:	2-[1-(3-*tert*-butyldimethylsiloxy)phenyl)-1-methoxymethylene]-tricyclo[3.3.1.1]decane – dissolved organic matter complex
$TPMAO_2$	:	4-methoxy-4-(3-tert-butyldimetylsilyoxyphenyl)spiro[1,2-dioxetane-3,2'-tricyclo[3.3.1.1]decane
TPP	:	5,10,15,20-Tetraphenyl-21H,23H-porphyrin
TPP-COOH	:	5-(4-Carboxyphenyl)-10,15,20-triphenyl-21H,23H-porphyrin
T_1	:	First excited triplet electronic state
UV	:	Ultra-violet
V	:	Volume
V_{tot}	:	Total volume
V_{DOM}	:	Dissolved organic matter volume
VXP	:	Vapor pressure osmometry and low-angle X-ray scattering
W	:	Watt
WSP	:	Wastewater stabilization ponds
Y	:	Yield
z	:	Depth

Chapter 1.

Introduction

Overview

Environmental photodegradation processes are important in the breakdown of pollutants, as well as in the global element cycles.[1] This thesis will describe several physical organic chemistry projects aimed at increasing our understanding of photodegradation processes as they pertain to specific environmental concerns and potential future technological applications. Following this introductory chapter, a reaction-diffusion theory of singlet oxygen is developed. This theory was developed to improve our understanding of photochemical reactions in systems that contain microenvironments. By thinking of these systems on the nanoscale, we are able to explain the enhanced photochemical reactivity of hydrophobic probe molecules and accurately estimate the physicochemical characteristics of the respective local microenvironment. Chapter 3 applies the reaction-diffusion theory towards explaining the observed enhanced inactivation of waterborne pathogens within wastewater stabilization ponds. The next chapter describes the synthesis of nanoscale photoreactors, a step towards a possible technological application, and a test of the reaction-diffusion theory. The final chapter focuses on another photochemically produced reactive intermediate, hydroxyl radical, and describes the development of fluorescent hydroxyl radical probes.

Photodegradation Processes

Photodegradation processes are sequences of events initiated by the absorption of electromagnetic radiation that result in the alteration of physicochemical characteristics of a molecule or system.[1] The two main types of photodegradation that are prevalent

throughout environmental, biological, and chemical systems are either *direct* or *indirect* processes. Both of these processes are described in below.

Direct photodegradation

Direct photodegradation is the simpler of the two photodegradation processes and refers to the instance where a substance directly absorbs electromagnetic radiation (e.g. visible light) that results in the alteration of that substance. The absorption of light results in an increase in energy of the molecule, where that molecule is now said to be "excited". Instead of transferring that energy, the excited molecule dissipates the energy through a change in the molecular structure. Direct photodegradation rates are dependent on the absorptivity of a substance and the energy of the light available for absorption.

The amount of light that a substance can absorb is generally understood by two experimentally determined relationships. Lambert's law states that the amount of light absorbed by a substance is independent of the intensity of the light emitted by the source given constant pressure, temperature, and composition as stated in the equation,

$$I = I_0 e^{-\alpha t} \quad (1)$$

where I and I_0 are the intensity of light leaving and entering a solution, respectively, α is the extinction coefficient, and t is time.[2] It specifically relates to the proportional relationship between light absorption and the path length of the solution. Beer's law states that the amount of light absorbed by a substance is directly proportional to the concentration of that substance, and when combined with the Lambert law, can be stated in the following equation,

$$A = \log \frac{I_0}{I} = \varepsilon b[S] \qquad (2)$$

where A is the absorbance of light, ε is the molar absorptivity of the absorbing species of a specific concentration, $[S]$, and b is the path length of light through the absorbing solution. This law dictates that the amount of light absorbed by a solution containing an absorbing species increases linearly with the concentration of that absorbing species given a constant path length. This relationship exists within dilute solutions, but deviates at high concentrations.

The light absorbing properties of the molecule are related to its chemical structure.[1] Any chemical moiety that absorbs light is called a *chromophore*. Some examples of chromophores within organic molecules that are important in environmental systems are conjugated double bonds and phenolates. These chromophores are found within molecules that participate in photosynthesis, natural organic matter, herbicides, pesticides, and organic pollutants.

The light source is the other factor responsible for direct photochemical degradation. Within environmental chemistry, the primary light source is the sun. The sun emits electromagnetic radiation across a broad range of wavelengths, yet the earth's atmosphere absorbs a large portion of the incident light.[1] Ozone, a component of the upper atmosphere, absorbs most high energy UV light. The majority of lower energy UV light is absorbed by water vapor and carbon dioxide. The resulting electromagnetic spectrum observed by the lower atmosphere is significantly different than that experienced by the upper atmosphere. There is very little light with wavelengths shorter than 300 nm available at the earth's surface, so in order to undergo direct

photodegradation, a molecule must be able to absorb light with wavelength greater than 300 nm. This is further restricted by the amount of light available; typically only UV light (λ < 400 nm) is energetic enough to induced physical transformation in the absorbing substance.

The absorption of a photon by a molecule is accompanied by an increase in energy. That energy can be dissipated in a variety of ways. Figure1.1 shows the pathways associated with the absorption and emission of photons by a molecule. A molecule in its singlet ground state, S_0, absorbs a photon and is excited to its first electronic excited state, S_1. The energy can be dissipated through radiative relaxation back to the ground state in the form of fluorescence, thermal interconversion back to the ground state without the emission of a photon, intersystem crossing, ISC, to the first electronic excited triplet state, T_1, or through degradation mechanisms. Examples of degradation mechanisms can be isomerization, bond cleavage, and chemical reactions with other molecules in singlet electronic states. Following ISC, radiative emission of a photon in the form of

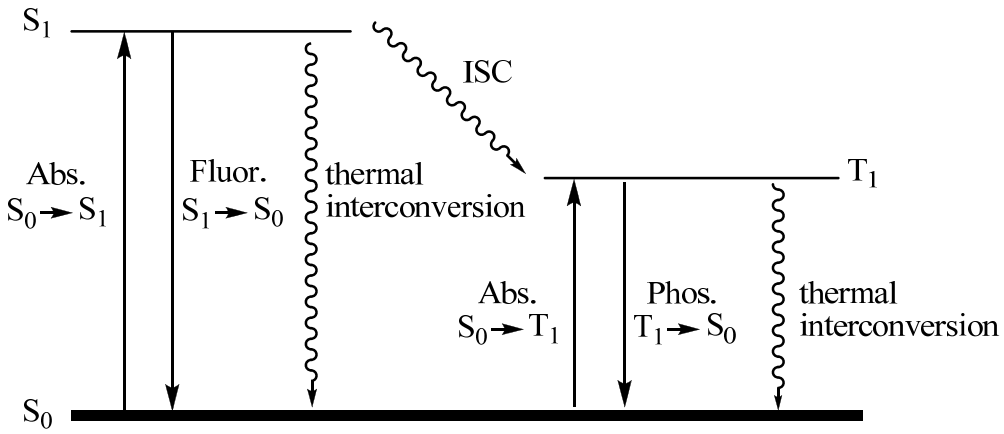

Figure 1.1. Jablonski diagram depicting light absorption and emission processes.

phosphorescence and thermal interconversion are also possible. While a molecule is in T_1 it can also undergo the same type of degradation mechanisms as when it was in the S_1, but now it primarily reacts with other molecules in a triplet electronic state. The interaction of triplet and singlet systems, though spin-forbidden, can occur provided the collision is strong enough to overcome the differences in angular momentum.[3] The T_1 process will become more important during our discussion of reactive oxygen species due to the triplet ground state of molecular oxygen.

An example of a direct photodegradation process of environmental significance can be found in the investigation of tetracycline, a commonly prescribed therapeutic and animal growth promoter found throughout surface waters.[4] Tetracycline degradation was found to be unaffected in the presence of nitrate, bicarbonate, and humic acid (all known participants in indirect photodegradation processes). Based on their investigation, Chen *et al.* concluded that tetracycline primarily undergoes direct photochemical degradation even in the presence of known reactive intermediate photosensitizers (i.e. nitrate, bicarbonate, ferric ions, and humic acid).

Indirect photodegradation

A substance is stated to go through indirect photodegradation when it undergoes chemical transformation stemming from reaction with a reactive intermediate species that received its increased energy either directly or indirectly from light absorption. As an example, a sensitizer is excited to a higher electronic state (either S_1 or T_1) by the absorption of a photon and then the sensitizer relaxes back to the ground state while

transferring its energy to a reactive substrate. Sensitizers in S_1 transfer their energy most efficiently to molecules in singlet states and T_1 transfer their energy most efficiently to molecules in triplet states, but spin-forbidden reactions can occur as mentioned above. This type of photodegradation mechanism is common in natural aqueous environments where chromophores within dissolved organic matter readily undergo ISC while in excited electronic states and then transfer their energy to ground state molecular oxygen to form a suite of well studied reactive oxygen species.[5]

An example of an indirect photodegradation process of environmental significance can be found in the investigation of biphenol A, a commonly used chemical in the production of plastics that has been found throughout natural surface waters.[6] Biphenol A is capable of undergoing both direct and indirect photochemical degradation, but due to light screening within natural waters the rate of direct degradation is significantly slower than the rate of indirect degradation. Chin *et al.* found that several photochemically produced reactive intermediates (e.g. hydroxyl radical and excited triplet state dissolved organic matter) are important in the indirect photochemical degradation of bisphenol A.[6]

Photochemically Produced Reactive Intermediates

Many environmental pollutants undergo indirect photodegradation mechanisms that do not stem from direct interaction with the S_1 or T_1 of a chromophore, but instead come from reaction with a daughter product of the initially excited sensitizer. These high-energy, transient species are called photochemically produced reactive intermediates,

PPRI. These species tend to be short-lived due to their numerous interactions with solvent molecules and other labile substrates. The oxygen-containing PPRI are a specific set of PPRI are formed called reactive oxygen species (Figure1.2).

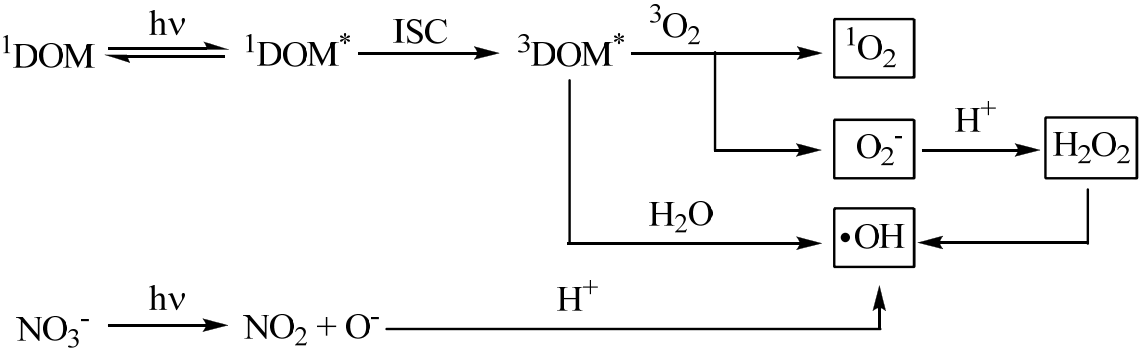

Figure 1.2. Reactive oxygen species formed from environmental photolysis conditions.[7]

Reactive oxygen species are generated in the environment through indirect photochemical processes. The chromophores present within dissolved organic matter (DOM, a topic discussed below) become excited from their singlet ground state to their first excited singlet stated (^{1}DOM*) upon absorption of light, undergo ISC to form their triplet excited state (^{3}DOM*), and then interact with molecular oxygen to form either singlet oxygen ($^1O_2$) and superoxide (O_2^-).[8] Hydroxyl radical (•OH), another common reactive oxygen species, can be formed from the interaction of water with ^{3}DOM*, the photolysis of hydrogen peroxide (H_2O_2), or the photolysis of nitrate (NO_3^-).[8] Organoperoxyl radicals (RO_2•) are another type of reactive oxygen species that are formed from the interaction of oxygen with carbon-centered radicals, but due to the difficulty in differentiating their reactivity from that of •OH, they have not been well

studied.[1] The remaining chapters of this thesis will emphasize the importance of $^1O_2$ and •OH, respectively, so we will now review in more detail the formation, reactivity, and environmental implication of these specific PPRI.

Singlet oxygen

Singlet oxygen is the first electronic excited state of ground state molecular oxygen.[8] The two unpaired valence electrons within ground state molecular oxygen ($^3\Sigma_g$) allows excited triplet sensitizers, (i.e. ^{3}DOM*) to transfer their energy readily to form $^1O_2$ (Figure1.3). A second excited state $^1O_2$ ($^1\Sigma_g$) is 37.5 kcal/mol higher in energy than $^3\Sigma_g$, but it quickly deactivates within solution to the lower excited state ($^1\Delta_g$), which lies 22.5 kcal/mol higher in energy than $^3\Sigma_g$.[9] Therefore, the $^1\Delta_g$ state is the predominate excited

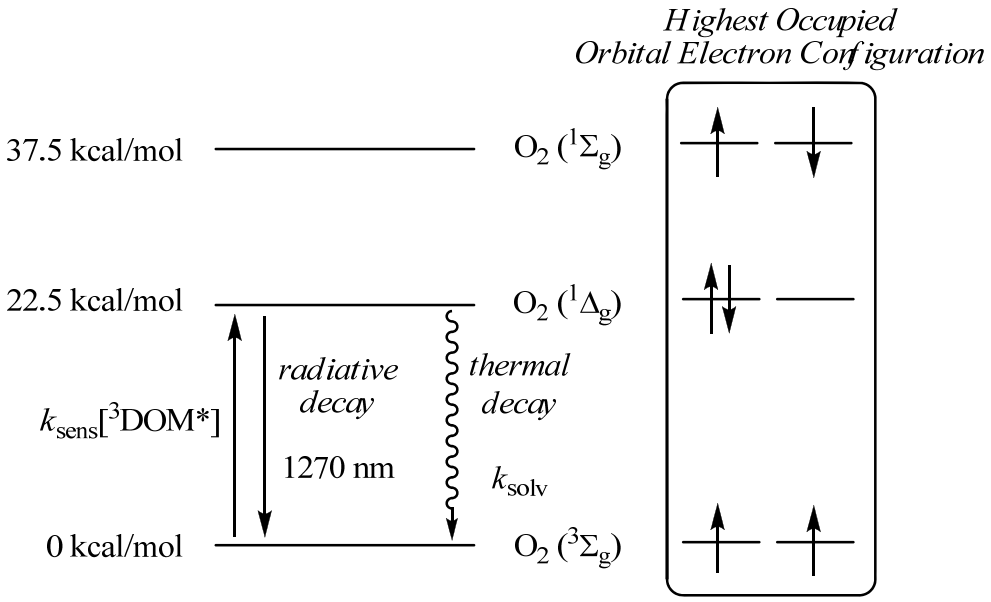

Figure 1.3. Energy level diagram for the environmental formation of $^1O_2$.

state species within solution and is exclusively responsible for the reactivity of $^1O_2$. Throughout the remainder of this thesis $^1O_2$ will refer to the $^1\Delta_g$ state.

The relatively low energy gap between ground state molecular oxygen and $^1O_2$ allows for a wide array of sensitizers that photochemically generate $^1O_2$. The phosphorescent decay of $^1O_2$ back to the ground state is accompanied by the emission of a photon in the near IR region of the electromagnetic spectrum (λ = 1270 nm).[10] The primary relaxation mechanism of $^1O_2$ within solution is through interaction with the solvent. The solvent deactivation rate of $^1O_2$, k_{solv}, for water is 2.5 x 10^5 s^{-1} and correlates to a lifetime of 4 μs.[11] Many molecules can also deactivate $^1O_2$ without reacting with it, such as diazobicyclo[2.2.2]octane (DABCO), β-carotene, and azide ion (N_3^-).[12-14]

The deactivation of $^1O_2$ can also occur through chemical reactions with organic molecules containing nucleophilic functional groups such as alkenes, aromatic rings, phenols, and sulfides.[1] Many of the common reactions involving $^1O_2$ and organic molecules are shown in Figure1.4. These reactions have been utilized through organic synthetic chemistry and in the understanding of environmental degradation of organic pollutants.[15, 16]

The cycloaddition of $^1O_2$ across alkene moieties have been thoroughly studied. The addition of $^1O_2$ across four carbon atoms possessing conjugated alkenes is classified as a formal [4+2] cycloaddition and is analogous to the Diels-Alder reaction.[16] The resulting endoperoxide can be isolated, but it is often too unstable and undergoes further reactions. The addition of $^1O_2$ across an electron-rich alkene is classified as a formal [2+2] cycloaddition and results in a 1,2-dioxetane product. Most of the resulting

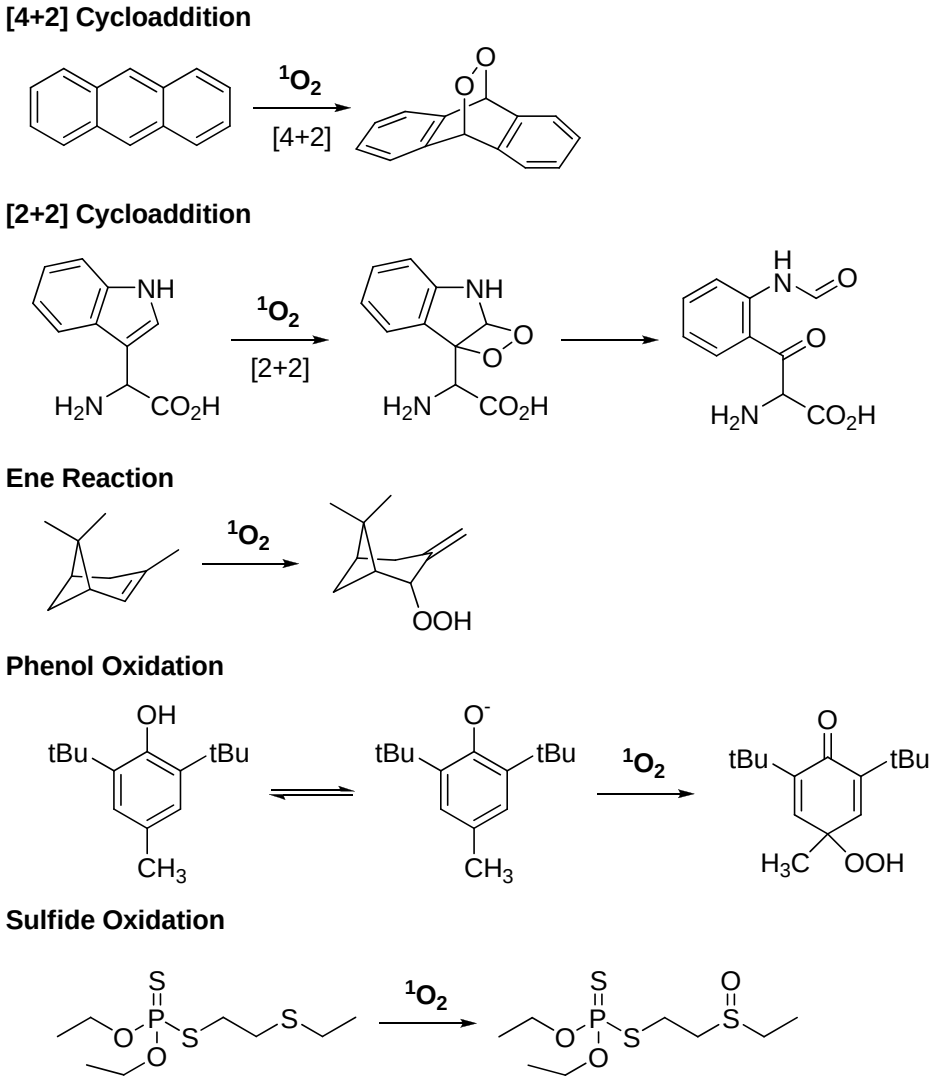

Figure 1.4. Reactivity of $^1O_2$. Adapted from Larson and Weber, 1994.[1]

dioxetanes are unstable due to the strain associated with a 4-membered ring and undergo ring opening mechanisms similar to that shown in Figure 1.4. The stability of 1,2-dioxetanes can be increased by adding sterically demanding substituents.[17] The incorporation of adamantyl moieties have been shown to drastically improve the stability of dioxetanes and subsequently been utilized in the development of trap-and-trigger $^1O_2$

probes.[18] The probes developed by MacManus-Spencer *et al*. were used extensively in the research described in Chapters 2-4 of this thesis.

Unsaturated organic molecules can also undergo the ene reaction with $^1O_2$ to form hydroperoxide products. This type of reaction has been well studied and incorporated in several organic syntheses of complicated natural products with strict stereochemical control.[16, 19] The oxidation of sulfides by $^1O_2$ has been reported for a variety of substrates.[20-22] The oxidation of phenolic compounds is of particular interest to environmental chemists. The prevalence of phenolic compounds within natural waters, drinking water, and wastewater emphasize the importance of studying their oxidation to the corresponding hydroperoxides.[23] Research has shown that the respective phenolate ion is much more reactive to $^1O_2$ and therefore the pH of the solution plays an integral role in phenol oxidation.[24] Numerous anthropogenic compounds contain phenol moieties and their remediation as environmental pollutants have been found to be enhanced through the use of $^1O_2$.[25, 26]

The role of $^1O_2$ throughout environmental and biological systems has been the subject of numerous studies, highlighting the importance of further understanding its chemical reactivity and technological applicability. In addition to its photochemical production within DOM, $^1O_2$ has been found to be produced from biological photosensitizers such as chlorophyll[27], flavins[28], and nicotinamide adenine dinucleotide dehydrogenase (NADH).[29] Singlet oxygen has been found to cause cytotoxic effects within biological systems by attacking crucial biological compounds such as DNA[30] and amino acids.[31-34] Another effect of $^1O_2$ within biological systems is the peroxidation of

lipid membranes. By reacting with unsaturated bonds within the fatty acid portion of lipid membranes, lipid hydroperoxides are formed which can go on to initiate chain reactions ultimately resulting in reduced membrane transport and diminished cellular signaling.[35, 36]

The biological cytotoxicity of $^1O_2$ has been applied to the medical and health fields through the advancement of photodynamic therapy and wastewater stabilization ponds (WSPs). Specific hydrophobic $^1O_2$ sensitizers, such as porphyrin species, have been introduced into cancerous cells and then irradiated with nonionizing electromagnetic radiation to cause cell death and tumor destruction through many of the mechanisms illustrated above.[37] Waterborne enteric viruses have been inactivated in WSPs through $^1O_2$-mediated photodegradation processes.[38-40] The third chapter in this thesis will further expand on this subject and focus on the enhanced inactivation of MS2 coliphage, a surrogate for human enteric viruses, when in close proximity to DOM and the elevated concentration of $^1O_2$ inherent to that microenvironment.

Despite the destructive effects of $^1O_2$ on biological systems, the environmental importance of $^1O_2$ has been questioned due to its relatively low environmental concentrations and selective chemical reactivity with respect to other PPRI (i.e. hydroxyl radical). Recently, $^1O_2$ has been suggested to play a more integral role in environmental degradation processes due to its elevated concentration within DOM micelles.[41] The second chapter in this thesis will deal specifically with this phenomenon and will further expand its theory and application to a wider range of DOM solutions.

Hydroxyl radical

Hydroxyl radical, •OH, is one of the most reactive oxygen species present in environmental chemistry. Its potency as a reactive intermediate derives from the bond dissociation energy of the parent hydrogen oxygen bond in water, 119 kcal/mol.[42] The resulting •OH is highly unstable and reacts with essentially any species that it encounters. This increased reactivity has lead to low level concentrations detected in the environment, yet its importance in the overall environmental photo-oxidation hierarchy has not been diminished. The steady-state concentration of •OH in natural waters has been estimated at 1×10^{-16} M, but in seawater its steady-state concentration has been estimated at 1×10^{-18} M.[43-45] Hydroxyl radical is formed in the environment in many processes (Figure 1.5).[1] Direct photolysis of ozone, water, and hydrogen peroxide in the atmosphere are important sources of atmospheric •OH (Figures 1.5A & 1.5E). Oxygen radical, one of the products of ozone photolysis (Figure 1.5A), can further react with water vapor in the atmosphere to form •OH (Figure 1.5F). The oxygen radical produced during the decomposition of ozone that reacts with water (Figure 1.5A & 1.5F) is in the ^{1}D electronic state and results in an exothermic reaction (-29.2 kcal/mol), as compared to the similar reaction of oxygen radical in the ^{3}P electronic state reacting with water in an endothermic reaction (+16.8 kcal/mol).[46] The production of •OH in environmental water solutions predominantly comes from the decomposition of hydrogen peroxide by reduced transition metal ions (i.e. Fenton reaction), and the photolysis of nitrate and nitrite anions. Hydroxyl radical has been found to be produced through

A) Photolysis of ozone in upper troposphere

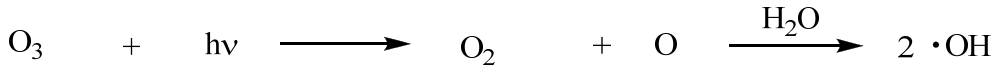

B) Fenton reaction

C) Photo-Fenton reaction

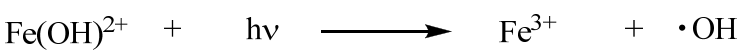

D) Nitric oxide reaction with hydroperoxyl radical

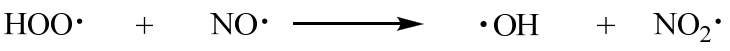

E) Photolysis of water and/or hydrogen peroxide

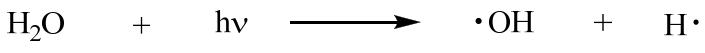

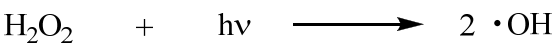

F) Reaction of oxygen atoms with water

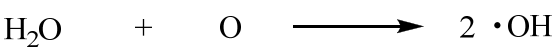

G) Photolysis of nitrate and nitrite anions

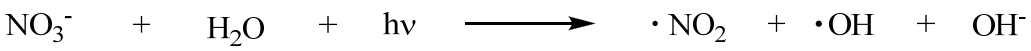

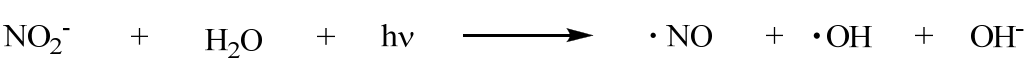

H) Reaction of superoxide with ozone

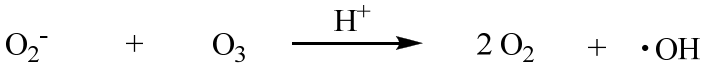

Figure 1.5. Production of •OH. Adapted from Larson and Weber, 1994.[1]

indirect photolysis of natural organic matter[47], but this process is diminished in importance in relation to the other two processes.[1]

Hydroxyl radical reacts with most compounds near the diffusion limit, whether they are organic or inorganic in nature.[48-51] The two main mechanisms of chemical reactivity are highlighted in Figure1.6. Hydrocarbons are susceptible to hydrogen atom abstraction and generally follow the rule that tertiary hydrogens are more reactive than secondary or primary hydrogens.[50] The second •OH reaction mechanism with organic molecules is that of addition to a double bond. This reactivity is governed by similar rules regarding to the stability of resulting radical species from unsymmetrical alkenes.[1] Hydroxyl radical adds to aromatic rings with little regard to electron density or steric hindrance.[44, 52] Substrates that possess both unsaturated bonds and abstractable

A) Hydrogen Abstraction

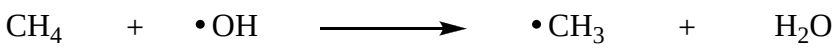

B) Unsaturated Bond Insertion

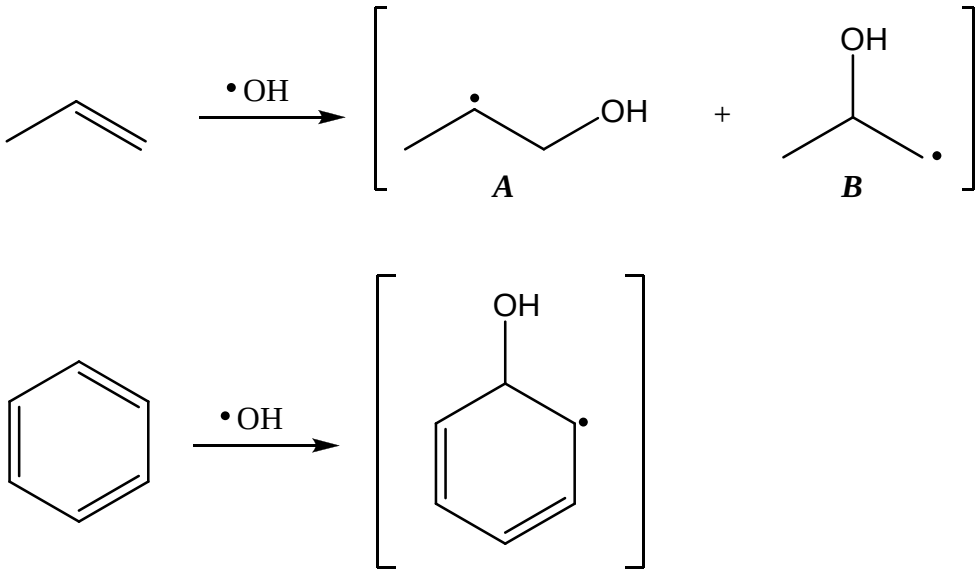

Figure 1.6. Dominant reaction mechanisms of •OH.

hydrogens undergo both reaction pathways, yet addition products dominate the product mixture by an order of magnitude.[51]

Hydroxyl radical can also react with inorganic species within aqueous solution.[48, 53, 54] The primary reaction mechanism of •OH with aqueous ions is analogous to the hydrogen abstraction from aliphatic compounds. Hydroxyl radical oxidizes most aqueous ions through electron abstraction to form the more stable hydroxide ion. In seawater, •OH predominately reacts with bromide present in solution to ultimately form the bromine radical anion, $\bullet Br_2^-$, despite the huge difference in concentration with chloride anion.[1] This reaction pathway dominates all other •OH reactivity in seawater solutions, but in freshwater solutions where the concentration of bromide anion is relatively low, •OH has been found to be reactive with bicarbonate, carbonate, and dissolved organic matter.

As stated above, •OH is produced in natural waters at very low steady-state concentrations that are an outcome of its indiscriminate, near diffusion-limit reactivity with both organic and inorganic species. Numerous probes have been developed that take advantage of the reactivity of •OH and incorporate a variety of detection methods.[55-63] Fluorescence detection has provided the sensitivity necessary for overcoming the problems associated with detecting low level concentrations of •OH.[55] Terephthalic acid has been proposed as a fluorescent probe that is very selective to •OH and is sensitive enough to detect low level concentrations in biological studies.[60] These characteristics have prompted several studies to use terephthalic acid to analyze •OH within environmental studies.[47, 64] Page *et al*. reported the production of •OH during the photolysis of DOM by observing the chemical reactivity of terephthalic acid.[47] The

inherent hydrophilicity of terephthalic acid restricts is application to only probing the concentration of •OH within aqueous environments. The previously mentioned observation of enhanced concentrations of reactive oxygen species within DOM micelles begins to question whether terephthalic acid adequately reports the reaction environment conditions experienced by many hydrophobic organic compounds that partition to DOM aggregates within natural waters.[41, 65] Based on these inadequacies, it is important to develop hydrophobic probes that still maintain the ability to detect low level concentrations of •OH. The last chapter in this thesis will describe the synthesis and characterization of such probe molecules.

Dissolved Organic Matter

Natural organic matter plays a crucial role within the global carbon cycle and in the photochemical transformation mechanisms of organic pollutant molecules.[1] Any carbon-containing chemical structure resulting from the breakdown of biological species (i.e. soil humus) can be classified as natural organic matter. The fraction of soil humus that is soluble in water (i.e. passes through a 0.2 μm filter) is defined as dissolved organic matter (DOM). In addition to its role as a photosensitizer described above, it is also key to the transport of hydrophobic organic pollutants due its mobile, hydrophobic, aqueous micelle-like structure. Hydrophobic organic pollutants, such as atrazine, are absorbed into the hydrophobic micellar pockets of DOM which increases the pollutants' bioavailability and biodegradation.[66, 67] Hydrophobic plasticizers have been shown to form complexes with DOM, increasing their mobility within aquatic ecosystems.[68]

Despite the well-studied utility within environmental degradation processes, the exact structure of DOM has not been established. Traditionally, DOM was envisioned as a large, covalently-attached conglomeration of small, ecologically-relevant building blocks (i.e. flavins, lignin, carbohydrates, and amino acids) capable of combining in various combinations and distributions.[69] The modern view of DOM still incorporates the small building blocks, but it is no longer thought to be composed of primarily of covalent linkages. Instead, the humic molecules self-assemble through various hydrogen-bonding, metal-chelation, and hydrophobic interactions to form micellar structures that are source and seasonally dependent.[70, 71]

The structural variability of DOM renders traditional analytical techniques aimed at quantitatively elucidating chemical structures (i.e. NMR, MS, FT-IR) to qualitative tools that give a vague idea of the organic moieties present within DOM. Traditional mass spectroscopy gives ranges of molecular weight values for DOM ranging from hundreds to thousands of Daltons. These results are dependent on isolation and analytical techniques.[72] Elemental analysis has shown typical DOM to be compromised largely of carbon and oxygen, with smaller contributions from hydrogen, nitrogen, and sulfur: C (43 – 50%), O (30 – 41%), H (3 – 5%), N (0.5 – 7%), and S (0.2 – 2%).[73] The vast amount of structurally similar moieties within DOM results in nuclear magnetic resonance (NMR) data that contains numerous superimposed signals.[73] Advances in NMR technology have provided insights towards the architecture of DOM. Specifically, solid state two-dimensional ^{1}H-^{13}C heteronuclear correlation spectroscopy (HETCOR) experiments conducted on terrestrial derived DOM have indicated that most of the methoxy (-O-CH_3)

moieties in DOM are connected to aromatic rings.[74] These results suggest that terrestrial DOM is largely derived from lignin and is further supported by fluorescence data.[75, 76] Cross polarization magic angle spinning ^{15}N NMR spectra indicate the presence of porphyrin substructures within DOM providing anionic cavities to bind to heavy metals in natural waters.[73] These structures are the remnants of humified photosynthetic material. The presence of other structural moieties, such as semiquinones, has been proven by the use of electron spin resonance (ESR) spectroscopy.[77]

The structural complexity of DOM has hindered scientific investigation into specific photochemical processes and their dependence on physicochemical characteristics. The elimination of photochemically neutral organic functionalities while maintaining the correct structural morphology of DOM would aid in future technological and scientific advances. The micellar qualities of DOM indicate that the most direct approach towards understanding the physicochemical dependence of DOM photochemistry would utilize known colloidal and surfactant systems of environmental and synthetic origin.

Microheterogeneous Systems

Traditional solution phase chemistry and physics strictly define systems to be either *homogeneous*, uniform throughout the entire sample, or *heterogeneous*, consisting of various pockets of dissimilar material sporadically dispersed throughout the entire solution. Heterogeneous solutions have been further divided into the subclasses of suspensions and colloids.[78] Suspensions refer to solutions with particles visible to the

naked eye ($\geq$ 1000 nm) that are dispersed throughout a solution and those particles are kept suspended in solution through constant agitation. These solutions separate upon standing. Colloids refer to solutions with particles 2 – 1000 nm in size that appear to be homogeneous to the naked eye, but with the help of microscopy can be correctly identified as heterogeneous solutions. These particles are small enough to remain in suspension due to the Brownian motion of the solvent and will not separate upon standing. Homogeneous solutions contain particles that are less than 2 nm in size, which do not scatter light or separate upon standing. Typical examples of colloidal suspensions include milk and fog, which contain large heterogeneous particles that cause scattering of light. Some colloidal particles with diameters in the nanometer range and little differences in the relative refractive indexes between the particle and the solvent scatter light at small angles. This behavior complicates the ability to accurately characterize solutions as either homogeneous or heterogeneous. Small angle light scattering techniques have been developed to address the problem of defining the boundary between homogeneous and heterogeneous solutions. For the remainder of this thesis, colloidal solutions with particles ranging from 2 – 50 nm in size will be referred to as microheterogeneous systems. Their position at the interface of homogeneous and heterogeneous solutions make them intriguing systems to investigate in regards to their ability to create miniscule, yet distinguishable, environments of different structure integrity and chemical reactivity.

Traditional colloids have ‘hard-soft’ interfaces between the suspended particle and the bulk solutions, but many microheterogeneous systems have ‘soft-soft’

interfaces.[79] The suspended water vapor in fog has a relatively 'hard' surface in comparison with the permeable 'soft' surface of the surrounding air. Microheterogeneous systems possess separate phases that may not exhibit the long-range three-dimensional order of solids, but do possess a level of local order similar to liquid phase interfaces.[79] Through a combination of short-range repulsive interactions between to the separate phases and long-range attractive interactions between molecules of the same phase, ordered separations form throughout the solutions provide a secure, yet 'soft', framework within bulk fluids. One particular class of molecules, amphiphiles, takes advantage of their ability to stabilize the hydrophilic-hydrophobic interface to create well-ordered microheterogeneous structures.

Amphiphiles possess both hydrophilic (water soluble) and hydrophobic (water insoluble) components that aid in their spatial placement at the surface between the two phases and aids in their alternative classification as surfactant molecules.[79] Examples of the four main types of amphiphiles are depicted in Figure1.7. Ionic surfactants can possess either cationic or anionic head groups on long hydrophobic alkyl tails. Nonionic surfactants utilize a hydrophobic alkyl chain typically connected to a hydrophilic polyether chain. Lipids are biological produced compounds that are soluble in organic solvents, sparingly soluble in water, and display amphiphilic behavior. Amphiphiles characteristically lower surface tension and interfacial tension between the two phases by

Anionic Surfactant

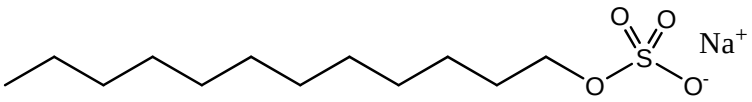

Sodium Dodecyl Sulfate, **SDS**

Cationic Surfactant

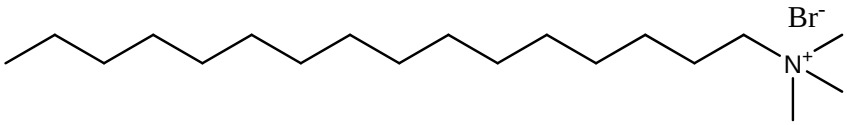

Cetyl Trimethylammonium Bromide, **CTAB**

Nonionic Surfactant

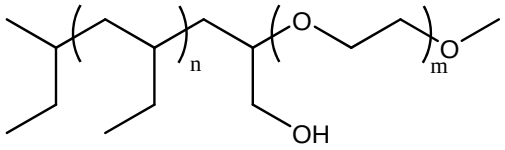

Poly(ethylethylene)-b-poly(ethyleneoxide) Block copolymer

Lipids

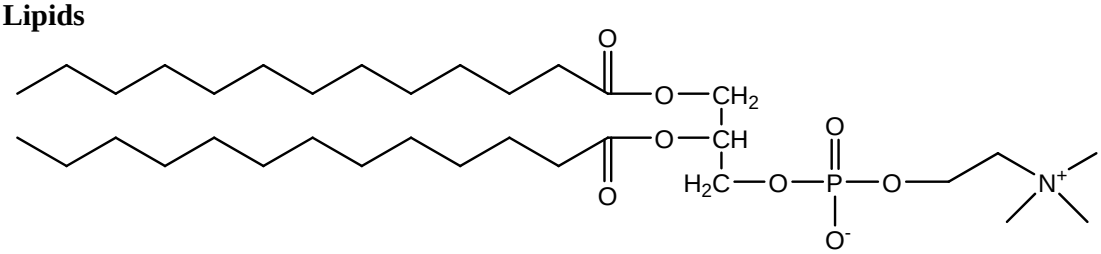

Phosphatidylcholine

Figure 1.7. Types of amphiphilic molecules.

balancing the intermolecular forces across the surface. This results in increased order across the hydrophilic-hydrophobic surface.

Within microheterogeneous systems of hydrophilic and hydrophobic microenvironments, amphiphiles help create several different structures (Figure1.8). Many water insoluble surfactants form monolayers at the water-air, or water-oil, interface

with the hydrophilic head pointed towards the water phase and the hydrophobic tail pointed away from that surface. Amphiphiles can also self-assemble in aqueous solution into micelles by surrounding the hydrophobic chains by the hydrophilic head groups. The shape of these micelles is dependent on the surfactant packing parameter, N_s, as stated in the following equation

$$N_s = \frac{V}{al} \quad (3)$$

where V is the volume per molecule, a is the estimated interface surface area, and l is the average fully extended hydrophobic chain length. Spherical micelles form when N_s is less

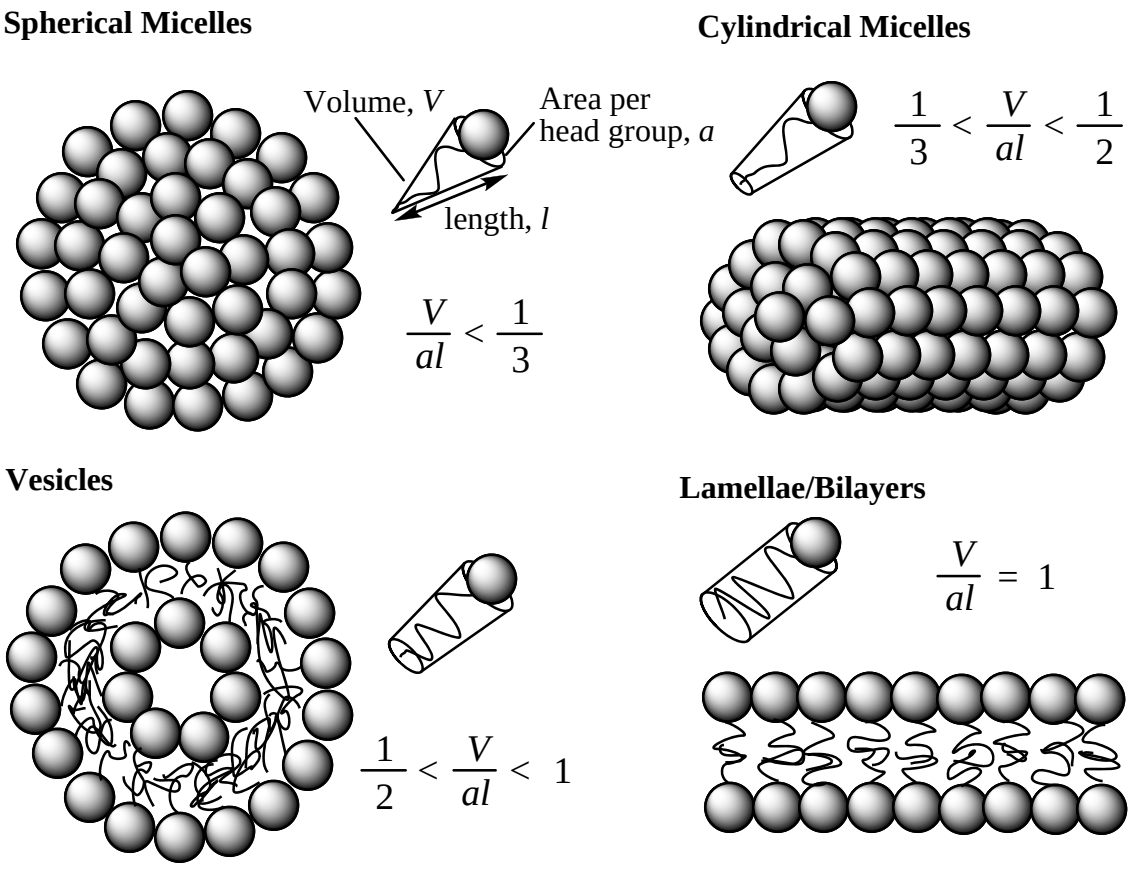

Figure 1.8. Amphiphilic microheterogeneous structures. Adapted from Hamley, 2000.[79]

than 1/3. Lamellar micelles form when N_s = 1. The surfactant packing parameter is related to the interfacial curvature and when it is equal to one, the curvature is equal to zero which present in planar sheets. Membranes are formed when two lamellar sheet form a hydrophobic barrier between separate aqueous compartments. Cell membranes are commonly built from phospholipid bilayers with embedded cellular machinery such as ion pumps and transport proteins. Vesicles are hollow aggregates that are formed from one or more amphiphilic bilayers.

Applications of Microheterogeneous Systems

The wide variety of natural and synthetic systems that utilize amphiphilic microheterogeneous structures provides a testament to their importance in human technology and biological ecosystems. DOM displays micellar behavior similar to other natural and synthetic surfactants.[80] Wu *et al*. found DOM to possess extremely low critical micelle concentration values with respect to other surfactants which aids in its ability to transport hydrophobic organic pollutants through the aqueous ecosystem. Interestingly, the hydrophobic partitioning of phenanthrene to the DOM micelles decreased at high DOM concentrations and this behavior was attributed to rearrangement of the DOM macromolecular structures into larger soluble aggregates. Numerous micelle systems have been prepared using traditional surfactants[81-83], dendrimers[84-88], and amphiphilic block copolymers[89-98] for use in technologies ranging from selective drug delivery[84, 85, 95, 98, 99] to nanoscale photoreactors[86, 91]. Micelles and vesicles formed from self-assembling block copolymers have been identified as potential transfer agents of

hydrophobic anticancer drugs into the body.[98] Through selective and controlled delivery of their payload, these microheterogeneous systems help remove many unwanted side effects from invasive chemical procedures. Amphiphilic dendrimers and block copolymers that form aqueous micelles have been studied as ways of encapsulating and transporting photosensitizers used in photodynamic therapy.[37, 91, 99-102]

The most fashionable reactive species for envisioned photodynamic therapeutic systems is $^1O_2$ and several studies have been conducted to optimize every facet of its production and reactivity.[100, 102-105] Porphyrin species have been championed by most studies due to their well known $^1O_2$-producing characteristics. Oar *et al*. have used fluorescence resonance energy transfer to increase the efficiency of $^1O_2$ production by porphyrin species.[102] Nishiyama *et al*. have developed light harvesting dendritic micelles that transfer energy to internal porphyrin photosensitizers that showed enhanced $^1O_2$-cyctotoxicity against cancerous cell lines in comparison to a hydrophobic porphyrin species, porphyrin IX, capable of penetrating cellular membranes.[101] Li *et al*. further showed that amphiphilic diblock copolymer micelles were capable of delivering porphyrin IX into cancerous cells twice as well as the free porphyrin and that micelle delivered porphyrin IX demonstrated an order of magnitude enhancement in phototoxicity over the free porphyrin.[91] Production of $^1O_2$ within microheterogeneous systems, such as micelles and vesicles, has demonstrated much potential within future technologies, yet there still exists a void in the understanding of the physical mechanisms at the molecular level within these systems.

Comprehension of the overall effects of a process aids in designing initial applications for that particular system, but an understanding of the complex relationships that make up the entirety of the process is necessary to refine the process for future generations of applications. The overall effect of microheterogeneous systems that photochemically produce $^1O_2$, such as DOM and photodynamic therapy micelles, is well understood. As mentioned above, the production of $^1O_2$ within these systems has also been extensively studied. Little understanding of the mechanisms that occur between the photochemical production step and the observed overall outcome exist. Latch and McNeill made great strides in understanding these intermediate processes by developing a theory of microheterogeneous production of $^1O_2$ within a commercially available DOM solutions.[41] Their theory was developed with the hope of further understanding environmental degradation processes involving DOM and $^1O_2$, yet there remained several details that needed to be addressed. The second chapter in this thesis will address the general applicability of the theory of microheterogeneity to all DOM solutions and further expand it into a means of examining the structure and size of the DOM micelles. The third chapter in this thesis demonstrates the strength of the microheterogeneous theory in understanding the inactivation of waterborne enteric viruses in natural waters. Finally, the fourth chapter explains the relationship between micelle size and $^1O_2$ reactivity, as predicted by the reaction-diffusion theory of microheterogeneity, and highlights current methods available in tailoring nano-scale photoreactors.

Conclusion

Examples of microheterogeneous structures are prevalent throughout environmental, biological, and technological systems. Many of these systems incorporate the production of high-energy, transient intermediates through indirect photochemical processes. Singlet oxygen and •OH are two examples of PPRIs that have been shown to be produced in microheterogeneous systems. The relatively indiscriminate reactivity of •OH has led to its observed low steady-state concentrations within natural waters. The possibility of its production within hydrophobic DOM micelles makes the development of hydrophobic •OH probes necessary to further understand its reactivity. Singlet oxygen, though more selective in its reactivity, has been shown to have enhanced reactivity within hydrophobic micelles as explained in an initial theory of microheterogeneous production. It is pertinent to further refine this theory into one that has general applicability to all systems that contain photochemically active micelles. Not only will this have direct impact on our understanding of photochemical degradation processes in the environment, but it will provide new insights into future technological applications of photochemically active microheterogeneous systems.

Chapter 2.

Microheterogeneous Concentrations of Singlet Oxygen in Natural Organic Matter Isolate Solutions

In part from:

Matthew Grandbois, Douglas E. Latch, and Kristopher McNeill. *Environmental Science & Technology*, **2008**, 42(*24*), 9184-9190.

Overview

The binding affinity of a hydrophobic singlet oxygen probe towards natural organic matter isolates was investigated. A Langmuir binding isotherm was used to calculate specific binding coefficients and intramicellar concentrations of singlet oxygen several orders of magnitude larger than reported by traditional singlet oxygen probes. From the obtained data, a kinetic model was developed to describe the microscopic environment experienced by hydrophobic compounds in natural water systems. Micellar radii and molecular weights were derived from the experimental data and evaluated. The data obtained provides additional support of a microheterogeneous environment within bulk natural solutions. The enhanced concentrations of photogenerated reactive intermediates within these microenvironments may improve understanding of hydrophobic pollutant degradation in the environment.

Introduction

Aquatic photochemical processes are important for the breakdown of pollutants and the biogeochemical cycling of the elements.[1] Due to the presence of numerous photoactive dissolved and particulate constituents, photochemistry in natural waters is more complex than in pure water. Dissolved natural organic matter (DOM) is arguably the most important of these constituents and is known to affect the photochemistry of organic chemicals in at least two ways.[2, 3] First, chromophoric DOM is a photosensitizer and is responsible for the formation of many photochemically produced reactive intermediates (PPRI).[4-6] Second, DOM can bind hydrophobic molecules, providing a

distinct photochemical environment that differs from the bulk aqueous phase in its polarity and in the concentration of PPRI.[7-16]

Humic substances, as components of the DOM pool, have long been discussed as large, macromolecular, covalently bonded remnants of biomaterials.[17] A more recent view holds that humic substances are better described as supramolecular assemblies held together through hydrogen bonding, hydrophobic interactions and cation complexation.[18, 19] These assemblies have micelle-like properties consistent with a hydrophobic interior and hydrophilic periphery.[20] The DOM interiors provide a binding site for hydrophobic organic contaminants, increasing their observed aqueous solubilities and possibly altering their reactivity.[7-16] The binding of different environmental contaminants, including chlorinated[8, 10, 16, 21] and polycyclic aromatics[13, 15, 21, 22], explosives[9, 14], pesticides[23], herbicides[12], and cholesterol[11] has been previously investigated. This binding behavior is a general phenomenon that occurs in rivers[22], pristine and human-influenced lakes[21], seawater[7], and waste stabilization ponds.[24]

Using hydrophobic singlet oxygen ($^1O_2$) probes, Latch and McNeill demonstrated that the $^1O_2$ concentration experienced by the probes is greater when they are bound to Aldrich humic acid (ALHA).[25] The results provide evidence for an intra-DOM microenvironment with elevated $^1O_2$ concentration. The probe molecule experiences microheterogeneous photooxidation while in association with DOM.[26] This is in agreement with other findings of enhanced photoreactivity of DOM-bound molecules.[27-29] While their work demonstrated the utility of hydrophobic probes for determining the

intra-DOM concentrations of $^1O_2$, it only focused on ALHA, whose limitations as a model DOM have been noted.[30, 31]

The objective of this thesis chapter is to extend the work of Latch and McNeill to include International Humic Substance Society (IHSS) reference material isolates (Pony Lake fulvic acid and Suwannee River humic and fulvic acids) and another widely used commercial humic acid, Fluka humic acid. In addition, the relative binding affinities of the natural organic matter samples towards one of the hydrophobic trap-and-trigger probes, TPMA (2-[1-(3-*tert*-butyldimethylsiloxy)phenyl)-1-methoxymethylene]-tricyclo[3.3.1.1]decane) and intra-DOM concentrations of $^1O_2$ were determined in low ionic strength aqueous solutions. These values were used in combination with our current theoretical model of microheterogeneity within DOM solutions to subsequently estimate DOM aqueous radii and molecular weights.

Methods and Materials

Materials

The organic matter isolates investigated were Aldrich humic acid (ALHA; Aldrich), Fluka humic acid (FLHA; Fluka), Suwannee River humic acid (SRHA; IHSS), Suwannee River fulvic acid (SRFA; IHSS), and Pony Lake fulvic acid (PLFA; IHSS). Furfuryl alcohol (FFA; Aldrich) was distilled prior to use. Acetonitrile (ACS grade, Mallinckrodt), ethyl ether (Aldrich), tetrabutylammonium fluoride (TBAF; 1.0 M in THF), sodium chloride (NaCl; Fischer), potassium phosphate monobasic (J.T.Baker), sodium phosphate dibasic (Fisher) were used as received. Tetrahydrofuran (THF; Aldrich), and methylene chloride (Aldrich) were dried prior to use. Stock solutions of the

organic matter isolates (25 mL, 500 mg/L) were created by dissolving the respective organic matter with water (MilliQ). Photolysis solutions contained 5 mM phosphate and 10 mM NaCl at pH 7.5. The synthesis of (TPMA) and the corresponding dioxetane, $TPMAO_2$, resulting from the reaction of TPMA with the thermal decomposition of triphenyl phosphate ozonide have previously been described.[32]

Dissolved organic carbon

Total dissolved organic carbon (DOC) content of the DOM stock solutions was determined via a Shimadzu TOC 5000A Total Organic Carbon Analyzer. The stock solutions were diluted by a factor of 5, acidified to pH ≤ 2 with 100 μL of 2N HCl, and analyzed as non-purgeable organic carbon. The DOC of each sample was compared to a standard calibration curve generated via potassium hydrogen phthalate.

Chemiluminescence measurements

All chemiluminescence measurements were recorded with a Turner Designs TD-20/20 luminometer. The sensitivity of the instrument was set to 30%. Aqueous photolyses were analyzed by diluting 5 μL aliquots of the reaction solution to 5 mL in acetonitrile. A 300 μL aliquot of the diluted reaction solutions were transferred to a 12 x 50 mm polypropylene tube for chemiluminescent analysis. The dioxetanes formed during photolysis were induced to decompose upon addition of 20 μL of 25 mM TBAF (acetonitrile). The chemiluminescent signal was recorded for 50 seconds and converted

to concentration of dioxetane via a calibration curve generated from the authentic standard dioxetane.

Steady state irradiation experiments

Steady state photolysis experiments were conducted with four medium pressure 175 W Hg vapor lamps (borosilicate-jacketed LumaPro lamps, GE HR175A39/CP bulbs) as the light source. The solutions were placed in quartz tubes (10 mL) on a turntable under the lamps. The test tubes were situated at 30° from normal. The photolyses were conducted at ambient temperature. Small sample aliquots (100 μL) were removed for analysis at specific time intervals. Furfuryl alcohol samples were analyzed via HPLC with a Supelco RP-Amide C_{16} (150 × 4.6 mm, 5μm particle size) column and a mobile phase of 10:90 acetonitrile:pH 5 acetate buffer. The flow rate was 1.0 mL/min and the detection wavelength was 219 nm. The rate of FFA degradation was analyzed to determine the steady state concentration of $^1O_2$ within the solution ($[^1O_2]_{aq}$). Reaction of TPMA was tracked by monitoring the formation of $TPMAO_2$ by chemiluminescence detection. Each dissolved organic matter isolate was irradiated at different concentrations of total organic matter (0.5 – 100 mg/L). All photolysis solutions (5 mL) consisted of 100 μM FFA, 10 μM TPMA, 5 mM pH 7.5 phosphate buffer, and 10 mM NaCl in addition to the desired concentration of dissolved organic matter.

Theory

Light screening factor

The $^1O_2$ concentrations determined via FFA probe degradation rate constant deviated from linear behavior at high concentrations of DOM. This was interpreted as the result of light screening from the organic matter within the reaction solution. The light screening correction factor was derived from the comparison of light intensity at the surface of the solution and the mean light intensity over a given solution thickness. At the optically thin surface layer, the rate of light absorption is given by the sum of the light absorbed over the light spectrum (eq. 1)

$$k_{abs,thin} = 2.303 \sum_{\lambda} \alpha_{\lambda} I_{\lambda,0} \quad (1)$$

where α_λ is the absorbance coefficient at a given wavelength and $I_{\lambda,0}$ is the light irradiance at a given wavelength. Outside the optically thin regime, one must use the mean light intensity, $\langle I_\lambda \rangle_z$, due to the significant absorption within solutions (eq. 2).

$$k_{abs,thick} = 2.303 \sum_{\lambda} \alpha_{\lambda} \left\langle I_{\lambda,} \right\rangle_z \quad (2)$$

The average irradiance at depth, z, is the irradiance at the surface multiplied by the light screening factor, S_λ (eq. 3).[1]

$$\left\langle I_{\lambda} \right\rangle_z = I_{\lambda,0} \frac{(1-10^{-\alpha_\lambda z})}{2.303 \alpha_{\lambda} z} = I_{\lambda,0} S_{\lambda} \quad (3)$$

In our calculations, z was optimized to a value of 1 cm, which gave the best linear fit of aqueous $^1O_2$ concentration data. The correction factor (*CF*) is then defined as the ratio of light absorbed at optically thin conditions over the light absorbed at optically thick conditions (eq. 4).

$$CF = \frac{k_{abs,thin}}{k_{abs,thick}} = \frac{\sum_{\lambda} \alpha_\lambda I_{\lambda,0}}{\sum_{\lambda} \alpha_\lambda \langle I_\lambda \rangle_z} = \frac{\sum_{\lambda} \alpha_\lambda I_{\lambda,0}}{\sum_{\lambda} \alpha_\lambda I_{\lambda,0} S_\lambda} \quad (4)$$

The need for a correction factor is clear from plots of $[^1O_2]_{ss}$ vs. [DOM] determined using FFA (Figure 2.1). These plots should be linear, but show a downward curvature. After application of the correction factor, the plots show linearity. The correction factor was also applied to the data acquired from TPMA photolysis in a similar manner to yield the results reported here.

Determining $[^1O_2]_{DOM}$ from hydrophobic probe binding

The hydrophobic $^1O_2$ probe used in this study, TPMA, associates with DOM, and this fact allows it to be used to estimate the intra-DOM $^1O_2$ concentration (Scheme 2.1). The amount of $TPMAO_2$ formed reflects the sum of the $^1O_2$ trapped in the DOM phase and in the aqueous phase. Since the concentrations in these two regions differ, the apparent singlet oxygen concentration, $[^1O_2]_{app}$ will vary according to the fraction of probe bound to the DOM phase, f_{DOM}, and in the aqueous phase, f_{aq} (eq. 5).

$$[^1O_2]_{app} = f_{DOM}[^1O_2]_{DOM} + f_{aq}[^1O_2]_{aq} \quad (5)$$

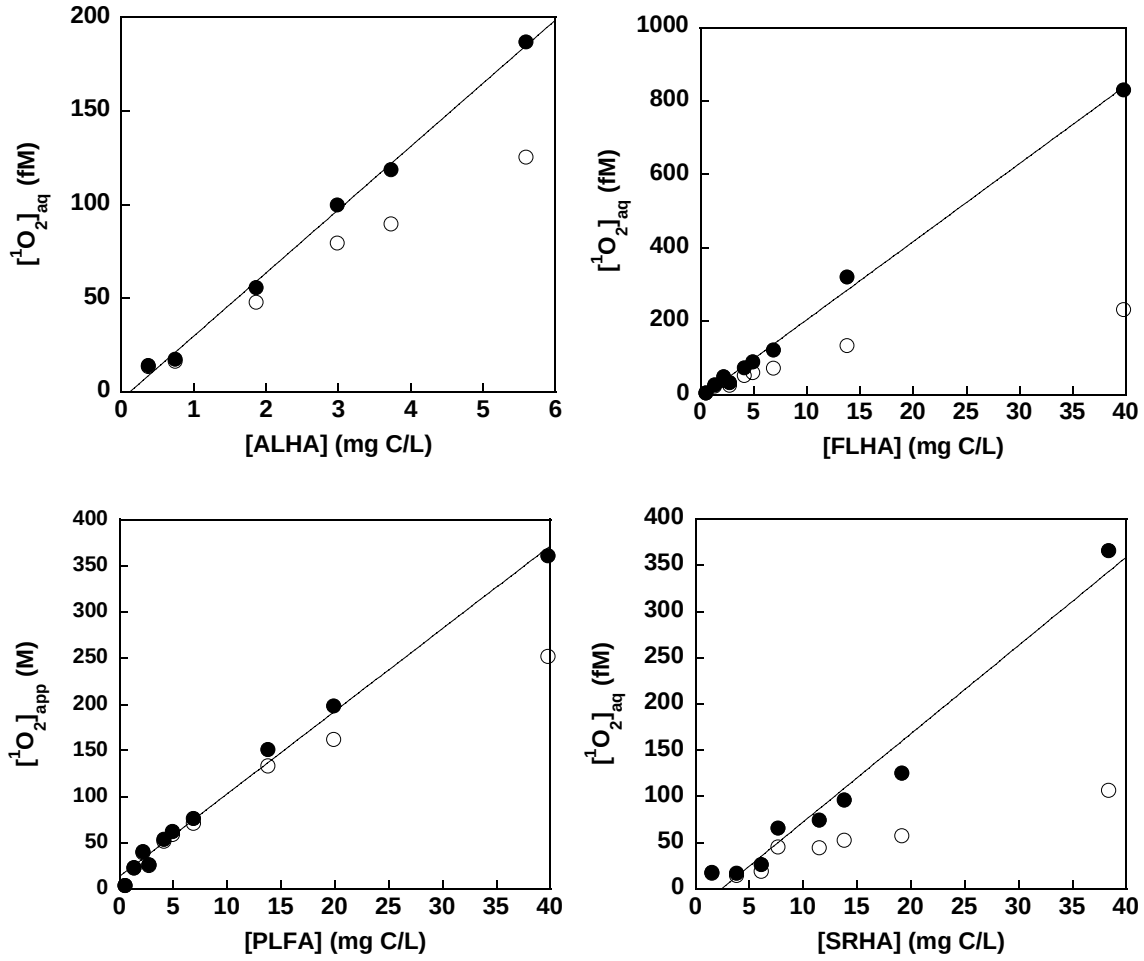

Figure 2.1. Concentration of $^1O_2$ within bulk dissolved organic matter solutions, as measured by FFA. Aldrich humic acid (ALHA), Fluka humic acid (FLHA), Pony Lake fulvic acid (PLFA), and Suwannee River humic acid (SRHA) were analyzed. Corrected values (●) fit a linear equation better than uncorrected values (○). Solid indicates fit of data to linear slope.

For a simple equilibrium binding model (Langmuir isotherm), as shown in equation 6, f_{DOM} is a function of the association constant, K_{OM} (eq. 7).

$$\text{TPMA} + \text{DOM} \underset{}{\overset{K_{OM}}{\rightleftharpoons}} \text{TPMA•DOM} \qquad (6)$$

$$f_{DOM} = \frac{K_{OM}[DOM]}{1 + K_{OM}[DOM]} \tag{7}$$

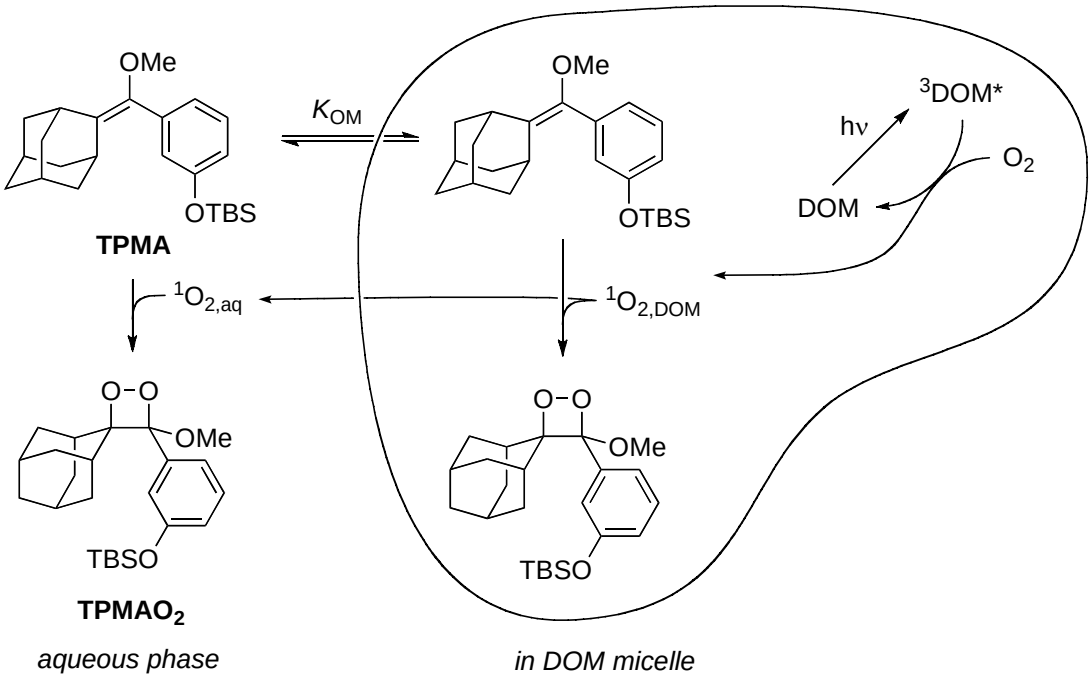

Scheme 2.1. Binding scheme for $^1O_2$ probe and DOM micelle. TBS = Dimethyl-*tert*-butyl silyl.

Given $f_{DOM} + f_{aq} = 1$, equations 5 and 7 can be rewritten as equation 8.

$$[^1O_2]_{app} = \frac{K_{OM}[DOM]}{1 + K_{OM}[DOM]}([^1O_2]_{DOM} - [^1O_2]_{aq}) + [^1O_2]_{aq} \tag{8}$$

The fraction of probe bound is not the only term in equation 8 that depends on [DOM], since the aqueous singlet oxygen concentration, $[^1O_2]_{aq}$, also varies linearly with [DOM] (eq. 9).

$$[^1O_2]_{aq} = k_{^1O_2}[DOM] \tag{9}$$

Here, $k_{^1O_2}$ is a DOM-normalized $^1O_2$ formation rate constant, which can be determined from measurements of $[^1O_2]_{aq}$ at various [DOM].

Combining equations 8 and 9 gives equation 10 that relates the apparent singlet oxygen concentration reported by the probe to the concentration of dissolved organic matter. The only fitting parameters in this equation are the binding constant, K_{OM}, and the interior $^1O_2$ concentration, $[^1O_2]_{DOM}$.

$$[^1O_2]_{app} = \frac{K_{OM}[DOM]}{1+K_{OM}[DOM]}([^1O_2]_{DOM} - k_{^1O_2}[DOM]) + k_{^1O_2}[DOM] \qquad (10)$$

DOM as a dispersed organic phase

Consider DOM as a distinct organic phase, inside which all of the sensitizing chromophores are located and all of the $^1O_2$ is produced. It follows that the rate of $^1O_2$ formation inside the DOM phase, $k_{f,DOM}$, will be much larger than the rate for the entire aqueous-DOM system, $k_{f,tot}$. Further, the magnitude of $k_{f,DOM}$ is related to $k_{f,tot}$ by the volume ratio, V_{tot}/V_{DOM}, eq 11.

$$k_{f,DOM} = k_{f,tot}\frac{V_{tot}}{V_{DOM}} \qquad (11)$$

For a 1 mg/L DOM solution, the volume ratio is *ca*. 10^6, and we therefore expect $k_{f,DOM}$ to be ca. 6 orders of magnitude higher than the measured $k_{f,tot}$. The $^1O_2$ formation rate, $k_{f,tot}$, is determined from $[^1O_2]_{aq}$ and the solvent-dependent electronic relaxation rate constant, k_{solv}, which is 2.5×10^5 s^{-1} for water (eq. 12).

$$k_{f,tot} = [^1O_2]_{aq} k_{solv} \qquad (12)$$

The diffusive transport of $^1O_2$ from the DOM phase to the aqueous phase serves both as a major sink for $^1O_2$ in the DOM phase and as the source of $^1O_2$ to the aqueous phase. The manner in which the DOM phase is dispersed in the aqueous phase, specifically the size, morphology, and density of the supramolecular aggregates, controls the transport rate of $^1O_2$ from the DOM phase to the aqueous phase. Despite decades of work on the structure of DOM, a detailed understanding remains limited. As a rough, but mathematically useful, approximation, we treat the DOM phase as monodisperse, spherical globules.

The kinetic scheme for this model is shown in Scheme 2.2. In this model, the sensitizer is excited by light (hν) with an absorption rate, k_{abs}. The excited sensitizer transfers energy to O_2 generating $^1O_2$ with a quantum yield, $\Phi_{^1O_2}$. The product of k_{abs} and $\Phi_{^1O_2}$ is k_f. There is a second source of $^1O_2$ to the DOM core, which is back-diffusion from the aqueous phase, k_{+diff}. The $^1O_2$ in the DOM phase is subject to two types of loss processes: diffusion out of the DOM phase, k_{-diff}, and electronic relaxation.

The above processes lead to a steady-state $^1O_2$ concentration in the DOM phase given by equation 13.

$$[^1O_2]_{DOM} = \frac{k_{f,DOM} + k_{+diff}[^1O_2]_{aq} K^{^1O_2}_{DOM/aq} \frac{V_{aq}}{V_{tot}}}{k_{DOM} + k_q[Q]_{DOM} + k_{-diff}} \qquad (13)$$

The volume normalizing term, $V_{aq}/V_{tot,}$ can be taken to be 1 for most DOM solutions. Further, a quick back-of-the-envelope analysis indicates that the diffusion term, k_{-diff},

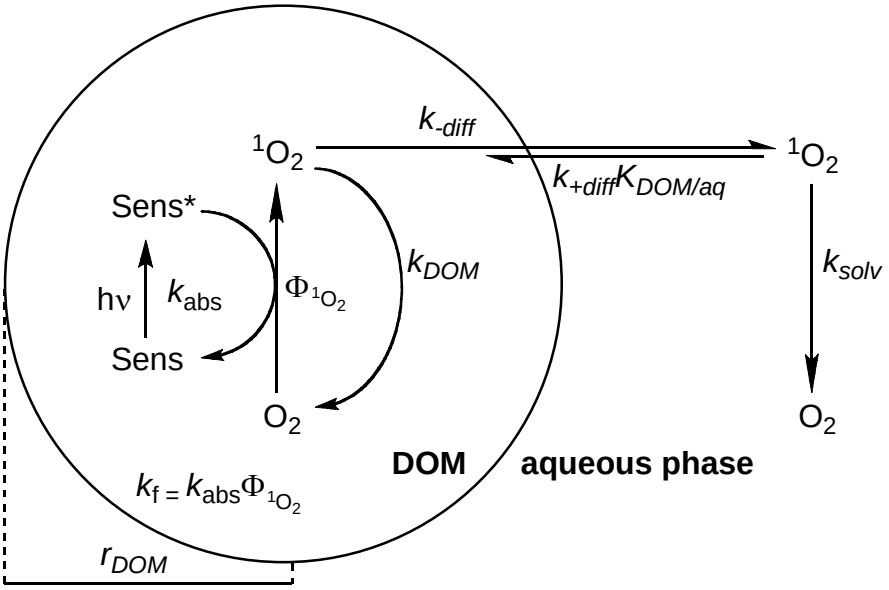

Scheme 2.2. Reaction-diffusion kinetic scheme for $^1O_2$ production inside a DOM globule.

is the only important term in the denominator. Thus, equation 13 can be simplified to equation 14.

$$[^1O_2]_{DOM} \approx \frac{k_{f,DOM} + k_{+diff}[^1O_2]_{aq} K^{^1O_2}_{DOM/aq}}{k_{-diff}} \qquad (14)$$

To a first approximation, back-diffusion (i.e., the second term of the numerator of eq. 14) can be ignored giving equation 15.

$$[^1O_2]_{DOM} \approx \frac{k_{f,DOM}}{k_{-diff}} \qquad (15)$$

For diffusion from a sphere, $k_{-diff} \approx 3D/r^2$, where D is the diffusivity of $^1O_2$ in the DOM phase and r is the sphere radius.[33] This substitution gives equation 16.

$$[^1O_2]_{DOM} \approx \frac{k_{f,DOM} r^2}{3D} \qquad (16)$$

Relating measurements of $[^1O_2]_{DOM}$ and $[^1O_2]_{aq}$ to the size of DOM based on mass transfer considerations

With values for both $[^1O_2]_{DOM}$ and $k_{f,DOM}$, equation 16, which relates $[^1O_2]_{DOM}$ to the mass transfer rate of $^1O_2$ from the micelle, gives an estimate of r^2/D. Solving for the micelle radius gives equation 17.

$$r \approx \left(\frac{[^1O_2]_{DOM}\, 3D}{k_{f,DOM}} \right)^{1/2} \tag{17}$$

The molecular weight of the DOM micelle can be expressed in terms of volume, volume of sphere = $^4/_3\pi r^3$, and the density of humic material within the micelle, ρ_{DOM}, where N_A is Avogadro's number (eq. 18).

$$MW \approx \frac{4}{3}\pi \left(\frac{[^1O_2]_{DOM}\, 3D}{k_{f,DOM}} \right)^{3/2} \rho_{DOM}\, N_A \tag{18}$$

Results and Discussion

Binding isotherms

Binding isotherms for association of TPMA with DOM isolates were constructed by determining the transformation rate of TPMA to its dioxetane analog, $TPMAO_2$, at various DOM concentrations (Figure 2.2). These transformation rates were converted to apparent $^1O_2$ concentrations, $[^1O_2]_{app}$, using the previously determined rate constant for the reaction of TPMA with $^1O_2$, $k_{rxn} = 1.7 \times 10^6\ M^{-1}\ s^{-1}$.[32]

Construction of these isotherms was performed in the face of two significant limitations that prevented measurements at very low and very high organic matter

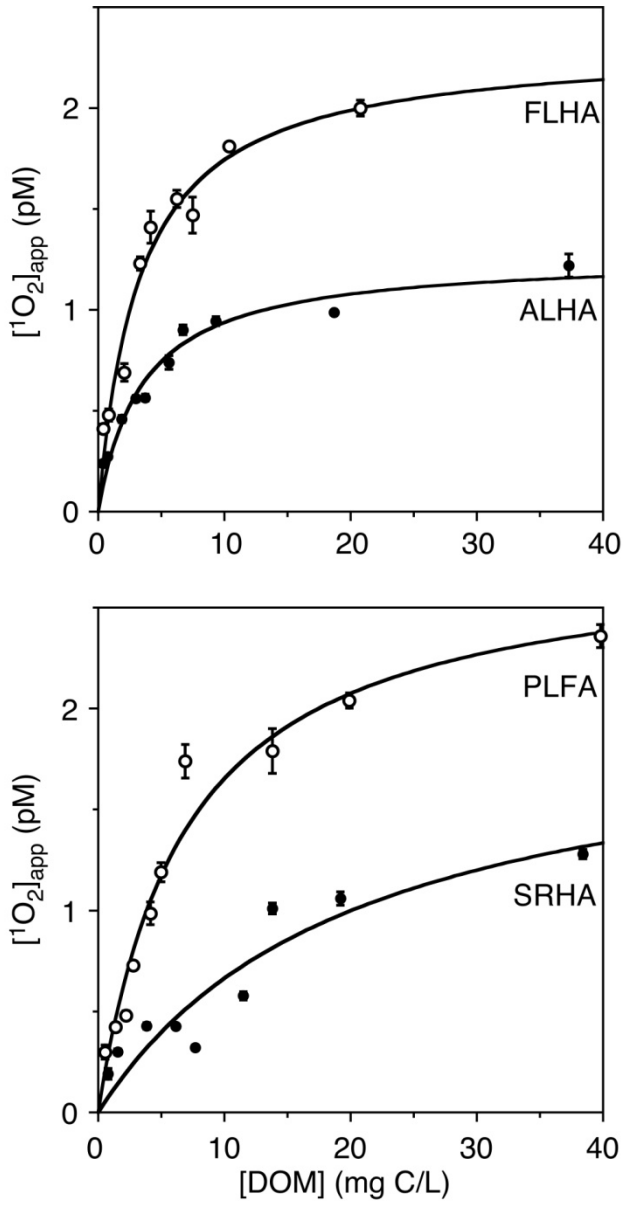

Figure 2.2. Binding isotherms of naturals DOM isolates. Top panel: Binding plots of commercial humic acids: ALHA and FLHA. Bottom panel: Binding plots of reference natural organic matter: PLFA and SRHA. Curves fit according to equation 12. Error bars represent the 95% confidence interval.

concentrations, namely, self-sensitization and light screening. In the absence of humic substances, irradiation of TPMA leads to slow formation of $TPMAO_2$. This self-sensitization occurs in water, but not alcohol solvents, indicating that aggregation of TPMA may be important in this process. The practical result is that when 10 μM TPMA is employed a "background" concentration of 2.5×10^{-13} M $^1O_2$ is observed even in the absence of organic matter. Data obtained at low organic matter concentrations (< 0.5 mg C/L), where the measured $^1O_2$ concentration was competitive with this background concentration, were not used in constructing the isotherm. Additionally, the background concentration of $^1O_2$ was subtracted from the measured $[^1O_2]_{app}$ values.

Light screening at high organic matter concentrations was also a problem. While a correction factor can be applied, we chose not to include data for which the correction factor was greater than two. This limited the organic matter concentrations to *ca*. 50 mg C/L. Thus, isotherms were constructed over a two-order of magnitude range of organic matter concentrations.

Plots of $[^1O_2]_{app}$ vs. the concentration of DOM were indicative of association between TPMA and DOM. First, the concentrations of $^1O_2$ reported by the TPMA probe were two to three orders of magnitude larger than those reported by the hydrophilic probe, FFA. We have previously shown that both probes report the same concentrations in ethanol, where hydrophobic binding is not expected to be important.[34] Second, the $[^1O_2]_{app}$ versus [DOM] plots are non-linear, consistent with the prediction of a simple association model (eq. 10). Four of the five DOM isolates examined, ALHA, FLHA,

PLFA, SRHA gave elevated $[^1O_2]_{app}$ values and non-linear $[^1O_2]_{app}$ versus [DOM] plots, indicating binding.

Values of log K_{OM} and $[^1O_2]_{DOM}$ for each DOM isolate are given in Table 2.1. The two commercial DOM isolates, ALHA and FLHA, showed almost identical K_{OM}, yet the $[^1O_2]_{DOM}$ for FLHA, 2.28 pM, was twice that for ALHA, 1.14 pM. PLFA, gave the highest $[^1O_2]_{DOM}$, 2.72 pM, and lowest K_{OM}. The values for SRHA are also listed in Table 2.1, albeit with higher estimated errors due to the weak association of TPMA with SRHA.

The TPMA-DOM binding constants and $[^1O_2]_{DOM}$ values for their respective DOM isolates have been reported in two prior publications using the same methodology as in the present work.[24, 25] Even though the same organic matter samples were examined, the results reported this chapter and in the previous studies differ. There are good reasons for the discrepancies, which are outlined below.

DOM	$[^1O_2]_{DOM}$ (pM)	log K_{OM}
ALHA	1.1 ± 0.1	5.5 ± 0.1
FLHA	2.3 ± 0.2	5.5 ± 0.1
PLFA	2.7 ± 0.2	5.0 ± 0.1
SRHA	1.9 ± 0.5	4.7 ± 0.2
SRFA		<2

Table 2.1. Isotherm fitting parameters for DOM isolates.

Latch and McNeill performed the initial study on the microheterogeneous distribution of $^1O_2$ in irradiated humic acid solutions with ALHA.[25] In that work, values of log K_{OM} and $[^1O_2]_{DOM}$ of 7.1 and 3 pM were found, contrasting with the values of 5.5 and 1.1 pM found here. One of the differences between this and the prior study is that the latter did not take into account light screening in construction of the binding isotherm. The application of screening factors to the values from the previous report give only modest changes (log K_{OM} = 6.9 and $[^1O_2]_{DOM}$ = 3.5 pM). A more important difference between this and the prior study was the ionic strength, μ, of the irradiated solutions. The ionic strength of the solutions in this report was ca. 10 mM, while the ionic strength in the previous study was ca. 460 mM. Hosee and Wilkinson have reported that the hydrodynamic radius of DOM micelles can be decreased (35-65%) by changes in ionic strength (1 − 100 mM).[35] The micelles at higher ionic strength would be denser and consequently more hydrophobic than the micelles at lower ionic strength. The K_{OM} values of ALHA presented in our previous work are expected to be higher due to the increased μ. Varying the ionic strength from μ = 0.01 to μ = 0.49 M while keeping [DOM] constant results in an increase of $[^1O_2]_{app}$ from 1.5 to 3.5 pM (Figure 2.3). We conclude that incongruities between this work and that of Latch and McNeill are due to the differences in experimental conditions, with the most important difference likely being ionic strength. These results suggest that significant differences in hydrophobic binding and singlet oxygen distribution will be observed between freshwater and marine samples.

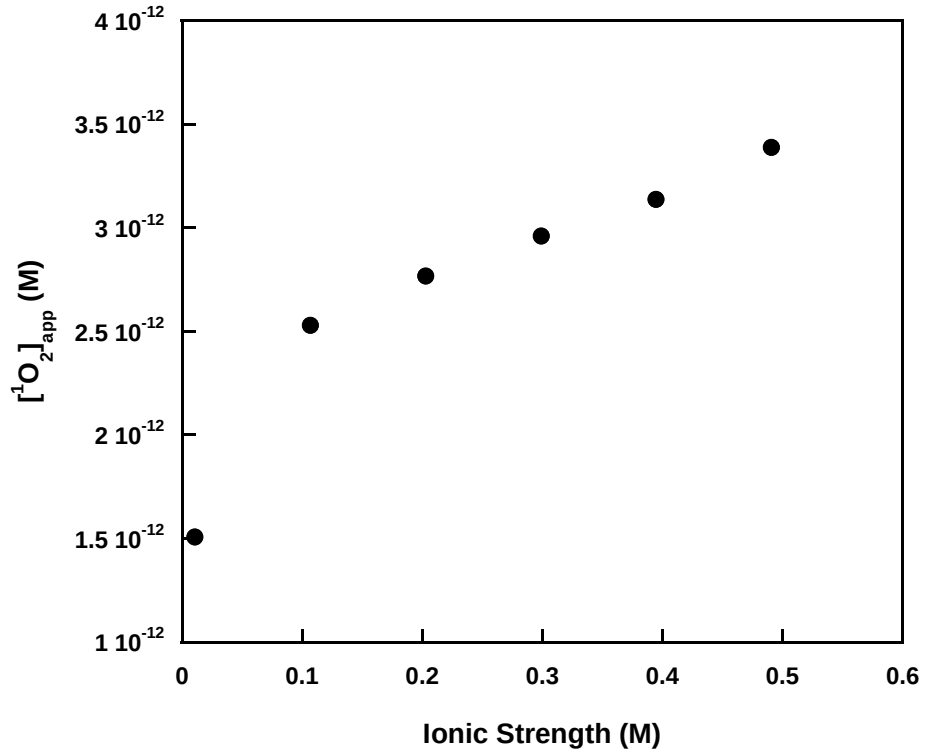

Figure 2.3. Relationship between ionic strength, μ, and $[^1O_2]_{app}$.

Chapter 3 of this thesis reports TPMA•DOM binding isotherms in conjunction with a study on the rate of association between MS2 virus and DOM in its photoinactivation.[24] The research conducted in that study utilized the same DOM isolates at the same ionic strength as the research presented in this chapter with the only methodological difference being the use of a solar simulator instead of Pyrex-filtered Hg-vapor lamps. In Chapter 2, for ALHA, FLHA, PLFA, and SRHA, $[^1O_2]_{DOM}$ /$[^1O_2]_{DOM,ALHA}$ values of 1, 2.2, 0.28, 1.1 and log K_{OM} values of 4.9, 4.2, 6.3, and 5.4 were found, respectively.

We have subsequently performed a study of the photostability of the dioxetane, $TPMAO_2$, under both solar simulator and Pyrex-filtered Hg-vapor lamp irradiation conditions. ALHA and SRHA were used in these experiments due to their similar behavior. We have found that $TPMAO_2$ is photochemically degraded under solar simulator conditions and not under Pyrex-filtered Hg-vapor lamp irradiation (Figure 2.4). For this reason, we have greater confidence in the K_{OM} and $[^1O_2]_{DOM}$ results presented here.

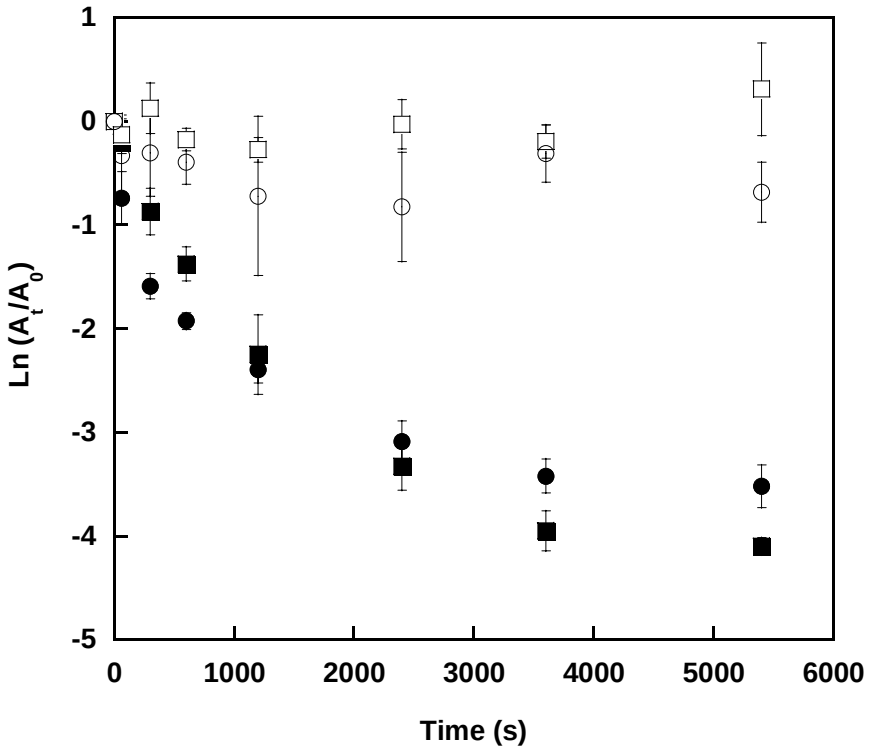

Figure 2.4. Degradation of $TPMAO_2$ within solutions of ALHA and SRHA under different photolysis conditions. Photolysis of ALHA (□) and SRHA (○) with Hg vapor led to little degradation of $TPMAO_2$. Photolysis of ALHA (■) and SRHA (●) with the solar simulator led to much faster degradation of $TPMAO_2$.

The research conducted in chapter 3 of this thesis concluded that the binding behavior and $^1O_2$ environment experienced by TPMA did not correlate with virus inactivation rates. Using the values determined by the research presented in this chapter, there is no change in that conclusion.

An especially noteworthy result of this study is the lack of binding behavior between TPMA and SRFA (Figure 2.5). This result highlights a potential deficiency of SRFA as a humic substance standard, in that it may not be representative in terms of hydrophobic binding.

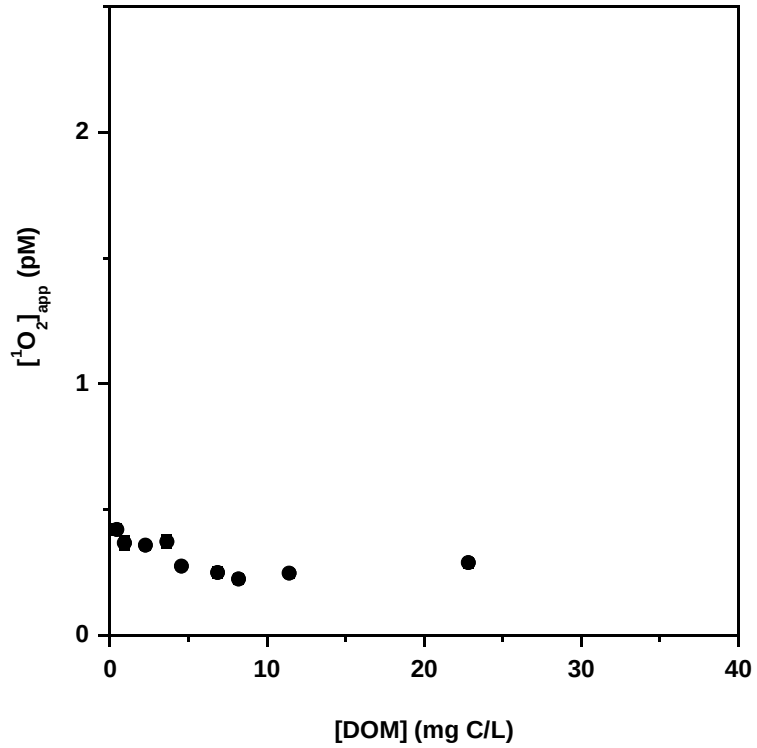

Figure 2.5. Plot of $[^1O_2]_{app}$ versus SRFA, showing no evidence for binding between TPMA and SRFA. $[^1O_2]_{app}$ values were determined by chemiluminescent analysis of $TPMAO_2$ generation at varied concentration of SRFA under Hg-vapor lamp photolysis. Error bar represent the 95% confidence interval.

Estimation of DOM micellar radii and molecular weights based on mass transfer considerations

Two radii were calculated for each DOM using eq. 17, one using the diffusivity of O_2 in water, 2.3×10^{-5} cm^2/s, and one using an order of magnitude lower value that corresponds to the diffusivity of O_2 in a polymer matrix (Table 2.2).[36] ALHA was calculated to have micellar radii ranging from 0.47 – 1.58 nm. These values agree well with radii calculated from experimentally determined molecular weights from other studies shown in Table 2.3.[37-40] The radii calculated for both FLHA, 1.06 – 3.60 nm, and SRHA, 0.65 – 2.19 nm also agree well with the experimentally determined values.[37,38,40-49] The least studied DOM, PLFA, is calculated to have radii ranging from 1.71 – 5.79 nm based on the results in this study. These values are significantly higher than the radius calculated, 0.77 nm, from the only other study estimating the size of PLFA by HP-SEC.[41]

Molecular weights were calculated using eq. 18 with both low and high density values of 0.7 and 1.5 g/mL (Table 2.4). These density values were chosen to represent the two extremes of micellar density. The latter value, 1.5 g/mL, is viewed as average density of humic acids as reported by IHSS.[42] A similar value, 1.66 g/mL, was used by Bendedetti *et al*. during their study of humic substances as a Donnan gel phase.[43] DOM micelles have the potential to take on 100% water at low ionic strength, reducing the intramicellar density to 0.7 g/mL.[44] De Wit *et al.* used a similar density range, 0.7 – 1.7 g/mL, in studying proton binding to humic substances.[45]

			$^1O_2$ formation rate constants			DOM sphere radius (nm)	
						D (cm^2/s)	
DOM	$[^1O_2]_{aq}$ (fM)[a]	$[^1O_2]_{DOM}$ (fM)[b]	$k_{f,tot}$ (nM/s)	$k_{f,DOM}$ (mM/s)	k_{-diff} (1/ns)	2.3×10^{-5}	2.3×10^{-6}
FLHA	9.71	1140	2.43	3.15	2.77	1.58	0.47
FLHA	3.74	2280	0.935	1.22	0.533	3.60	1.06
SRHA	8.55	1940	2.14	2.78	1.43	2.19	0.65
PLFA	1.73	2720	0.431	0.561	0.206	5.79	1.71

[a]Aqueous steady-state $[^1O_2]$ in the bulk solution determined by FFA degradation experiments

[b]Concentration of $^1O_2$ within DOM micelles extrapolated from TPMA binding isotherms

Table 2.2. Calculated radii of DOM micelles.

It is possible, in principle, to work backward from DOM molecular weight or radius data to an expected value of the interior singlet oxygen concentration, $[^1O_2]_{DOM}$. Such an estimate is based on three different values: the sum of light absorption, quantum yield of singlet oxygen formation, and approximate size of the DOM micelle. While the light absorbance properties are simple to measure, and the quantum yield for singlet oxygen formation is likely to fall in a narrow range (ca. 1 – 5 %), the size of the DOM micelle is difficult to determine. The widely variable estimates of DOM radii from different techniques given in Table 2.3 suggest that we are currently not able to give good *a priori* estimates of $[^1O_2]_{DOM}$.

Relationship between average measured values and the microscopic physical picture

While the measured $[^1O_2]_{DOM}$ values for each DOM are on the order of 1 pM, this does not correlate with a microscopic physical picture in which each micelle has $[^1O_2]$ of 1 pM. In fact, this is physically impossible since a singly occupied micelle of 1 nm radius has a $^1O_2$ concentration of 400 μM. Rather, the microscopic picture is envisioned as a mixture of unoccupied micelles ($[^1O_2]$ = 0 M) and singly occupied micelles ($[^1O_2]$ ~ 100 μM) governed by Poisson statistical distribution.[46] Burns *et al*., have utilized similar distribution statistics governing scavenger molecule occupation of humic micelles during photodegradation of mirex.[47] The distribution of $^1O_2$ within an aqueous solution of DOM micelles is governed by the probability, *P(n)*, of a certain number of molecules, *n*, residing within a micelle at a given molecule-to-micelle ratio, *R*, as denoted in the Poisson equation (eq. 19).

$$P(n) = \frac{R^n e^{-R}}{n!} \tag{19}$$

DOM	MW (kDa)	Radius (nm)	Method	Reference
ALHA	4.1	1.08	HP-SEC[a]	[37]
	6.06	1.23	HP-SEC	[38]
	13.0	1.58	SEC[b]	[39]
	14.5	1.64	FFF[c]	[40]
		0.47 – 1.58	*this work*	
FLHA	2.28	0.89	HP-SEC	[48]
	16.8	1.72	HP-SEC	[49]
	20	1.83	SEC	[50]
	3280	10	TEM[d]	[51]
	51200	25	DLS[e]	[52]
		1.06 – 3.60	*this work*	
SRHA	1.49	0.77	FFF	[40]
	1.5	0.77	VPX[f]	[40]
	3.67	1.04	HP-SEC	[38]
	3.82	1.05	HP-SEC	[37]
	3.94	1.06	HP-SEC	[53]
	4.31	1.10	HP-SEC	[54]
	4.39	1.10	FFF	[40]
	410000	50	PCS[g]	[55, 56]
		0.65 – 2.19	*this work*	
PLFA	1.47	0.77	HP-SEC	[41]
		1.71 – 5.79	*this work*	

[a]High performance size exclusion chromatography
[b]Size exclusion chromatography
[c]Flow field-flow fractionation
[d]Transmission electron microscopy
[e]Dynamic light scattering
[f]Vapor pressure osmometry and low-angle X-ray scattering
[g]Photon correlation spectroscopy

Table 2.3. Comparison of molecular weight and radii of DOM micelle. All radii were calculated from experimentally determined molecular weights using equations 17 and 18, except directly measured radii reported from TEM and DLS.

			Molecular Weight (kDa)	
DOM	D (cm^2/s)	radius (nm)	ρ = 1.5 g/mL	ρ = 0.7 g/mL
ALHA	2.3×10^{-5}	1.58	14.9	9.93
	2.3×10^{-6}	0.47	0.38	0.26
FLHA	2.3×10^{-5}	3.60	176	117
	2.3×10^{-6}	1.06	4.52	3.01
SRHA	2.3×10^{-5}	2.19	40.0	26.6
	2.3×10^{-6}	0.65	1.03	0.68
PLFA	2.3×10^{-5}	5.79	734	489
	2.3×10^{-6}	1.71	18.8	12.5

Table 2.4. Calculated molecular weights of DOM based on micelle radii.

Environmental Significance

The above findings add further support to the presence of microenvironments within natural waters with increased concentrations of PPRI. The solubility of hydrophobic pollutants in natural water systems have been shown to be increased by the presence of DOM consistent with binding of hydrophobic contaminants to DOM.[57] This study, along with others, demonstrates increased concentrations of PPRI within DOM micelles, facilitating photodegradation of hydrophobic pollutants in the environment.

The effect of increased concentrations of PPRI within DOM micelles is not limited to the fate of hydrophobic contaminants, but may also have relevance to the photobleaching of DOM. The role of $^1O_2$ in the weathering of DOM has been assumed to be minimal due to its previously reported low concentrations in natural aquatic systems. Hefner et al. found that a solution of SRHA made of 1:1 D_2O:H_2O showed no increase in

photobleaching of the solution.[58] These findings, though correct in observation of the bulk solution, do not take into account the effect on the concentration of $^1O_2$ in the hydrophobic DOM phase by the longer $^1O_2$ lifetime in the bulk aqueous phase. The enhanced concentrations reported in this and our previous work show that the concentration of $^1O_2$ is roughly one thousand fold higher than previously thought. The role of singlet oxygen in photoweathering of DOM in light of its heightened intra-DOM concentrations is intriguing and remains an open question.

Chapter 3.

Association with natural organic matter enhances the sunlight-mediated inactivation of MS2 coliphage by singlet oxygen

In part from:

Tamar Kohn, Matthew Grandbois, Kristopher McNeill, and Kara L. Nelson.

Environmental Science & Technology, **2007**, 41(*13*), 4626-4632.

Overview

The reaction-diffusion theory of singlet oxygen ($^1O_2$) production within natural dissolved organic matter (DOM) isolates developed in the previous chapter is applied to the further understanding the sunlight-mediated inactivation of MS2 coliphage, a surrogate for human enteric viruses, in the presence of DOM. The concentration of $^1O_2$ within the DOM supramolecular assemblies ($[^1O_2]_{DOM}$) is orders of magnitude higher than in the bulk aqueous solution ($[^1O_2]_{aq}$). While in close proximity to the DOM assembly, MS2 is exposed to the higher $[^1O_2]_{DOM}$ and any inactivation caused by $^1O_2$ would be expected to be enhanced in comparison to the bulk solution.

In the presence of simulated sunlight, experiments were conducted to determine $[^1O_2]_{aq}$, $[^1O_2]_{DOM}$, and the association of MS2 with four DOM isolates. The effect of each DOM isolate on the inactivation of MS2 was determined by fitting the observed MS2 inactivation rate constants, k_{obs}, over a range of DOM concentrations according to a Langmuir-type binding isotherm. Despite differences in binding behaviour between the DOM isolates, MS2 inactivation was dominated by $[^1O_2]_{DOM}$ rather than $[^1O_2]_{aq}$.

Introduction

Sunlight is important in the inactivation of viral and bacterial pathogens within sewage-impacted surface waters.[1-5] This disinfection process has been utilized in several low-cost water and wastewater treatment systems, such as solar disinfection processes[6] and wastewater stabilization ponds (WSP).[7, 8] Photo-inactivation of waterborne pathogens can occur either through direct or indirect photodegradation mechanisms.[9] Direct photo-

inactivation occurs via degradation of nucleic acids by UVB light, while indirect photo-inactivation occurs by the reaction of vital cellular components with reactive oxygen species (ROS) that are formed by sensitizers within the system. Reactive oxygen species are formed by both internal sensitizers (e.g. flavins[10]) or sensitizers present within the water solution (e.g. DOM[11]) during indirect photochemical mechanisms discussed in the first chapter of this thesis.

Kohn and Nelson demonstrated that the indirect inactivation of MS2 coliphage occurred in solutions of DOM isolates and in WSP water.[12] Of all the ROS produced by these external photosensitizers, $^1O_2$ was found to dominate the inactivation of MS2. As demonstrated in the previous chapter, the concentration of $^1O_2$ within DOM supramolecular assemblies, ($[^1O_2]_{DOM}$), was found to be several orders of magnitude higher than the steady-state concentrations of $^1O_2$ within the bulk solutions, ($[^1O_2]_{aq}$).[13, 14] The local concentration of $^1O_2$ quickly approaches $[^1O_2]_{aq}$ with increasing distance from the DOM supramolecular assembly, therefore molecules that are in close proximity to DOM assemblies would be subjected to the increased concentrations of $^1O_2$.[14] Based on these studies, it should follow that the photo-inactivation of MS2 would proceed more rapidly when in close proximity to external sensitizers (i.e. DOM or particulate organic matter) and be subjected to concentrations of $^1O_2$ closer to $[^1O_2]_{DOM}$ compared to $[^1O_2]_{aq}$.

The degree of association between DOM and waterborne pathogens is likely to important for several transportation and treatment processes, yet very little is known about these interactions due to the difficulty associated with separating free and DOM-associated pathogens. Waterborne enteric viruses have been postulated to associate with

small particles in rivers[15] and wastewater.[16] Bixby and O'Brien have reported that fulvic acids, the fraction of DOM soluble at all pH levels, bind to MS2.[17] The mechanisms in which viruses attach to various soils and clays have been well studied, but in these studies DOM is generally viewed as a *competing species* for any sorption sites on the soil instead of a *providing species* of sorption sites.[18] These results must be viewed with a sceptical eye, given that much of the literature on the subject suggest that the interactions are more complex than initially hypothesized and many of the results often contradict one another.

The goal of the study described in the remainder of this chapter was to determine the role of DOM association on the external inactivation of MS2 by $^1O_2$ within sunlit waters. MS2 was chosen as a subject because it is a common model for enteric viruses.[19] This research was completed in collaboration with Dr. Tamar Kohn and Dr. Kara Nelson at University of California – Berkeley, CA, experts in MS2 photoinactivation[12], and consequently, all experiments involving MS2 were executed by them. The same four DOM isolates investigated in the previous chapter (Aldrich humic acid, ALHA; Fluka humic acid, FLHA; Suwannee River humic acid, SRHA; and Pony Lake fulvic acid, PLFA) were investigated in context of the inactivation of MS2. In addition to each aqueous sensitizer's respective association behaviour with MS2, their $[^1O_2]_{DOM}$ and $[^1O_2]_{aq}$ production capacity were characterized using methods similar to the previous chapter. Additional experiments were also performed by Kohn and Nelson to further understand the factors that enhance MS2-DOM association and the results were interpreted with respect to the inactivation of MS2. The results of this study provided much needed quantitative data on virus-DOM interactions, as well as on their inactivation

by external $^1O_2$ photosensitizers. Furthermore, the results of this study provide additional data that will aid in the development of low-cost water and wastewater treatment processes that can contribute to the water purification infrastructure in both developing and developed nations.

Methods and Materials

Chemicals and Organisms

Sample solutions contained deionized water, D_2O (99.9%, Aldrich), or water obtained from a waste stabilization pond (WSP) described previously,[12] NaCl (Fisher), and either phosphate (NaH_2PO_4, Fisher) or bicarbonate ($NaHCO_3$, Fisher) as a buffer. The natural organic matters (NOM) tested were Fluka humic acid (FLHA; Fluka), Aldrich Humic Acid (ALHA; Aldrich), Suwannee river humic acid (SRHA; International Humic Substance Society) and Pony Lake Fulvic Acid (PLFA; International Humic Substance Society). $MgCl_2$ (Fisher) was added to enhance MS2-NOM interactions. The probe compound for measuring $[^1O_2]_{aq}$ concentrations was furfuryl alcohol (FFA; 99%, Aldrich). Iron analysis included ferroZine iron reagent (98%, Acros), hydroxylamine hydrochloric reagent (Acros), ammonium acetate (Fisher Chemicals) and sulfuric acid (Fisher Chemicals). Chemiluminescent measurements included tetrabutylammonium fluoride (TBAF 1.0 M in tetrahydrofuran; Aldrich), acetonitrile (ACS grade, Mallinckrodt), and 2-[1-(3-tert-butyldimethylsiloxy)phenyl)-1-methoxy-methylene]-tricyclo[3.3.1.1]decane (TPMA, synthesized according to literature).[20]

MS2 coliphage (ATCC 15597-B1) was cultured and enumerated as described in literature[21] using the materials listed previously.[12] Selected MS2 samples were analyzed in triplicate and yielded reproducible results (95% confidence intervals of 0.08 log units). Several MS2 inactivation and $^1O_2$ formation experiments were conducted in duplicate with high reproducibility.

Dissolved organic carbon and iron analysis

Dissolved organic carbon (DOC) was determined using a Shimadzu TOC-5000 A analyzer. The total iron concentration of DOM was determined in solutions of 100 or 200 mg DOM/L, using the ferrozine method described in literature.[22]

Chemiluminescence measurements

All chemiluminescence measurements were recorded with a Turner Designs TD-20/20 luminometer. The sensitivity of the instrument was set to 30%. Aqueous photolyses were analyzed by diluting 5 μL aliquots of the reaction solution to 5 mL in acetonitrile. A 300 μL aliquot of the diluted reaction solutions were transferred to a 12 × 50 mm polypropylene tube for chemiluminescent analysis. The dioxetanes formed during photolysis were induced to decompose upon addition of 20 μL of 25 mM TBAF (acetonitrile). The chemiluminescent signal was recorded for 50 seconds and converted to concentration of dioxetane via a calibration curve generated from the authentic standard dioxetane.

Steady state irradiation experiments

Irradiation experiments to measure $[^1O_2]_{aq}$ and MS2 inactivation were conducted in stirred 150-mL reactors using the Oriel 1000-W solar simulator and sampling procedures described in literature.[12] A UVB filter blocking most light below 320 nm was used for all experiments conducted under this setup, to minimize the direct damage of the nucleic acid by UVB light.[12] Measurements of $[^1O_2]_{DOM}$ and the ratio $[^1O_2]_{DOM} : [^1O_2]_{aq}$ were conducted in 13 × 100-mm quartz cuvettes using an Atlas Suntest CPS+ solar simulator.

Samples for the inactivation experiments contained 5 mM phosphate buffer, 10 mM NaCl and 10^7 plaque forming units of MS2 per mL. DOM stock solutions (500 mg/L) were prepared in pH 9 buffer solutions. Aliquots of the DOM stock were added to the sample solutions to obtain the DOM concentration specified. Solution pH values were adjusted using NaOH and HCl. The pH remained constant over the time course of the experiments.

Experiments involving Mg^{2+} were conducted in 2 mM $NaHCO_3$. Magnesium was added from a 1 M $MgCl_2$ stock solution to a final concentration of 2 mM. Control samples without Mg^{2+} contained an additional 6 mM NaCl for ionic strength control. Inactivation experiments were conducted over 24-60 h. Experiments involving SRHA were limited to less than 35 hours to minimize synergistic effects with accumulating H_2O_2.[12] Experiments at low pH, in D_2O, or the presence of Mg^{2+} were also shorter. During the timeframe of these experiments, some inactivation of MS2 in phosphate buffer without sensitizers was observed. This inactivation was not observed in dark

controls and may be due to direct RNA damage by small amounts of UVB light not blocked by the cut-off filter,[12] a slow endogenous inactivation process, or exogenous inactivation resulting from impurities in the phosphate buffer. The average rate constant for this "blank" inactivation, k_{obs}(blank), was 0.046 (± 0.014) h^{-1}.

Measurement of $^1O_2$ concentrations

The solutions were placed in quartz tubes (10 mL) on a turntable under the lamps. The test tubes were situated at 30° from normal. The photolyses were conducted at ambient temperature. Small sample aliquots (100 μL) were removed for analysis at specific time intervals. Furfuryl alcohol samples were analyzed via HPLC with a Supelco RP-Amide C_{16} (150 × 4.6 mm, 5μm particle size) column and a mobile phase of 10:90 acetonitrile:pH 5 acetate buffer. The flow rate was 1.0 mL/min and the detection wavelength was 219 nm. The rate of FFA degradation was analyzed to determine the steady state concentration of $^1O_2$ within the solution ($[^1O_2]_{aq}$). Reaction of TPMA was tracked by monitoring the formation of $TPMAO_2$ by chemiluminescence detection. Each dissolved organic matter isolate was irradiated at different concentrations of total organic matter (0.5 – 100 mg/L). All photolysis solutions (5 mL) consisted of 100 μM FFA, 10 μM TPMA, 5 mM pH 7.5 phosphate buffer, and 10 mM NaCl in addition to the desired concentration of dissolved organic matter. The concentration of singlet oxygen apparent to TPMA, $[^1O_2]_{app}$, for each irradiation experiment with varied concentration of DOM. These data were fit to equation 1 according to the theory developed in the previous chapter.[13]

$$[^1O_2]_{app} = \frac{K_{OM}[DOM]}{1+K_{OM}[DOM]}([^1O_2]_{DOM} - k_{1_{O_2}}[DOM]) + k_{1_{O_2}}[DOM] \quad (1)$$

Light screening factor

The values of $[^1O_2]_{app}$ determined from the irradiation of DOM isolates in the presence of TPMA were corrected for light screening according to the theory developed in the previous chapter.[13] The correction factor (*CF*) is then defined as the ratio of light absorbed at optically thin conditions over the light absorbed at optically thick conditions (eq. 2).

$$CF = \frac{k_{abs,thin}}{k_{abs,thick}} = \frac{\sum_{\lambda} \alpha_\lambda I_{\lambda,0}}{\sum_{\lambda} \alpha_\lambda \langle I_\lambda \rangle_z} = \frac{\sum_{\lambda} \alpha_\lambda I_{\lambda,0}}{\sum_{\lambda} \alpha_\lambda I_{\lambda,0} S_\lambda} \quad (2)$$

Data analysis

Inactivation followed first-order kinetics with respect to MS2 concentration.[12] Inactivation rate constants were determined from the slope of plots of a linear regression of ln(PFU/mL) vs. time exposed to light, and reported as k_{obs} (h^{-1}) ± 95% confidence intervals. The regressions generally included five or more data points, and resulted in $R^2 \geq 0.97$. Both $[^1O_2]_{aq}$ and k_{obs} were corrected for light screening. Furthermore, significant light shielding and shorter reaction times prevented a measurable k_{obs}(blank).

Results and Discussion

MS2 inactivation as a function of DOM concentration

As expected, an increase in $[^1O_2]_{aq}$ was observed by increasing the concentration of DOM, [DOM] (Figure 3.1). This linearity was not apparent until the values were corrected for light screening. As expected based on the results from the first chapter, the observed inactivation rate constant, k_{obs}, did not increase linearly with increased [DOM], but instead saturated in behaviour indicative of a Langmuir-type binding isotherm (Figure 3.2). The saturation behaviour was observed even after the k_{obs} values were corrected for light screening. According to Figure 3.2, FLHA and SRHA exhibited strong binding behaviour that resulted in a levelling of k_{obs} despite increased [DOM]. Based on the work of Kohn and Nelson, $^1O_2$ was assumed to be the only ROS involved in MS2 photo-inactivation, therefore k_{obs} saturation was expected to follow $[^1O_2]$ saturation at increased [DOM]. Irradiation of DOM in the presence of TPMA resulted in increased $[^1O_2]_{app}$ that scaled according to the Langmuir-type binding isotherm represented in equation 1 (Figure 3.3).

The data represented by Figures 3.2 and 3.3 provide strong evidence for the enhanced inactivation of MS2 while the virus is in close proximity to, or in association with, DOM supramolecular assemblies. While in close proximity to DOM, $^1O_2$ produced within the hydrophobic assembly has a significantly shorter distance to travel to react with MS2, therefore a smaller amount of the $^1O_2$ will be quenched through interaction with the solvent. The DOM supramolecular assemblies have an elevated concentration of $^1O_2$ within their hydrophobic interiors ($[^1O_2]_{DOM}$) with respect to the concentration in the

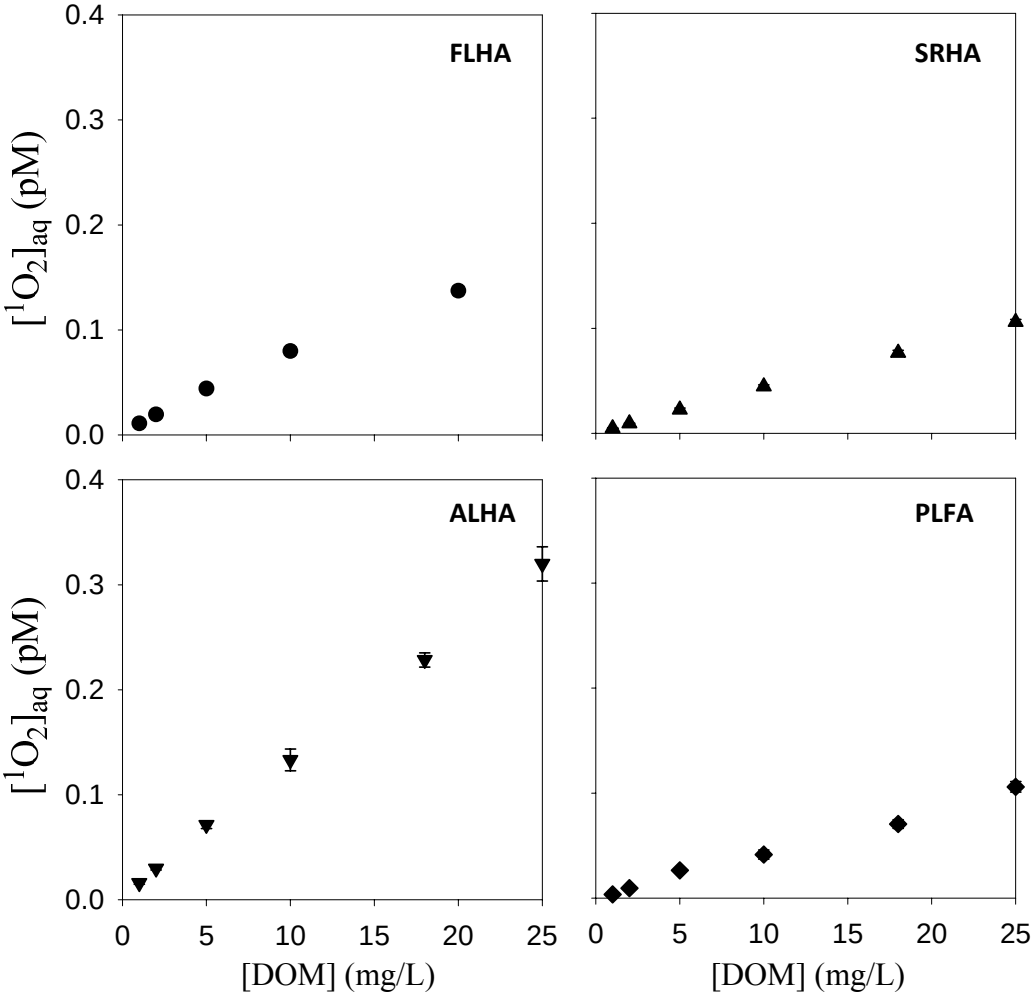

Figure 3.1. [$^1O_2$]$_{aq}$ as a function of DOM concentration. The values of [$^1O_2$]$_{aq}$ were corrected for light screening according to equation 2. Error bars indicate 95 % confidence intervals.

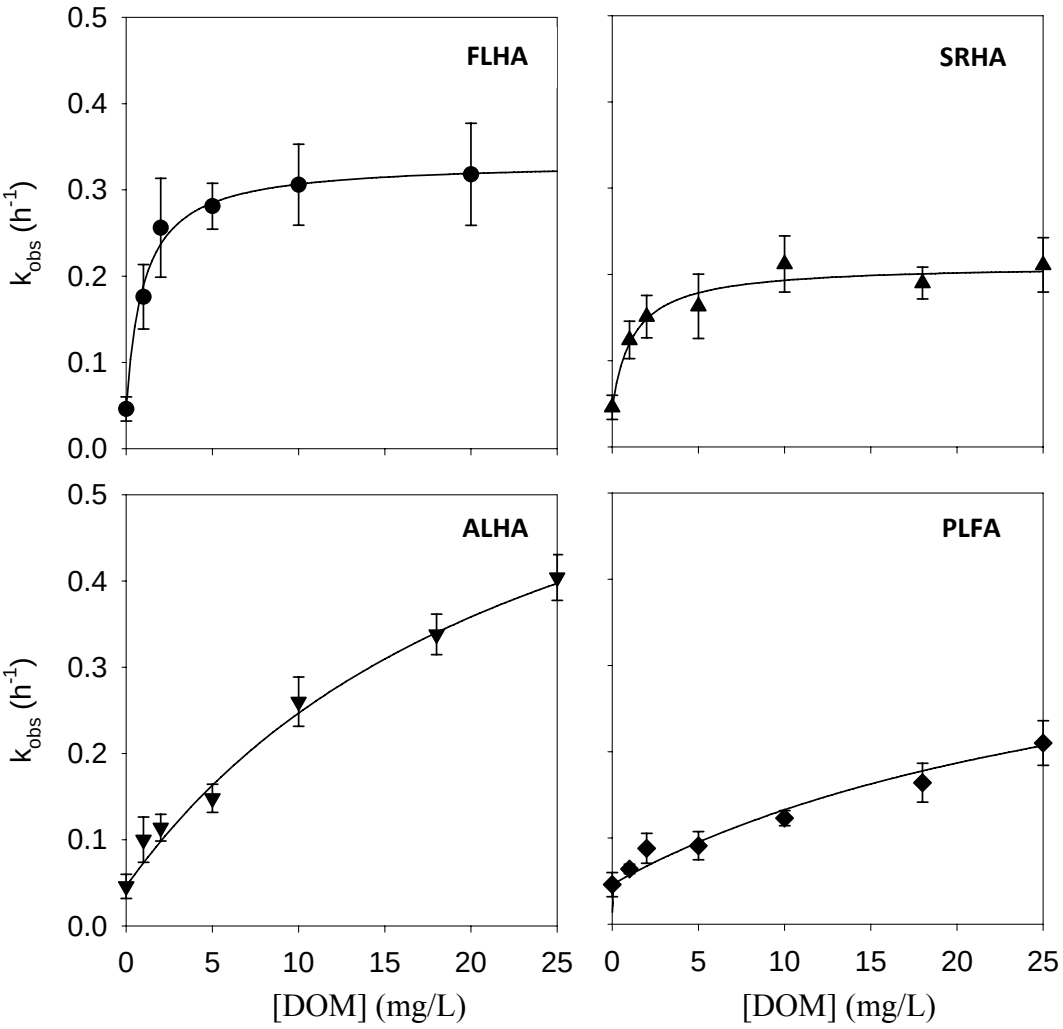

Figure 3.2. Virus inactivation rate constant, k_{obs}, as a function of DOM concentration. The values of k_{obs} are corrected for light screening according to equation 2. Solid lines indicate model fits to equation 5. Error bars indicate 95 % confidence intervals.

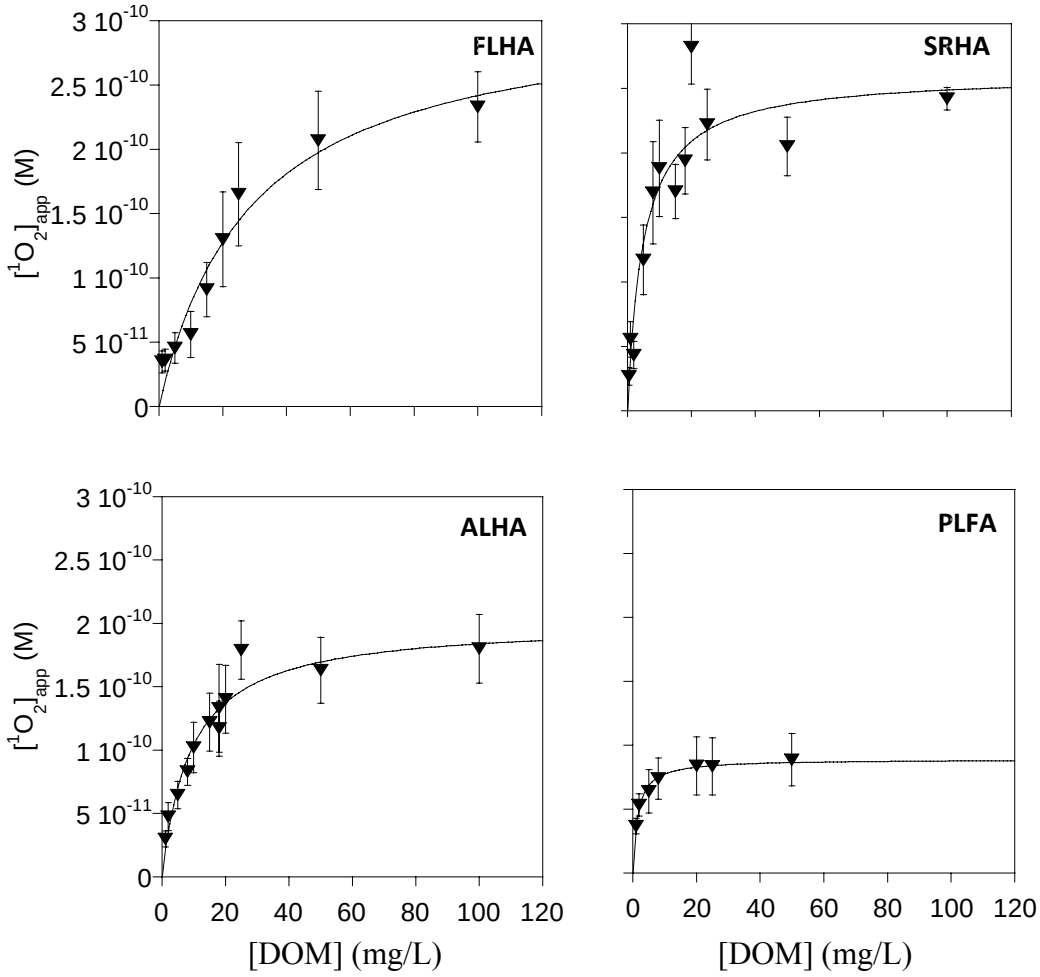

Figure 3.3. TPMA-DOM binding isotherms. Values of $[^1O_2]_{app}$ were corrected for light screening according to equation 2. Solid line indicates fit to equation 1. Error bars indicate 95% confidence intervals.

bulk solution ($[^1O_2]_{aq}$). This phenomenon can be observed by plotting the ratio of $[^1O_2]_{DOM}$: $[^1O_2]_{aq}$ in relation to increased concentration of DOM (Figure 3.4). The concentration of $^1O_2$ within the bulk solution is relatively low at low concentrations of DOM, yet $[^1O_2]_{DOM}$ remains constant highlighting the difference between bulk solution reactivity and reactivity dispersed in microheterogeneous solutions.

Determining $k_{obs,DOM}$ by MS2-DOM binding

In order to accurately quantify the association between MS2 and DOM and its effect on k_{obs}, a model similar to the one proposed in the previous chapter was developed which takes into account the inactivation of MS2 bound to DOM and subjected to the enhanced $[^1O_2]_{DOM}$, the inactivation of MS2 within the bulk solution when subjected to $[^1O_2]_{aq}$, and by inactivation observed in the absence of DOM:

$$k_{obs} = f_{DOM} k_{DOM} + f_{aq} k_{aq} + k_{obs}(blank) \quad (3)$$

Where f_{DOM} and f_{aq} are the fraction of MS2 bound to the DOM supramolecular assembly and unbound within the bulk solution, respectively, k_{DOM} is the theoretical first-order inactivation rate constant of MS2 inactivation obtained at maximum coverage by DOM, k_{aq} is the pseudo-first-order inactivation rate constant of MS2 inactivation in the bulk solution. The variable k_{DOM} corresponds to the second order rate constant for the inactivation of MS2 by $^1O_2$, $k_{MS2\text{-}1O2}$, and the enhanced $[^1O_2]_{DOM}$. MS2 is significantly larger than average DOM supramolecular assemblies, and consequently MS2 is not expected to bind to DOM in the same manner as TPMA, which is significantly smaller

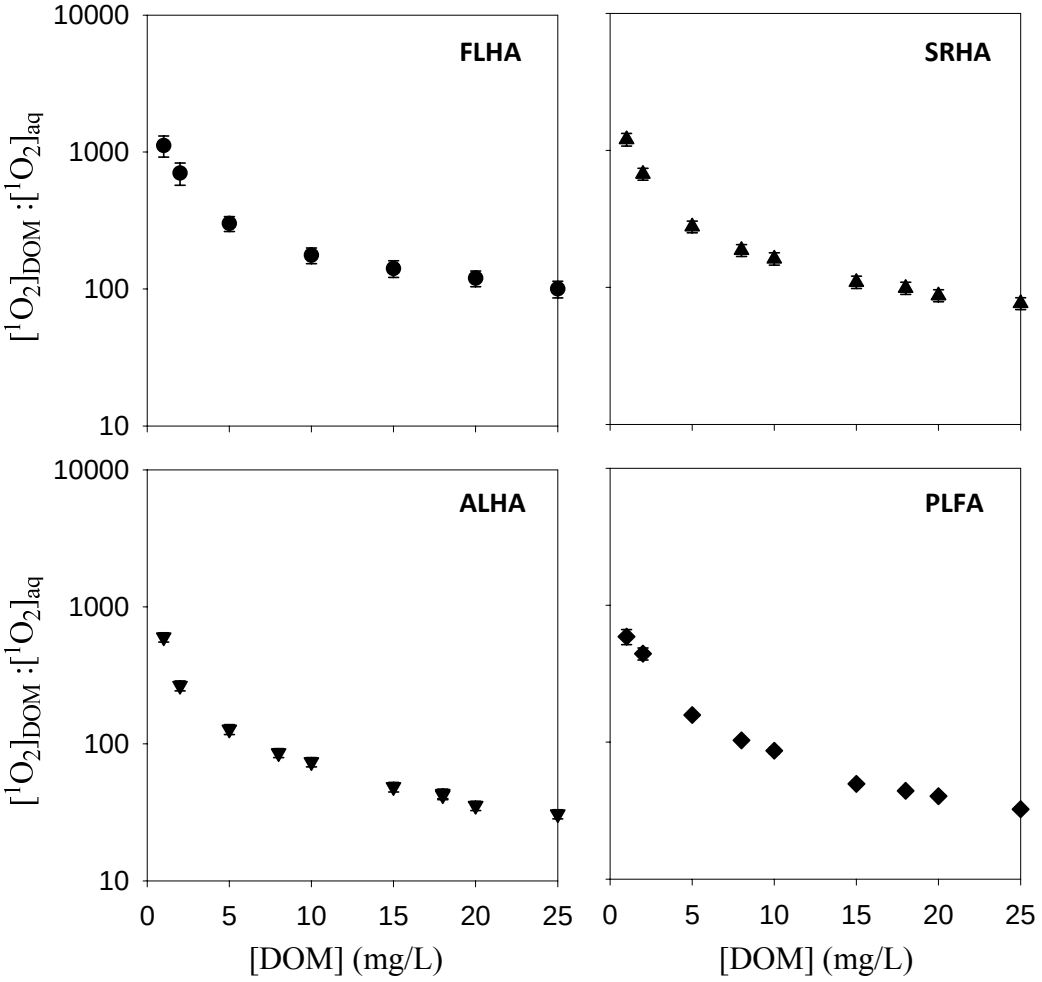

Figure 3.4. Ratio of $[^1O_2]_{internal} : [^1O_2]_{bulk}$ (obtained using the Atlas Suntest CPS+ solar simulator and corrected for light screening) as a function of [DOM]. Error bars indicate 95 % confidence intervals.

than average DOM supramolecular assemblies.[13, 23] Subsequently, k_{DOM} was treated as a lump parameter for each DOM isolate.

The variable k_{aq} corresponds to $k_{MS2\text{-}1O2}$ and $[^1O_2]_{aq}$. Figure 3.1 demonstrates that $[^1O_2]_{aq}$ is a linear function of [DOM] and can be expressed by equation 4:

$$k_{aq} = k_{MS2-1O2} k_{1O2} [DOM] \tag{4}$$

where k_{1O2} is a DOM-normalized $^1O_2$ formation rate constant determined from the linear slope of each plot in Figure 3.1.

Assuming a simple Langmuir-type binding isotherm, f_{DOM} is expressed in terms of MS2-DOM association constant K_{OM} (equation 5).

$$f_{DOM} = \frac{K_{OM}[DOM]}{1 + K_{OM}[DOM]} \tag{5}$$

Given $f_{DOM} + f_{aq} = 1$, equations 3, 4, and 5 can be rewritten as equation 6.

$$k_{obs} = \frac{K_{OM}[DOM]}{1 + K_{OM}[DOM]} (k_{DOM} - k_{MS2-1O2} k_{1O2} [DOM]) + k_{obs}(blank) \tag{6}$$

The value for $k_{MS2\text{-}1O2}$ is an intrinsic parameter and therefore independent of the DOM isolate investigated. It was determined by simultaneously fitting equation 6 to the k_{obs} from all four DOM isolates to yield a value of 10^{12} M^{-1} h^{-1}. This value is slightly lower than the value obtained previously by Kohn and Nelson, which attributed all MS2 inactivation to reaction with $[^1O_2]_{aq}$ and neglected any contribution based on MS2 binding to DOM supramolecular assemblies.[12] Nevertheless, the value determined in the current study is still high when compared to the second-order rate constants of $^1O_2$ reaction with various individual amino acids.[24] The difference between these values is

likely due to the numerous $^1O_2$-labile reaction sites within MS2, therefore making $k_{MS2\text{-}1O2}$ not a true bi-molecular rate constant. Rate constants for the reaction between $^1O_2$ and proteins that contain several $^1O_2$-labile amino acids have been found to be higher than those for the free amino acids.[25]

The values of K_{OM} and k_{DOM} were obtained by fitting the data in Figure 3.2 to equation 6 by using the value of $k_{MS2\text{-}1O2}$ set to 10^{12} M^{-1} h^{-1} (Table 3.1). Additionally, the data from the irradiation of WSP water in the presence of MS2 and TPMA were analyzed in the same manner and the resulting parameters are shown in Table 3.1. The DOM isolates that exhibited the larger K_{OM} are FLHA and SRHA. Those DOM isolates demonstrate a much large binding affinity than that of either ALHA or PLFA. Both FLHA and SRHA reached their maximum adsorption density at low [DOM], whereas the

	K_{OM} (L/mg)	k_{DOM} (h^{-1})	R^2	$[^1O_2]_{DOM}$ (M)
FLHA	1.00 ± 0.33	0.28 ± 0.02	0.99	3.1 (±0.3)×10^{-10}
SRHA	0.81 ± 0.44	0.16 ± 0.02	0.96	2.6 (±0.2)×10^{-10}
ALHA	0.04 ± 0.03	0.39 ± 0.07	0.99	2.0 (±0.1)×10^{-10}
PLFA	0.03 ± 0.03	0.24 ± 0.14	0.96	8.0 (±0.2)×10^{-11}

Table 3.1: Parameters obtained from model fits and $[^1O_2]_{DOM}$. K_{OM} is the adsorption equilibrium constant of DOM and MS2; k_{DOM} is the theoretical inactivation rate constant at maximum coverage. Errors indicate 95 % confidence intervals.

maximum adsorption densities for ALHA and PLFA would have occurred at [DOM] several times higher than the range investigated.

The differences in MS2 adsorption and MS2 inactivation between the individual DOM isolates was expected considering that many properties of DOM vary with regards to their size, structure, and abundance of functional groups.[26] This variability resulted in differences between DOM isolates regarding their interactions with molecules and surfaces. Gauthier *et al*. found that DOM isolates with a high degree of aromaticity demonstrate higher sorption of pyrene[27], whereas Tipping demonstrated that anionic functional groups located on the periphery of DOM supramolecular assemblies enables adsorption onto iron oxide surfaces by ligand-exchange with surface hydroxyl groups.[28]

The individual forces involved in DOM adsorption vary depending on the properties of the surface or molecule. Electrostatic interactions combined with non-coulombic interactions were implicated in the adsorption of DOM onto charged hematite surfaces.[29] In another study, Ochs *et al*. demonstrated that hydrophobic interactions dominated the adsorption of DOM onto hydrophobic mercury surfaces.[30] The different structural properties attributed to each DOM isolate complicated the comparison of their respective adsorption properties. This is especially the case during the investigation of DOM adsorption to a complex surface such as a virus capsid. Therefore, the values of K_{OM} determined in this study reflect the overall contribution of all modes of adsorption (i.e. hydrophobic, hydrophilic, ligand-exchange) for each DOM isolate. The values of K_{OM}, however, do not contain detailed adsorption information, such as the maximal DOM coverage of the virus capsid, the number of points of interaction between

MS2 and DOM, or the distance between MS2 reaction sites and the $^1O_2$-producing entities of DOM.

The difference in adsorption behavior between DOM isolates reported in Table 3.1 may help explain some of the contradictory results on the role of organic matter in the adsorption of viruses onto soils.[18] The fact that the DOM isolates readily adsorb to MS2 has significant implications for the existing literature on the transport of viruses in soil. In addition to competiting for adsorption sites on soil and clay surfaces, DOM may adsorb on the viruses and change their surface properties, and thereby exert a dual influence on virus transport and adsorption.

Kinetic isotope effect on $[^1O_2]_{aq}$ and MS2 inactivation

In order to confirm the importance of DOM association with MS2 during its inactivation, experiments were conducted using 99.9% D_2O, which is a less efficient quencher of $^1O_2$ than H_2O. Rodgers and Snowden demonstrated that experiments conducted in pure D_2O lead to a 13-fold increase in $[^1O_2]_{aq}$, while not affecting the concentration of any other reactive oxygen species.[31] Based on their work, 99.9% D_2O was calculated to yield a 12-fold maximum enhancement in $[^1O_2]_{aq}$. Therefore, if k_{obs} was only a function of $[^1O_2]_{aq}$, a 12-fold increase in k_{obs} would be expected. Latch and McNeill demonstrated that compounds associated with DOM supramolecular assemblies are only mildly sensitive to this kinetic isotope effect (KIE) because they react with $^1O_2$ at its source before any significant quenching by the solvent can occur.[14] The KIE of D_2O on k_{obs} was expected to be low during strong adsorption of DOM to MS2.

	$k_{obs}(D_2O) / k_{obs}(H_2O)$ *(experimental)*	$k_{obs}(D_2O) / k_{obs}(H_2O)$ *(calculated)*[a]	$k_{obs} / k_{obs}(Mg^{2+})$
FLHA	3.0	1.4	2.8
SRHA	5.0	1.4	1.2
ALHA	8.1	6.4	3.8
PLFA	10.3	6.5	4.1

[a] Values were calculated based on eq. 6 and the fitting parameters in Table 3.1, and assuming that $[^1O_2]_{aq}$ increases 13-fold in D_2O.

Table 3.2: Enhancement of k_{obs} (at 5 mg/L DOM) in D_2O and upon addition of 2mM Mg^{2+}. k_{obs} in H_2O and D_2O are corrected for a baseline inactivation (without DOM) of 0.046 h^{-1}. k_{obs} in Mg^{2+} are corrected for a baseline inactivation (without DOM, but with Mg^{2+}) of 0.084 h^{-1}.

As shown in Table 3.2, the enhancement of k_{obs} values for the DOM isolates conducted in D_2O ranged from 3.0– 10.3. None of the DOM isolates exhibited the maximum KIE, indicating that all DOM isolates exhibited some degree of association with MS2. The effect of D_2O on k_{obs} for the DOM isolates was weaker for FLHA and SRHA, and stronger for ALHA and PLFA. This trend corresponds well with K_{OM} obtained from the model fits in Table 3.1 and is further evidence that association between MS2 and DOM supramolecular assemblies occurs.

In addition to the experimental values of enhanced k_{obs} due to D_2O, Table 3.2 also shows calculated values of enhanced k_{obs} based on equation 6 and the fitting parameters in Table 3.1. The calculated values assumed that $[^1O_2]_{aq}$ (and therefore also k_{1O2} and k_{aq}) increased 13-fold in D_2O, but that $[^1O_2]_{DOM}$ (and k_{DOM}) remained constant. All of the

calculated values were lower than the experimentally determined values. The discrepancy between these values may reflect that $[^1O_2]_{DOM}$ is subject to a small KIE in D_2O solutions. Latch and McNeill found the KIE on $[^1O_2]_{DOM}$ to be minimal (0.9 – 1.2) as determined by TPMA, but the effect may be more pronounced for $[^1O_2]_{DOM}$ experienced by MS2.[14] The large size and complex surface of MS2 likely resulted in a looser association of MS2 with DOM compared to TPMA, allowing for more exposure of DOM to the solvent and therefore higher susceptibility of $[^1O_2]_{DOM}$ to a KIE.

Contribution of internal vs. bulk singlet oxygen toward MS2 inactivation

Within the four DOM isolates investigated, $[^1O_2]_{DOM}$ was 30 − 1200 times higher than the corresponding bulk concentration $[^1O_2]_{aq}$ (Figure 3.4). The bulk concentration $[^1O_2]_{aq}$ was lowest at low [DOM], which combined with the concentration independent $[^1O_2]_{DOM}$ gave the highest ratio of $[^1O_2]_{DOM}$:$[^1O_2]_{aq}$ at low [DOM]. This ratio states that MS2 inactivation was still dominated by $^1O_2$ produced from MS2-associated DOM, even when the DOM coverage of the virus was low. As an illustration of this point, in a solution of 5 mg/L ALHA, the ALHA-MS2 association was only 18% of its maximum (equation 5). The contribution of $[^1O_2]_{ALHA}$ to the total k_{obs}, C_{DOM}, as determined by equation 7:

$$C_{DOM} = \frac{k_{DOM} f_{DOM}}{k_{obs}} \times 100\% \qquad (7)$$

was found to be 48%. The contribution from the remaining 82% of MS2 exposed to the bulk of the solution, C_{aq}, as determined by equation 8:

$$C_{aq} = \frac{k_{aq} f_{aq}}{k_{obs}} \times 100\% \quad (8)$$

was found to be only 39% of the total k_{obs}. The remaining 13% resulted from inactivation not attributed to DOM (i.e. k_{obs}(blank)). This example illustrates that even at a low coverage of MS2 by ALHA, $[^1O_2]_{DOM}$ was the dominant factor governing k_{obs}. This behavior was true for all DOM isolates investigated. Regardless of [DOM], the contribution of DOM-associated inactivation to the total k_{obs} was always more significant than inactivation in the bulk phase.

In the case of the more strongly adsorbing DOM isolates, k_{obs} was almost fully governed by $[^1O_2]_{DOM}$. At a [FLHA] of 1 mg/L, 50% of the maximal FLHA-MS2 association was achieved, which accounted for 80% of the overall k_{obs} according to equation 7. The contribution of the bulk solution to k_{obs} never exceeded 3% over the entire FLHA range investigated according to equation 8.

As can be seen in Table 3.1, $[^1O_2]_{DOM}$ does not scale with k_{DOM}. To further understand this discrepancy, it should be reiterated that the measurement of $[^1O_2]_{DOM}$ was obtained with a hydrophobic probe (TPMA) that only approximates the $[^1O_2]_{DOM}$ experienced by the virus. As stated above, other factors besides the degree of MS2-DOM association and $[^1O_2]_{DOM}$ may influence k_{DOM}, such as the distance between MS2 particle and the associated DOM, and the pattern of DOM coverage on the viral capsid. Specifically, the presence of metal cations within the DOM supramolecular assemblies would enhance the ionic interactions between the DOM-bound cation and the negatively charged capsid regions. When tested for iron content, FLHA was found to have the highest Fe_{TOT}/mg DOM at 4.2, whereas PLFA was found to have the lowest at 0.3. The

higher iron content would enable a closer and more comprehensive coverage of FLHA than that of PLFA.[32] The topic of DOM coverage of MS2 is very interesting and warrants further investigation.

Effect of divalent cations on DOM mediated MS2 inactivation

Cations can exert several effects that enable a closer approach between negatively charged viruses with other charged entities. They can neutralize the negative charge by compressing the electric double layer surrounding the charged particle, they can complex the negatively charged functional groups and lead to partial charge neutralization or reversal, or they may act as antichaotropic agents and accommodate hydrophobic interactions.[18, 33]

Divalent cations are more effective at enhancing the interactions between negatively charged entities than monovalent cations. Redman *et al*. showed that divalent cations enhanced the adsorption of bacteriophage SJC3 to quartz more effectively than Na^+.[34] Sobsey *et al.* demonstrated an enhancing effect of Mg^{2+} on polio- and rheovirus adsorption onto sand.[35]

In the presence of 2 mM Mg^{2+}, MS2 samples demonstrated k_{obs} of 0.084 h^{-1} in the absence of DOM. This rate constant was interpreted as a combination of MS2 aggregation upon addition of $Mg^{2+}$and residual k_{obs}(blank) observed in the absence of DOM and Mg^{2+}. In the presence of both 2 mM Mg^{2+} and 5 mg/L DOM, significantly faster MS2 inactivation was observed than in the absence of Mg^{2+}, even after correcting for virus aggregation (Table 3.2). The rate enhancement was most pronounced for ALHA (3.8-fold) and PLFA (4.1-fold), which adsorb weakly onto MS2 in the absence of Mg^{2+}.

The DOM isolates that displayed nearly maximal cover of MS2 at concentration of 5 mg/L DOM in the absence of Mg^{2+}, SRHA (1.2-fold) and FLHA (2.8-fold), exhibited a lower, but still significant effect of Mg^{2+}.

The observed enhancement was interpreted as a result of enhanced association between MS2 and the DOM supramolecular assembly. The presence of Mg^{2+} did not increase $[^1O_2]_{DOM}$ or $[H_2O_2]$, so the effect of Mg^{2+} was not contributed to higher concentrations of reactive oxygen species.[36] The observed Mg^{2+}-mediated enhancement of DOM interaction with MS2 would result from charge shielding and compression of the electric double layer. An increase in ionic strength would exhibit a similar effect; however, Kohn and Nelson found that increased concentrations of NaCl led to slower inactivation of MS2 in solutions of FLHA.[12] Therefore, double layer compression was not the cause of the observed Mg^{2+} effect in the case of FLHA.

Charge neutralization through complexation of negatively charged functional groups was a more likely cause for enhanced MS2-DOM association. If both virus and DOM supramolecular assembly undergo (partial) charge neutralization, electrostatic repulsion would be decreased, and additional areas on the MS2 capsid would become accessible to DOM adsorption. Alternatively, charge neutralization would cause DOM molecules to coil into a denser, smaller structure, which may be accommodated on the MS2 particle more easily.[37]

Due to the structural diversity of the DOM isolates investigated, it is highly unlikely that the response to the presence of Mg^{2+} was due to similar mechanisms for all DOM isolates. While the observed increases in k_{obs} indicated that Mg^{2+} enhanced MS2-

DOM interactions for all DOM isolates investigated, these experiments were not suited to determine the increase in k_{obs} that might occur due to increased association of DOM under different conditions.

Conclusion

Association of viruses with particles or DOM is usually viewed as inhibiting disinfection, because particles interfere with the access of an external disinfectant to the virus. For example, particle-association impeded the inactivation of MS2 by UV.[38] In the system we investigated, however, the disinfectant ($^1O_2$) was produced inside the DOM supramolecular assembly, leading to enhanced inactivation through DOM association. Association with large particles, such as those present in WSP water, is also expected to enhance disinfection.[12] A similar phenomenon has been observed with photocatalytic inactivation of MS2 by hydroxyl radicals formed on TiO_2 particles; a linear correlation between MS2 adsorption on to the catalyst and inactivation rates was found.[39] Accordingly, a promising area of future research focuses on the promotion virus-sensitizer complexes in wastewater and other purification devices.

In summary, the irradiation of aqueous DOM isolates with a solar simulator mimicked the conditions experienced by waterborne pathogens in surface waters. The $^1O_2$-mediated inactivation of MS2 did not scale linearly with increased [DOM], instead k_{obs} saturated at increased [DOM] indicative of Langmuir-type binding isotherm behaviour. The inactivation of MS2 was understood in terms of the enhanced concentration of $^1O_2$ within DOM supramolecular assemblies dominating k_{obs} at all concentrations of DOM. Kinetic isotope effect experiments further supported the theory

of MS2-DOM association dominating the observed enhanced inactivation of the virus. The presence of increased divalent cations (i.e. Mg^{2+}) did provide an enhancement in the observed inactivation of MS2, as interpreted by increased association between MS2 and the DOM supramolecular assembly, yet further research needs to be conducted to fully understand this mechanism.

Chapter 4.

The Effect of Hydrophobic Nanodomain Size on the Spatial Distribution of Photochemically Produced Singlet Oxygen

Overview

Aqueous spherical micelles composed of amphiphilic block copolymers were utilized to encapsulate singlet oxygen ($^1O_2$) photosensitizers. The internal concentration of $^1O_2$ within the hydrophobic micellar core produced during irradiation experiments was found to scale with the square of the micellar core radius as predicted by a reaction-diffusion model of microheterogeneous production of singlet oxygen. Hydrophobic, chemiluminescent molecular probes were utilized to quantify the interior concentration of $^1O_2$ and these results corresponded with experiments that showed enhanced $^1O_2$-mediated photooxidation of the hydrophobic pesticide disulfoton in the presence of photosensitizer encapsulated micelles. Hydrophobic and hydrophilic $^1O_2$ quenchers were utilized to selectively suppress the $^1O_2$ reactivity within the micellar cores and bulk aqueous phase, respectively. The results of this research are relevant to the understanding of microheterogeneous systems in synthetic and natural contexts (e.g. photodynamic light therapy and humic substances).

Introduction

The emergence of nanotechnology over the past decade has solidified its role within technologies important to the future (e.g. energy[1-5], health[6-8], communications[9-13], water purification[14-21], and food production[22]). Nanostructures of various shapes and sizes are readily available using techniques such as nanolithography or by taking advantage of the self-assembling nature of amphiphilic block copolymers.[23-28] Biomimetic nanostructures have provided numerous applications across a variety of fields.[29-31] Taking

a page from nature, nanoarchitecture incorporating hydrogen-bonding[32, 33], metal chelation[34-37], and amphiphilic moieties[37-43] to provide organized microenvironments can be found throughout the literature. Polymer chemistry has provided numerous examples of vesicles[6, 28, 42, 44], lipid membranes[45, 46], self-assembling mono-layers[47], and micellar structures[6, 37, 42, 48-55] within hydrophobic and aqueous media.

As discussed in previous chapters of this thesis, dissolved organic matter (DOM) is the fraction of natural organic matter that forms ill-defined, supramolecular, chromaphoric assemblies with significant micellar character within aqueous environments.[56] DOM plays two vital roles within the natural remediation of hydrophobic organic pollutants. The hydrophobic interior of DOM micelles aides in the transport of hydrophobic compounds through aqueous systems and the inherent chromophores within DOM photochemically produce reactive intermediates that participate in the photodegradation of labile pollutants and organisms.[57-60] Of these photochemically produced reactive intermediates, reactive oxygen species (e.g. $^1O_2$) have been found to play a prominent role in environmental photodegradation processes.[61-64] In a similar fashion, dendritic micelles with $^1O_2$ producing moieties have been utilized as nanoscale photoreactors within protic and aprotic polar solvents, yet limited investigation within aqueous environments have been performed.[38, 39, 65-69]

The previous two chapters of this thesis describe a reaction-diffusion model of $^1O_2$ reactivity within aqueous DOM solutions that accurately described the photodegradation of hydrophobic compounds, yet the ill-defined nature of DOM provides some limitations to the model.[70, 71] The composition of DOM is *source* and *seasonally*

dependent, producing large variation in both $^1O_2$ production and hydrophobic partitioning capacity.[58] DOM forms self-assembling aggregates that vary in size as evident by the wide array of micellar radii and molecular weight values reported throughout the literature.[70] By making well-founded assumptions on the intra-DOM micellar density and the diffusivity of $^1O_2$ within DOM, the size of the supramolecular assemblies and their molecular weights for a suite of natural organic matter isolates were estimated, yet more concrete evidence for the reaction-diffusion model lies within the realm of nanotechnology.

Amphiphilic block copolymers have demonstrated the ability to self-assemble into monodisperse, spherical micelles similar in size to DOM capable of utilizing known $^1O_2$ photosensitizers within their microenvironments, making them ideal candidates as model systems of natural aqueous photoreactors.[28, 42, 53, 72] The variety of polymer block permutations and relative ease in their synthesis has made them the targets of numerous research studies.[6, 25, 27] Polymeric micelles with incorporated photosensitizers have been proposed as targets for photodynamic light therapy.[73] Well-characterized aqueous micelles incorporating $^1O_2$ photosensitizers are the ideal system for investigating the reaction-diffusion model described in the previous two chapters of this thesis by removing the ill-defined compositional and structural properties associated with DOM.

All systems incorporating the production of short-lived, diffusible species (e.g. $^1O_2$) within a microheterogeneous environment, such as photodynamic light therapy and photovoltaic technology, must address the problem of spatial distribution throughout the solution.[74-80] $^1O_2$ has a short lifetime (4 μs in H_2O) and thus a short diffusion length of *ca*.

100 nm (e.g., 99% quenching in 240 nm).[81] When $^1O_2$ is produced within a membrane, a micelle, a dendrimer, or some other macro- or supramolecular nanostructure, its short diffusion length leads to a steep concentration gradient with high internal and low external concentrations. Any external labile species that associate with the hydrophobic interior with enhanced $^1O_2$ concentrations would be expected to display enhanced reactivity as a function of its partitioning and the structural characteristics of the hydrophobic micellar interior.

The goal of the work presented in this thesis chapter was to go beyond the *qualitative* demonstration of a nano-scale photoreactor by working toward a *quantitative* understanding of such systems. Specifically, we sought to test the prediction that in spherical $^1O_2$-producing micelles, the internal $^1O_2$ concentration will increase with the square of the radius. This prediction comes from a reaction-diffusion kinetic model presented in Chapter 2 of this thesis.[70] Two key challenges that need to be addressed are the construction of spherical micelle systems that significantly differ in radius and the determination of the concentration of $^1O_2$ inside and outside these photosensitizer-doped nanostructures. Here we describe the use of structurally well-defined block copolymer micelles[28] that contain both covalently bound and non-covalently bound sensitizers, combined with the use of sensitive and selective molecular probes for $^1O_2$ that partition into the hydrophobic micellar cores.[71, 82, 83] These assemblies constitute a new set of nanoscale photoreactors that demonstrate that doubling the micellar core radius indeed results in a fourfold increase in the internal $^1O_2$ concentration.

Methods and Materials

Materials

The PEE-PEO(2-9) (PEE: poly(ethylethylene), PEO: poly(ethylene oxide)) diblock copolymer was synthesized by two successive anionic polymerizations, as described previously.[72] PEP-PEO(6.7-16.5) (PEP: poly(ethylene-*alt*-propylene)) diblock copolymer was purchased from Polymer Source, Inc. and was used as received. The numbers denote the block molecular weights, in kg/mol. The synthesis of 2-[1-(3-*tert*-butyldimethylsiloxy)phenyl)-1-methoxymethylene]tricyclo[3.3.1.1]decane (TPMA) and the corresponding dioxetane, $TPMAO_2$, resulting from the reaction of TPMA with the thermal decomposition of triphenyl phosphate ozonide have previously been described.[83] 5,10,15,20-Tetraphenyl-21H,23H-porphyrin (TPP, Sigma-Aldrich), 5-(4-carboxyphenyl)-10,15,20-triphenyl-21H,23H-porphyrin (TPP-COOH, TCI Europe), polyDMAP resin (100-200 mesh, Acros), disulfoton (PESTANAL®, Sigma-Aldrich), disulfoton-sulfoxide (PESTANAL®, Sigma-Aldrich), sodium azide (Acros), β-carotene (BioChemika, Fluka), and oxalyl chloride (*Reagent Plus®,* $\geq$ 99.9%, Sigma-Aldrich) were used as received. Acetonitrile (ACS grade, Mallinckrodt), ethyl ether (Aldrich), tetrabutylammonium fluoride (TBAF; 1.0 M in THF), sodium chloride (NaCl; Fischer), potassium phosphate monobasic (J.T.Baker), sodium acetate (Mallinckrodt), acetic acid (glacial, Mallinckrodt), and phosphoric acid (85%, Mallinckrodt) were used as received. Furfuryl alcohol (FFA; Aldrich) was distilled prior to use. Tetrahydrofuran (THF; Aldrich), and methylene chloride (Aldrich) were dried according to literature procedures prior to use.[84]

General methods

Size exclusion chromatography (SEC) was performed on a Hewlett-Packard series 1100 liquid chromatography system equipped with a Hewlett-Packard 1047A refractive index (RI) detector, a Gilson model 166 ultraviolet-visible light detector, and three Jordi poly(divinylbenzene) columns of 10^4, 10^3, and 500 Å pore sizes, calibrated with polystyrene standards (Polymer Laboratories). Proton nuclear magnetic resonance spectroscopy (^{1}H NMR) was performed using a Varian 500 MHz NMR spectrometer. Ultraviolet-visible light spectroscopy (UV-vis) was conducted using an Ocean Optics USB2000 spectrophotometer. Fluorescence spectroscopy was conducted using a Varian Cary Eclipse Fluorescence spectrometer. High performance liquid chromatography (HPLC) analysis was performed on an 1100 Series Agilent liquid chromatograph equipped with a UV-absorbance detector or a multiwavelength diode array detector.

Synthesis of TPP-PEE-PEO

The covalently attached TPP-PEE-PEO diblock copolymer was synthesized via the coupling of TPP-COOH and PEE-PEO(1.4-15) through an acid chloride intermediate. To a solution of TPP-COOH (0.112 g, 0.17mmol) in THF (25 mL) was added oxalyl chloride (300 uL, 3.54mmol) and the resulting dark green solution was refluxed for 18 hours. After the solution was cooled to room temperature, excess oxalyl chloride was removed *in vacuo*. To the crude intermediate was added polyDMAP resin (0.647g) and PEE-PEO(2-9) (0.164g, 0.01mmol) dissolved in THF (25 mL). The solution was heated to reflux and allowed to react for 72 hours, upon which the reaction mixture was cooled

to room temperature and the polyDMAP was removed via filtration. To the filtrate was added an equal volume of water and the resulting mixture was extracted with methylene chloride (3×). The combined organic fractions were dried over anhydrous sodium sulfate, filtered to remove the drying agent, and then excess solvent was removed via rotary evaporator. The crude, dark purple solid was recrystallized from cold acetone (3×) to yield the desired product as a light purple solid (0.062 g). Absence of free dye was confirmed by SEC using refractive index and UV-vis detection based on the absorption properties of the dye (λ = 410 nm). The PDI of the resulting polymeric product was calculated to be 1.15. The ratio of dye-modified polymer to unmodified polymer was determined by ^{1}H NMR and calculated to be 0.014:1.0. UV-Vis analysis of the product resulted in the characteristic Soret-band at 419 nm and Q-bands at 515 nm, 550 nm, 589 nm, and 645 nm.

Formation of polymer micelle solutions

The block copolymer micelle solutions were generated via a thin layer deposition method. Stock solutions of the respective block copolymers were formed by first dissolving the respective polymeric solid in methylene chloride (5 mL) in a vial. The solvent was removed via rotary evaporation to form a thin layer of polymer on the walls of the vial. Any remaining solvent was removed *in vacuo* over 24 hours. The remaining solid was dissolved in enough water (MilliQ) to form 1 wt % solutions and then allowed to stir in sealed vials at room temperature for over one week. The micelle solution containing the covalently attached sensitizer was used without further modification. The hydrophobically encapsulated TPP micelle solutions were prepared by diluting the

respective micelle solution to 0.5 wt % and then adding a small amount of TPP. The resulting mixture was sealed in vials and allowed to stir at room temperature and in the dark for over one week. After this time, the solution was filtered through 0.45μm filters (Nalgene) to yield clear, light yellow solutions. The presence of TPP was confirmed via fluorescence spectroscopy and the amount of TPP was determined via UV-vis spectroscopy. The importance of the hydrophobic micelles in the solubilization of TPP was confirmed by a lack of UV-vis absorption typical of TPP within a solution prepared with no amphiphilic block copolymer (not shown).

Cryogenic transmission electron microscopy (Cryo-TEM)

Cryo-TEM samples were prepared in a controlled environment vitrification system (CEVS) at room temperature. A micropipette was used to load a drop of micelle solution onto a lacey Formvar-Carbon supported TEM grid, which was held by tweezers. The excess solution was blotted with a piece of filter paper, resulting in the formation of thin films with thicknesses of ca. 100-300 nm in the mesh holes. After at least 20 s was allowed for relaxation of any stresses induced during the blotting, the samples were quickly plunged into a reservoir of liquid ethane at its melting temperature (-183 ^{o}C) cooled by liquid nitrogen. The vitrified samples were then stored in liquid nitrogen until they were transferred to a cryogenic sample holder (Gatan 626) and examined with a JEOL 1210 TEM (120 keV) at approximately – 178 ^{o}C. The phase contrast was enhanced by underfocus. The images were recorded on a Gatan 724 multiscan CCD and processed with Digital Micrograph, version 3.6.5. The ramp-shaped optical density gradients in the background were digitally corrected.

Dynamic light scattering (DLS)

The micelle solutions were placed into 0.25 in. diameter glass tubes. The samples were investigated using a home-built photometer equipped with an electrically heated silicon oil index-matching bath, a Lexel 75 Ar^+ laser operating at 488 nm, a Brookhaven BI-DS photomultiplier, and a Brookhaven BI-9000 correlator. Intensity autocorrelation functions, $g_2(t)$, were recorded at room temperature, and the measurements were typically made at 6 scattering angles from 45^o to 90^o. When the measured and the calculated baselines were in a good agreement (difference < 0.1%), the correlation function was accepted. For the decay rate distribution, an inverse Laplace transform of the field correlation functions was performed using REPES. The corresponding micelle size distributions were then obtained using the Stokes-Einstein equation (eq. 1)

$$R_h = \frac{k_b T}{6\pi\eta D_0} \qquad (1)$$

where k_b, T, η, and D_0 are the Boltzmann constant, absolute temperature, solvent viscosity, and diffusion coefficient, respectively.

Steady state irradiation experiments

Steady state photolysis experiments were conducted with four medium pressure 175 W Hg vapor lamps (borosilicate-jacketed LumaPro lamps, GE HR175A39/CP bulbs) as the light source. The solutions were placed in quartz tubes (5 mL) on a turntable under the lamps. The test tubes were situated at 30° from normal. The photolysis experiments were conducted at ambient temperature. Small sample aliquots (150 μL) were removed

for analysis at specific time intervals. Furfuryl alcohol samples were analyzed via HPLC with a Supelco RP-Amide C_{16} (150 × 4.6 mm, 5μm particle size) column and a mobile phase of 10:90 acetonitrile:pH 5 acetate buffer. The flow rate was 1.0 mL/min and the detection wavelength was 219 nm. The rate of FFA degradation was analyzed to determine the steady state concentration of $^1O_2$ within the solution ($[^1O_2]_{aq}$). Reaction of TPMA was tracked by monitoring the formation of $TPMAO_2$ by chemiluminescence detection. Disulfoton samples were analyzed via HPLC with a Supelco RP-Amide C_{16} (150 × 4.6 mm, 5μm particle size) column and a mobile phase of 60:40 acetonitrile:pH 3 phosphate buffer. The flow rate was 1.0 mL/min. and the detection wavelength was 200 nm. The rate of disulfoton-sulfoxide growth was analyzed by comparison to a calibration curve generated with its authentic standard. TPMA photolysis solutions (5 mL) consisted of 100 μM FFA, 10 μM TPMA, 5 mM pH 7.5 phosphate buffer, and 10 mM NaCl in addition to the desired concentration of micelles. Disulfoton photolysis solutions (5 mL) consisted of 100 μM FFA, 80 μM Disulfoton, 5 mM pH 7.5 phosphate buffer, and 10 mM NaCl in addition to the desired concentration of micelles.

Chemiluminescence measurements

All chemiluminescence measurements were recorded with a Turner Designs TD-20/20 luminometer. The sensitivity of the instrument was set to 30%. Aqueous samples were analyzed by diluting 5 μL aliquots of the reaction solution to 5 mL in acetonitrile. A 300 μL aliquot of the diluted reaction solution was transferred to a 12 × 50 mm polypropylene tube for chemiluminescent analysis. The dioxetanes formed during

photolysis were induced to decompose upon addition of 20 μL of 25 mM TBAF (acetonitrile). The chemiluminescent signal was recorded for 50 seconds and converted to concentration of dioxetane via a calibration curve generated from the authentic standard dioxetane.

Quenching experiments

Steady-state irradiation experiments in the presence of the hydrophobic quencher, β-carotene, or the hydrophilic quencher, sodium azide, were employed to investigate the quenching effect on the indirect photodegradation of disulfoton. The photolysis solutions (5 mL) consisted of 2.66×10^{-3} mL Org./L of TPP-PEE-PEO(2-9), 100 μM FFA, 80 μM disulfoton, 5 mM pH 7.5 phosphate buffer, and 10 mM NaCl in addition to a range of β-carotene ([β-carotene] = 0 – 120 nM) or sodium azide ([azide] = 0 – 1.7 mM). The quenching effect was visible by plotting the data according to the Stern-Volmer equation (eq. 2)

$$\frac{R_0}{R_q} = 1 + \frac{k_q}{k_{solv}}[Q] \qquad (2)$$

where R_0/R_q is the ratio of unquenched to quenched rates of disulfoton-sulfoxide formation, k_{solv} is the deactivation rate constant of $^1O_2$ due to the solvent interaction ($k_{water} = 2.5 \times 10^5$ M^{-1} s^{-1}), k_q is the deactivation rate constant of $^1O_2$ due to interaction with the quencher ($k_{\beta\text{-carotene}} = 2.5 \times 10^{10}$ M^{-1} s^{-1} and $k_{azide} = 7 \times 10^8$ M^{-1} s^{-1}), and [Q] is the concentration of the quencher.[85]

Theory

The detection of microheterogeneous environments of enhanced $^1O_2$ reactivity is based on a reaction diffusion model described previously in this thesis (Scheme 4.1).[70, 71] The steady-state production of $^1O_2$ within the distinct hydrophobic micellar core, $[^1O_2]_{MIC}$, is given by equation 3

$$[^1O_2]_{MIC} = \frac{k_f + k_{+diff}[^1O_2]_{aq} K^{^1O_2}_{MIC} \frac{V_{aq}}{V_{total}}}{k_{MIC} + k_q[Q]_{MIC} + k_{-diff}} \quad (3)$$

where k_f is the formation rate constant of $^1O_2$ expressed in Scheme 4.1 as the product of the light absorption rate constant of TPP, k_{abs}, and the quantum yield of $^1O_2$ production, Φ_{1O2}, k_{+diff} and k_{-diff} are the diffusion of $^1O_2$ into and out of the hydrophobic micellar core, respectively, $K^{1O2}{}_{MIC}$ is the partition coefficient of $^1O_2$ between the hydrophobic micellar core and the bulk aqueous phase, k_{MIC} is the deactivation rate constant of $^1O_2$ due to interaction with the hydrophobic micelle environment, and k_q is the deactivation rate constant of $^1O_2$ due to interaction with any quenchers, [Q]. The production of $^1O_2$ is localized within the hydrophobic micellar core, and consequently any $^1O_2$ present in the bulk aqueous phase, $[^1O_2]_{aq}$, is solely a product of $^1O_2$ diffusion from the hydrophobic micellar core. As depicted in Scheme 4.1, $[^1O_2]_{aq}$ can undergo relaxation back to ground state O_2 by interaction with the solvent at a given rate constant, k_{solv}. The difference between k_{MIC} and k_{solv}, in addition to the localized production of $^1O_2$ within the hydrophobic micellar core, results in two environments with different concentrations of $^1O_2$.

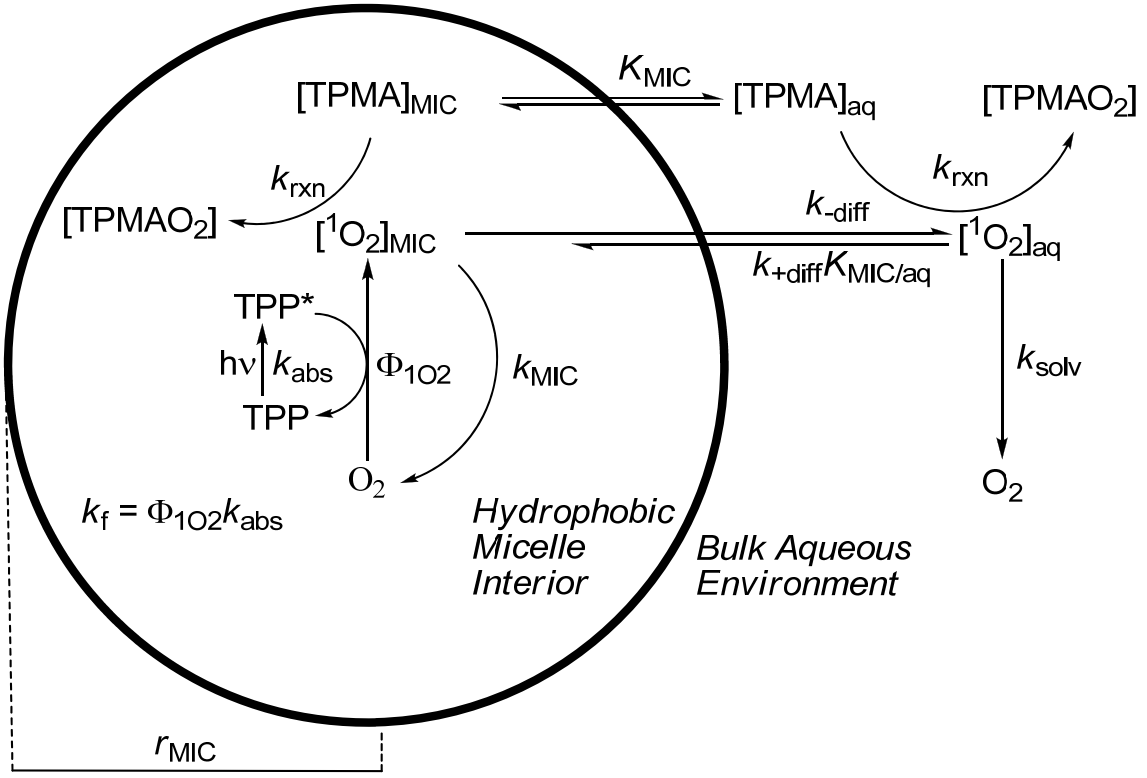

Scheme 4.1. Reaction-diffusion model of $^1O_2$ within block copolymer micelles.

To a first approximation, equation 3 can be simplified by assuming that k_f and k_{-diff} are the only significant terms in the numerator and denominator, respectively. The relatively low value of $[^1O_2]_{aq}$ in comparison to k_f makes any contribution of back-diffusion into the hydrophobic micellar core negligible. The same argument can be made for the omission of $k_q[Q]$ and k_{MIC} from the denominator. These assumptions allow us to rewrite equation 3 as the simplified equation 4.

$$[^1O_2]_{MIC} \approx \frac{k_f}{k_{-diff}} \qquad (4)$$

The diffusion of $^1O_2$ from a spherical micelle is assumed to follow a simple Fickian diffusion model[86] and allows us to express $[^1O_2]_{MIC}$ as a function of hydrophobic micellar core radius, $r_{MIC,}$ (eq. 5)

$$[^1O_2]_{MIC} \approx \frac{k_f r_{MIC}^{\ 2}}{3D} \qquad (5)$$

where D is the diffusivity of $^1O_2$ within the hydrophobic micellar core. From equation 5 we are able to predict that $[^1O_2]_{MIC}$ scales with the square of r_{MIC}. Therefore, micelle systems with similar k_f and D are expected to display a square relationship between experimentally determined values of $[^1O_2]_{MIC}$ and r_{MIC}. The r_{MIC} of aqueous micelles can be determined via cryo-TEM, yet $[^1O_2]_{MIC}$ can only be determined by using probe molecules that bind to the hydrophobic micellar core.

Hydrophobic substrates (i.e. TPMA) associate with the hydrophobic micellar core based on a simple Langmuir-type binding isotherm with an association constant, K_{MIC} (Scheme 4.1). Within the hydrophobic micellar core, TPMA associated within the micelle, $[TPMA]_{MIC}$, react with the enhanced $[^1O_2]_{MIC}$ to form the respective product, $TPMAO_2$. Similarly, TPMA within the bulk aqueous environment, $[TPMA]_{aq}$, react with $[^1O_2]_{aq}$ to form $TPMAO_2$. The reaction rate constant of TPMA forming $TPMAO_2$, k_{rxn}, is independent of the solvent and therefore identical for both the hydrophobic micellar core and the bulk aqueous solvent.[71, 83] It is impossible to differentiate between $TPMAO_2$ generated in the hydrophobic micellar core from that generated within the bulk aqueous environment, but by assuming a Langmuir-type binding isotherm of TPMA it is possible to estimate $[^1O_2]_{MIC}$ and K_{MIC} via equation 6

$$[^1O_2]_{app} = \frac{K_{MIC}[MIC]}{1+K_{MIC}[MIC]}([^1O_2]_{MIC} - k_{1_{O_2}}[MIC]) + k_{1_{O_2}}[MIC] \qquad (6)$$

where k_{1O2} is organic volume-normalized $^1O_2$ formation rate constant determined from measurements of $[^1O_2]_{aq}$ at various micelle concentrations.

Results and Discussion

Characterization of sensitizer encapsulated micelles

The morphology and size of the PEE-PEO (2-9) aqueous micelles have previously been reported.[28] The hydrophobic encapsulation of TPP did not result in significant changes in aqueous micelle morphology or size (Table 4.1). The TPP-PEE-PEO (2-9) micelle systems were found to have hydrodynamic (r_h) and hydrophobic core (r_{MIC}) radii of 24 nm and 6.3 nm, respectively. As expected, the larger block copolymer, PEP-PEO (6.7-16.5), formed spherical micelles larger than the PEE-PEO (2-9) micelles as observed in cryo-TEM experiments (Figure 4.1).[42] The TPP-PEP-PEO (6.7-16.5) micelles were found to have r_h and r_{MIC} of 59 nm and 12.6 nm, respectively. By utilizing 0.861 g/cm^3 and 0.866 g/cm^3 as the respective densities of the PEP and PEE hydrophobic cores[87], the concentration of micelles within the 0.5 wt % solutions were calculated to be 3.4×10^{-7} M and 1.6×10^{-6} M. The difference in micelle concentration was attributed to the relative molecular weight of the respective hydrophobic block and the calculated aggregation number of each micelle system based on the above stated densities and the experimentally determined micellar core radii (Table 4.1).

Micelle System	r_h[a]	r_{MIC}[b]	$[TPP]_{MIC}$[d]	$[TPP]_{Tot}$[d]	Log K_{MIC}	$[^1O_2]_{MIC}$[e]
TPP-PEE-PEO(2-9)	24[c]	6.3[c]	7.47×10^{-5}	9.93×10^{-8}	3.2 ± 0.1	6.7 ± 0.7
TPP-PEP-PEO(6.7-16.5)	59	12.6 ± 0.3	7.47×10^{-5}	1.25×10^{-7}	3.1 ± 0.04	24.6 ± 0.9
Cov-TPP-PEE-PEO(2-9)	24	6.3 ± 0.1	1.63×10^{-3}	1.56×10^{-6}	1.1 ± 0.1	10.5 ± 0.4

Table 4.1. Micelle system characteristics and TPMA binding isotherm fitting parameters. [a]Hydrodynamic radii were calculated from DLS data using the Stokes-Einstein equation and are reported in nm. [b]Micelle hydrophobic core radii were tabulated from cryo-TEM data along with their 95% confidence intervals. The values are reported in nm. [c]Hydrodynamic radii and hydrophobic core radii for PEE-PEO (2-9) micelles were taken from literature.[28] [d]Concentration of TPP within the micelle phase and within the total solution are expressed in M. [e]Concentration of $^1O_2$ within the micelle phase are expressed in 10^{-11} M.

The concentration of sensitizer hydrophobically encapsulated within each micelle solution was determined by UV-vis spectroscopy. The absorbance properties of TPP are solvent dependent. The absorbance maximum (λ_{max} = 419 nm) and Soret absorption bands (λ = 515, 550, 589, and 645 nm) observed in both TPP-PEE-PEO (2-9) and TPP-PEP-PEO (6.7-16.5) have been observed in other TPP-micelle systems.[88] Characteristic fluorescence properties of TPP (λ_{ex} = 419 nm, λ_{em} = 650 and 717 nm) within aprotic environments were observed in both micelle systems, providing further evidence for the location of TPP within the hydrophobic micelle cores.[89] Comparison of absorptivities at 419 nm for each micelle solution to standardized solutions of TPP within squalane, an aprotic hydrocarbon similar in structure and salvation properties to PEE and PEP, was utilized to calculate the concentration of TPP within the bulk solutions (Table 4.1).

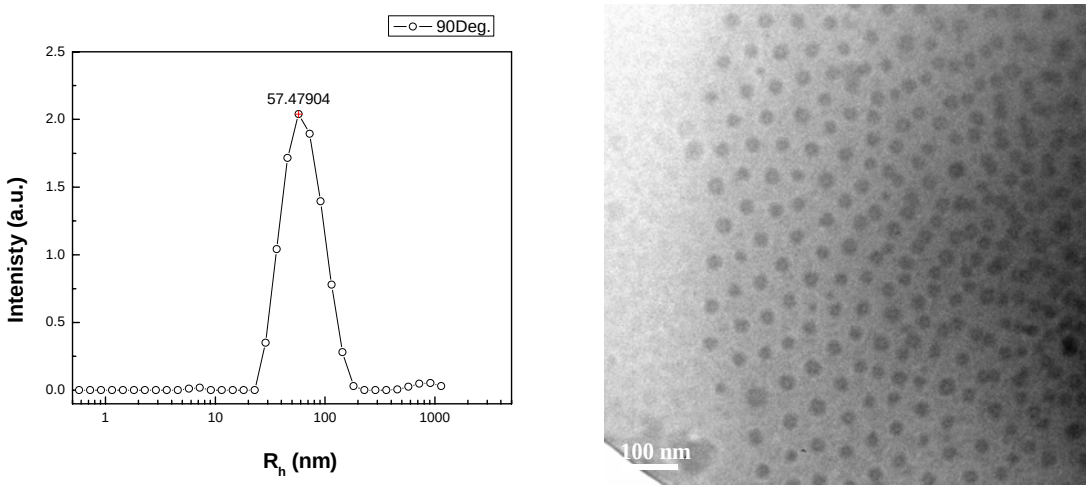

Figure 4.1. Inverse Laplace transform from DLS analysis at 90^{o} and cryo-TEM image of hydrophobically encapsulated TPP-PEP-PEO (6.7-16.5) micelle solution. DLS results display uniform micelles with hydrodynamic radii of 59 nm according to the Stokes-Einstein equation (eq. 1). Cryo-TEM image displays micelles with interior hydrophobic core radii calculated to be 12.6 ± 0.3 nm.

In order to investigate the effect of micelle radius on the microheterogeneous $^1O_2$ production, it was necessary to normalize the solutions in terms of sensitizer per hydrophobic organic volume. By using both the total concentration of TPP within the micelle solutions, $[TPP]_{Tot}$, as determined by UV-vis, and the concentration of micelles (calculated above), the concentration of TPP within the hydrophobic organic volume, $[TPP]_{MIC}$, was determined to be 7.47×10^{-8} M for TPP-PEP-PEO (6.7-16.5) and 1.66×10^{-7} M for TPP-PEE-PEO (2-9). The more concentrated TPP-PEE-PEO (2-9) system was diluted with 1 wt. % PEE-PEO containing no TPP until both micelle systems possessed $[TPP]_{MIC}$ of 7.47×10^{-8} M. Despite the apparent dilution of microenvironments of enhanced $^1O_2$ reactivity, this normalization procedure was consistent with the Poisson distribution model of TPP.[70, 71, 90] Maintaining a consistent ratio of TPP to hydrophobic

organic volume between the two solutions was envisioned to have the same effect as dividing an identical amount of organic volume into uniform spheres with radii of 6.3 nm or 12.6 nm, respectively. The majority of the spherical micelles contain no TPP, and hence no $^1O_2$. The concentration of micelles used in this study dictated an intermicellar distance that exceeds the diffusion length of $^1O_2$ produced in a micelle containing TPP towards reaching a micelle that contains no TPP. The molecular probes employed in this study reported $[^1O_2]_{MIC}$ and R_{MIC} for the average micelle according to the above proposed model.

TPMA binding isotherms and micelle radius effect

Binding isotherms based on the association of TPMA to the hydrophobic core of the block copolymer micelles were generated by analyzing the concentration of $^1O_2$ apparent to TPMA, $[^1O_2]_{app}$, at increasing amounts of TPP-micelles (Figure 4.2). Increased amounts of TPP-micelles did not have a linear effect on $[^1O_2]_{app}$, but instead displayed behavior attributed to Langmuir-type binding of TPMA between microenvironments with different concentrations of $^1O_2$.[70, 71] By fitting the resulting data to equation 6, $[^1O_2]_{MIC}$ and log K_{MIC} for the two hydrophobically encapsulated TPP-micelle systems were estimated (Table 4.1). As can be seen in Table 4.1, the expected squared relationship between micellar core radius and $[^1O_2]_{MIC}$ was observed and provides additional support towards our theory of microheterogeneous production of $^1O_2$ within aqueous micelles.

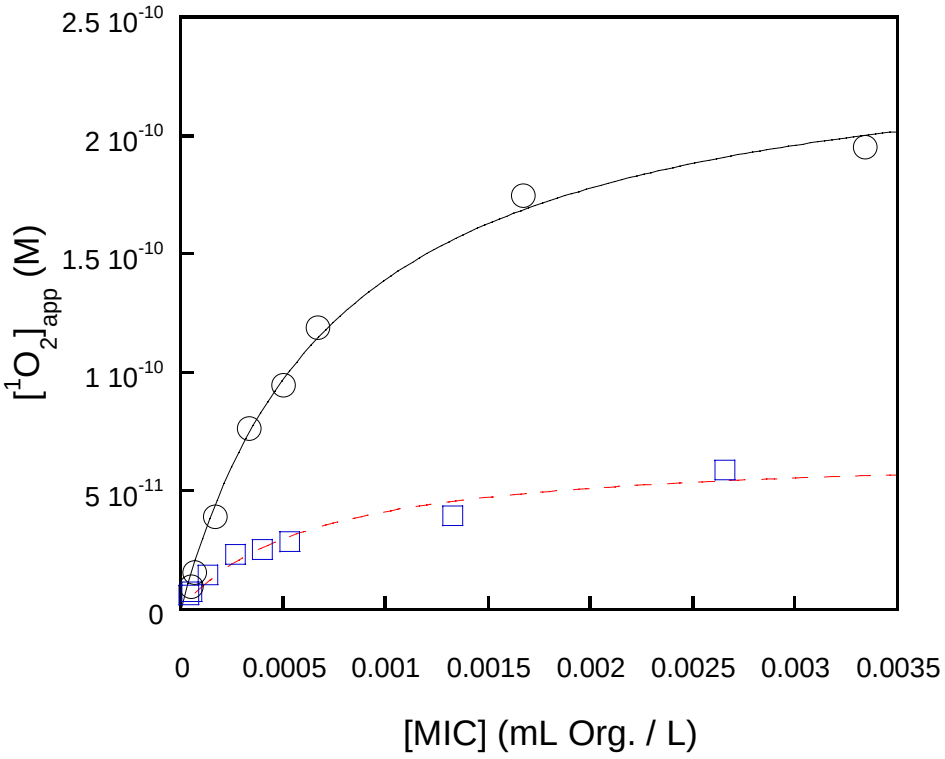

Figure 4.2. Fitting of $[^1O_2]_{app}$ determined by TPMA photolysis with TPP-PEP-PEO (6.7-16.5) (O) and TPP-PEE-PEO (2-9) (□) to Langmuir binding isotherm. Binding parameters are tabulated in Table 4.1.

Disulfoton binding isotherms

The reaction of singlet oxygen with the pesticide disulfoton to form disulfoton-sulfoxide is depicted in Scheme 4.2.

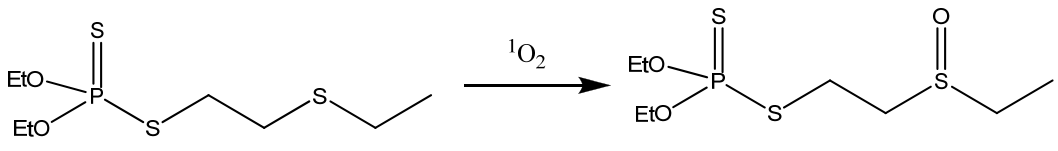

Scheme 4.2. Reaction of disulfoton with singlet oxygen to form disulfoton-sulfoxide.

Binding isotherms based on the association of disulfoton to the hydrophobic core of the block copolymer micelles were generated in the same manner described for TPMA (Figure 4.3). The resulting data was fit to the Langmuir-type binding equation similar to equation 6, but more specific to the observed growth of disulfoton-sulfoxide (eq. 7)

$$R_{sulfoxide} = \frac{K_{MIC}[MIC]}{1 + K_{MIC}[MIC]}(R_{MIC} - R_{aq}) + R_{aq} \quad (7)$$

where $R_{\text{sulfoxide}}$ is the observed rate of disulfoton-sulfoxide growth, and R_{MIC} is the enhanced rate of disulfoton-sulfoxide growth due to binding of disulfoton to the hydrophobic micellar core, and R_{aq} is the rate of disulfoton-sulfoxide growth within the aqueous environment. The rate of disulfoton-sulfoxide growth is a function of $[^1O_2]$ according to steady-state assumptions (equation 8)

$$R_{sulfoxide} = k'_{obs}[^1O_2] \quad (8)$$

where k'_{obs} is the pseudo-first order reaction rate constant of disulfoton-sulfoxide formation ($k'_{\text{obs}} = k_{\text{obs}}$[disulfoton]). Combining equations 6 and 8 resulted in equation7, allowing for the analysis of $R_{\text{sulfoxide}}$ in terms of Langmuir-type binding of the parent disulfoton with the microenvironment of enhanced $^1O_2$ reactivity within the hydrophobic micellar cores.

The binding parameters of R_{MIC} and log K_{MIC} determined from the fit are displayed alongside the respective $[^1O_2]_{\text{MIC}}$ determined by the TPMA probe experiments (Table 4.2). In contrast to the TPMA binding isotherms, K_{MIC} between the two different micelle systems are not consistent. The discrepancy in K_{MIC} between the PEE-PEO(2-9)

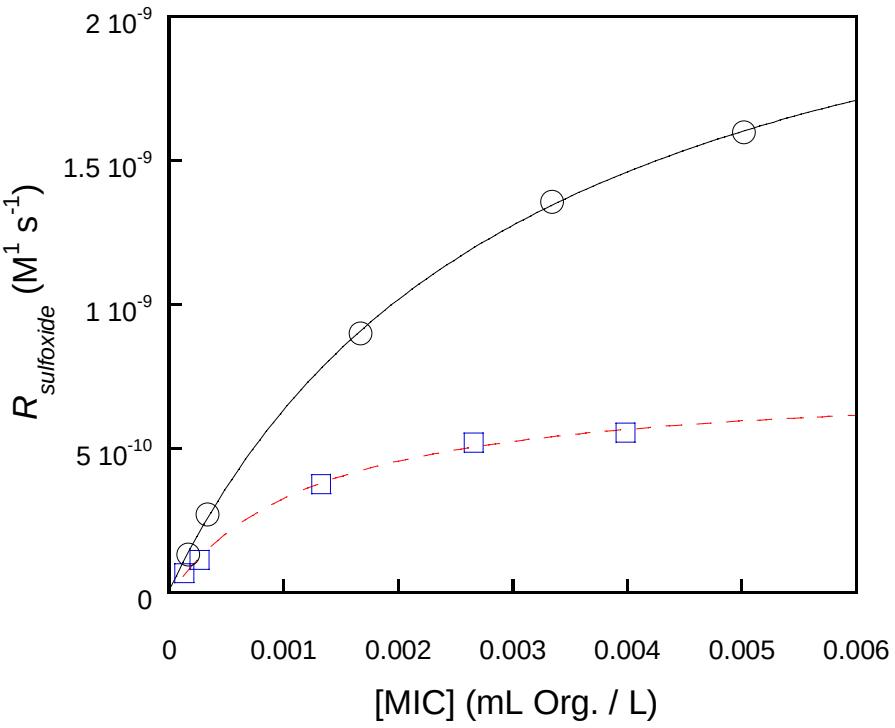

Figure 4.3. Fitting of observed disulfoton-sulfoxide growth rates during photolysis of TPP-PEP-PEO (6.7-16.5) (O) and TPP-PEE-PEO (2-9) (□) to Langmuir binding isotherm. Binding parameters are tabulated in Table 4.2.

and PEP-PEO(6.7-16.5) micelles was interpreted as a difference in mechanisms of binding. The two block copolymers investigated in this study were chosen based on their ability to form well-behaved spherical micelles in aqueous solutions. The synthetically prepared PEE-PEO(2-9) block copolymer possesses a primary hydroxyl group at the interface between the two blocks, and subsequently a hydroxyl functional group at the micelle-corona interface. The commercially obtained PEP-PEO(6.7-16.5) block copolymer does not have a hydroxyl functionality at the micelle-corona interface. The difference in the K_{MIC} values between disulfoton-micelle systems was interpreted as additional binding interactions (i.e. hydrogen bonding at the PEE-PEO micelle interface)

Micelle System	$[^1O_2]_{MIC}$ (10^{-11} M)[a]	Log K_{MIC}	R_{MIC} (10^{-10} M^1 s^{-1})
TPP-PEE-PEO(2-9)	6.7	2.9 ± 0.1	7.5 ± 0.5
TPP-PEP-PEO(6.7-16.5)	24.6	2.5 ± 0.04	26.0 ± 0.1

Table 4.2. Disulfoton binding isotherm fitting parameters. [a]$[^1O_2]_{MIC}$ determined by TPMA photolysis studies tabulated in Table 4.1.

playing a role in the dynamics at the neutral micelle interface.[91] The effect of the physicochemical structure at the micelle interface on the binding of substrates is an interesting result when the reactivity of the substrate is dominated by processes within that micelle. This phenomenon warrants additional investigation.

The decreased K_{MIC} for disulfoton-micelle binding has significant influence on the estimation of R_{MIC}.[70] The error associated with R_{MIC} estimation decreases with increased micelle concentrations due to the presence of acquired data points closer to the actual R_{MIC}. Solubility and intermicellar distance restrict the upper range of micelle concentration in the current study and have been previously encountered in our research.[70] The relatively low error associated with the R_{MIC} reported in Table 4.2 is attributed to the ideal fitting of data to the proposed binding curve throughout the micelle concentration range used in this study. Despite the low K_{MIC} of disulfoton-micelle systems, the estimated R_{MIC} exhibits the same square relationship between micellar core radius and $^1O_2$ reactivity predicted by the reaction diffusion model described above.

The microheterogeneous production of $^1O_2$ within aqueous micelles was additionally investigated by probing the effect of compartmentalizing TPP within the hydrophobic microenvironment in comparison to its effect when it is present in the bulk

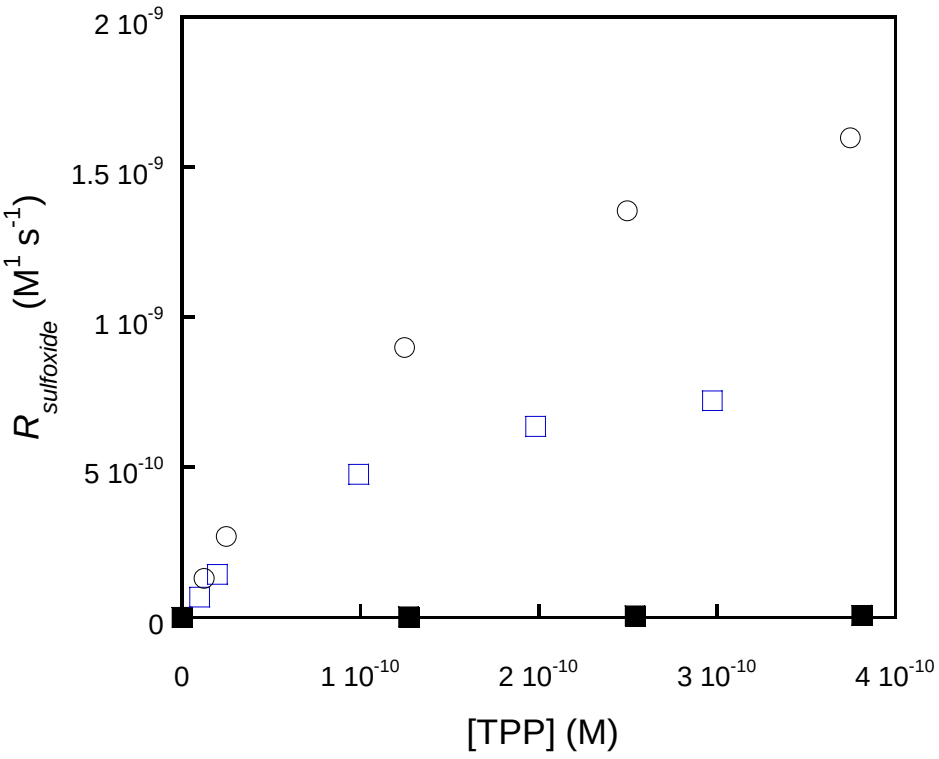

Figure 4.4. Effect of compartmentalizing TPP within organic micelles on photodegradation of disulfoton. Bulk TPP (■) displays a much lower k_{obs} in comparison to TPP encapsulated in PEP-PEO (6.7-16.5) (○) and PEE-PEO (2-9) (□).

environment. Figure 4.4 displays the results of Figure 4.3 in terms of bulk concentration of sensitizer with the addition of control experiments demonstrating the inefficiency of TPP to induce photodegradation of disulfoton within the bulk solution. It is interesting to note that the concentration of TPP with respect to the bulk solution was in the range of 10^{-10} M and little growth of disulfoton-sulfoxide due to $^1O_2$ production occurred at these concentrations, but by compartmentalizing the hydrophobic components of the photolysis experiment into hydrophobic micellar cores a significant enhancement was observed.

Quenching experiments necessary to determine microheterogeneous effect

Control experiments employing known $^1O_2$ quencher molecules were utilized to suppress the $^1O_2$ reactivity within their respective microenvironments. Sodium azide was used as a hydrophilic quencher and its results on the photodegradation of disulfoton within TPP-PEE-PEO (2-9) solutions are displayed in Figure 4.5. According to Figure 4.3, the majority of disulfoton within the solution would be bound to the hydrophobic micellar core, and consequently not be subjected to the expected quenching effect on the bulk aqueous environment. At 10^{-3} M concentrations of sodium azide, the observed disulfoton-sulfoxide growth would be expected to be significantly lower than the unquenched rate. The lack of quenching behavior exhibited in Figure 4.5 supports the

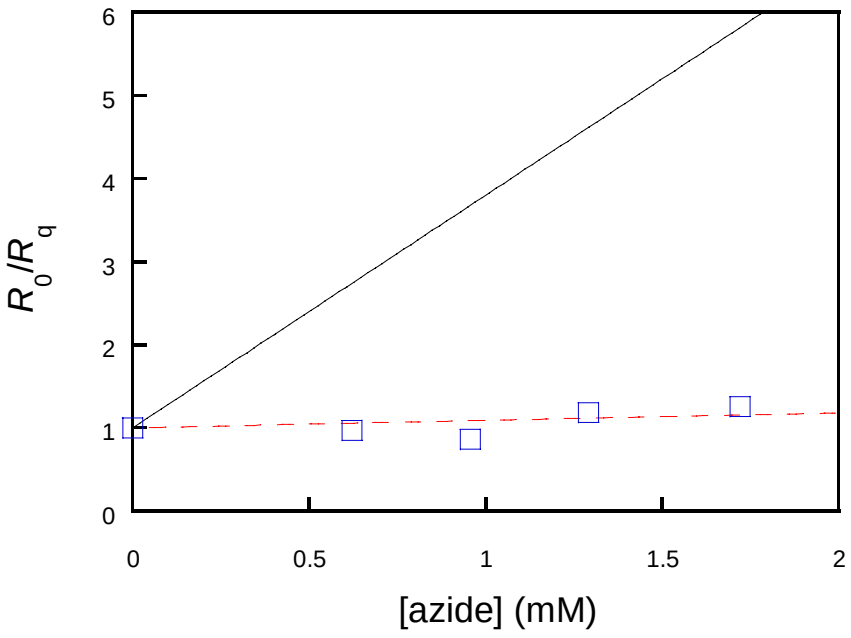

Figure 4.5. Effect of hydrophilic quencher, azide ion, on photodegradation of disulfoton within hydrophobically encapsulated TPP-PEE-PEO (2-9) micelle solutions. Solid line represents expected quenching effect for conventional distribution with $k_{H2O} = 2.5 \times 10^5$ M^{-1} s^{-1} and $k_q = 7 \times 10^8$ M^{-1} s^{-1}.

theory of enhanced $^1O_2$ reactivity within the hydrophobic micelle core being the most important factor in disulfoton degradation.

The enhanced $^1O_2$ reactivity within the hydrophobic micelle core was selectively suppressed by using known hydrophobic $^1O_2$ quencher β-carotene (Figure 4.6). β-carotene is a very efficient quencher of $^1O_2$ (k_q = 2.5 × 10^{10} M^{-1} s^{-1})[85], but at the concentrations used in our control experiments very little quenching would be expected to occur within a traditional distribution model of $^1O_2$ reactivity. Despite the low concentration of β-carotene, significant quenching was observed. The results are consistent with a picture in which, due to the high hydrophobicity of β-carotene, it localized within the hydrophobic micellar cores and quenched $^1O_2$ in that microenvironment.

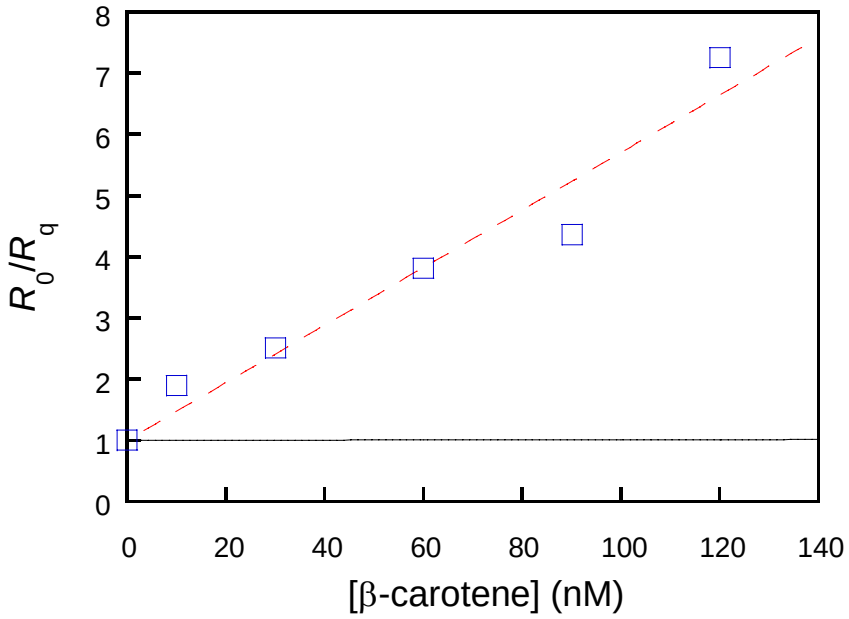

Figure 4.6. Effect of hydrophobic quencher, β-carotene, on photodegradation of disulfoton within hydrophobically encapsulated TPP-PEE-PEO (2-9) micelle solutions. Solid line represents expected quenching effect for conventional distribution with k_{H2O} = 2.5 × 10^5 M^{-1} s^{-1} and k_q = 2.5 × 10^{10} M^{-1} s^{-1}.

Covalently-attached sensitizer micelles

The modification of PEE-PEO (1.4-15) by creating an ester linkage to a TPP sensitizer at the interface of the two blocks is depicted in Scheme 4.3. The intermediate acid chloride of the asymmetric TPPCOOH was not isolated, but instead reacted with primary hydroxyl group at the interface of PEE-PEO (1.4-15). The yield of the reaction was very low despite prolonged exposure to the reaction conditions, 1.4% conversion to the ester. This low reactivity was expected due to the relatively low reaction rates at mid-functional polymers.[92] Despite the low conversion to product, enough material was generated to create the polymer blend described below. The presence of the covalently attached TPP was confirmed by SEC with refractive index and UV-vis detection (Figure 4.7) and ^{1}H NMR (Figure 4.8). The amount of TPP was determined by quantitative ^{1}H NMR studies employing long acquisition time and calculated based on the integrated signals from the aromatic TPP peaks to the aliphatic PEE-PEO peaks.

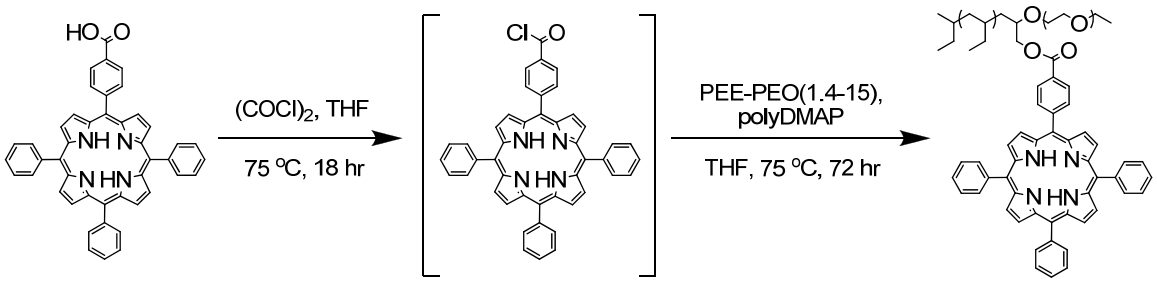

Scheme 4.3. Synthesis of covalently-attached TPP-PEE-PEO (1.4-15).

The preparation of PEE-PEO micelles with the covalently attached TPP involved blending the covalently attached TPP-PEE-PEO (1.4-15) with unmodified PEE-PEO (2-9) at a ratio that would place one TPP sensitizer within a micelle that maintained the characteristics of the unblended PEE-PEO (2-9) micelles. The aggregation number for PEE-PEO (2-9) micelles was determined to be 297 by utilizing the experimentally determined hydrophobic core radius and density of PEE stated above. The modified and unmodified polymers were combined at a ratio of one TPP-PEE-PEO (1.4-15) to 296 PEE-PEO (2-9) and subjected to the same thin layer deposition micelle formation technique as the micelle systems used in hydrophobic encapsulation experiments. After thermal equilibration, DLS and cryo-TEM experiments demonstrated that spherical micelles were generated and they possessed the same hydrodynamic and hydrophobic core radii of the unblended polymer micelles (Figure 4.9).

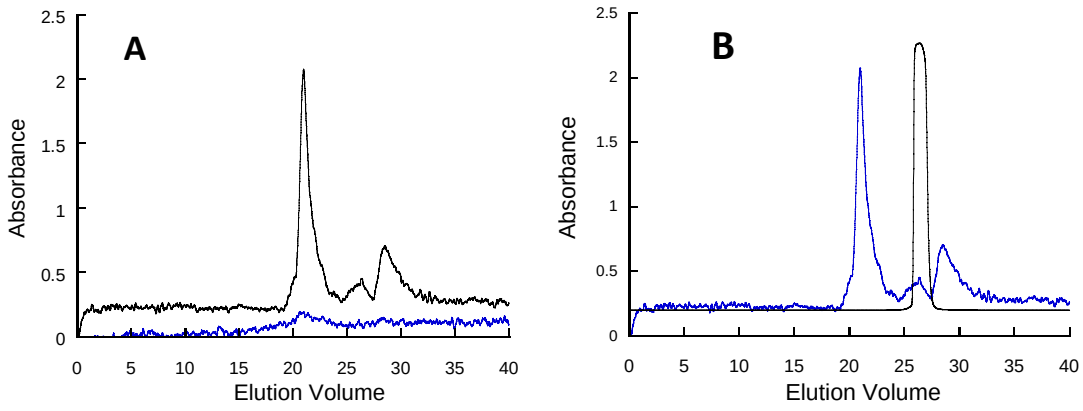

Figure 4.7. Size exclusion chromatography (SEC) with UV-VIS detection of covalently-attached TPP-PEE-PEO (1.4-15). Plot A compares pre-modified PEE-PEO (1.4-15) to post-modified TPP-PEE-PEO (1.4-15) at 410 nm. The post-modified polymer contained a significant absorbance at 410 nm. Plot B compares post-modified TPP-PEE-PEO (1.4-15) with the later eluting TPP starting material at 410 nm.

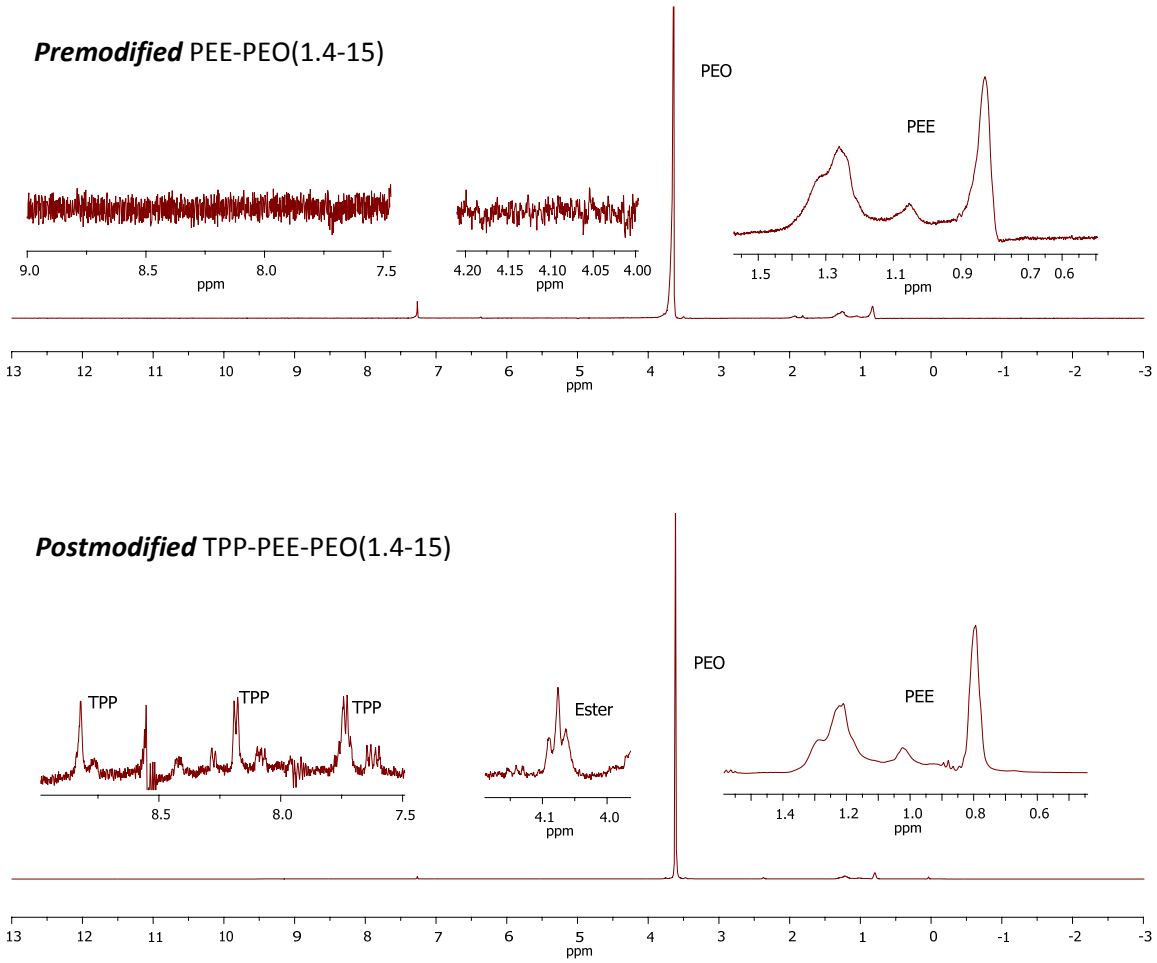

Figure 4.8. ^{1}H NMR spectroscopy of premodified and postmodified block copolymers.

The resulting polymer micelles were subjected to steady-state photolysis experiments in the presence of TPMA and the resulting binding plot and parameters are displayed in Figure 4.10 and Table 4.1, respectively. The concentration of TPP within the covalently modified PEE-PEO (2-9) micelles was significantly higher than the hydrophobically encapsulated TPP-PEE-PEO (2-9) system, so it was predicted to exhibit an increased $[^{1}O_2]_{MIC}$ based on the reaction diffusion model described above. The

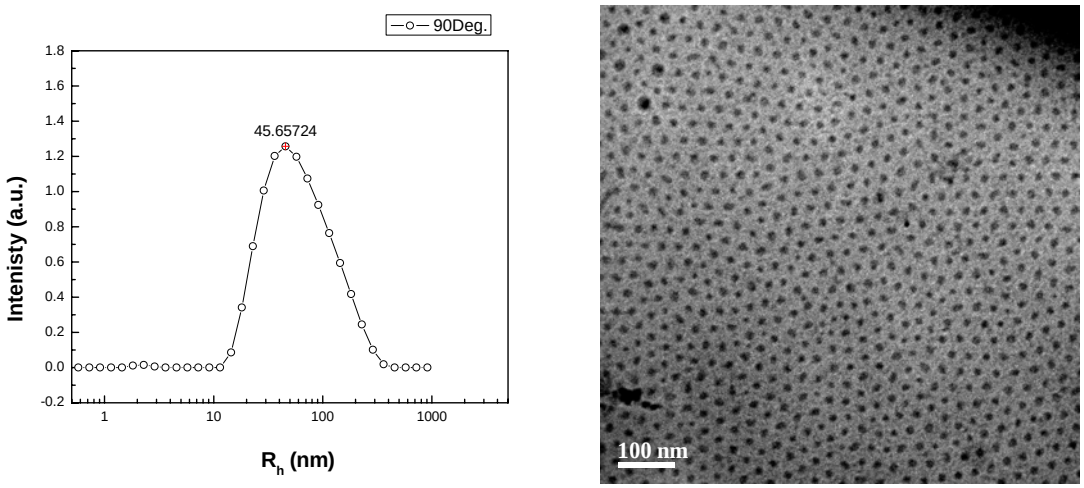

Figure 4.9. Inverse Laplace transform from DLS analysis at 90^{o} and cryo-TEM image of covalently-attached TPP-PEE-PEO (2-9) micelle solution. DLS results display moderate uniformity of micelles with hydrodynamic radii of 24 nm according to the Stokes-Einstein equation. Cryo-TEM images displays micelles with interior hydrophobic core radii calculated to be 6.3 ± 0.1 nm.

difference in $[^1O_2]_{MIC}$ was not as large as expected and this could be due to the relative location of TPP within the respective micelles. The theory of microheterogeneous production of $^1O_2$ assumes uniform production of $^1O_2$ within hydrophobic organic microenvironments and hydrophobic encapsulation of TPP by the micelle system employs the same assumption in regards to its distribution within the hydrophobic microenvironment. Covalently attached TPP-PEE-PEO (2-9) micelles have the sensitizer located at the micelle-bulk interface, so the production of $^1O_2$ occurs at the interface and any $^1O_2$ within the micelle is a product of its diffusion into the micelle. Due to the increased solubility of $^1O_2$ within the hydrophobic microenvironment and its relative proximity to the site of $^1O_2$ production, $[^1O_2]_{MIC}$ is still expected to be significantly higher than $[^1O_2]_{aq}$ and our experimental data is consistent with this hypothesis.

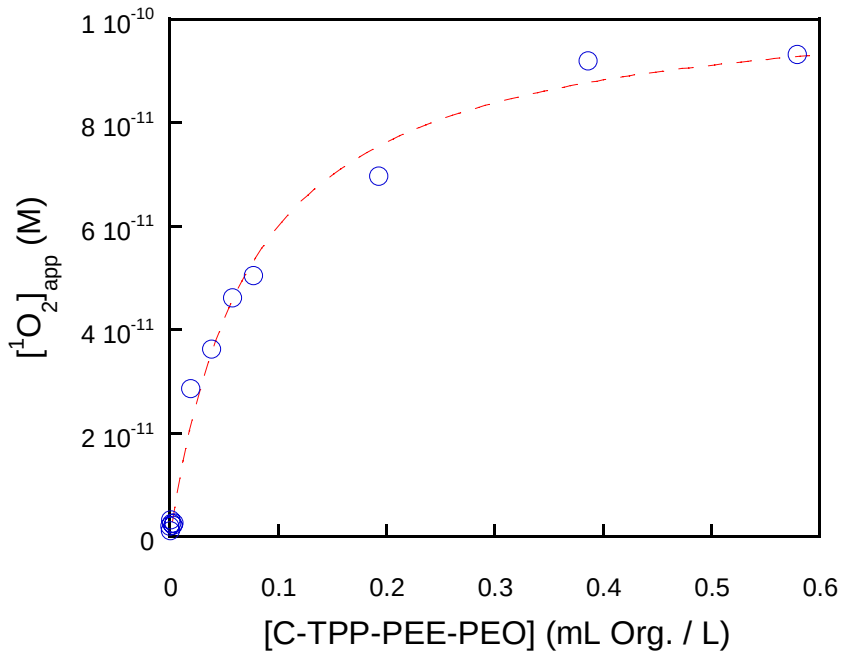

Figure 4.10. Fitting of covalently-attached TPP-PEE-PEO (2-9) micelles to Langmuir binding isotherm (eq. 6). $[^1O_2]_{app}$ determined by chemiluminescent detection of $TPMAO_2$, selective product of TPMA reacting with $^1O_2$.

An interesting and unexpected result derived from the comparison of hydrophobically encapsulated TPP and covalently attached TPP micelle systems is their difference in K_{MIC} with respect to TPMA. The data in Table 4.1 shows that K_{MIC} for the covalently attached TPP-PEE-PEO (2-9) micelles is 100-fold lower than that for the hydrophobic TPP-micelles. The micelle morphology and hydrophobic core radius of the covalently attached TPP-PEE-PEO (2-9) did not significantly differ from that of the unmodified PEE-PEO (2-9) micelles utilized in the hydrophobic encapsulation studies. The molecular structure of the hydrophobic micelle core and the micelle-bulk interface are identical except for the presence of the ester linkage and TPP in the covalently attached TPP-PEE-PEO (2-9). One possible explanation of the 100-fold difference in

K_{MIC} could be the effect of the approximately 100-fold difference in $[TPP]_{MIC}$ on the hydrophobic binding capacity of the micelle system. TPP within the covalently attached TPP-PEE-PEO (2-9) micelles does not engage in the partitioning behavior utilized in generating hydrophobically encapsulated TPP-micelles, but instead occupies a constant volume that would impede the partitioning of other hydrophobic components (i.e. TPMA) from binding to the hydrophobic micelle core. Despite the observed differences in K_{MIC}, binding behavior is still observed within both covalently attached and hydrophobically encapsulated TPP-micelle systems.

Conclusion

Block-copolymers have shown to be ideally suited to form well-controlled aqueous nanostructures that display photochemical properties similar to natural aqueous photochemical systems. Hydrophobic encapsulation and covalent attachment of a well-characterized $^1O_2$ photosensitizer, TPP, within synthesized and commercially available block copolymers provide easily accessible nanoscale photoreactors for applications ranging from photodynamic light therapy to nanoscale light harvesting for energy storage and conversion. Known hydrophobic probe, TPMA, and hydrophobic pesticide, disulfoton, displayed Lagmuir-type binding behavior with respect to block copolymer micelles similar to binding behavior exhibited between hydrophobic molecules and natural organic matter. By observing their photochemistry within TPP-micelle systems differing in both sensitizer concentration and micelle radius, the expected square relationship between micelle radius and $[^1O_2]_{MIC}$ was observed. The application of hydrophobic and hydrophilic quenchers of $^1O_2$ further demonstrated the significant

difference in $^1O_2$ reactivity between the hydrophobic microenvironment within aqueous micelles and within the bulk aqueous environment. Control experiments using hydrophobic and hydrophilic quenchers of $^1O_2$ are necessary when attributing enhanced reactivity within heterogeneous systems to the microheterogeneity similarly displayed in this study. The localization of TPP at the micelle-bulk solution interface had an interesting effect on the binding behavior of disulfoton with respect to PEE-PEO (2-9) micelles and must be taken into consideration in future studies.

Chapter 5.

Synthesis and Reactivity of Fluorescent Hydroxyl Radical Probes

Overview

The detection and quantification of hydroxyl radical within aqueous solutions is an ongoing area of research across many areas of chemistry and biology. The high reactivity of hydroxyl radical, in combination with its general lack of reaction partner specificity, has led to a lack of selective molecular probes. In addition, the fact that hydroxyl radical is produced inside the macromolecular environment of humic substances leads to difficulty in accurately describing the oxidative environment experienced by most hydrophobic organic pollutants. The research within this thesis chapter focused on the development of a class of selective hydroxyl radical probes that have the potential to specifically report the concentration inside the humic microenvironment. The synthesis of hydrophobic hydroxyl radical molecular probes and investigations into their reactivity with hydroxyl radical to produce fluorescent benzocoumarin products is described.

Introduction

Hydroxyl radical, •OH, is a highly reactive oxygen species important to a variety of synthetic and natural systems. It is photochemically produced in the environment through several processes: photolysis of nitrate and nitrite, indirect sensitization of dissolved organic matter (DOM), and Fenton processes.[1] Within biological systems, Fenton processes are a dominant source of •OH.[2] Titanium dioxide (TiO_2) nanoparticles have been used to produce •OH that led to increased oxidative stress on malignant cells, ultimately leading to cell necrosis.[3] In the area of nanotechnology, TiO_2-carbon films have been found to produce •OH through two mechanisms: electron transfer to the carbon

nanoparticles to sensitize the production of H_2O_2 and subsequential Fenton reaction with iron impurities and from the reaction of water at the electron hole within TiO_2 created by the electron transfer event.[4]

Once produced, •OH plays an active role in the reduction/oxidation chemistry within its local environment. Hydroxyl radical reacts with most organic compounds near the bimolecular diffusion controlled limit through either hydrogen/electron abstraction or alkene-insertion type mechanisms.[5-7] Within biological systems, •OH causes severe damage to living organisms through several processes: oxidation of DNA base pairs,[8, 9] lipid peroxidation,[10] protein fragmentation via attack on the α-carbon of aliphatic amino acids,[11] and the disabling of protein folding mechanisms by the formation of covalently cross-linked protein aggregates.[12, 13] Despite the apparent damages caused by •OH within biological systems, it is also a necessary component for cellular organisms to function properly.[14] Organic pollutants within the environment are readily degraded by •OH produced by DOM, Fenton, and nitric oxide processes.[15-19]

The reactive nature of •OH has led to low steady-state concentrations within environmental and biological systems. In natural surface freshwaters, the steady-state concentration of •OH, $[•OH]_{ss}$, has been estimated at 10^{-16} M,[20-22] but within seawaters the concentration has been estimated at two orders of magnitude lower due to lower concentrations of DOM and nitrite anion, NO_2^-, (photosensitizers of •OH) and increased concentrations of bromide (a strong quencher of •OH).[21, 22] Despite the difficulty associated with detecting $[•OH]_{ss}$ within living systems by traditional analytical methods, $[•OH]_{ss}$ within cells has been estimated as high as 10^{-9} M.[23, 24] The extreme range of

concentrations experienced between environmental and biological samples highlights one of the many difficulties encountered while investigating the chemistry of •OH.

The accurate quantification of •OH within complex natural, biological, and synthetic systems has been an ongoing effort over the past fifty years. Electron spin resonance (ESR) has been used to detect "spin-trap" radicals, but the expense and availability of ESR instrumentation and expertise limits its use.[25-27] A more common approach has been the implementation of molecular probes that take advantage of their reactivity with •OH to accurately describe the concentrations within solution.[28-44] Aromatic organic compounds such as substituted benzenes[39, 42, 43], salicylic acid[44], *para*-chlorobenzoic acid[32], phenylalanine[28], coumarins[35, 36], and terephthalate[31, 41, 45] have all been proposed as competent molecular probes for the detection of •OH. Molecular probes that utilize fluorescence detection methods have offered increased sensitivity over traditional absorbance detection methods.[46] Fluorescence detection offers the additional benefit of being able to report the local environment of the molecular probe within biological systems.[30, 38] Terephthalate undergoes reaction with •OH to form 2-hydroxyterephthalate, a highly fluorescent compound that was proposed to be stable *in vitro* via Fenton reaction conditions.[47] Page *et al*. utilized terephthalate to determine the production of •OH within DOM solutions and found that 2-hydroxylterphthalate was not stable under the reaction conditions.[41] This discrepancy within the literature highlights the shortcomings associated with terephthalate as an environmental •OH probe despite its popularity as a detection method.

The detection of •OH within natural surface waters is plagued by an additional problem: the microheterogeneous production of reactive oxygen species within DOM solutions, as highlighted in the previous chapters of this thesis.[48-52] As stated above, nitrate and nitrite as well as Fenton process are dominant in the photoproduction of •OH within marine waters, but within freshwater systems, DOM plays an increased role.[21, 22] The generation of •OH within DOM supramolecular assemblies creates a spatial distribution that can only be assessed by molecular probes within a detection scheme aimed at the quantification of •OH within hydrophobic microenvironments in contrast to the bulk aqueous solution.[49, 51] Terephthalate is hydrophilic and cannot accurately describe the different oxidation environments within hydrophobic DOM supramolecular assemblies. The first step in determining the presence of a spatial distribution of •OH within natural waters is the development of a hydrophobic, sensitive, and selective •OH molecular probe to work in tandem with a hydrophilic •OH probe, such as terephthalate.

A proposed hydrophobic probe molecule and its •OH reaction product are shown in Scheme 5.1. 2-Biphenylcarboxylic acids (BPA) are fluorescent molecules capable of undergoing hydroxylation at the more electron-rich aromatic ring. The resulting phenol intermediate undergoes rapid intramolecular cyclization to form the fluorescent benzocoumarin (BZC).[53, 54] Although •OH typically inserts into aromatic rings with little regard to electronic density, there is a slight preference to electron-rich aromatic rings with respect to electron-poor aromatic rings.[7, 21, 55] The pseudo-symmetry of BPA dictates that 50% of the electron-rich aromatic ring •OH insertion events would result in the desired fluorescent benzocoumarin product. Tremblay and Sames utilized a similar

analytical method to investigate the *in vivo* reduction of a quinone moiety/lactonization by coenzyme Q to form a fluorescent benzocoumarin.[54]

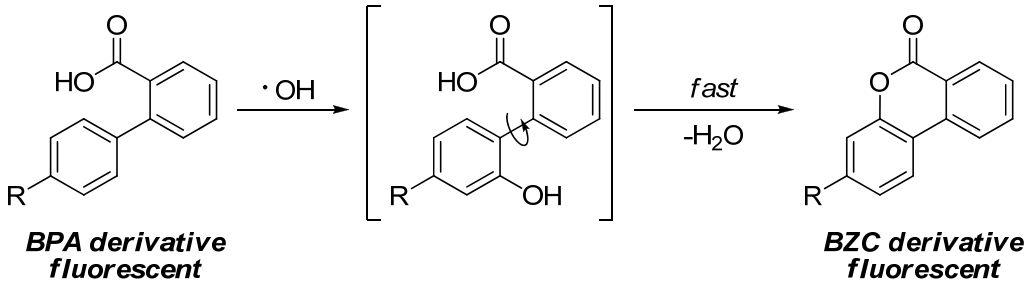

Scheme 5.1. Proposed •OH molecular probe and its reactivity.

The aim of the research described in this thesis chapter is to describe the synthesis and reactivity of a suite of BPA derivatives as potential •OH molecular probes. Eight potential probe molecules that deviated at the 4'-aromatic position (R = H, Me, ^{t}Bu, HO, MeO, NMe_2, CF_3, Cl) and their respective 3'-substituted BZC products were efficiently synthesized and investigated in respect to their •OH reactivity within aqueous solutions. Competition kinetic analysis was used to quantify their reactivity with •OH. The results of this research are important to the ongoing effort to accurately quantify the concentration of •OH within complex aqueous solutions.

Methods and Materials

Materials and general methods

All reagents were purchased from commercial suppliers. Solvents were dried according to literature procedures prior to use.[56] Proton and carbon nuclear magnetic

resonance spectra (^{1}H NMR and ^{13}C NMR) were acquired with a Varian Inova 500 MHz NMR spectrometer. Fluorine nuclear magnetic resonance spectroscopy (^{19}F NMR) was performed using a Varian Inova 300 MHz NMR spectrometer. Electrospray mass spectrometry (ESI-MS) and electrospray high resolution mass spectrometry (ESI-HRMS) was conducted with a BIO-TOF mass spectrometer. Ultraviolet-visible light spectroscopy (UV-vis) was conducted using an Ocean Optics USB2000 spectrophotometer. Fluorescence spectroscopy was conducted using a Varian Cary Eclipse Fluorescence spectrometer. High performance liquid chromatography (HPLC) analysis was performed on an 1100 Series Agilent liquid chromatograph equipped with a UV-absorbance detector and a multiwavelength fluorescence detector.

Synthesis

The BPA and BZC derivatives, along with their synthetic intermediates, were synthesized according to the following methods. Compounds synthesized in previous studies were characterized and compared to known ^{1}H NMR, ^{13}C NMR, ESI, and m.p. characterization values as indicated below.

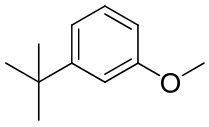

3-tert-butylanisole: To a solution of 3-tert-butylphenol (5.60 g, 37 mmol) in aqueous sodium hydroxide (38 mL, 1.0 M) was added dimethyl sulfate (3.6 mL, 38 mmol). The solution was heated to reflux and allowed to stir overnight, upon which the solution was cooled to room temperature and extracted with diethyl ether (3×).

Vacuum distillation gave the desired compound as a colorless liquid (4.48 g, 73%). ^{1}H NMR (500 MHz, $CDCl_3$) δ = 7.28 (dd; J = 8.0, 8.0; 1H; 5-H), 7.03 (d; J = 8.0; 1H; 4-H), 7.00 (d; J = 2.5; 1H; 2-H), 6.77 (dd; J = 2.5, 8.0; 1H; 6-H), 3.85 (s; 3H; OCH_3), 1.36 (s; 9H; CCH_3) ppm. ^{13}C NMR (500 NMR, $CDCl_3$) δ = 159.42 (1-C), 153.00 (3-C), 129.00 (5-C), 117.91 (4-C), 112.07 (2-C), 109.97 (6-C), 55.17 (OCH3), 34.79 (Ar-CH_3), 31.36 (CH_3) ppm. The characterization matches literature values.[57]

General procedure for biphenyl-2-carboxylic acids: To a Schlenk flask containing 2-iodobenzoic acid (1.00 eq), palladium (II) acetate (0.1 mol%), and boronic acid (1.05 eq) was added aqueous potassium hydroxide (3.00 eq, 2.0 M). The reaction was slowly heated to 75 °C and stirred for 12 hours. The solution was cooled to room temperature and acidified (pH ≤ 2). The resulting precipitate was dissolved by partitioning the mixture with methylene chloride (3×). The organic fractions were combined and the solvent was removed via rotary evaporator to yield the product as a crude white solid. Recrystallization from ethanol/water gave pure target material.

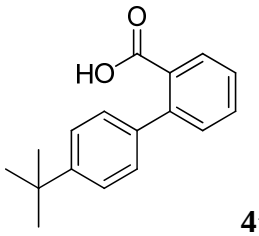

4'-*tert*-butylbiphenyl-2-carboxylic acid (^{t}Bu-BPA): The desired compound was isolated as a white crystalline solid (0.145 g, 25%). m.p. = 134-136 ^{o}C. ^{1}H NMR (500 MHz, $CDCl_3$) δ = 7.94 (d; J = 7.0; 1H, 3-H), 7.56 (dd; J = 7.5, 7.5; 1H; 5-H),

7.41 (d; J = 8.5, 2H; 2',5'-H), 7.39 (m; 2H; 4,6-H), 7.29 (d; J = 8.0; 2H; 3',5'-H), 1.36 (s, 9H, CH_3) ppm. ^{13}C NMR (500 NMR, $CDCl_3$) δ = 150.29 (CO_2H), 137.88 (1-C), 132.02 (3-C), 131.35 (4-C), 130.67 (5-C), 129.29 (1'-C), 128.18 (3',5'-C), 126.98 (6-C), 125.11 (2',6'-C), 34.58 (Ar-C), 31.40 (CH_3) ppm. ESI-HRMS: calculated m/z/ = 253.1234, observed m/z = 253.1214 $[C_{17}H_{17}O_2]^-$.

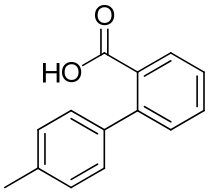

4'-methylbiphenyl-2-carboxylic acid (Me-BPA): The desired compound was isolated as a white solid (0.568 g, 78%). m.p. = 148-150 ^oC. ^1H NMR (500 MHz, $CDCl_3$) δ = 7.97 (d; J = 7.5; 1H; 3-H), 7.58 (dd; J = 7.5, 7.5; 1H; 5-H), 7.43 (dd; J = 7.0, 7.0; 1H; 4-H), 7.40 (d; J = 7.5; 1H; 6-H), 7.28 (d; J = 8.0; 2H; 2',5'-H), 7.23 (d; J = 8.0; 2H; 3',5'-H), 2.43 (s; 3H, CH_3) ppm. ^{13}C NMR (500 NMR, $CDCl_3$) δ = 174.10 (CO_2H), 143.35 (2-C), 138.06 (1-C), 137.17 (1'-C), 132.16 (3-C), 131.29 (4-C), 130.75 (5-C), 129.33 (6-C), 128.93 (2',6'-C), 128.41 (3',5'-C), 127.03 (4'-C), 21.29 (Ar-CH_3) ppm. ESI-HRMS: calculated m/z = 211.0765, observed m/z = 211.0759 $[C_{14}H_{11}O_2]^-$. The characterization matches literature values.[58]

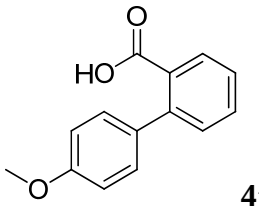

4'-methoxybiphenyl-2-carboxylic acid (MeO-BPA): The desired compound was isolated as a white solid (0.504 g, 91%). m.p. = 146 ^{o}C. ^{1}H NMR (500 MHz, $CDCl_3$) δ = 11.66 (s; 1H; CO_2H), 7.94 (d; J = 7.5; 1H; 3-H), 7.55 (dd; J = 7.5, 7.5; 1H; 5-H), 7.40 (dd; J = 7.5, 7.5; 1H; 4-H), 7.37 (d; J = 7.5; 1H; 6-H), 7.29 (d; J = 7.5; 2H; 2',6'-H), 6.94 (d; J = 7.5; 2H; 3',5'-H). 3.86 (s; 3H; CH_3) ppm. ^{13}C NMR (500 NMR, $CDCl_3$) δ = 174.02 (CO_2H), 159.10 (4'-C), 142.96 (1-C), 133.34 (1'-C), 132.11 (5-C), 131.26 (3-C), 130.74 (4-C), 129.67 (2',6'-C), 129.30 (2-C), 126.87 (6-C), 113.64 (3',5'-C), 55.28 (CH_3) ppm. ESI-HRMS: calculated m/z = 227.0714, observed m/z = 227.0703 $[C_{14}H_{11}O_3]^-$. The characterization matches literature values.[59]

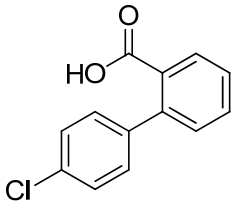

4'-chlorobiphenyl-2-carboxylic acid (Cl-BPA): The desired compound was isolated as a white solid (0.137 g, 27%). m.p. = 167-168 ^{o}C. ^{1}H NMR (500 MHz, $CDCl_3$) δ = 8.00 (d; J = 8.0; 1H; 3-H), 7.59 (dd; J = 7.5, 7.5; 1H; 5-H), 7.46 (dd; J = 7.5, 7.5; 1H; 4-H), 7.37 (d; J = 8.5; 2H; 2',6'-H), 7.34 (d; J = 7.5; 1H; 6-H), 7.27 (d; J = 8; 2H; 3',5'-H) ppm. ^{13}C NMR (500 NMR, $CDCl_3$) δ = 173.41 (CO_2H), 142.38 (1'-C), 139.56 (1-C), 133.52 (4'-C), 132.42 (5-C), 131.20 (3-C), 131.02 (4-C), 129.84 (2',6'-C), 128.96 (2-C), 128.27 (3',5'-C), 127.61 (6-C) ppm. ESI-MS: m/z [ion] (rel.

int%) = 231.1 $[M-H]^-$ (100), 233.1 $[M+2-H]^-$ (31), 232.1 $[M+1-H]^-$ (11), 234.1 $[M+3-H]^-$ (3). ESI-HRMS: calculated m/z = 231.0218, m/z = 231.0216 $[C_{13}H_8ClO_2]^-$. The characterization matches literature values.[59]

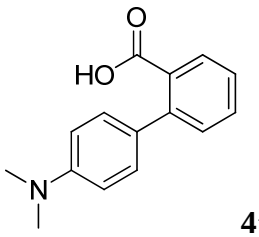

4'-N,N-dimethylaminobiphenyl-2-carboxylic acid (NMe_2-BPA): The desired compound was isolated as a white solid (0.044 g, 9%). m.p. = 192-194 ^oC. ^1H NMR (500 MHz, $CDCl_3$) δ = 7.90 (d; J = 7.5; 1H; 3-H), 7.52 (dd; J = 8.0, 8.0; 1H; 5-H), 7.38 (d; J = 8.5; 1H; 6-H), 7.36 (dd; J = 7.0, 7.0; 1H; 4-H), 7.26 (d; J = 8.5; 2H; 2',6'-H), 6.77 (d; J = 8.5; 2H; 3',5'-H), 2.99 (s; 6H; CH_3) ppm. ^{13}C NMR (500 NMR, $CDCl_3$) δ = 173.20 (CO_2H), 149.90 (4'-C), 143.08 (1-C), 131.83 (5-C), 131.02 (3-C), 130.61 (4-C), 129.40 (2',6'-C), 128.83 (1'-C), 126.28 (6-C), 113.25 (2-C), 112.42 (3',5'-C), 40.62 (NCH_3) ppm. ESI-HRMS: calculated m/z = 240.1030, observed m/z = 240.1033 $[C_{15}H_{14}NO_2]^-$.

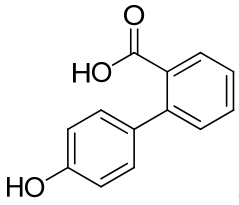

4'-hydroxybiphenyl-2-carboxylic acid (HO-BPA): To a mixture of concentrated hydrobromic acid and glacial acetic acid (3:1 V/V) was added 4'-methoxybiphenyl-2-carboxylic acid (0.149 g, 0.65 mmol). The reaction mixture was

heated to reflux and allowed to stir for 3 hours and then cooled to room temperature. The solution was extracted with diethyl ether (3×), dried over Na_2SO_4, filtered and the solvents were removed by rotary evaporation to yield the target material as a white solid (0.135 g, 97%). m.p. = 203-205 ^oC. ^1H NMR (500 MHz, CD_3OD) δ = 7.72 (d; J = 8.0; 1H; 6-H), 7.48 (dd; J = 7.5, 7.5; 1H, 5-H), 7.35 (dd; J = 8.0, 8.0; 1H, 4-H), 7.34 (d; J = 8.0; 1H; 3-H), 7.17 (d; J = 8.5; 2H; 2',6'-H), 6.81 (d; J = 8.5; 2H; 3',5'-H) ppm. ^{13}C NMR (500 NMR, CD_3OD) δ = 171.67 (CO_2H), 156.67 (4'-C), 141.84 (1-C), 132.37 (1'-C), 130.63 (5-C), 130.30 (3-C), 129.33 (2',6'-C), 128.93 (4-C), 126.19 (6-C), 114.61 (3',5'-C) ppm. ESI-HRMS: calculated 213.0557, observed m/z = 213.0558 $[C_{13}H_9IO_3]^-$. The characterization matches literature values.[60]

General procedure for 2-methoxybenzoic acids: Dimethyl sulfate (3.0 eq) was added to a solution of the substituted salicylic acid (1.0 eq) and potassium carbonate (3.0 eq) in acetone. The solution was heated at reflux for 12 hours, upon which the liquid was removed via rotary vacuum. The residue was dissolved in aqueous sodium hydroxide (1.0 M) and heated at reflux for 12 hours. The solution was then cooled in an ice bath and acidified (pH ≤ 2). The resulting precipitate was filtered and washed with cold water. Recrystallization from ethanol/water gave the target compound

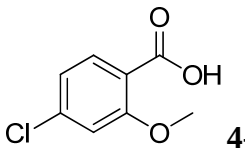

4-chloro-2-methoxybenzoic acid: The desired compound was isolated as a white solid (4.54 g, 84%). m.p. = 144-146 ^oC. ^1H NMR (500 MHz, $CDCl_3$) δ = 10.82

(s; 1H; CO_2H), 8.07 (d; J = 8.0; 1H; 6-H), 7.10 (d; J = 8.5; 1H; 5-H), 7.05 (s; 1H; 3-H), 4.06 (s; 3H; OCH_3) ppm. ^{13}C NMR (500 NMR, $CDCl_3$) δ = 165.56 (CO_2H), 158.74 (2-C), 140.99 (4-C), 134.71 (6-C), 122.30 (5-C), 116.30 (1-C), 112.56 (3-C), 57.00 (OCH_3) ppm. ESI-HRMS: calculated m/z = 185.0011, observed m/z = 185.0029 $[C_8H_6ClO_3]^-$.

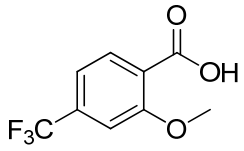

4-trifluoromethyl-2-methoxybenzoic acid: The desired compound was isolated as a white solid (8.94 g, 90%). m.p. = 126-127^o C. ^1H NMR (500 MHz, $CDCl_3$) δ = 10.88 (s; 1H; CO_2H), 8.23 (d; J = 8.0; 1H; 6-H), 7.37 (d; J = 8.0; 1H; 5-H), 7.27 (s; 1H; 3-H), 4.11 (s; 3H; OCH_3) ppm. ^{13}C NMR (500 NMR, CD_3OD) δ = 165.56 (CO_2H), 157.28 (2-C), 132.75 (q; J = 32.0; 4-C), 130.11 (6-C), 122.43 (1-C), 121.93 (q; J = 271; CF_3), 114.78 (d; J = 3.0; 5-C), 106.95 (d; J = 4.0; 3-C), 53.68 (OCH_3) ppm. ESI-HRMS: calculated m/z = 219.0275, observed m/z = 219.0282 $[C_9H_6F_3O_3]^-$. The characterization matches literature values.[61]

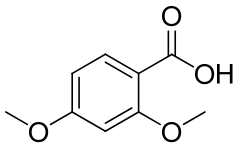

2,4-dimethoxybenzoic acid: To a solution of 2,4-dihydroxybenzoic acid (7.24 g, 47.0 mmol) and potassium carbonate (19.6 g, 141.9 mmol) in acetone was added dimethyl sulfate (13.4 mL, 140.9 mmol). Purification yielded the desired material as a white solid (5.81 g, 68%). m.p. = 107-108 ^{o}C. ^1H NMR (500 MHz, $CDCl_3$) δ = 10.68 (s, 1H, CO_2H), 8.10 (d; J = 9.0; 1H; 6-H); 6.62 (dd; J = 2.0, 8.5; 1H; 5-H), 6.52 (d; J =

2.0; 1H; 3-H), 4.02 (s, 3H, 2-OCH_3), 3.87 (s; 3H; 4-OCH_3) ppm. ^{13}C NMR (500 NMR, $CDCl_3$) δ = 165.64 (CO_2H), 165.17 (4-C), 159.64 (2-C), 135.51 (6-C), 110.33 (1-C), 106.54 (5-C), 98.63 (3-C), 56.62 (2-OCH_3), 55.77 (4-OCH_3) ppm. ESI-HRMS: calculated m/z = 181.0506, observed m/z = 181.0505 $[C_9H_9O_4]^-$. The characterization matches literature values.[62]

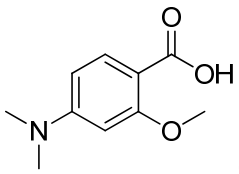

4-N,N-dimethylamino-2-methoxybenzoic acid: To a solution of sodium hydride (8.31 g, 60% dispersion in mineral oil, 207.6 mmol) in tetrahydrofuran (50 mL) was added 4-aminosalicylic acid (7.04 g, 46.0 mmol) dissolved in tetrahydrofuran (25 mL). The solution was cooled in an ice bath and was added methyl iodide (14.4 mL, 231.3 mmol) in tetrahydrofuran (25 mL) drop wise. The solution was allowed to stir at 0 °C for 3 hours. Aqueous sodium hydroxide (50 mL, 1M) was added to the solution was heated to reflux for 12 hours. The solution was then cooled in an ice bath and neutralized with aqueous hydrochloric acid (1 M). The resulting precipitate was filtered and washed with cold water. Recrystallization from ethanol/water gave the target compound as a pale yellow solid (1.51 g, 18%). m.p. = 112-113^o C. ^1H NMR (500 MHz, $CDCl_3$) δ = 10.53 (s; 1H; CO_2H), 7.96 (d; J = 8.5; 1H; 6-H), 6.35 (dd; J = 1.5, 8.5; 1H; 5-H), 6.10 (d; J = 2.0; 1H; 3-H), 4.02 (s, 3H, OCH_3), 3.06 (s, 6H, NCH_3) ppm. ^{13}C NMR (500 NMR, $CDCl_3$) δ = 166.12 (CO_2H), 159.78 (2-C), 155.07 (4-C), 134.84 (6-C),

105.49 (5-C), 104.50 (1-C), 93.43 (3-C), 56.19 (OCH_3), 40.17 (NCH_3) ppm. ESI-HRMS: calculated m/z = 194.0823, observed m/z = 194.0826 $[C_{10}H_{12}NO_3]^-$.

General procedure for 2-methoxy-bromobenzenes: Oxalyl chloride (4.0 eq) was added to pear-shaped flask containing the substituted benzoic acid (1.0 eq) and the solution was allowed to stir overnight, after which the solvent was removed under vacuum to yield the crude acid chloride. In a second pear-shaped flask containing AIBN (40% eq) was added $CBrCl_3$ and the resulting solution was transferred to the acid chloride. The resulting solution was added drop wise to a refluxing solution of 2-mercaptopyridine *N*-oxide sodium salt (2.0 eq) in $CBrCl_3$. Upon complete addition, the solution was cooled and the solvent was removed via rotary evaporation. The residue was dissolved in CH_2Cl_2 and the solution was washed with H_2O (2×) and 1M NaOH (2×). The organic fraction was dried over Na_2SO_4, filtered, and the solvent was removed via rotary evaporation. Column chromatography (CH_2Cl_2:hexanes) provided the target material.

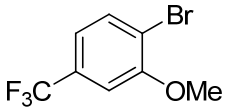

4-Trifluoromethyl-2-methoxy-bromobenzene. The desired compound was isolated as a pale yellow oil (0.258 g, 50%). ^{1}H NMR (500 MHz, $CDCl_3$) δ = 7.62 (d; J = 8.7; 1H; 6-H), 7.08 (s; 1H; 3-H), 7.06 (s; 1H; 5-H), 3.93 (s; 3H; OCH_3) ppm. ^{13}C NMR (500 NMR, $CDCl_3$) δ = 156.01 (2-C), 133.56 (6-C), 130.72 (q; J = 32.6; 4-C), 123.57 (q; J = 270.8; CF_3), 118.18 (q; J = 4.1; 5-C), 115.62 (1-C), 108.20 (q; J =

3.5; 3-C) ppm. ^{19}F NMR (300 NMR, $CDCl_3$) δ = -63.35 (CF_3) ppm. GCMS (rel. %) m/z = 254.0 (100), 256.0 (97), 255 (9), 257 (9).

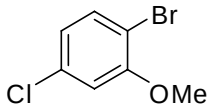

4-Chloro-2-methoxy-bromobenzene. The desired compound was isolated as a pale yellow oil (0.186 g, 41%). ^{1}H NMR (500 MHz, $CDCl_3$) δ = 7.43 (d; J = 8.5; 1H; 6-H), 6.86 (s; 1H; 3-H), 7.82 (d; J = 8.5; 1H; 5-H), 3.88 (s; 3H; OCH_3) ppm. ^{13}C NMR (500 NMR, $CDCl_3$) δ = 156.38 (2-C), 134.01 (4-C), 133.75 (6-C), 121.77 (5-C), 112.59 (3-C), 109.76 (1-C), 56.41 (OCH_3) ppm. GCMS (rel. %) m/z = 222.0 (100), 220.0 (78), 224 (25).

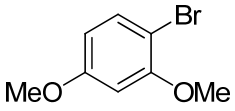

2,4-Dimethoxy-bromobenzene. To a solution of 5,5-dimethyl-N,N-dibromo-hydantoin (5.978 g, 20.9 mmol) in THF (50 mL) in a round bottom flask equipped with a magnetic stir bar was added 1,3-dimethoxybenzene (5.5 mL, 42.5 mmol). The solution was allowed to stir overnight upon which the solvents were removed via rotary evaporator. The resulting liquid was diluted with diethyl ether and the precipitate was removed by filtration. The crude product was purified via vacuum distillation to provide the desired compound (2.57 g, 28%) as a colorless oil. ^{1}H NMR (500 MHz, $CDCl_3$) δ = 7.40 (d; J = 9.0; 1H; 6-H), 6.48 (s; 1H; 3-H), 6.39 (dd; J = 3.0, 9.0; 1H; 5-H), 3.86 (s; 3H; 2-OCH_3), 3.79 (s; 3H; 4-OCH_3) ppm. ^{13}C NMR (500 NMR, $CDCl_3$) δ = 160.24 (4-C), 156.52 (2-C), 133.15 (6-C), 105.88 (5-C), 102.40 (1-C), 99.95

(3-C), 56.15 (4-OCH_3), 55.58 (2-OCH_3) ppm. The characterization matches literature values.[63]

General Procedure for 2-methoxyphenylboronic acids: To a solution of 2-methoxy-bromobenzene (1.0 eq) in THF cooled to -78°C was added *tert*-butyl lithium (2.0 eq, 1.7 M in heptane). The solution was allowed to stir for one hour upon which trimethylborate (2.0 eq) was added. The solution was allowed to stir for an additional hour and then warmed to room temperature and let stir for an additional 2 hours. Upon completion of the reaction, the solution was poured into an ice/water bath and then acidified to pH ≤ 2 with concentrated hydrochloric acid. The resulting precipitate was extracted with diethyl ether (3×), dried with Na_2SO_4, filtered, and the solvents were removed via rotary evaporator. The crude material was purified via recrystallization to yield the target material.

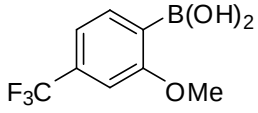

4-Trifluoromethyl-2-methoxyphenylboronic acid. The target material was recrystallized from hot water to yield a white solid (0.0614 g, 30%). ^{1}H NMR (500 MHz, $CDCl_3$) δ = 7.98 (d; J = 7.5; 1H; 6-H), 7.32 (d; J = 8.0; 1H; 5-H), 7.31 (s; 2H; BOH), 7.264 (s; 1H; 3-H), 4.04 (s; 3H; OCH_3) ppm. ^{19}F NMR (300 NMR, $CDCl_3$) δ = -64.00 ppm.

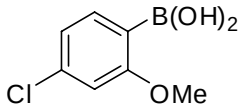

4-Chloro-2-methoxyphenylboronic acid. The target material was recrystallized from hot water to yield a white solid (0.124 g, 90%). ^{1}H NMR (500 MHz, $CDCl_3$) δ = 7.78 (d; J = 8.0; 1H; 6-H), 7.03 (d; J = 8.0; 1H; 5-H), 6.91 (s; 1H; 3-H), 6.22 (s; 2H; BOH), 3.92 (s; 3H; OCH_3) ppm. ^{13}C NMR (500 NMR, $CDCl_3$) δ = 164.95 (2-C), 138.50 (4-C), 137.85 (6-C), 121.56 (5-C), 114.17 (1-C), 110.90 (3-C), 55.86 (OCH_3) ppm. ESI-MS: m/z [ion] (rel. int%) 237.0 $[M+Na]^+$ (100), 236.0 $[M+Na-1]^+$ (37), 239.0 $[M+Na+2]^+$ (28), 238.0 $[M+Na+1]^+$ (17). ESI-HRMS: calculated m/z = 237.0466, observed m/z = 237.0489 $[C_9H_{12}BClNaO_3]^+$.

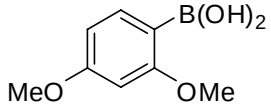

2,4-Dimethoxyphenylboronic acid. The target material was recrystallized from hot water to yield a white solid (0.583 g, 29%). ^{1}H NMR (500 MHz, $CDCl_3$) δ = 7.79 (d; J = 8.0; 1H; 6-H), 6.57 (dd; J = 2.0, 8.0; 1H; 5-H), 6.47 (d; J = 1.5; 1H; 3-H), 6.26 (s; 2H; BOH), 3.89 (s; 3H; 2-OCH_3), 3.85 (s; 3H; 4-OCH_3) ppm. ^{13}C NMR (500 NMR, $CDCl_3$) δ = 165.98 (2-C), 163.70 (4-C), 138.12 (6-C), 112.92 (1-C), 105.28 (5-C), 97.86 (3-C), 55.48 (2-OCH_3), 55.37 (4-OCH_3) ppm. ESI-HRMS: calculated m/z = 233.0956, observed m/z = 233.0959 $[C_{10}H_{15}BNaO_4]^+$.

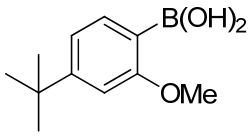

4-^{t}Butyl-2-methoxyphenyboronic acid. A solution of 3-*tert*-butylanisole (0.578 g, 3.52 mmol) in diethyl ether (20 mL) was cooled to -78 ^{o}C.

N,N,N,N-Tetramethylethylenediamine (1.6 mL, 10.7 mmol) was added and followed by drop wise addition of *tert*-butyl lithium (6.2 mL, 1.7 M in pentane). The solution was allowed to warm up to room temperature and stirred for 5 hours. The solution was then cooled back to -78 ^{o}C upon which trimethyl borate (1.2 mL, 10.8mmol) was added. The solution was allowed to slowly warm to room temperature overnight. The solution was then cooled to 0 ^{o}C upon which hydrochloric acid (30 mL, 20%) was added and extracted with diethyl ether (2×, 30 mL), The combined organic fractions were further extracted with aqueous sodium hydroxide (1M, 3×, 20 mL) and then the combined aqueous extracts were reacidified (pH ≤ 2) with concentrated hydrochloric acid to precipitate the crude product. The precipitate was extracted out with diethyl ether (2×, 30 mL) and the combined organic extracts were washed with water (2×), dried over Na_2SO_4, filtered, and the solvent was removed *in vacuo*. The crude residue was recrystallized from hexanes to yield a white solid (0.598 g, 82%). m.p. = 101-103 ^{o}C. ^{1}H NMR (500 MHz, $CDCl_3$) δ = 7.78 (d; J = 7.5; 1H; 6-H), 7.08 (d; J = 7.5; 1H; 5-H), 6.94 (s; 1H; 3-H), 6.17 (s; 2H; BOH), 3.94 (s; 3H; OCH_3); 1.34 (s; 9H: CH_3) ppm. ^{13}C NMR (500 NMR, $CDCl_3$) δ = 164.45 (2-C), 156.68 (4-C), 136.33 (6-C), 118.21 (5-C), 107.04 (3-C), 105.36 (1-C), 55.16 (OCH_3), 35.03 (Ar-C), 30.99 (CH_3) ppm. ESI-HRMS: calculated m/z = 259.1476, observed m/z = 259.1484 $[C_{13}H_{21}BNaO_3]^{+}$.

General Procedure for 2'-methoxy-biphenyl-2-carboxylic acids: To a Schlenk flask containing 2-iodobenzoic acid (1.00 eq), palladium (II) acetate (0.1 mol%), and boronic acid (1.05 eq) was added aqueous potassium hydroxide (3.00 eq, 2.0 M). The reaction

was slowly heated to 75°C and stirred for 12 hours. The solution was cooled to room temperature and acidified (pH ≤ 2). The resulting precipitate was dissolved by partitioning the mixture with methylene chloride (3×). The organic fractions were combined and the solvent was removed via rotary evaporator to yield the product as a crude white solid. Recrystallization from ethanol/water gave pure target material.

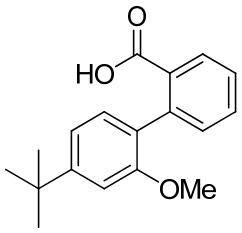

4'-^{t}Butyl-2'-methoxy-biphenyl-2-carboxylic acid. The desired compound was isolated as a white crystalline solid (0.0508 g, 11%). ^{1}H NMR (500 MHz, $CDCl_3$) δ = 9.59 (s; 1H; CO_2H), 7.80 (d; J = 8.0; 1H; 6-H), 7.43 (dd; J = 7.5, 7.5; 1H; 4-H), 7.31 (dd; J = 7.5, 7.5; 1H; 5-H), 7.29 (d; J = 7.5; 1H; 3-H), 7.20 (d; J = 7.5; 1H; 3'-H), 7.00 (d; J = 8.0; 1H; 4'-H), 6.87 (s; 1H; 6'-H), 3.66 (s; 3H; OCH_3), 1.35 (s; 9H; CCH_3) ppm. ^{13}C NMR (500 NMR, $CDCl_3$) δ = 173.31 (CO_2H), 156.08 (1'-C), 151.70 (5'-C), 137.88 (1-C), 134.95 (2'-C), 131.18 (5-C), 130.17 (3'-C), 129.69 (3-C), 129.01 (4-C), 128.30 (2-C), 126.71 (6'-C), 117.46 (4'C), 108.08 (6-C), 55.22 (OCH_3), 34.85 (Ar-C), 31.49 (CH_3) ppm. ESI-HRMS: calculated m/z 283.1340, observed m/z = 283.1334 $[C_{18}H_{19}O_3]^-$.

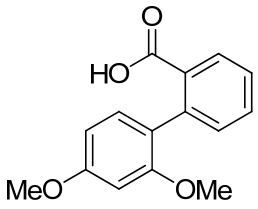

2',4'-Dimethoxy-biphenyl-2-carboxylic acid. The desired compound was isolated as a white crystalline solid (0.522 g, 29%). ^{1}H NMR (500 MHz, $CDCl_3$) δ = 10.61 (br, 1H; CO_2H), 7.92 (d; J = 7.5; 1H; 6-H), 7.57 (dd; J = 7.5, 7.5; 1H; 4-H), 7.39 (dd; J = 7.5, 7.5; 1H; 5-H), 7.33 (d; J = 8.0; 1H; 3-H), 7.20 (d; J = 8.5; 1H; 5'-H), 6.58 (dd; J = 2.5, 8.5; 1H; 4'-H), 6.47 (d; J = 2.5; 1H; 2'-H), 3.86 (s; 3H; 2'-OCH_3), 3.69 (s; 3H; 4'-OCH_3) ppm. ^{13}C NMR (500 NMR, $CDCl_3$) δ = 205.15 (CO_2H), 160.71 (1'-C), 157.11 (3'-C), 138.72 (2-C), 132.30 (5-C), 131.58 (5'C), 130.26 (3-C), 129.82 (4-C), 126.87 (2'-C), 122.88 (1-C), 114.17 (6'-C), 104.50 (4'-C), 98.60 (6-C), 55.38 (2'-OCH_3), 55.02 (4'-OCH_3) ppm.

General Procedures for benzocoumarins: Method A) To a mixture of concentrated hydrobromic acid and glacial acetic acid (3:1 V/V) was added the 2'-methoxy-biphenyl-2-carboxylic acid. The reaction mixture was heated to reflux and allowed to stir for 3 hours and then cooled to room temperature. If the pure material crystallized, it was filtered off and dried in a vacuum oven overnight to yield the pure target material. Otherwise, the reaction mixture was extracted with dichloromethane, dried over Na_2SO_4, filtered and the solvent was removed via rotary evaporator. Flash column chromatography provided the desired compound. **Method B)** Benzocoumarins were synthesized from their respective biphenyl-2-carboxylic acids following a procedure similar to Togo *et al.*[64] A solution of [bis(trifluoroacetoxy)iodo]benzene (1.1 eq) and

respective biphenyl-2-carboxylic acid (1.0 eq) in a mixed solvent of dry benzene and dry methylene chloride (62.5 mM; 13:3 V/V) was stirred in the dark for 3 hours, upon which iodine (0.1 eq) was added. The reaction was heated to 70 ^{o}C and irradiated with a tungsten lamp (300 W) for 4 hours. The reaction mixture was poured in saturated $NaHCO_3$ (aq.), extracted with methylene chloride (3×), and the organic fractions were combined before washing with saturated Na_2SO_3 (aq.). The mixture was separated, extracted with methylene chloride (2×), and the organic fraction was dried over Na_2SO_4, filtered and the solvent was removed via rotary vacuum. Flash column chromatography on the resulting crude oil delivered the desired compound.

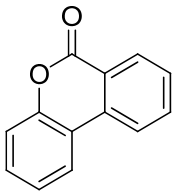

3,4-benzocoumarin (H-BZC): The desired compound was isolated using Method B as a white crystalline solid (0.170 g, 86%). m.p. 91-92 ^{o}C. ^{1}H NMR (500 MHz, $CDCl_3$) δ = 8.39 (d; J = 8.0; 1H; 6-H), 8.11 (d; J = 8.0; 1H; 3-C), 8.04 (d; J = 8.0; 1H; 6'-H), 7.82 (dd; J = 7.5, 7.5; 1H; 4'-H), 7.57 (dd; J = 7.5, 7.5; 1H; 4-H), 7.48 (d; J = 7.5,7.5; 1H; 5-H), 7.34 (m; 2H; 3'-H, 5'-H) ppm. ^{13}C NMR (500 NMR, $CDCl_3$) δ = 161.19 (CO), 151.28 (2'-C), 134.85 (5-C), 134.76 (1'-C), 130.57 (3-C), 130.45 (4'-C), 128.88 (6'-C), 124.56 (4-C), 122.77 (5'-C), 121.69 (6-C), 121.24 (2-C), 118.03 (1-C), 117.78 (3'-C) ppm. ESI-HRMS: $[M+H]^+$ calculated m/z = 197.0597, observed m/z = 197.0603 $[C_{13}H_9O_2]^+$. The characterization matches literature values.[65]

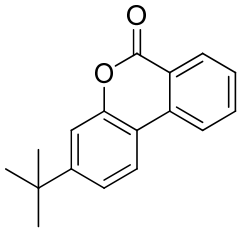

4'-^{t}Butyl-benzocoumarin (^{t}Bu-BZC): The desired compound was isolated using Method A as a white crystalline solid (0.0475 g, 78%). m.p. 159-160 ^{o}C. ^{1}H NMR (500 MHz, $CDCl_3$) δ = 8.41 (d; J = 7.5; 1H; 6-H), 8.11 (d; J = 8.0; 1H; 3-C), 8.00 (d; J = 9.0; 1H; 6'-H), 7.82 (dd; J = 7.5, 7.5; 1H; 5-H), 7.47 (dd; J = 7.5, 7.5; 1H; 4-H), 7.40 (s; 1H; 3'-H), 7.40 (d; J = 7.0; 1H; 5'-H), 1.37 (s; 9H; CCH_3) ppm. ^{13}C NMR (500 NMR, $CDCl_3$) δ = 161.41 (CO), 154.62 (2'-C), 151.13 (4'-C), 134.82 (1'-C), 134.74 (5-C), 130.42 (3-C), 128.36 (6'-C), 122.38 (4-C), 121.96 (5'-C), 121.48 (6-C), 120.90 (2-C), 115.30 (1-C), 114.42 (3'-C) ppm. ESI-HRMS: calculated m/z = 275.1043, observed m/z = 275.1042 $[C_{17}H_{16}NaO_2]^{+}$.

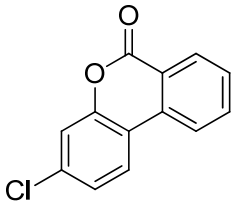

4'-Chloro-benzocoumarin (Cl-BZC): The desired compound was isolated using Method B as a white solid (0.0268 g, 84%). m.p. 152-153^{o} C. ^{1}H NMR (500 MHz, $CDCl_3$) δ = 8.34 (d; J = 8.0; 1H; 6-H), 8.02 (d; J = 8.5; 1H; 3-H), 8.93 (d; J = 8.5; 1H; 6'-H), 7.81 (dd; J = 7.5, 7.5; 1H; 5-H), 7.57 (dd; J = 8.0, 8.0; 4-H), 7.29 (m; 2H; 3'-H, 5'-H) ppm. ^{13}C NMR (500 NMR, $CDCl_3$) δ = 160.51 (CO), 151.46 (2'-C), 135.92 (1'-C), 135.08 (5-C), 133.93 (4'-C), 130.68 (3-C), 129.18 (6'-C), 125.01 (4-C), 123.78 (5'-C), 121.65 (6-C), 120.86 (2-C), 117.90 (3'-C), 116.68 (1-C) ppm. ESI-MS: m/z [ion]

(rel. int%) = 231 $[M+H]^+$ (100), 233 $[M+2+H]^+$ (28), 232 $[M+1+H]^+$ (12), 234 $[M+3+H]^+$ (3). ESI-HRMS: $[M+H]^+$, calculated m/z = 231.0207, observed m/z = 231.0207 $[C_{13}H_8ClO_2]^+$.

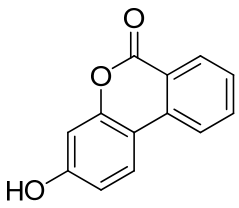

4'-Hydroxy-benzocoumarin (HO-BZC): The desired compound was isolated using Method A as a white crystalline solid (0.031 g, 72%). m.p. 220 – 222 ^oC. ^1H NMR (500 MHz, $CDCl_3$) δ = 9.25 (s; 1H; Ar-OH), 8.25 (d; J = 8.0; 1H; 6-H), 8.20 (d; J = 8.0; 1H; 3-H), 8.11 (d; J = 8.8; 1H; 2'-H), 7.86 (dd; J = 7.2, 6.8; 1H; 5-H), 7.56 (dd; J = 7.2, 8.0; 1H; 4-H), 6.91 (dd; J = 2.4, 8.8; 1H; 3'-H), 6.80 (d; J = 2.4; 1H; 5'-H) ppm. ^{13}C NMR (500 NMR, $CDCl_3$) δ = 160.11 (4'-C), 153.09 (2'-C), 135.29 (5-C), 130.22 (3-C), 128.76 (2-C), 127.87 (6'-C), 124.88 (4-C), 121.70 (6-C), 120.09 (1-C), 113.32 (5'-C), 110.52 (1'-C), 103.54 (3'-C) ppm. ESI-HRMS: calculated m/z = 235.0366, observed m/z = 235.0365 $[C_{13}H_8NaO_3]^+$. The characterization matches literature values.[66]

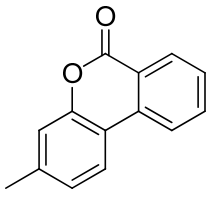

4'-Methyl-benzocoumarin (Me-BZC): The desired compound was isolated from Method B as a white crystalline solid (0.0940 g, 94%). m.p. 129-130 ^oC. ^1H NMR (500 MHz, $CDCl_3$) δ = 8.39 (d; J = 8.0; 1H; 6-H), 8.08 (d; J = 8.0; 1H; 3-H), 7.94

(d; J = 8.0; 1H; 6'-H), 7.80 (dd; J = 8.0, 8.0; 1H; 5-H), 7.55 (dd; J = 8.0, 8.0; 1H; 4-H), 7.16 (m; 2H; 3'-H, 5'-H) ppm. ^{13}C NMR (500 NMR, $CDCl_3$) δ = 161.46 (CO), 151.29 (2'-C), 141.31 (4'-C), 135.01 (1'-C), 134.79 (5-C), 130.56 (3-C), 128.38 (6'-C), 125.69 (4-C), 122.53 (5'-C), 121.44 (6-C), 120.90 (2-C), 117.90 (3'-C), 115.45 (1-C), 21.47 (CH_3) ppm. ESI-HRMS: $[M+Na]^+$ calculated m/z = 233.0573, observed m/z =233.0573 $[C_{14}H_{10}NaO_2]^+$.

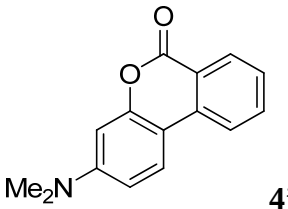

4'-Dimethylamino-benzocoumarin (NMe_2-BZC): The desired compound was isolated from Method B as a white crystalline solid (0.001 g, 3 %). ^{1}H NMR (500 MHz, $CDCl_3$) δ = 8.32 (d; J = 7.5; 1H; 6-H), 7.94 (d; J = 8.0; 1H; 3-H), 7.86 (d; J = 8.0; 1H; 6'-H), 7.73 (dd; J = 7.5, 7.5; 1H; 5-H), 7.41 (dd; J = 7.5, 7.5; 1H; 4-H), 6.70 (d; J = 8.5; 1H; 5'-H), 6.60 (s; 1H; 3'-H) ppm. ESI-HRMS: calculated m/z = 240.1019, observed m/z = 240.1019 $[C_{15}H_{14}NO_2]^+$.

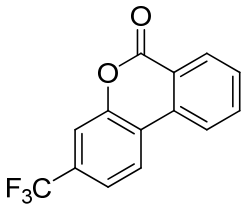

4'-Trifluoromethyl-benzocoumarin (CF_3-BZC): The desired compound was isolated from Method B as a white solid (0.106 g, 40%). m.p. 141-142 ^{o}C. ^{1}H NMR (500 MHz, $CDCl_3$) δ = 8.43 (d; J = 7.5; 1H; 6-H), 8.18 (d; J = 9.0; 1H; 6'-H),

8.16 (d; J = 9.0; 1H; 3-H), 7.89 (dd; J = 7.5, 7.5; 1H; 5-H), 7.68 (dd; J = 7.5, 7.5; 1H; 4-H), 7.57 (m; 2H; 3'-H, 5'-H) ppm. ^{13}C NMR (500 NMR, $CDCl_3$) δ = 160.25 (CO), 150.97 (2'-C), 135.22 (5-C), 133.38 (1'-C), 132.22 (d; J = 33.2, 4'-C), 130.86 (3-C), 130.15 (6'-C), 123.64 (4-C), 122.21 (6-C), 121.66 (2-C), 121.10 (d; J = 3.0; 5'-C), 115.25 (d; J = 4.0; 3'-C), 113.12 (1-C) ppm. ^{19}F NMR (300 NMR, $CDCl_3$) δ = -64.42 ppm. ESI-HRMS: $[M+Na]^+$ calculated m/z = 287.0290, observed m/z = 287.0296 $[C_{14}H_7F_3NaO_2]^+$.

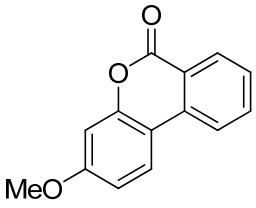

4'-Methoxy-benzocoumarin (MeO-BZC): To a solution of HO-BZC (0.0068 g, 0.03 mmol) and anhydrous potassium carbonate (0.0386 g, 0.28 mmol) in dry acetone was added dimethyl sulfate (6.1 μL, 0.06 mmol). The solution was heated to reflux and allowed to stir overnight, upon which the solution was cooled to temperature and 5% HCl (aq) was added to the solution. The reaction mixture was extracted with diethyl ether, dried over Na_2SO_4, filtered, and the solvent was removed via rotary evaporator. Flash column chromatography yielded the desired compound as a white solid (0.0072 g, 100%). ^{1}H NMR (500 MHz, $CDCl_3$) δ = 8.34 (d; J = 7.5; 1H; 6-H), 7.98 (d; J = 7.5; 1H; 3-H), 7.93 (d; J = 9.0; 1H; 6'-H), 7.77 (dd; J = 7.0, 7.0; 1H; 5-H), 7.49 (dd; J = 7.0, 7.0; 1H; 4-H), 6.90 (dd; J = 3.0, 9.0; 1H; 5'-H), 6.85 (d; J = 3.0; 1H; 3'-H) ppm. ^{13}C NMR (500 NMR, $CDCl_3$) δ = 161.48 (4'-C), 158.08 (2'-C), 134.86 (5-C), 130.53 (3-C), 127.72 (6'-C), 123.77 (4-C), 121.07 (6-C), 119.96 (2-C), 112.73 (1-C),

112.43 (5'-C), 111.14 (1'-C), 101.62 (3'-C), 55.70 (Ar-OCH_3) ppm. ESI-HRMS: calculated m/z = 249.0522, observed m/z = 249.0528 $[C_{14}H_{10}NaO_3]^+$. The characterization matches literature values.[67]

Steady state irradiation experiments

Steady state photolysis experiments were conducted with four medium pressure 175 W Hg vapor lamps (borosilicate-jacketed LumaPro lamps, GE HR175A39/CP bulbs) as the light source. The solutions were placed in quartz tubes (10 mL) on a turntable under the lamps. The test tubes were situated at 30° from normal. The photolyses were conducted at ambient temperature. Small sample aliquots were removed for analysis at specific time intervals. The aliquots were analyzed via HPLC chromatography with a Supelco C_{18} (150 x 4.6 mm, 5μm particle size) column and a mobile phase consisting of acetonitrile and pH 3 acetate buffer at a mixture sufficient to separate all the analyzed peaks. The flow rate was 1.0 mL/min and the detection was accomplished via absorbance (λ = 250 nm) or fluorescence specific to the investigated compound. The decay rates were analyzed according to steady-state assumptions of •OH with the solution ($[•OH]_{ss}$). Formation of product peaks were converted to concentrations based on HPLC calibration experiments for each investigated compound. Each photolysis solution (5 mL) contained 5.00 mM $NaNO_2$, 100 μM benzene, and a concentration of BPA within the range 1.2 – 0.05 mM. A concentration of BPA was determined so that the observed growth rate was within an order of magnitude of the reference compound according to competition kinetic analysis (discussed further below). Acetonitrile was used as a cosolvent to ensure

solubility throughout the course of the photolysis. Direct photodegradation experiments were identical to the previous solutions with the exception being the absence of $NaNO_2$. Singlet oxygen control experiments were conducted in the presence of 100 μM perinaphthenone and 100 μM furfuryl alcohol.

Results and Discussion

Synthesis of 4'-substituted-2-biphenylcarboxylic acids

The BPA derivatives were synthesized using a ligandless Suzuki-Miyaura coupling under mild aqueous conditions (Scheme 5.2).[68] The reaction conditions were chosen due to their ease in execution, despite the inherent low stability of catalytic systems within aqueous ligandless coupling reactions. The low stability was observed by the low product yields for the more hydrophobic boronic acids (R = ^{t}Bu and Cl) as seen in Scheme 5.2. Another interesting result was the low yield acquired during the synthesis of NMe_2-BPA. In their initial studies, Korolev and Bumagin never reported a coupling

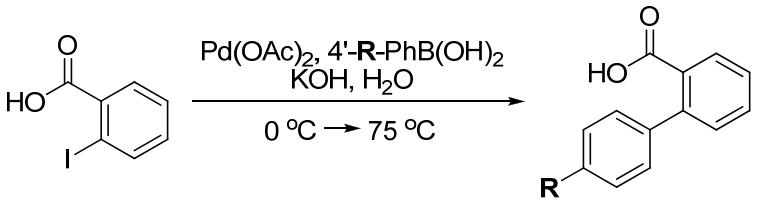

R = Me (78)
^{t}Bu (25)
MeO (91)
NMe_2 (9)
Cl (27)

Scheme 5.2. Synthesis of 4'-substituted-2-biphenylcarboxylic acids.

Percent yield are given in parentheses.

reaction involving a NMe_2-substituent, but due to the broad range of substrates investigated it was hypothesized that the NMe_2-derivative would behave similarly to the MeO-derivative.[68] Nevertheless, enough NMe_2-BPA was isolated to characterize its optical and chemical reactivity.

As seen in Scheme 5.2, the coupling conditions were utilized to synthesize only five of the proposed eight BPA derivatives. The parent compound, 2-biphenylcarboxylic acid (i.e. H-BPA), and CF_3-BPA were commercially available. The remaining derivative, HO-BPA, was synthesized from MeO-BPA via an acid-catalyzed hydrolysis of the methyl ether functionality (Scheme 5.3). Despite the increased synthetic sequence, the overall yield over the two steps was satisfactory.

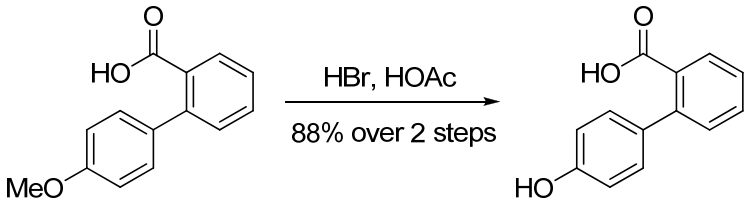

Scheme 5.3. Synthesis of 4'-hydroxy-2-biphenylcarboxylic acid (HO-BPA)

Synthesis of 3'-benzocoumarins

The synthesis of the 3'-substituted-BZC derivatives was initially proposed to undergo a multi-step synthesis based on the retrosynthetic analysis in Scheme 5.4. The desired 3'-substituted-BZC derivative was envisioned to come from the acid-catalyzed hydrolysis of a 2'-MeO-2-biphenylcarboxylic acid, which in turn was synthesized from the Suzuki-Miyaura coupling of commercially available 2-iodobenzoic acid and the

independently synthesized boronic acid, ***1***. The synthesis of ***1*** was envisioned to proceed from a lithium-halogen exchange of the corresponding bromobenzene trapped by a boron electrophile. The bromobenzene would be generated via a Barton decarboxylation with the phenyl radical trapped by a bromine radical source, $CBrCl_3$.[69-73] The 2-MeO-benzoic acid intermediate would be easily obtained by selective protection of the phenyl-hydroxyl functionality on a range of commercially available salicylic acids.

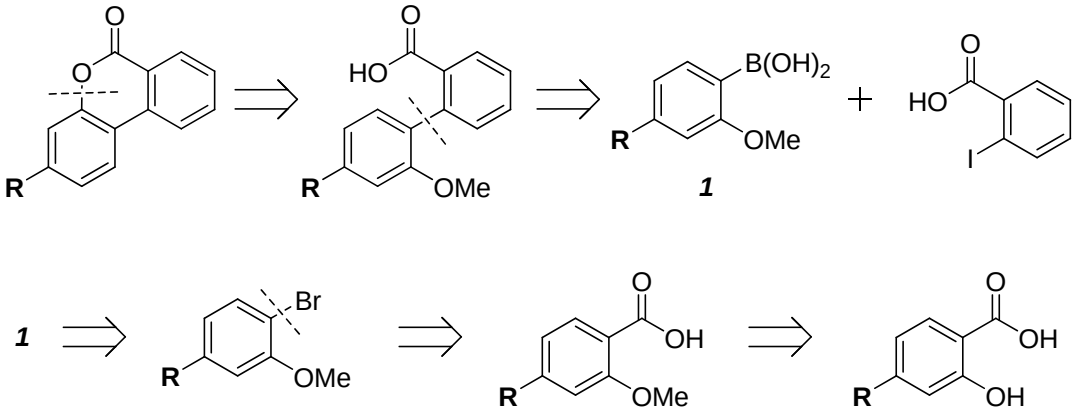

Scheme 5.4. Retrosynthetic analysis of 3'-substituted benzocoumarins I.

With a synthetic strategy in hand, the commercially available salicylic acid derivatives were globally protected with dimethyl sulfate and then the methyl esters were saponified to yield the desired 2-MeO-benzoic acid derivatives (Scheme 5.5). The NMe_2-derivative gave poor yield despite the mild reaction conditions and this initial set-back was further compounded with the complete degradation of the NMe_2-derivative under the Barton decarboxylation conditions to form the corresponding bromobenzene. All of the derivatives prepared showed poor to moderate yields attributed to the harsh reaction conditions and the inefficient radical decarboxylation/bromine radical trap.

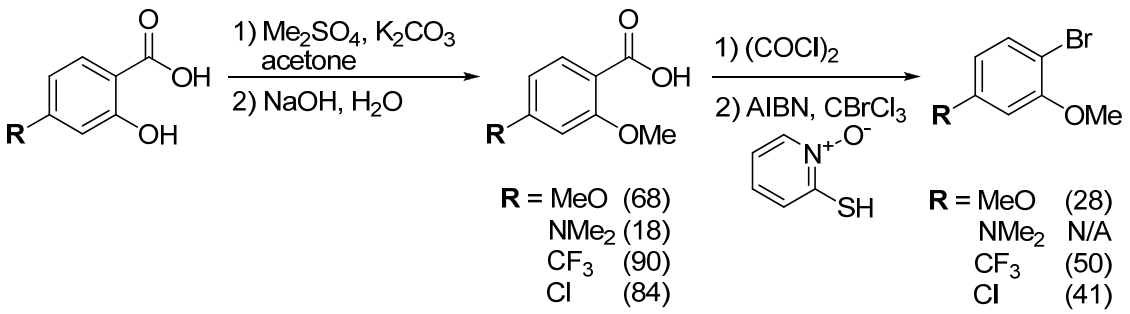

Scheme 5.5. Synthesis of 2-methoxy-bromobenzenes.
Percent yield are given in parentheses.

The remaining 2-MeO-bromobenzene derivatives were subjected to lithium-halogen exchange to form the intermediate phenyl lithium anion that was trapped by trimethylborate (Scheme 5.6). Hydrolysis upon workup yielded the desired 2-MeO-phenylboronic acids in moderate to good yield. The CF_3-derivative gave poor yield part due to degradation of the CF_3- moiety in the presence of *tert*-butyl lithium. The MeO-derivative also gave poor yield, but that was attributed to poor recrystallization; the crude yield of the MeO-derivative was >90%. Utilizing the same aqueous ligandless Suzuki-Miyaura coupling procedure, the desired 2'-MeO-2-BPA derivatives were synthesized in poor yield due to the sterically crowded reaction center and poor electronic compatibility between the boronic acid and iodoarene. For example, the CF_3- and Cl-derivatives yielded only starting material due to the electron-poor nature of the boronic acid involved in the Suzuki-Miyaura coupling.

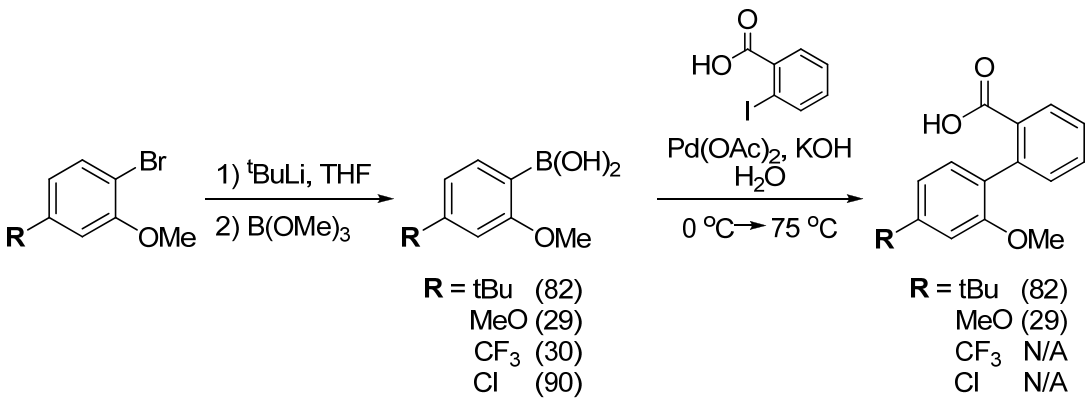

Scheme 5.6. Synthesis of 2'-methoxy-4'-substituted-2-biphenylcarboxylic acids. Percent yield are given in parentheses.

Despite the poor yield during the synthesis of the 2'-MeO-2-BPA intermediates, the final step of the synthetic strategy was still investigated (Scheme 5.7). Both ^{t}Bu-BZC and HO-BZC were isolated in good yield. The HO-BZC derivative was synthesized from the corresponding 2', 4'-dimethoxy-2-BPA, but the MeO-BZC derivative was synthesized from the HO-BZC in near quantitative yield by dimethyl sulfate.

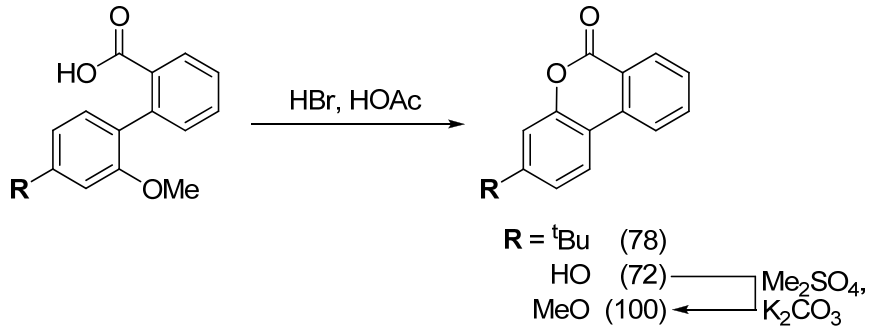

Scheme 5.7. Acid-catalyzed hydrolysis to form 3'-substituted-benzocoumarins. Percent yield are given in parentheses.

The inability to generate the NMe_2-, Cl-, CF_3-, and Me-BZC derivatives by the proposed synthetic strategy in Scheme 5.4 led to renewed effort towards efficiently synthesizing the BZC derivatives from the corresponding BPA derivatives (Scheme 5.8). The initial synthetic strategy utilized a readily hydrolyzed 2'-MeO- functionality that lead to the intramolecular lactonization necessary to complete the desired BZCs. There were few examples in the literature that were able to affect the same cyclization. The use of a 2'-fluoride functionality would result in the same cyclization through an intramolecular S_N2' mechanism, but installation of the fluoride would be troublesome at every stage of the synthetic sequence.[74] Oxidation of the electron-rich aromatic ring at the *ortho*-position could be accomplished, but most methods used harsh conditions that would degrade the 4'-substituents.[75] The most promising method involved the formation of an oxygen-centered radical on the carboxylic acid functionality via (diacetoxyiodo)arenes that would undergo rapid intramolecular radical-mediated cyclization.[64]

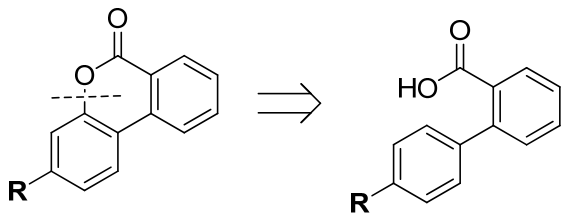

Scheme 5.8. Retrosynthetic analysis of 3'-substituted benzocoumarins II.

The new synthetic strategy was more efficient than the previously one and resulted in the synthesis of the remaining BZC derivatives (Scheme 5.9). The BZC derivatives were isolated in good to excellent yield except for NMe_2-BZC. The bis-(trifluoroacetoxy)-iodobenzene reagent readily demethylated the starting material NMe_2-BPA as seen in crude ^1H NMR and ESI spectrometry. CF_3-BPA also underwent degradation in the presence of the iodobenzene, but to a lesser extent as noted by the lower yield of CF_3-BZC (Scheme 5.9).

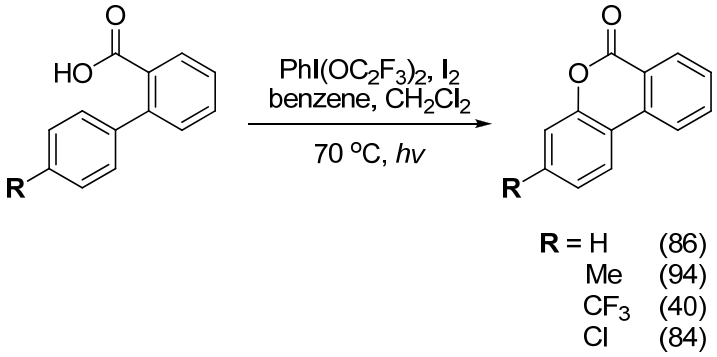

Scheme 5.9. Bis-(trifluoroacetoxy)-iodobenzene mediated cyclization of 4'-substituted biphenylcarboxylic acids. Percent yield are given in parentheses.

A milder iodobenzene derivative, (diacetoxy)-iodobenzene, was investigated and found to be more suitable to the synthesis of NMe_2-BZC when used at ambient temperature instead of at reflux temperature (Scheme 5.10). The yield was poor, but enough material was isolated to further investigate the optical properties and chemical reactivity of the eight proposed BZC derivatives.

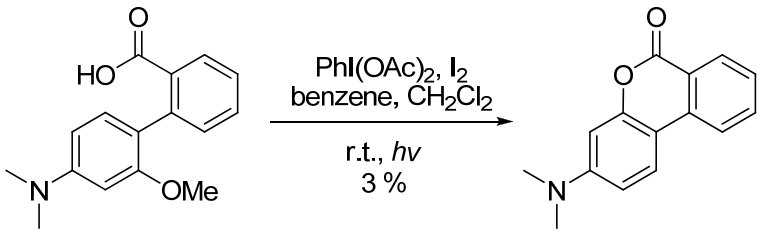

Scheme 5.10. Synthesis of 3'-dimethylamino-benzocoumarin

Optical properties of BPA and BZC derivatives

The use of the investigated compounds during the photochemical production of •OH makes the understanding of their optical properties a priority. Any light absorbed by the BPA, or BZC, derivatives would interfere with the photochemical production capacity of the solutions they would be used to investigate. Therefore, it was important to determine their molar absorptivites according to the Beer-Lambert law (equation 1)

$$A = \log\frac{I_0}{I} = \varepsilon b[S] \qquad (1)$$

where A is the absorbance of light, ε is the molar absorptivity of the absorbing species of a specific concentration, $[S]$, and b is the path length of light through the absorbing solution. The light absorption across the UV-Vis spectrum by the corresponding compound was plotted against its concentration within a 1 cm quartz cuvette according to equation 1. Only absorbance values < 2.0 and linear relationships with R^2 > 95% were used in the calculation of ε. The absorbance plots at varied concentration and the corresponding molar absorptivity plots for the 16 compounds investigated are shown in Figures 5.1-5.16.

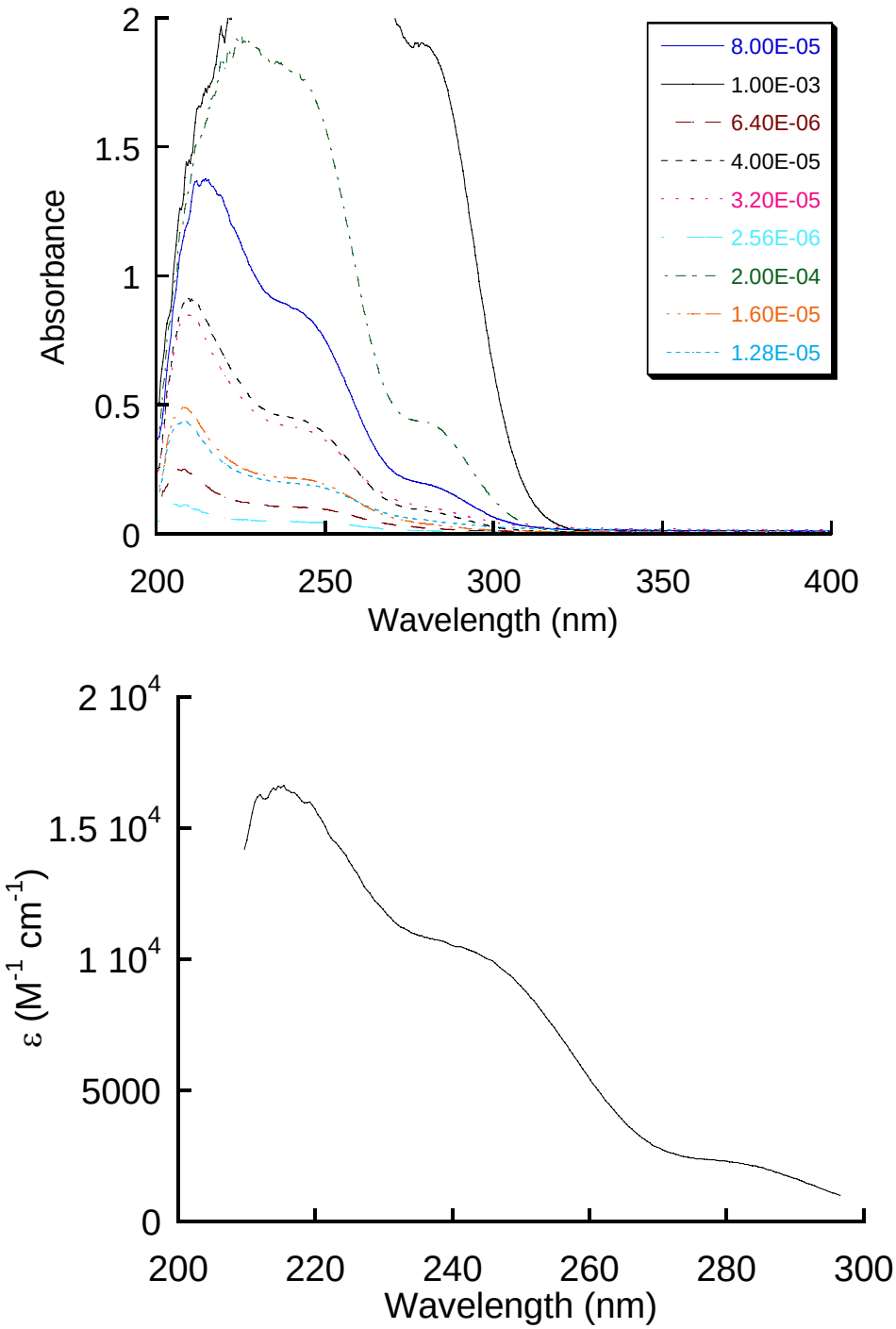

Figure 5.1. Molar absorptivity plots of 2-biphenylcarboxylic acid (H-BPA) in ethanol. Values in the legend indicate concentration in M.

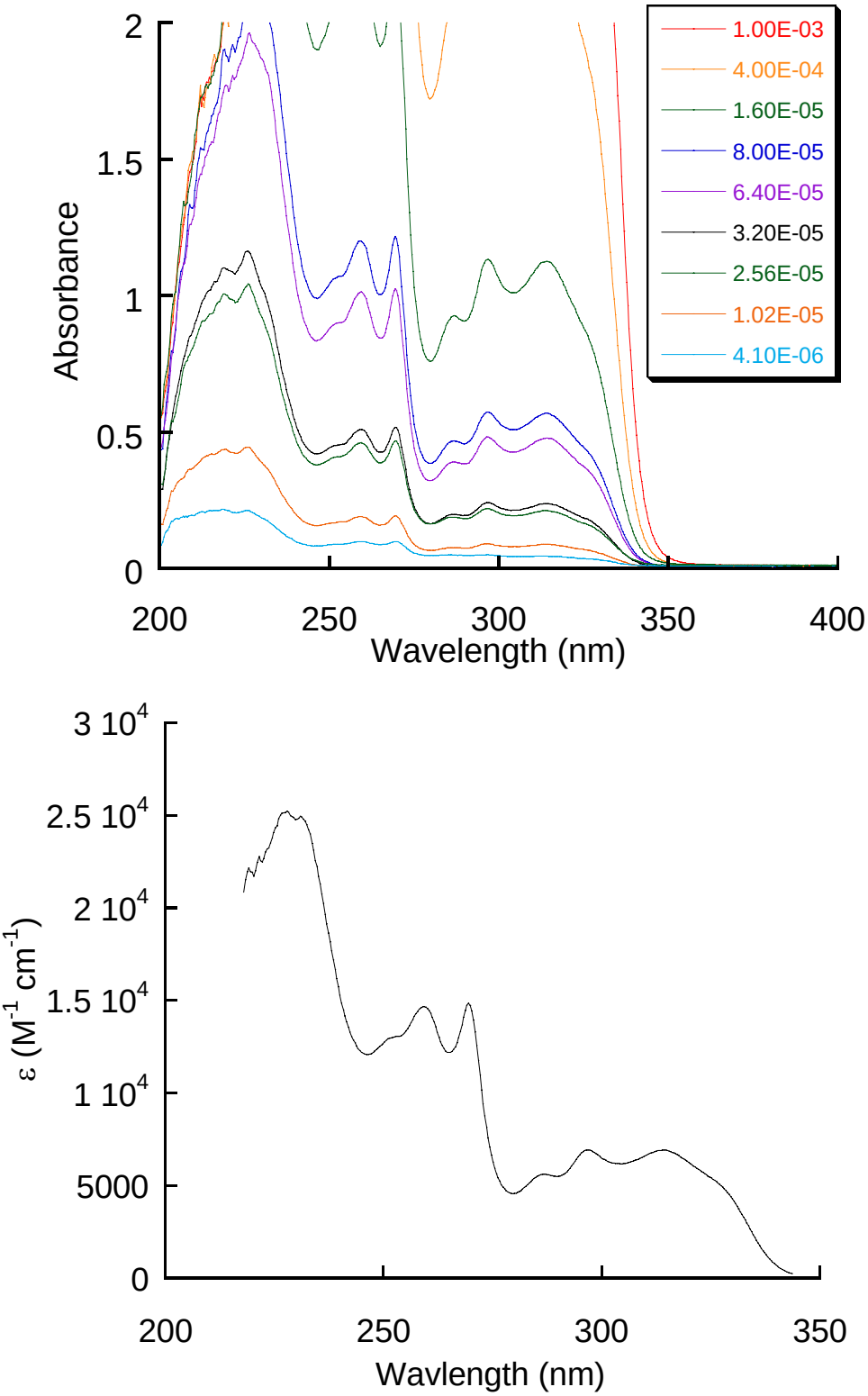

Figure 5.2. Molar absorptivity plots of 3,4-benzocoumarin (H-BZC) in ethanol. Values in the legend indicate concentration in M.

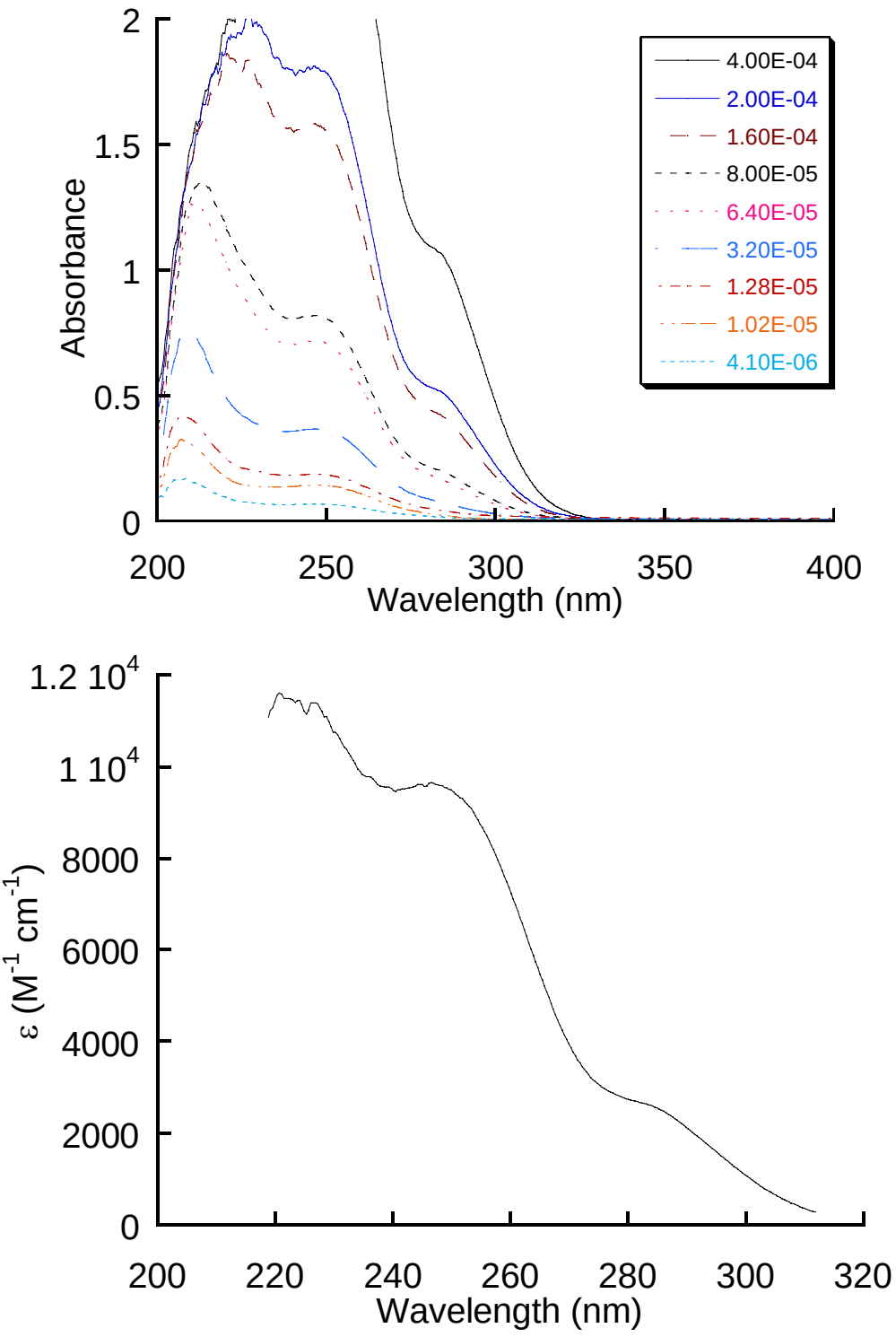

Figure 5.3. Molar absorptivity plots of 4'-methyl-2-biphenylcarboxylic acid (Me-BPA) in ethanol. Values in the legend indicate concentration in M.

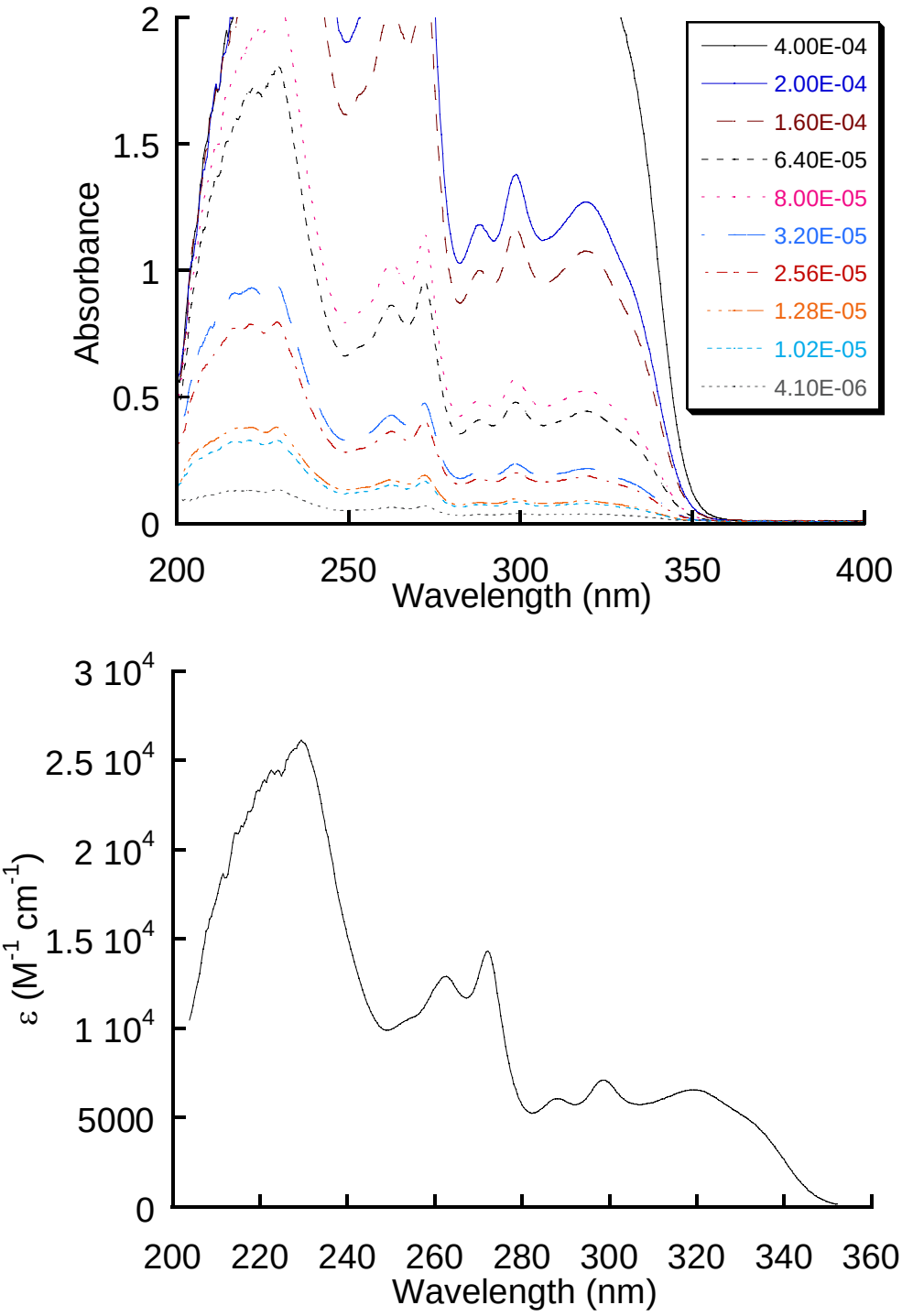

Figure 5.4. Molar absorptivity plots of 3'-methyl-benzocoumarin (Me-BZC) in ethanol. Values in the legend indicate concentration in M.

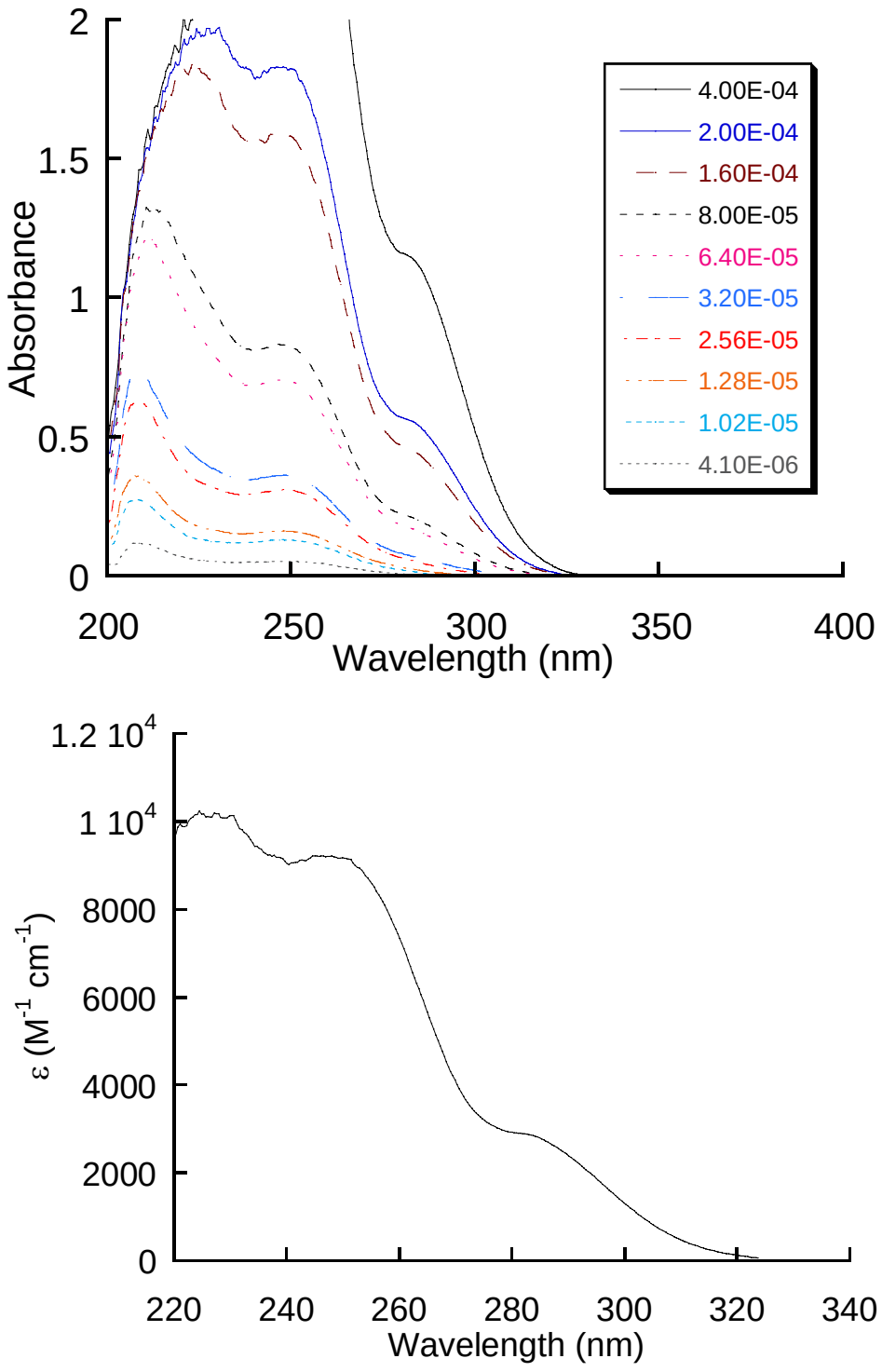

Figure 5.5. Molar absorptivity plots of 4'-*tert*-butyl-2-biphenylcarboxylic acid (^{t}Bu-BPA) in ethanol. Values in the legend indicate concentration in M.

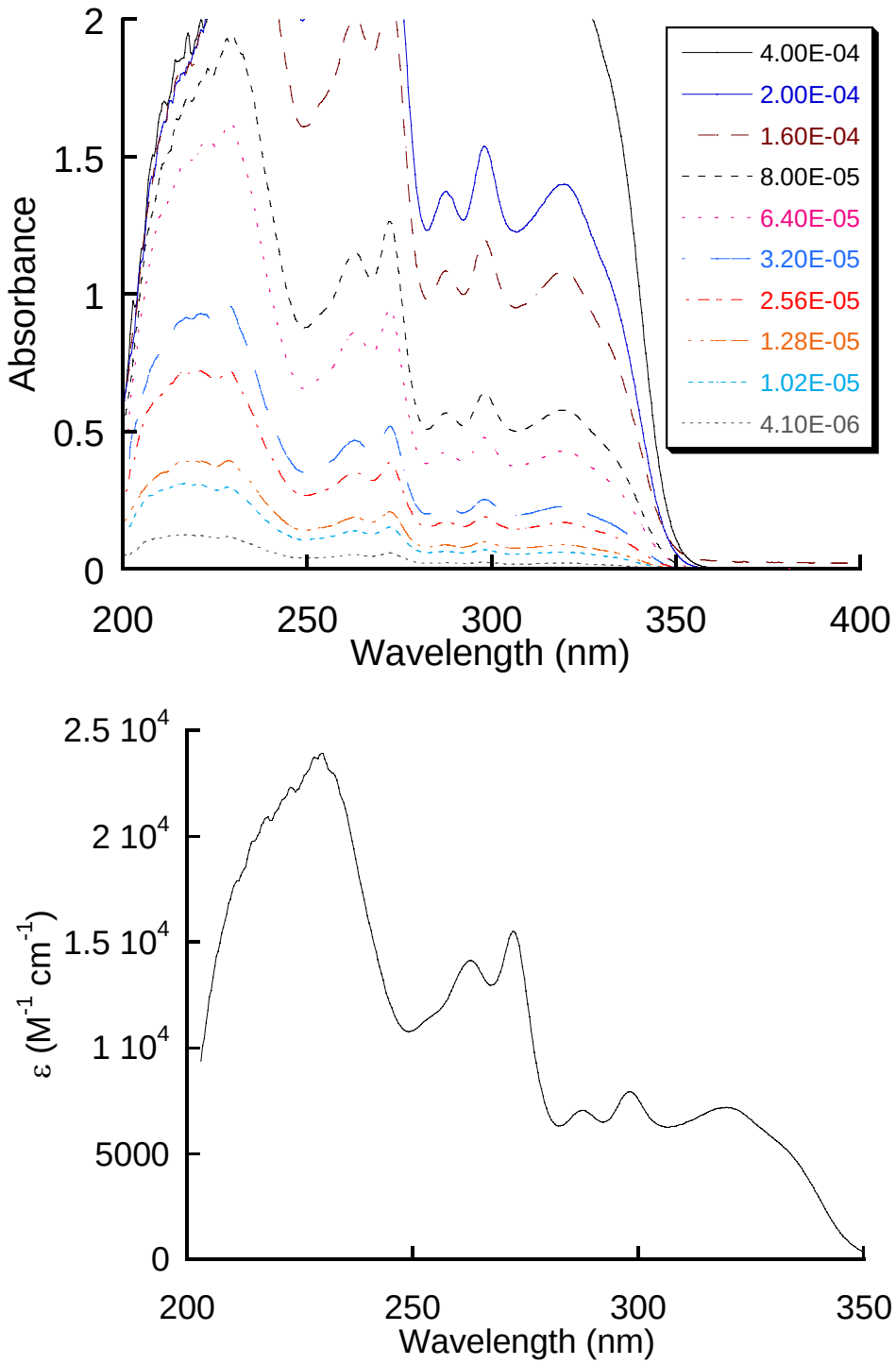

Figure 5.6. Molar absorptivity plots of 3'-*tert*-butyl-benzocoumarin (^{t}Bu-BZC) in ethanol. Values in the legend indicate concentration in M.

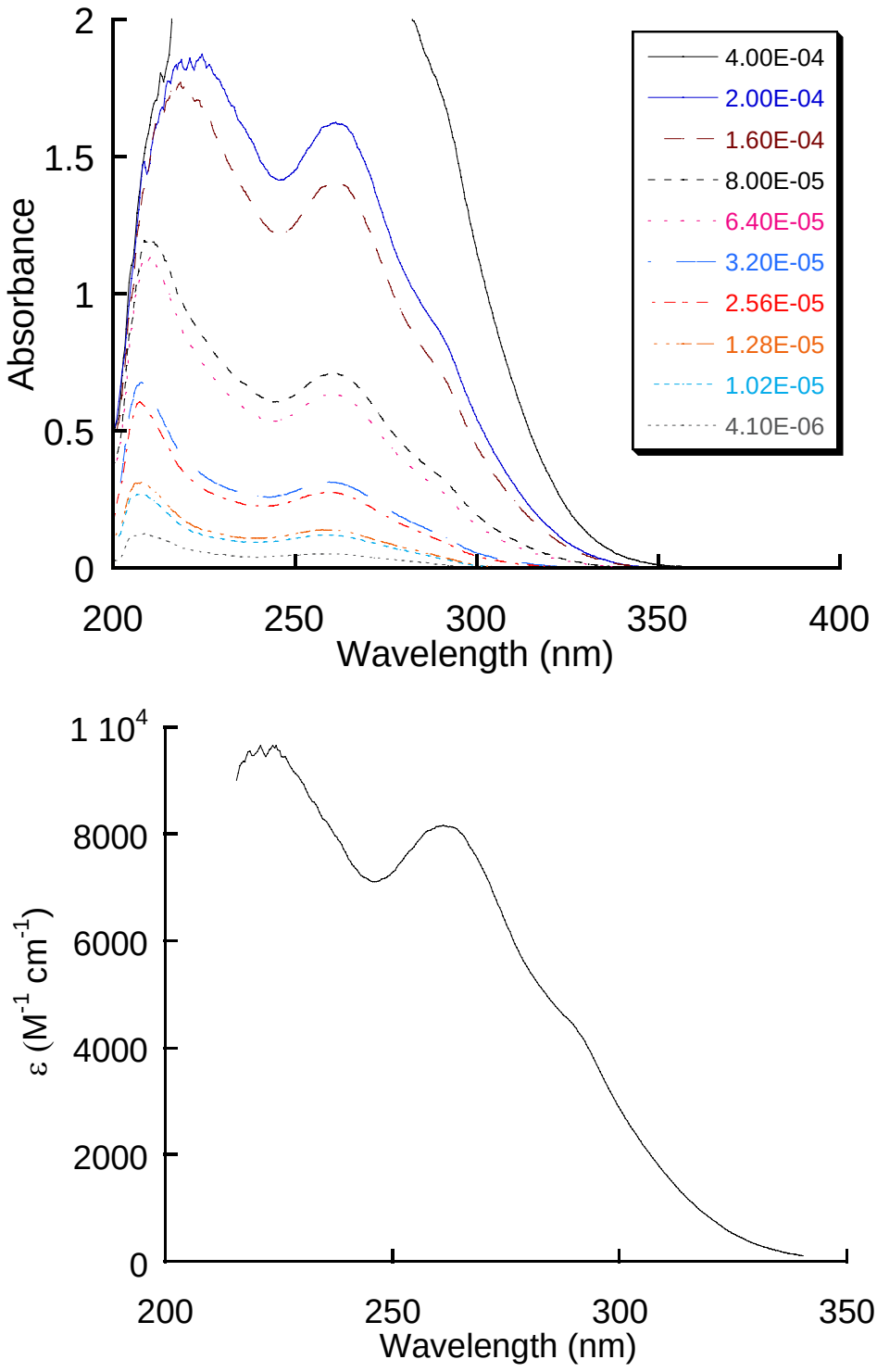

Figure 5.7. Molar absorptivity plots of 4'-hydroxy-2-biphenylcarboxylic acid (HO-BPA) in ethanol. Values in the legend indicate concentration in M.

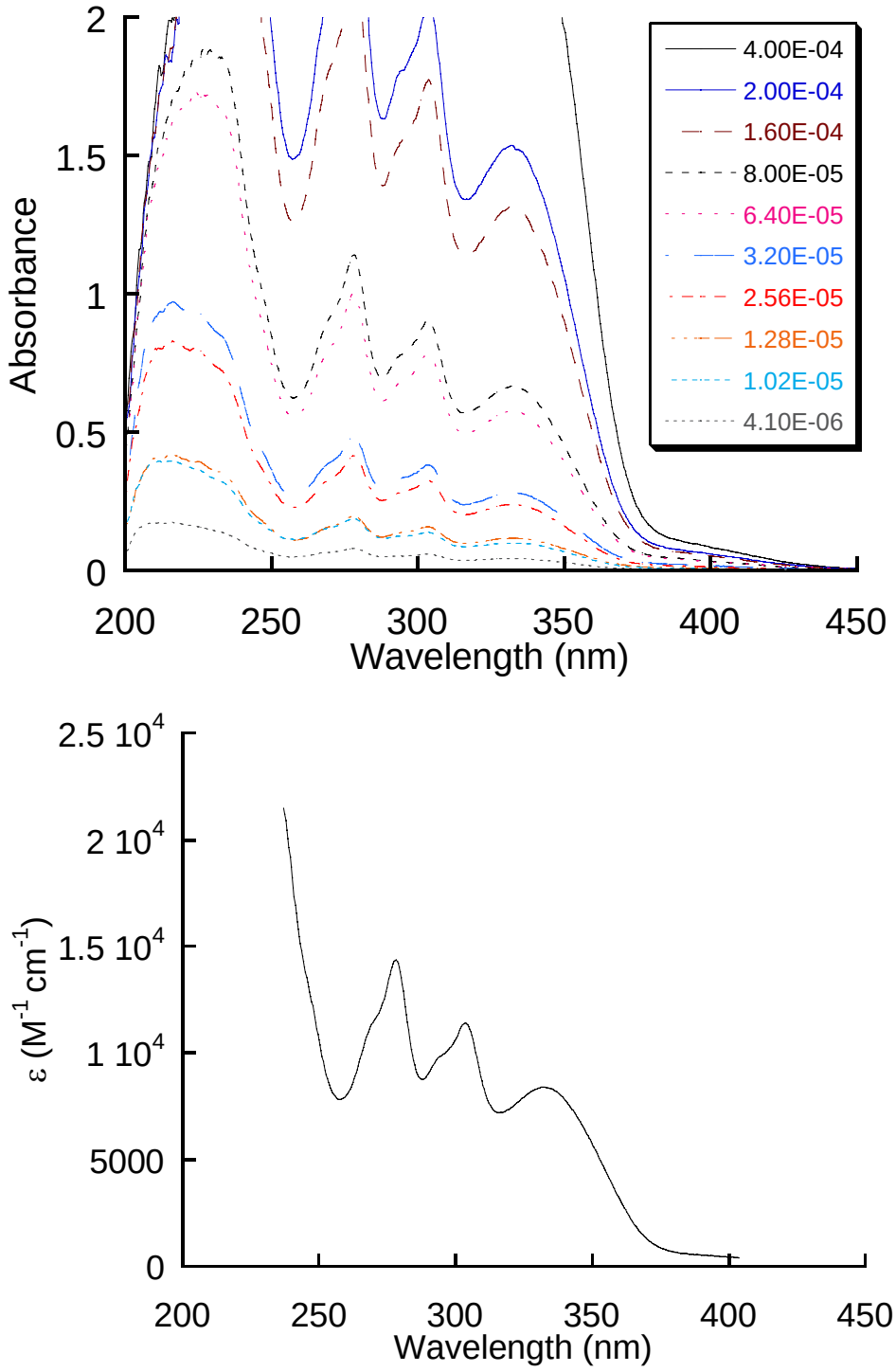

Figure 5.8. Molar absorptivity plots of 3'-hydroxy-benzocoumarin (HO-BZC) in ethanol. Values in the legend indicate concentration in M.

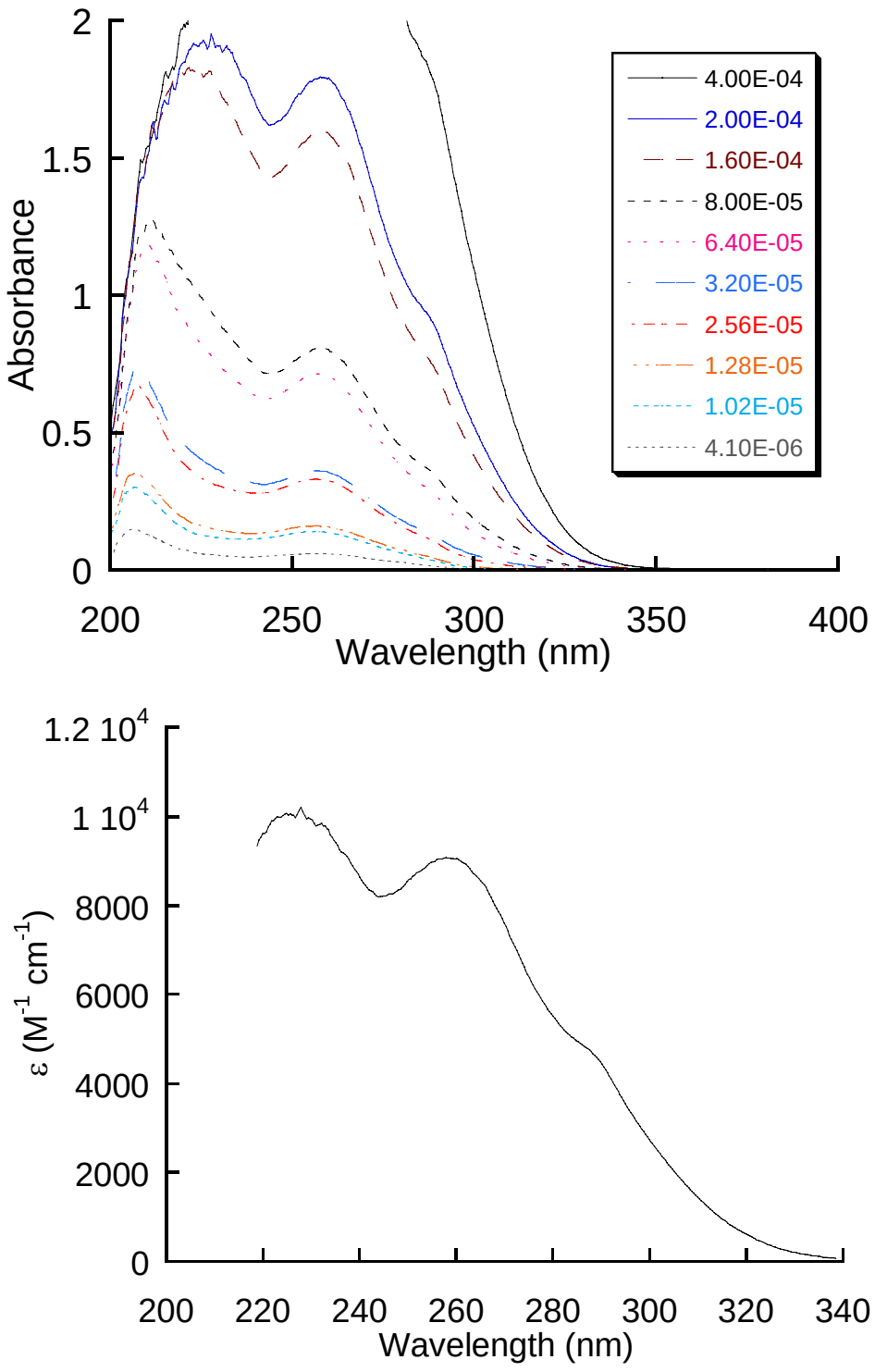

Figure 5.9. Molar absorptivity plots of 4'-methoxy-2-biphenylcarboxylic acid (MeO-BPA) in ethanol. Values in the legend indicate concentration in M.

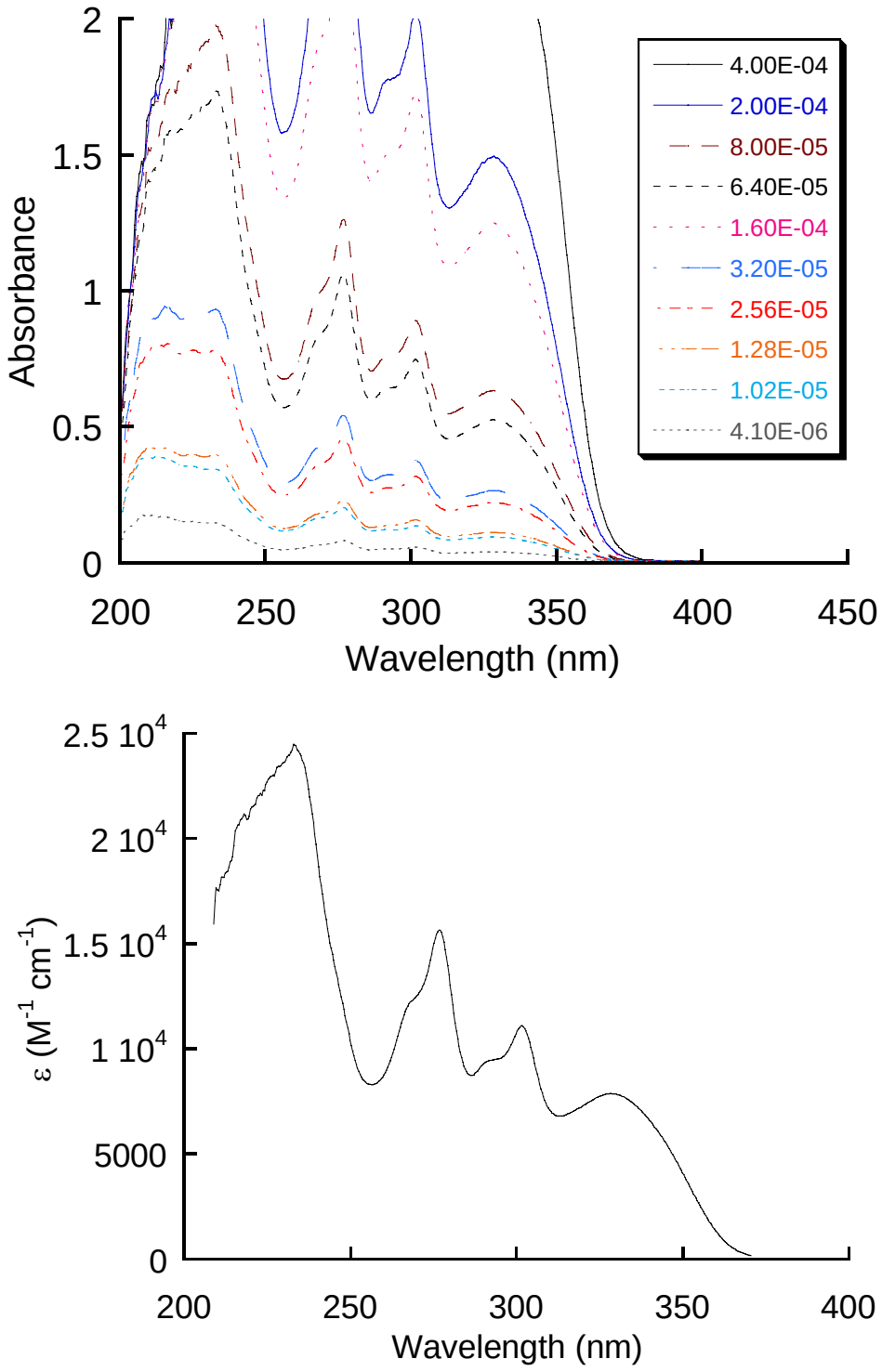

Figure 5.10. Molar absorptivity plots of 3'-methoxy-benzocoumarin (MeO-BZC) in ethanol. Values in the legend indicate concentration in M.

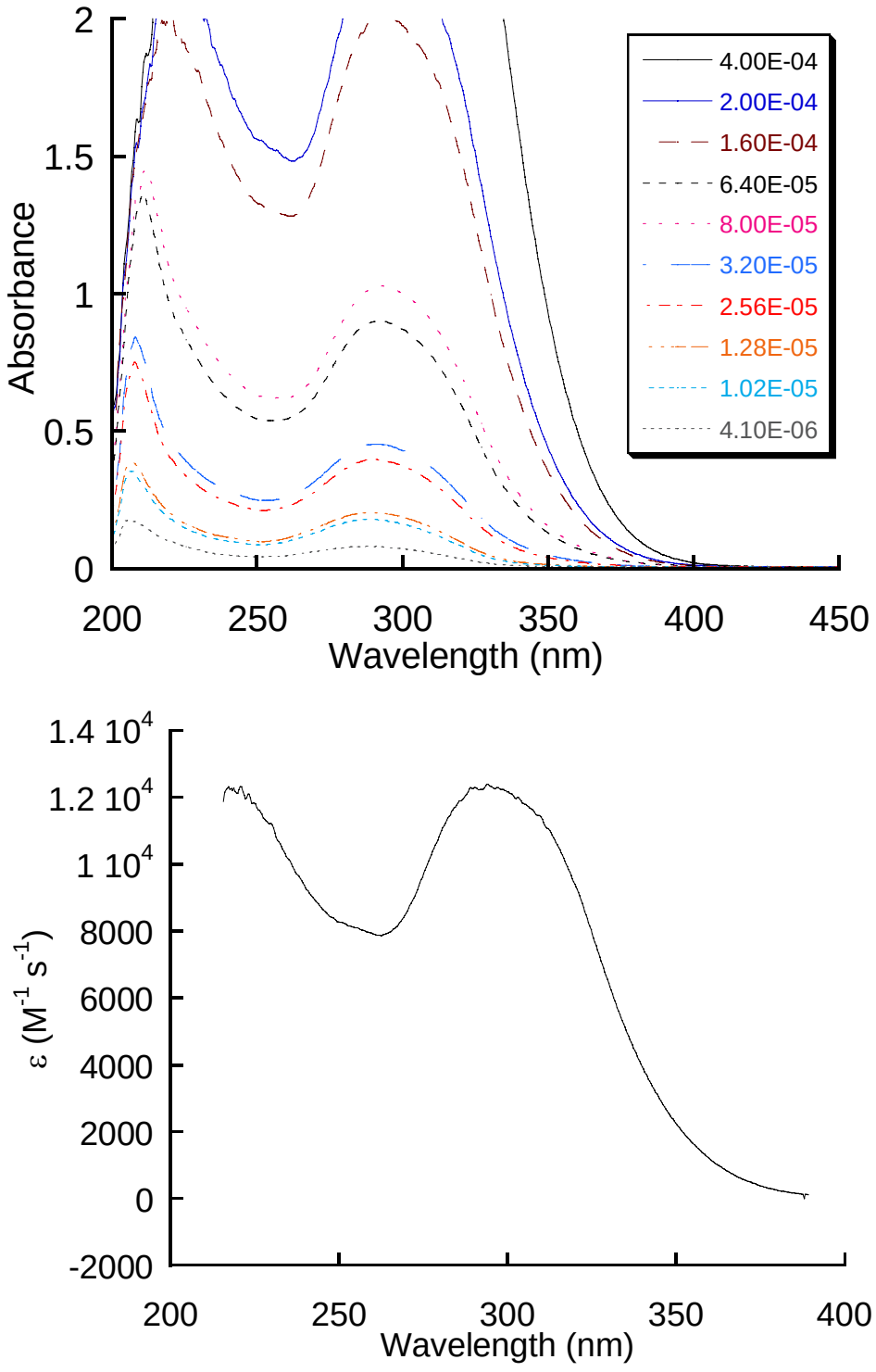

Figure 5.11. Molar absorptivity plots of 4'-dimethylamino-2-biphenylcarboxylic acid (NMe_2-BPA) in ethanol. Values in the legend indicate concentration in M.

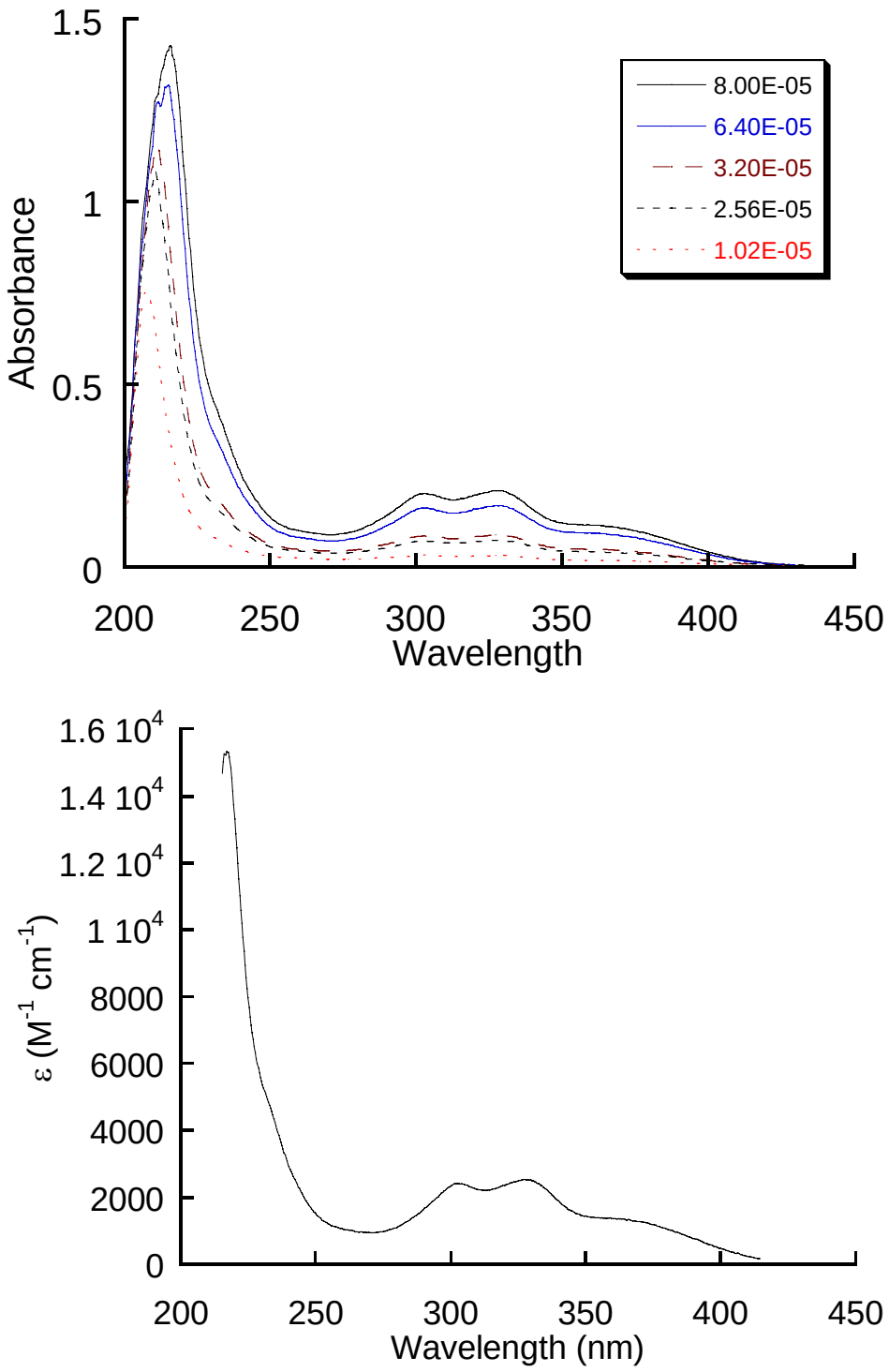

Figure 5.12. Molar absorptivity plots of 3'-dimethylamino-benzocoumarin (NMe_2-BZC) in ethanol. Values in the legend indicate concentration in M.

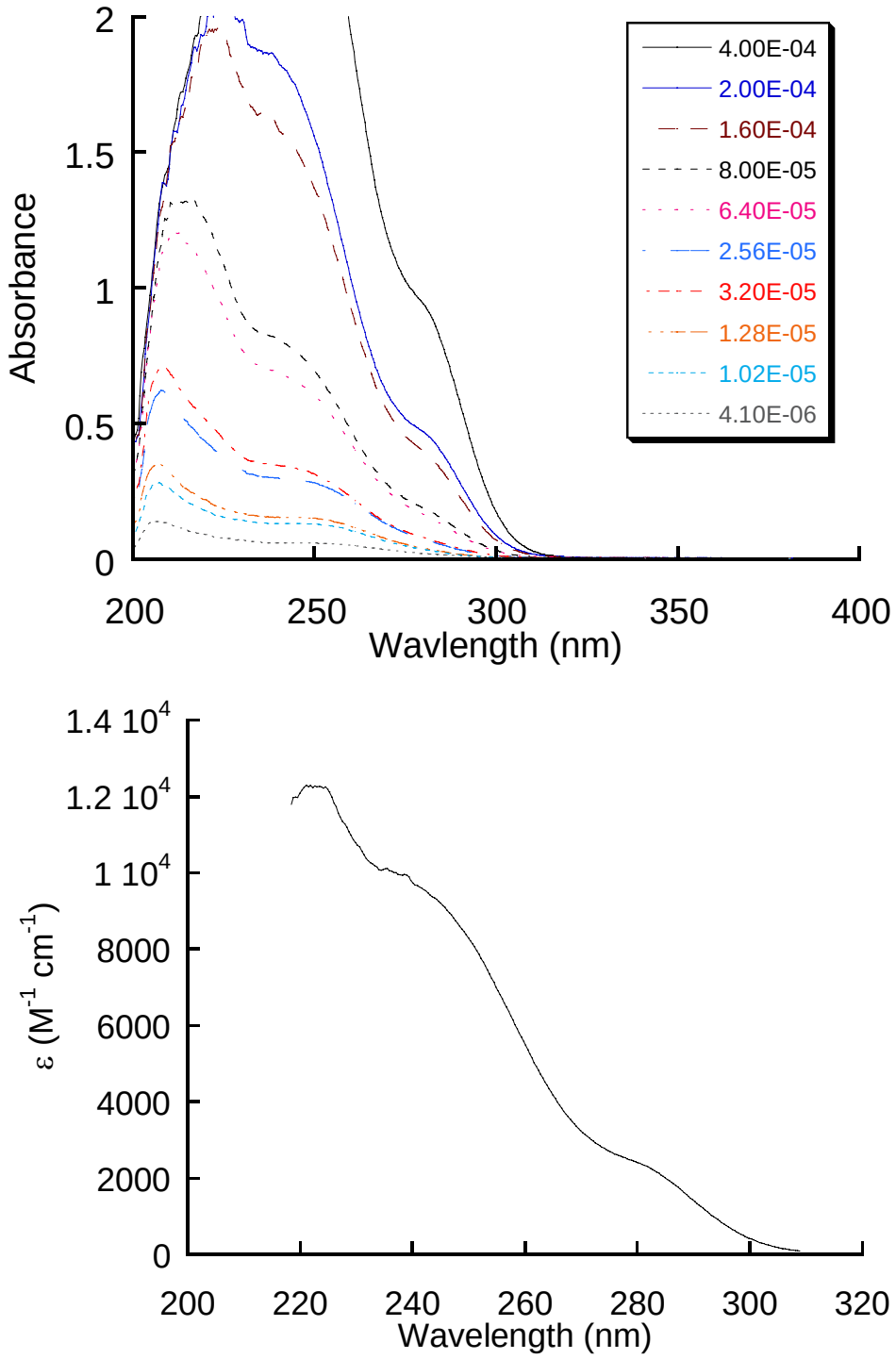

Figure 5.13. Molar absorptivity plots of 4'-trifluoromethyl-2-biphenylcarboxylic acid (CF_3-BPA) in ethanol. Values in the legend indicate concentration in M.

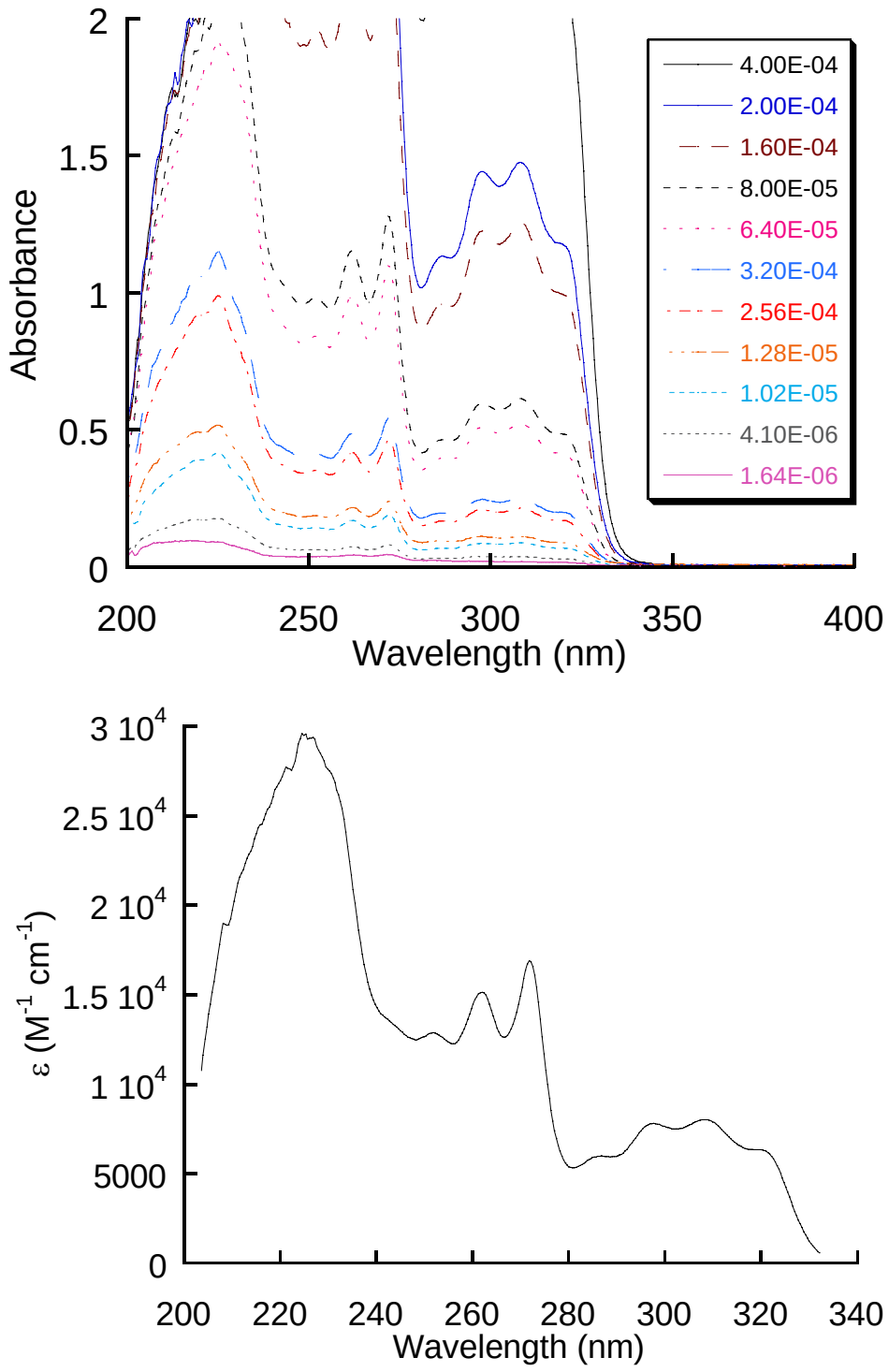

Figure 5.14. Molar absorptivity plots of 3'-trifluoromethyl-benzocoumarin (CF_3-BZC) in ethanol. Values in the legend indicate concentration in M.

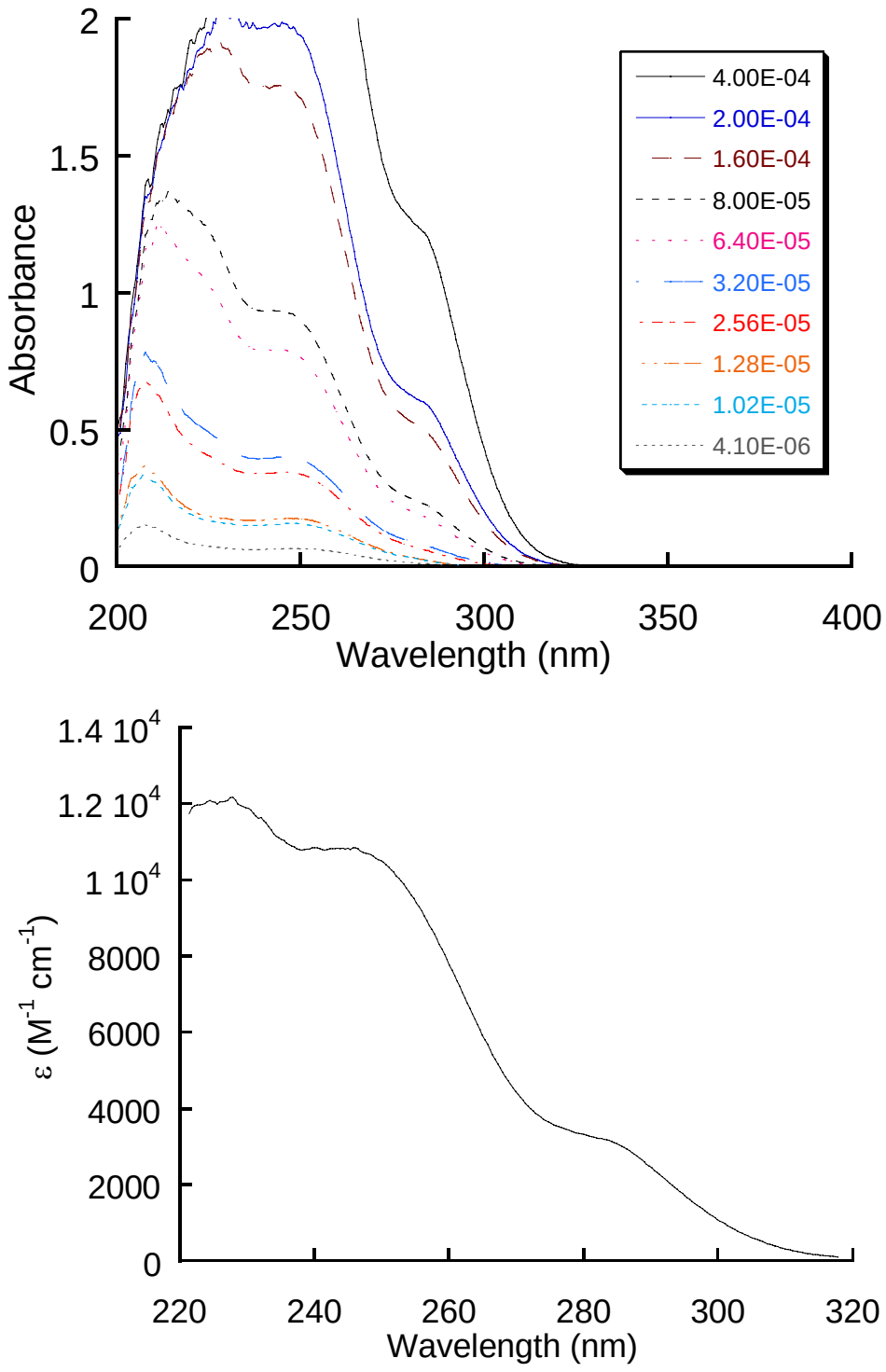

Figure 5.15. Molar absorptivity plots of 4'-chloro-2-biphenylcarboxylic acid (Cl-BPA) in ethanol. Values in the legend indicate concentration in M.

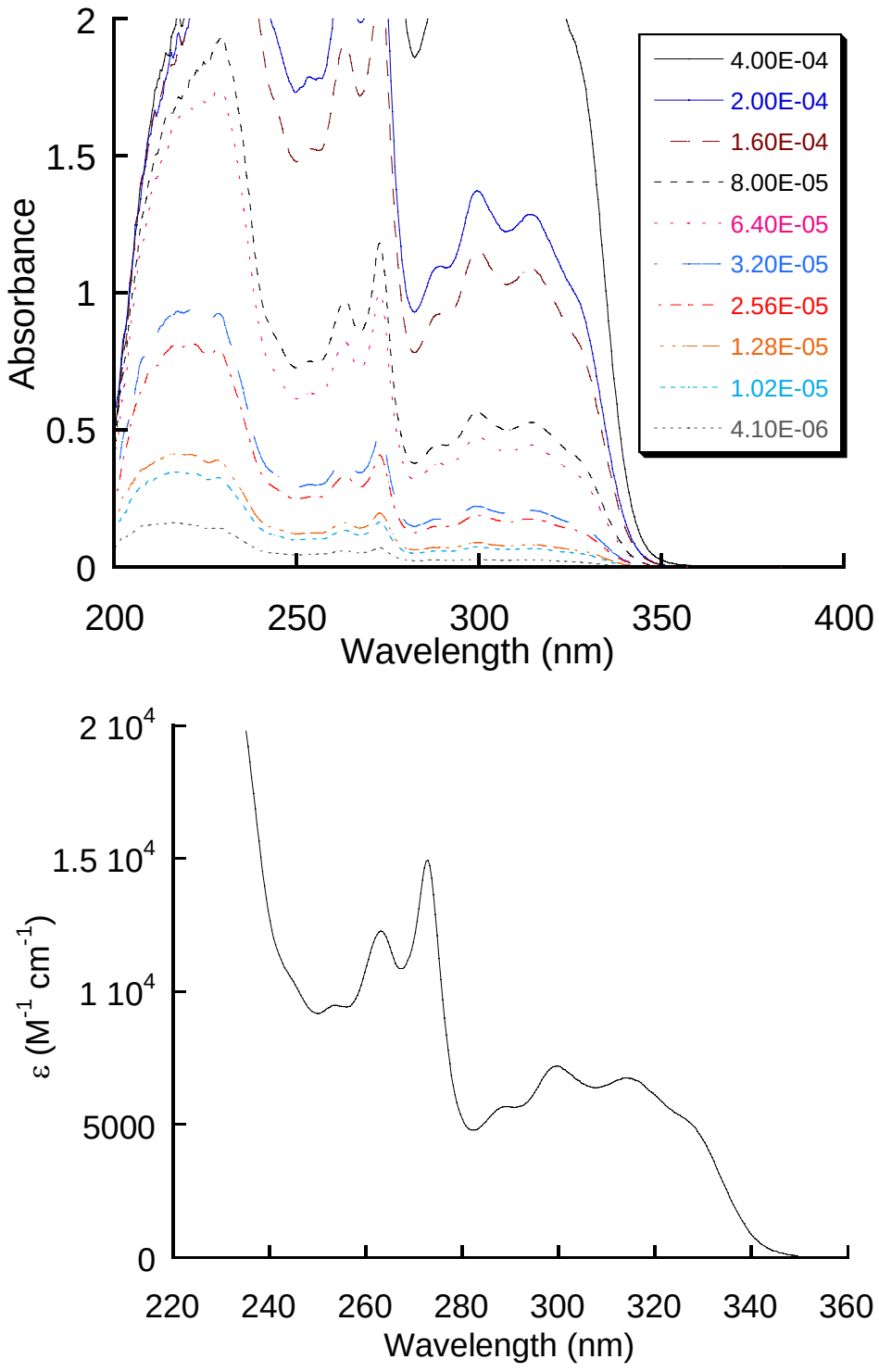

Figure 5.16. Molar absorptivity plots of 3'-chloro-benzocoumarin (Cl-BZC) in ethanol. Values in the legend indicate concentration in M.

The BZCs displayed a red shift in absorbance values compared to their corresponding BPAs. The BPAs generally had an absorbance maxima near λ = 280 nm, where the BZCs had a broad absorbance maxima near λ = 320 nm. Most of the BPAs did not absorb light with λ > 350 nm, with the lone exception being NMe_2-BPA (Figure 5.11). The observation of NMe_2-BPA absorbing more red light may hinder its effectiveness as an environmental •OH probe due to direct degradation of the probe.

Fluorescence detection methods

The fluorescence properties of the eight BPAs (Figure 5.17) and the eight BZCs (Figure 5.18) were characterized within the polar, protic solvent ethanol in order to determine the ideal optical conditions for quantitative analysis. The observed maximum wavelengths for the excitation and emission spectra of the investigated compounds are listed in Table 5.1. The aliphatic (H-, Me-, and ^{t}Bu-), electron-donating (NMe_2-, MeO-, HO-), and electron-withdrawing (CF_3- and Cl-) BZC derivatives display similar characteristics within each respective group (Figure 5.18.). All of the BPA derivatives display qualitatively similar excitation spectra with the main exception being NMe2-BPA which possesses a larger absorption maxima at λ = 291 nm. All of the compounds investigated display singular emission peaks within their spectra with the exception being CF_3-BZC, which displays a broad peak with two fluorescence maxima. This phenomenon has been seen in other CF_3-biphenyl molecules and corresponds to two electronic states capable of emitting visible photons.[76]

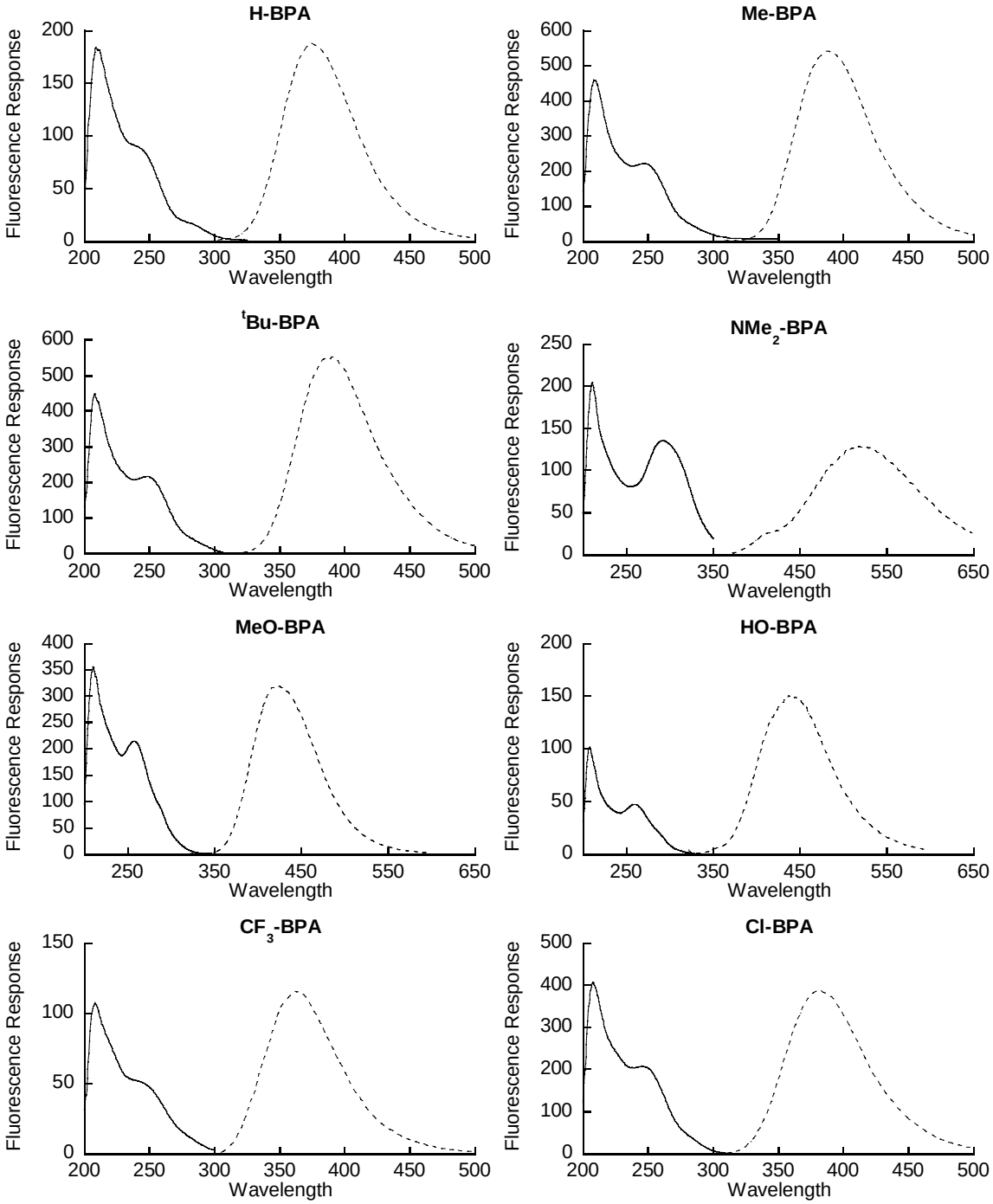

Figure 5.17. Fluorescence spectra of 4'-derivatized-2-biphenylcarboxylic acids in ethanol. Solid line indicates excitation spectra and dashed line indicates emission spectra. Wavelength was reported in nm.

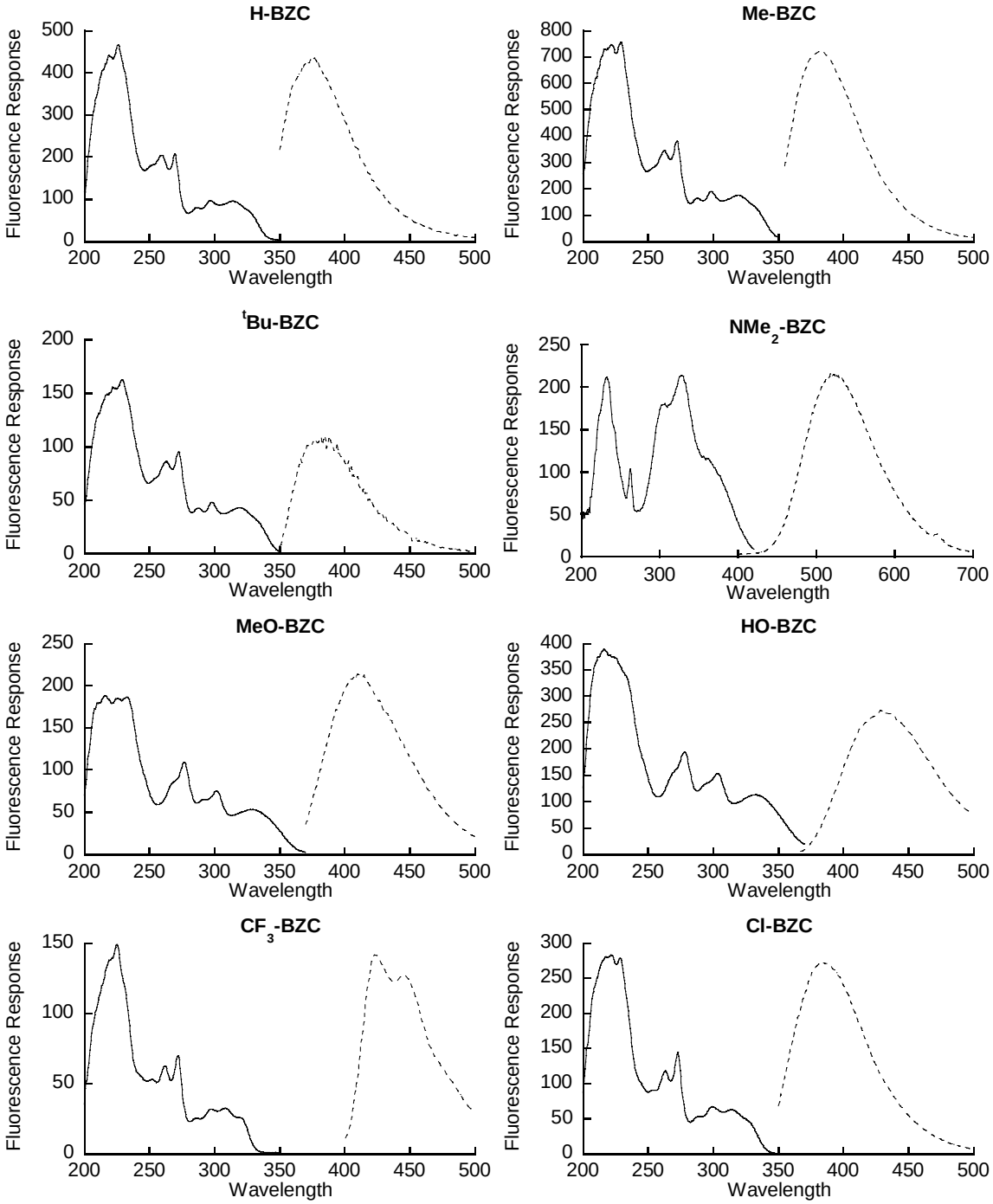

Figure 5.18. Fluorescence spectra of 3'-derivatized-benzocoumarins in ethanol. Solid line indicates excitation spectra and dashed line indicates emission spectra. Wavelength was reported in nm.

BPA	λ_{ex} (nm)	λ_{em} (nm)	$\Delta\lambda$ (nm)	HPLC response (M^{-1})[a]
H[a]	294	373	93	2.12×10^6
Me	300	389	104	1.75×10^6
^{t}Bu	304	389	105	1.00×10^6
NMe_2	291	523	232	**N/A**
MeO	314	419	132	3.43×10^6
HO[a]	318	435	155	2.08×10^6
CF_3	296	363	83	1.64×10^5
Cl	302	381	96	6.03×10^5
benzene[77]	214	280	66	1.36×10^6
BZC				
H	339	375	48	1.01×10^8
Me	346	382	62	6.79×10^8
^{t}Bu	348	381	61	2.74×10^8
NMe_2	328	526	198	2.57×10^8
MeO	370	410	81	9.12×10^9
HO	366	409	77	2.53×10^7
CF_3	333	368	61	4.62×10^7
Cl	343	385	71	3.11×10^8
phenol[39]	270	298	28	8.30×10^8

Table 5.1. Fluorescence properties and HPLC response values for the BPA and BZC derivatives in ethanol. Values were calculated from the excitation and emission spectra in Figures 5.1 – 5.16. [a]The HPLC response corresponds to the fluorescence detection values at the corresponding λ_{ex} and λ_{em}, except for H-BPA and HO-BPA, where the response values are based on absorbance detection at λ = 250 nm.

The BPA derivatives possess increased Stokes shifts ($\Delta\lambda$) in comparison to their corresponding BZC derivatives. This loss in energy between absorbed and emitted photons from the excited BPA derivatives is attributed to the ability of the intramolecular charge transfer (ICT) intermediate to twist around the axis of the aryl-aryl bond, resulting in a lower energy planar conformation in the excited state.[78] In comparison, the BZC derivatives are rigid and therefore display a decreased Stokes shift. The rigidity leads to an increase in fluorescence yield due to the decreased amount of energy loss pathways available to the BZCs in comparison to the BPAs.[79] The BZCs display a 2-3 order of magnitude enhancement in their HPLC fluorescence response over that of the BPAs. It is important to note that both H-BPA and HO-BPA displayed poor response to fluorescence detection and were subsequently analyzed by absorbance detection at λ = 250 nm.

The HPLC fluorescence response values for the BPA and BZC derivatives displayed in Table 5.1 were determined by analyzing solutions of varying concentration of either BPA or BZC at their respective wavelength excitation/emission pair. The fluorescence response was taken from the linear slope of the corresponding calibration plots (Figures 5.19-5.21). The HPLC response values across a concentration range of BPA derivatives are shown in Figure 5.19. As mentioned before, H-BPA and HO-BPA displayed poor HPLC fluorescent analysis and were subsequently analyzed by absorbance detection at λ = 250 nm. All of the compounds displayed linear behavior across the concentration range investigated. The linear HPLC fluorescence response across the investigated concentration range of the reference compound, benzene, is shown in Figure 5.20. The HPLC response values across a concentration range of BZC

derivatives, except MeO-BZC, are shown in Figure 5.21. The observed HPLC response was linear across the concentrations investigated. As noted in Table 5.1, MeO-BZC possesses over an order of magnitude greater fluorescence response than any of the other BZC derivatives, therefore it was plotted separately from the others (Figure 5.22). The linear HPLC response values across the investigated concentration of phenol, the product of benzene reacting with •OH, are also shown in Figure 5.22. With the analytical response values in hand, it was then possible to investigate the reactivity of the BPA derivatives with respect to •OH.

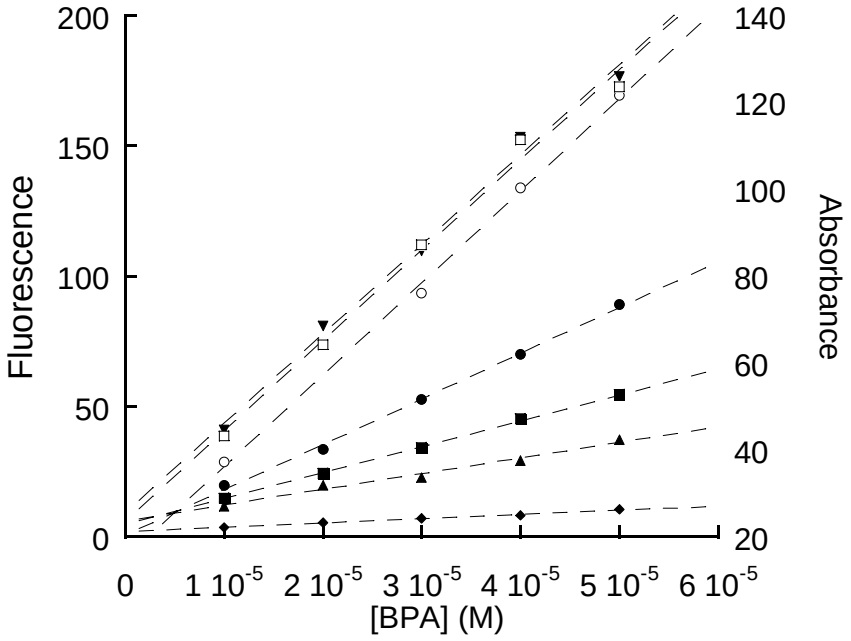

Figure 5.19. HPLC response calibration plot for H-BPA (○), Me-BPA(●), ^{t}Bu-BPA (■), MeO-BPA(▼), HO-BPA (□), CF_3-BPA(◆) and Cl-BPA(▲). Dashed line indicates linear fit. H-BPA and HO-BPA were detected via absorbance response and the remaining BPAs were detected via fluorescence response. Error bars indicate 95 % confidence interval. Fluorescence and absorbance values from Table 5.1 were used for the analysis of each BPA derivative.

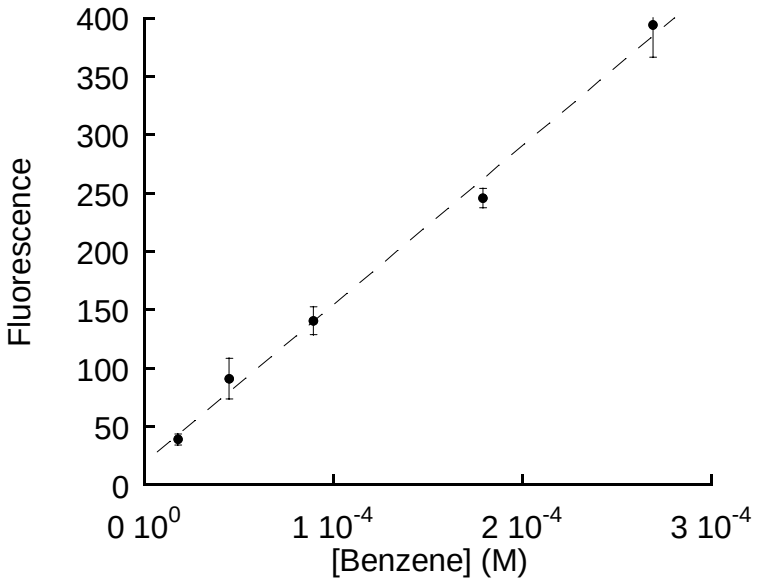

Figure 5.20. HPLC fluorescence response calibration plot for benzene. Dashed line indicates linear fit. Error bars indicate 95 % confidence interval. Fluorescence values from Table 5.1 were used during the analysis.

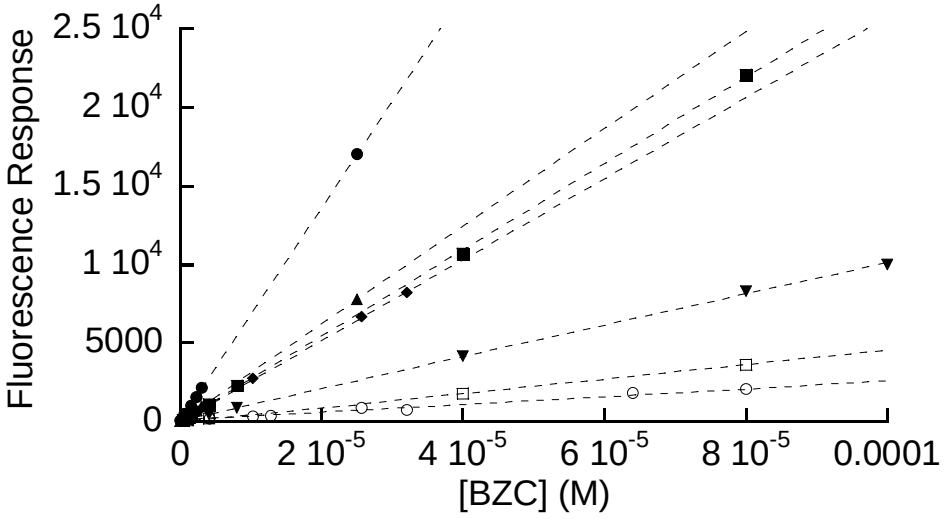

Figure 5.21. HPLC Fluorescence response calibration plot for H-BZC (▼), Me-BZC (●), ^{t}Bu-BZC (■), NMe_2-BZC (◆), HO-BZC (O), CF_3-BZC (□), and Cl-BZC (▲). Dashed line indicates linear fit. Error bars indicate 95 % confidence interval. Fluorescence values from Table 5.1 were used in the analysis for each BZC derivative.

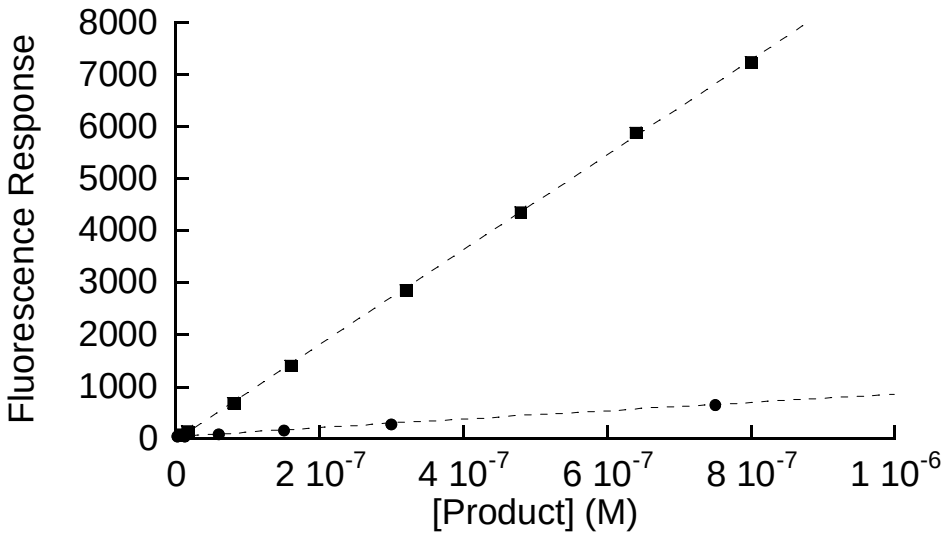

Figure 5.22. HPLC Fluorescence response calibration plot for MeO-BZC (■) and phenol (●). Dashed line indicates linear fit. Error bars indicate 95 % confidence interval. Fluorescence values from Table 5.1 were used in the analysis of MeO-BZC and phenol

Competition kinetic analysis and probe sensitivity

Competition kinetic analysis was used to compare the reactivity of the BPA derivatives towards •OH with that of benzene in the same solution and, thus, under identical reaction conditions.[22, 39, 80] Benzene was used as a reference compound due to its extensive use as a probe for •OH in previous studies.[43, 81-83] Under the reaction conditions described above, light (λ = 200-400 nm) applied to a solution of nitrite anion would produce •OH according to the following reaction scheme (equations 2-4):[84]

$$NO_2^- \xrightarrow{hv} [NO_2^-]^* \quad (2)$$

$$[NO_2^-]^* \rightarrow NO\cdot + O\cdot^- \quad (3)$$

$$O\cdot^- + H_2O \rightleftharpoons \cdot OH + OH^- \quad (4)$$

The production of •OH from the proton extraction by oxygen radical anion ($O^{\bullet -}$) from water (eq 4) has a rate constant value of 1.7×10^6 M^{-1} s^{-1}.[84] Benzene and the BPA probes would react with the photochemically produced •OH according to equations 5 and 6 to produce phenol and BZC, respectively, and other products

$$\cdot \mathrm{OH} + \mathrm{benzene} \rightarrow \mathrm{phenol} + \mathrm{other\ products} \quad k_{OH,benzene} \tag{5}$$

$$\cdot \mathrm{OH} + \mathrm{BPA} \rightarrow \mathrm{BZC} + \mathrm{other\ products} \quad k_{OH,BPA} \tag{6}$$

where $k_{\mathrm{OH,benzene}}$ and $k_{\mathrm{OH,BPA}}$ is the overall •OH reaction rate constant of benzene and BPA, respectively. Benzene has a k_{OH} value of 7.8×10^9 M^{-1} s^{-1}.[85] The overall •OH reaction rate constant can be expressed as the sum of the individual component reaction rate constants, $k_{\mathrm{rxn}}^{\mathrm{x}}$, (equation 7) and the formation of the individual reaction products in equations 5 and 6 can be expressed as a percentage of k_{OH}, respectively (equations 8 and 9).

$$k_{rxn} = \sum k_{\mathrm{rxn}}^{\mathrm{x}} \tag{7}$$

$$k_{phenol} = k_{OH,benzene} Y_{\mathrm{phenol}} \tag{8}$$

$$k_{BZC} = k_{OH,BPA} Y_{\mathrm{BZC}} \tag{9}$$

where k_{phenol} is the reaction rate constant of phenol formation from the reaction of benzene with •OH, k_{BZC} is the reaction rate constant of BZC formation from the reaction of BPA with •OH, Y_{phenol} is the yield of phenol formation per reaction of benzene with •OH ($Y_{\mathrm{phenol}} = 0.75 \pm 0.07$)[86], and Y_{BZC} is the yield of BZC formation per BPA reaction with •OH. The value of $k_{\mathrm{OH,BPA}}$ was determined via the observed decay of BPA during steady-state irradiation experiments with nitrite anion. During the course of experiments, these values were corrected for any direct photodegradation processes.

The bimolecular reactions depicted in equations 5 and 6 are the rate-limiting steps, thus the rate laws for the formation of phenol and BZC are obtained by equations 10 and 11

$$R_{phenol} = \frac{\partial[phenol]}{\partial t} = k_{phenol}[\cdot\,\mathrm{OH}][\mathrm{benzene}] \quad (10)$$

$$R_{BZC} = \frac{\partial[BZC]}{\partial t} = k_{BZC}[\cdot\,\mathrm{OH}][\mathrm{BPA}] \quad (11)$$

where R_{phenol} and R_{BZC} are the rates of phenol and BZC formation, respectively.

Assuming steady-state •OH concentration, $[\bullet\mathrm{OH}]_{ss}$, conditions allows us to express equations 10 and 11 as their pseudo-first order equations 12 and 13

$$R_{phenol} = k'_{phenol}[\cdot\,\mathrm{OH}]_{ss} \quad (12)$$

$$R_{BZC} = k'_{BZC}[\cdot\,\mathrm{OH}]_{ss} \quad (13)$$

Where $k'_{\mathrm{OH\text{-}phenol}}$ and $k'_{\mathrm{OH\text{-}BZC}}$ are psuedo-first-order rate constants ($k'_{\mathrm{OH\text{-}phenol}} = k_{\mathrm{OH\text{-}phenol}}[\mathrm{benzene}]_0$ and $k'_{\mathrm{OH\text{-}BZC}} = k_{\mathrm{OH\text{-}BZC}}[\mathrm{BPA}]_0$). By combining the two previous equations and inserting experimentally determined values (i.e. $[\mathrm{benzene}]_0$, $[\mathrm{BPA}]_0$, R_{phenol}, R_{BZC}) allowed for the calculation of k_{BZC} based on the ratio of intial probe compounds, the ratio of observed rates of product growth, and the literature accepted value of k_{phenol} (equation 14).

$$k_{BZC} = \frac{[\mathrm{benzene}]_0}{[\mathrm{BPA}]_0} \cdot \frac{R_{BZC}}{R_{phenol}} \cdot k_{phenol} \quad (14)$$

It was found necessary for several of the values of R_{phenol} and R_{BZC} to use the intial rates due to further oxidation of the respective BZC derivatives and phenol by photochemically produced reactive intermediates.

In order to characterize the utility of each BPA derivative as a •OH probe, the sensitivity, *S*, was reported as the product of k_{BZC} and its HPLC fluorescence response shown in Table 5.1 (equation 15).

$$S = k_{BZC} \cdot Fluorescence\ response \quad (15)$$

•OH reactivity studies

Competition kinetic experiments between benzene and each BPA derivative were conducted to determine k_{OH} and k_{BZC} by observing the growth of BZC and phenol (Figure 5.23 and Table 5.2). The plots do not give an accurate representation of their relative •OH sensitivity due to the necessity of a cosolvent (i.e. acetonitrile) to ensure the solubility of the hydrophobic BPA substrates. ^{t}Bu-BPA, Me-BPA, CF_3-BPA, and Cl-BPA all required additional acetonitrile to remain soluble in the aqueous media. The presence of a cosolvent in competition kinetic studies is not preferred, but has been used in literature studies.[87, 88] Initial studies incorporated ethanol as a cosolvent due to its increased solvation capacity at low concentrations, but the relatively high value of k_{OH} for ethanol ($k_{OH} = 1.9 \times 10^9\ M^{-1}\ s^{-1}$) resulted in low yields of both phenol and BZC.[85] Acetonitrile, on the other hand, has a value of $k_{OH} = 2.2 \times 10^7\ M^{-1}\ s^{-1}$ which led to decreased competition for •OH in respect to benzene and the BPA derivatives.[89]

The plots in Figure 5.23 demonstrate that indeed BZC is formed from the reaction of BPA with •OH. Negligible amounts of BZC derivatives were formed in the absence of NO_2^-, indicating that direct photolysis contributed little to the formation of BZC. Additional experiments were conducted in the presence of perinaphthenone to test the

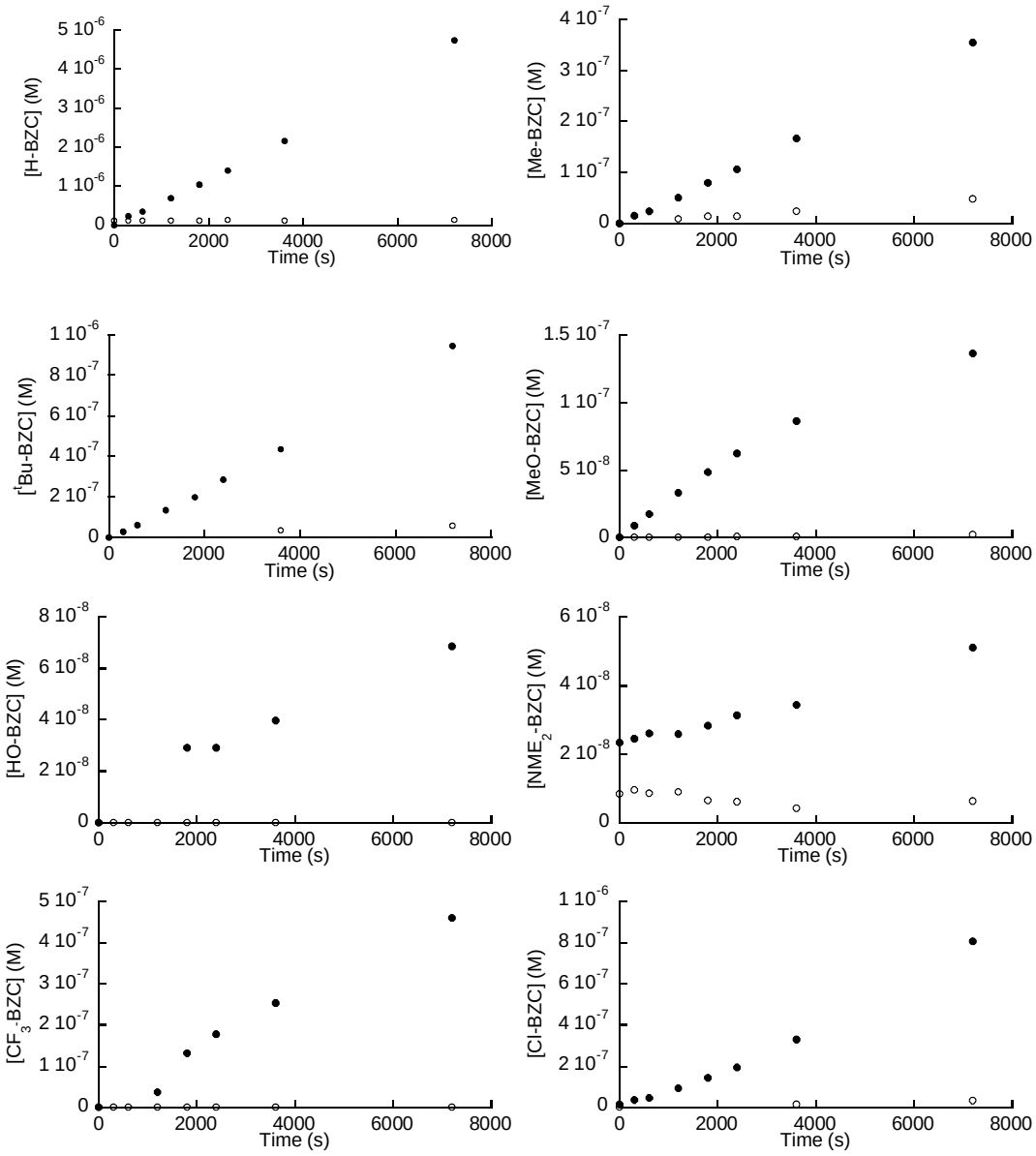

Figure 5.23. Growth of 3'-BZC derivatives during steady state irradiation experiments in the presence of nitrite anion (●) and in the absence of nitrite anion (○). Photolysis solutions conducted in the presence of benzene as reference compound.

BPA	k_{OH} ($\times 10^9$ M^{-1} s^{-1})	k_{BZC} ($\times 10^9$ M^{-1} s^{-1})	Y_{BZC}	*Normalized Sensitivity*[a]
H	40.5 (± 10.3)	2.75 (± 0.07)	0.068	0.057
Me	109.7 (± 85.7)	***12.44*** (± 0.52)	0.113	***1.739***
^{t}Bu	***404.8*** (± 69.8)	1.48 (± 0.04)	0.004	0.083
MeO	32.6 (± 8.4)	0.07 (± 0.00[1])	0.002	0.138
HO	11.4 (± 19.1)	0.08 (± 0.01)	0.007	*0.000*
NMe_2	***261.0*** (± 137.0)	0.30 (± 0.02)	0.001	0.016
CF_3	7.8 (± 1.7)	0.51 (± 0.03)	0.066	0.005
Cl	***157.3*** (± 49.0)	1.18 (± 0.05)	0.007	0.075
benzene	7.80	5.85	0.750	1.000

[a]Sensitivity normalized to benzene

Table 5.2. Reaction rate data of BPA derivatives and benzene with hydroxyl radical. k_{OH} was determined by BPA decay by $[•OH]_{ss}$ (determined by phenol growth). k_{BZC} was calculated according to equation 14. Y_{BZC} was calculated according to equation 9. Sensitivity was calculated according to equation 15 and normalized to benzene. Benzene values of k_{OH} and Y_{phenol} from literature.[39, 85, 86]

selectivity of the BPA probes for •OH over singlet oxygen, $^1O_2$ (data not shown). Despite high steady-state concentrations of $^1O_2$, as detected by furfuryl alcohol degradation, no BPA decay or BZC growth were observed.[90] No control experiments for the selectivity of BZC formation from other reactive oxygen species (e.g. superoxide (O_2^-) or hydrogen peroxide (H_2O_2)) were conducted, yet the photolysis of NO_2^- does not yield any of these reactive intermediates and their contribution in this study was considered neglible.[84]

In addition to the observation of BZC growth during photolysis, the decay of the respective BPA derivative was also observed in order to calculate k_{OH}. The resulting steady-state decay plot for the BPA derivatives can be seen in Figure 5.24. The decay of BPA was more difficult to observe than the growth of BZC by HPLC analysis due to the tendency of carboxylic acids to tail during reverse phase chromatography.[91] The BPA derivatives were present in the photolysis solutions at ca. [BPA] = 100 μM, and resulted in broad, tailing peaks during the analysis of the concentrated reaction mixture. The incorporation of a 100-fold dilution reduced the peak tailing to minimum and increased the reliability between samples. Nevertheless, the amount of BPA degradation remained difficult to accurately quantify (Figure 5.24) and several of the values of k_{OH} calculated from the resulting data were beyond the diffusion limit for bimolecular reactions in aqueous media (Table 5.2).[92]

The high calculated k_{OH} values for Me-BPA, ^{t}Bu-BPA, NMe_2-BPA, and Cl-BPA, which were all found to be above the diffusion limit, highlight potential problems with determining the reaction rate constant between the molecular probes and •OH (Figure 5.24). One possible explanation for the increased k_{OH} values for these compounds was the contribution of other physical and chemical 'decay' mechanisms. Me-BPA, tBu-BPA, and Cl-BPA all required acetonitrile as a cosolvent in order to remain soluble throughout the course of the photolysis, but any process that would lead to a decrease in cosolvent (e.g. evaporation) would result in adsorption of the hydrophobic BPA compounds on the

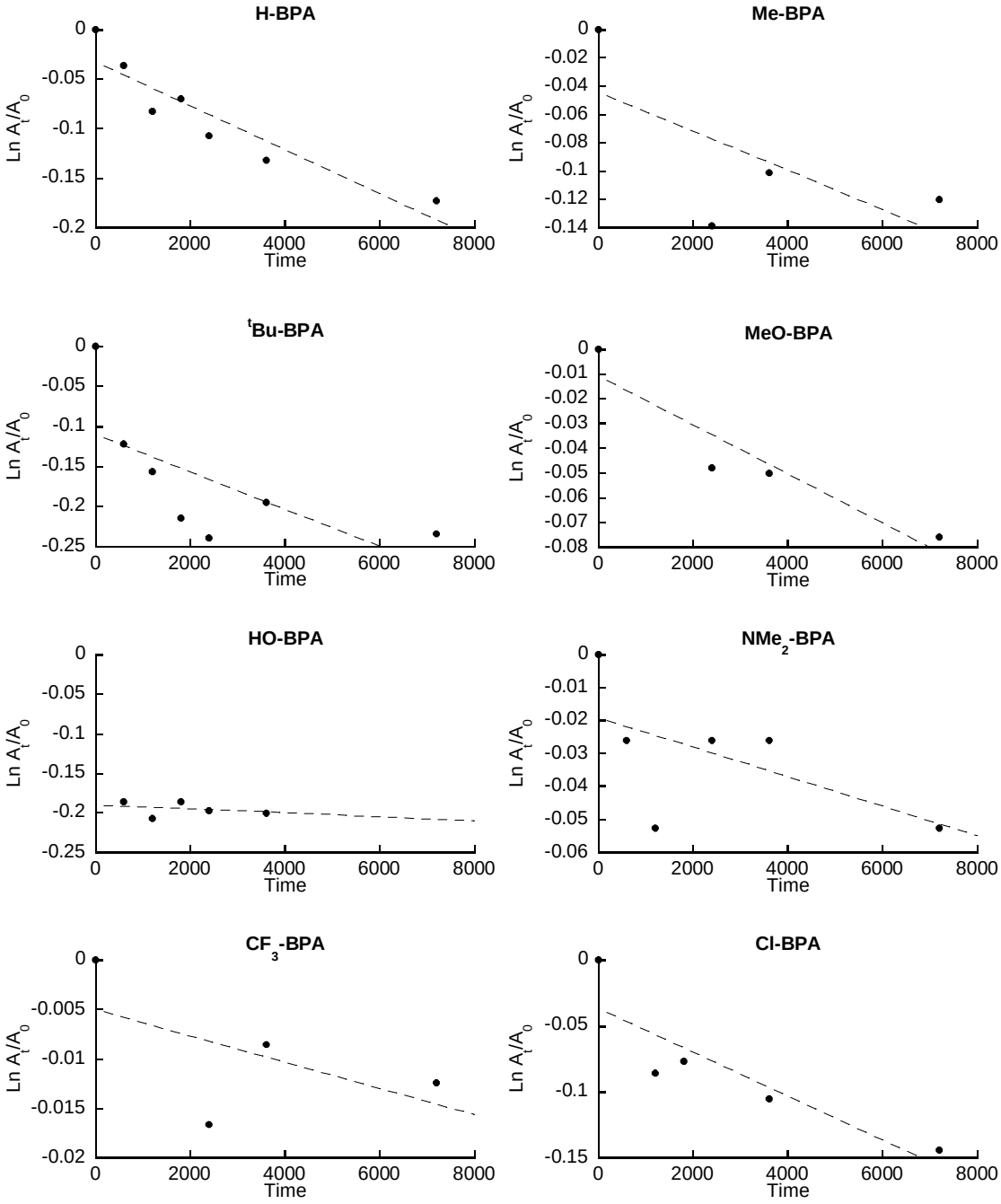

Figure 5.24. Steady-state decay of BPAs during irradiation of nitrite anion corrected for direct degradation. Dashed lines indicate fit to linear slope.

walls of the quartz test tubes. This unimolecular loss process, in addition to any bimolecular decay mechanism, would result in the observed k_{OH} for these compounds. As seen in equation 3, the photolysis of nitrite also produces other radical species (e.g. O• and NO•) that may have increased reactivity with the four BPA derivatives with k_{OH} above the diffusion limit. Any combination of the above processes would result in an over-estimation of k_{OH}.

The rate of BZC growth was used to calculate k_{BZC} according to equations 14 (Table 5.2). All of the values of k_{BZC} were calculated with little attributed error (i.e. error ≤ 10%), with the only exception being HO-BPA. Me-BPA was the only compound that exhibited $k_{BZC} > k_{phenol}$ for the reaction of benzene with •OH and highlights the possible use of Me-BPA in future studies as a probe for •OH. Overall, the BPA derivatives formed their respective BZCs at rates similar to other BPAs within their group. The electron-rich BPAs (i.e. MeO-, HO-, and NMe_2-) exhibited the lowest k_{BZC} values despite previous studies reporting the preferred reactivity of •OH with electron-rich aromatic compounds over electron-poor aromatic compounds.[21] As seen in Table 5.2, the electron-poor BPAs (i.e. CF_3- and Cl-) had higher k_{BZC} than the electron-rich BPAs. The aliphatic BPAs (i.e. H-, Me-, and ^{t}Bu-) were found to have the largest k_{BZC} values despite their increased susceptibility to hydrogen abstraction. Hoshino *et al.* found that molecules containing both aliphatic and aromatic moieties undergo hydroxylation at both positions, but the majority of the products were the result of aromatic insertion.[93]

Only BPA derivatives with k_{OH} values below the diffusion limit were considered during the calculation of Y_{BZC} according to equation 9 (Table 5.2). Given the problems in

determining k_{OH}, all values should be regarded with caution. Of these values, none were found to be as high as that of the reference compound benzene ($Y_{phenol} = 0.75$)[85], but that was to be expected due to the symmetrical nature of benzene in comparison to the BPA derivatives. Me-BPA possessed the highest value of Y_{BZC} which could be attributed to a combination of electronic and steric factors in the formation of Me-BZC. Both H-BPA and CF_3-BPA had Y_{BZC} values half the magnitude of that for Me-BZC. Considering the electronic differences between H-BPA and CF_3-BPA, the similar values of Y_{BZC} are an interesting phenomenon. The electron-rich BPAs, MeO-BPA and HO-BPA, had the lowest Y_{BZC} values despite electronic effects promoting •OH reaction at the substituted aromatic rings. One possible explanation would be that •OH insertion into the more electron-rich aromatic ring of both HO-BPA and MeO-BPA occurred *ortho*- to the substituent (i.e. 3'- or 5'-positions). Matsuura and Omura found that the addition of •OH to phenol gave a mixture of *ortho*- to *para*-dihydroxybenzenes in a 2:1 ratio in favor of the *ortho*-insertion product.[55] The electron-rich HO- and MeO- substituents are stronger directing groups than the aryl substituent and would result in •OH insertion that would be incapable of intramolecular lactonization.

The overall effectiveness of the BPA derivatives as potential •OH probes were determined by calculating their sensitivity in relation to the known •OH scavenger benzene. In general, benzene possessed greater k_{phenol} (in comparison to k_{BZC}) and Y_{phenol} (in comparison toY_{BZC}) values than all of the BPA derivatives (Table 5.2) and based on these factors seemed more suitable as a •OH molecular probe. The analytical response is just as important as the chemical reactivity as a factor for developing a product-growth

based analytical method because of its contribution in detecting low concentrations (i.e. detection limit) and subtle concentration changes (i.e. sensitivity).[94] The accepted definition of sensitivity focuses on both concentration of analyte and its calibrated instrumental response factor. The concentration of our analyte (i.e. phenol or BZC) is a function of its production rate (eqs. 10 and 11) and leads to an estimation of probe molecule sensitivity (eq. 15). The sensitivity of all the BPA derivatives were calculated according to equation 15 and normalized to the calculated sensitivity of benzene (Table 5.2). All of the BPA derivatives were less sensitive than benzene as •OH probes with the exception of Me-BPA, which was nearly twice as sensitive as benzene. Due to these results, Me-BPA demonstrates promise as a selective and sensitive hydrophobic •OH probe within aqueous media. Of the remaining BPA derivatives, MeO-BPA demonstrated moderate sensitivity as a •OH probe in comparison to the others in due to its relatively high fluorescence response factor (Table 5.1). HO-BPA possessed low values of k_{BZC} and fluorescence response, resulting in its complete insensitivity as a •OH probe.

Conclusion

The chemical reactivity of eight BPA derivatives were investigated in respect to the photochemical production of •OH in aqueous media. Chapters 2 – 4 of this thesis focused on the production of $^1O_2$ within microheterogeneous environments resulting in enhanced localized concentration of $^1O_2$ within dissolved organic matter supramolecular assemblies. The production of •OH within DOM would be expected to follow a similar distribution resulting in microenvironments of increased •OH reactivity. The

development of well-behaved hydrophobic probe molecules was the first step towards investigating this phenomenon. The eight BPA derivatives and the corresponding BZC derivatives were synthesized in acceptable yields. In additional to their traditional chemical characterization, absorbance and fluorescence properties were also characterized in order to develop analytical methods for their detection and for future considerations in regard to light screening processes. Their reactivity with •OH was determined via competition kinetic experiments with benzene in the presence of irradiated NO_2^-.

In general, the BPA derivatives reacted with •OH to form the expected BZC product, but the reaction rates and corresponding fluorescence properties of the BZC compounds resulted in poor sensitivity with respect to benzene as a molecular probe. The only exception to this claim was Me-BPA, which demonstrated high sensitivity towards •OH and shows promise as a potential •OH molecular probe. Additional selectivity experiments need to be completed before it can be effectively implemented. Several BPA molecules were found to have high disappearance rates that could not be attributed to reaction with •OH alone and require additional investigation.

References

Chapter 1

1) Larson, R.A.; Weber, E.J., eds. *Reaction Mechanisms in Environmental Organic Chemistry*. 1994, Lewis Publishers: Boca Raton, FL.

(2) Ingle, J.D.; Crouch, S.R., *Spectrochemical Analysis*. 1988, Englewood Cliffs, NJ: Prentice Hall.

(3) Trindle, C.; Halevi, E.A. *Int. J. Quantum Chem.* **2009**, *14*, 281-290.

(4) Chen, Y.; Hu, C.; Qu, J.; Yang, M. *J. Photochem. Photobiol., A* **2007**, *197*, 81-87.

(5) Blough, N.V.; Zepp, R.G. *Struct. Energ. React. Chem. Ser.* **1995**, *2*, 280-333.

(6) Chin, Y.-P.; Miller, P.L.; Zeng, L.; Cawley, K.; Weavers, L.K. *Environ. Sci. Technol.* **2004**, *38*, 5888-5894.

(7) Blough, N.V.; Zepp, R.G., *Reactive oxygen species in natural waters*, in *Active Oxygen in Chemistry*, C.S. Foote, et al., Editors. 1995, Chapman and Hall: New York. p. 280-333.

(8) Coti, K.K.; Belowich, M.E.; Liong, M.; Ambrogio, M.W.; Lau, Y.A.; Khatib, H.A.; Zink, J.I.; Khashab, N.M.; Stoddart, J.F. *Nanoscale* **2009**, *1*, 16-39.

(9) Turro, N.J., *Modern Molecular Photochemistry*. 1978, Menlo Park, CA: Benjamin/Cummings Publishing Co.

(10) Schmidt, R.; Tanielian, C. *J. Phys. Chem. A* **2000**, *104*, 3177-3180.

(11) Merkel, P.B.; Kearns, D.R. *J. Am. Chem. Soc.* **1972**, *94*, 7244-53.

(12) Young, R.H.; Martin, R.L.; Feriozi, D.; Brewer, D.; Kayser, R. *Photochem. Photobiol.* **1973**, *17*, 233-244.

(13) Darmanyan, A.P.; Jenks, W.S.; Jardon, P. *J. Phys. Chem. A* **1998**, *102*, 7420-7426.

(14) Clennan, E.L.; Noe, L.J.; Wen, T.; Szneler, E. *J. Org. Chem.* **1989**, *54*, 3581-3584.

(15) Montagnon, T.; Tofi, M.; Vassilikogiannakis, G. *Acc. Chem. Res.* **2008**, *41*, 1001-1011.

(16) Wasserman, H.H.; Ives, J.L. *Tetrahedron* **1981**, *37*, 1825-52.

(17) Adam, W.; Reinhardt, D. *J. Chem. Soc., Perkin Trans. 2* **1997**, 1453-1463.

(18) MacManus-Spencer, L.A.; Latch, D.E.; Kroncke, K.M.; McNeill, K. *Anal. Chem.* **2005**, *77*, 1200-1205.

(19) Srikrishna, A.; Ravi Kumar, P. *Tetrahedron Lett.* **2004**, *45*, 6867-6870.

(20) Aubry, J.-M.; Bouttemy, S. *J. Am. Chem. Soc.* **1997**, *119*, 5286-5294.

(21) Kacher, M.L.; Foote, C.S. *Photochem. Photobiol.* **1979**, *29*, 765-9.

(22) Monroe, B.M. *Photochem. Photobiol.* **1979**, *29*, 761-4.

(23) Thomas, M.J.; Foote, C.S. *Photochem. Photobiol.* **1978**, *27*, 683-693.

(24) Scully, F.E.; Hoigne, J. *Chemosphere* **1987**, *16*, 681-694.

(25) Garcia, N.A. *J. Photochem. Photobiol., B* **1994**, *22*, 185-196.

(26) Palumbo, M.C.; Garcia, N.A.; Gutierrez, M.I.; Luiz, M. *Toxicol. Environ. Chem.* **1990**, *29*, 85-94.

(27) Krieger-Liszkay, A. *J. Exp. Bot.* **2005**, *56*, 337-346.

(28) Baier, J.; Maisch, T.; Maier, M.; Engel, E.; Landthaler, M.; Baeumler, W. *Biophys. J.* **2006**, *91*, 1452-1459.

(29) Tanaka, M.; Ohkubo, K.; Fukuzumi, S. *J. Phys. Chem. A* **2006**, *110*, 11214-11218.

(30) Piette, J.; Decuyper-Debergh, D.; Van de Vorst, A. *NATO ASI Ser., Ser. H* **1988**, *15*, 201-10.

(31) Boreen, A.L.; Edhlund, B.L.; Cotner, J.B.; McNeill, K. *Environ. Sci. Technol.* **2008**, *42*, 5492-5498.

(32) Michaeli, A.; Feitelson, J. *Photochem. Photobiol.* **1995**, *61*, 255-60.

(33) Matheson, I.B.C.; Lee, J. *Photochem. Photobiol.* **1979**, *29*, 879-81.

(34) Nilsson, R.; Merkel, P.B.; Kearns, D.R. *Photochem. Photobiol.* **1972**, *16*, 117-24.

(35) Kim, H.J.; Min, D.B. *Lipid Oxid. Pathways* **2008**, *2*, 1-30.

(36) Tejero, I.; Gonzalez-Lafont, A.; Lluch, J.M.; Eriksson, L.A. *Chem. Phys. Lett.* **2004**, *398*, 336-342.

(37) Dougherty, T.J.; Gomer, C.J.; Henderson, B.W.; Jori, G.; Kessel, D.; Korbelik, M.; Moan, J.; Peng, Q. *J. Natl. Cancer Inst.* **1998**, *90*, 889-905.

(38) Kohn, T.; Grandbois, M.; McNeill, K.; Nelson, K.L. *Environ. Sci. Technol.* **2007**, *41*, 4626-4632.

(39) Pecson, B.M.; Martin, L.V.; Kohn, T. *Appl. Environ. Microbiol.* **2009**, *75*, 5544-5554.

(40) Kohn, T.; Nelson, K.L. *Environ. Sci. Technol.* **2007**, *41*, 192-197.

(41) Latch, D.E.; McNeill, K. *Science* **2006**, *311*, 1743-1747.

(42) Sawyer, D.T. *J. Phys. Chem.* **1989**, *93*, 7977-8.

(43) Mill, T.; Hendry, D.; Richardson, D. *Science* **1980**, *207*, 886-887.

(44) Zepp, R.G.; Hoigne, J.; Bader, H. *Environ. Sci. Technol.* **1987**, *21*, 443-450.

(45) Zhou, X.; Mopper, K. *Mar. Chem.* **1990**, *30*, 71-88.

(46) McGrath, W.D.; Norrish, R.G.W. *Proc. R. Soc. London, Ser. A* **1960**, *254*, 317-26.

(47) Page, S.E.; Arnold, W.A.; McNeill, K. *Abstracts of Papers, 239th ACS National Meeting, San Francisco, CA, United States, March 21-25,* **2010**, GEOC-188.

(48) Farhataziz; Ross, A.B., *Selected Specific Rate of Reaction of Transients from Water in Aqueous Solutions. III. Hydroxyl radical and perhydroxyl radical and their radical ions*, W. National Bureau of Standards, DC, Editor. 1977.

(49) Shemer, H.; Sharpless, C.M.; Elovitz, M.S.; Linden, K.G. *Environ. Sci. Technol.* **2006**, *40*, 4460-4466.

(50) Atkinson, R. *Chemical Reviews* **1986**, *86*, 69-201.

(51) Dorfman, L.M.; Adams, G.E., *Reactivity of the hydroxyl radical in aqueous solutions*, W. National Bureau of Standards, DC, Editor. 1973.

(52) Matsuura, T.; Omura, K. *J. Chem. Soc. Chem. Commun.* **1966**, 127-128.

(53) Buxton, G.V.; Greenstock, C.L.; Helman, W.P.; Ross, A.B. *J. Phys. Chem. Ref. Data* **1988**, *17*, 513-886.

(54) Ross, F.; Ross, A.B., *Selected specific rates of reactions of transients from water in aqueous solution. III. Hydroxyl radical and perhydroxyl radical and their radical ions*. 1977, Radiat. Lab.,Notre Dame Univ.,Notre Dame,IN,USA. p. 122 pp.

(55) Newton, G.L.; Milligan, J.R. *Radiation Physics and Chemistry* **2006**, *75*, 473-478.

(56) Pi, Y.; Schumacher, J.; Jekel, M. *Ozone: Sci. Eng.* **2005**, *27*, 431-436.

(57) Powell, S.R.; Hall, D. *Free Radical Biol. Med.* **1990**, *9*, 133-41.

(58) Maleknia Simin, D.; Kiselar Janna, G.; Downard Kevin, M. *Rapid Commun. Mass Spectrom.* **2002**, *16*, 53-61.

(59) Vermilyea, A.W.; Voelker, B.M. *Environ. Sci. Technol.* **2009**, *43*, 6927-6933.

(60) Barreto, J.C.; Smith, G.S.; Strobel, N.H.P.; McQuillin, P.A.; Miller, T.A. *Life Sci.* **1994**, *56*, PL89-96.

(61) Soh, N.; Makihara, K.; Ariyoshi, T.; Seto, D.; Maki, T.; Nakajima, H.; Nakano, K.; Imato, T. *Anal. Sci.* **2008**, *24*, 293-296.

(62) King, M.; Kopelman, R. *Sens. Actuators, B* **2003**, *B90*, 76-81.

(63) Manevich, Y.; Held, K.D.; Biaglow, J.E. *Radiat. Res.* **1997**, *148*, 580-591.

(64) Syrychova, I.; Hideg, E. *Funct. Plant Biol.* **2007**, *34*, 1105-1111.

(65) Grandbois, M.; Latch, D.E.; McNeill, K. *Environ. Sci. Technol.* **2008**, *42*, 9184-9190.

(66) Means, J.C.; Wijayaratne, R. *Science* **1982**, *215*, 968-70.

(67) Wershaw, R.L. *Soil Sci.* **1999**, *164*, 803-813.

(68) Ogner, G.; Schnitzer, M. *Science* **1970**, *170*, 317-18.

(69) *Humic Substances in Soil, Sediment, and Water*, ed. G.R. Aiken, et al. 1985, New York, NY: John Wiley & Sons. 692.

(70) Sutton, R.; Sposito, G.; Diallo, M.S.; Schulten, H.-R. *Environ. Toxicol. Chem.* **2005**, *24*, 1902-1911.

(71) Piccolo, A. *Soil Sci.* **2001**, *166*, 810-832.

(72) Choudhry, G.G., *Humic Substances. Structural, Photophysical, Photochemical and Free Radical Aspects and Interactions with Environmental Chemicals*. Current Topics in Environmental and Toxicological Chemistry. Vol. 7. 1984, London, UK: Gordon and Breach Science Publishers. 185.

(73) *Refractory Organic Substances in the Environment*, ed. F.H. Frimmel, et al. 2002, Weinheim, Germany: Wiley-VCH.

(74) Mao, J.D.; Xing, B.; Schmidt-Rohr, K. *Environ. Sci. Technol.* **2001**, *35*, 1928-1934.

(75) Gjessing, E.T., *Physical and Chemical Characteristics of Aquatic Humus*. 1976, Ann Arbor, MI: Ann Arbor Science. 120.

(76) McKnight, D.M.; W., B.; Westerhoff, P.K.; Doran, P.T.; Kulbe, T., Elizabeas; Andersen, D.T. *Limnol. Oceanogr.* **2001**, *46*, 38-48.

(77) Scott, D.T.; McKnight, D.M.; Blunt-Harris, E.L.; Kolesar, S.E.; Lovley, D.R. *Environ. Sci. Technol.* **1998**, *32*, 2984-2989.

(78) Hunter, R.J.; White, L.R., *Foundations of Colloid Science*. 1987-1989, New York: Oxford University Press.

(79) Hamley, I.W., *Introduction to Soft Matter. Polymers, Colloids, Amphiphiles and Liquid Crystals*. 2000, West Sussex, England: John Wiley & Sons, LTD.

(80) Wu, W.; Sun, H.; Wang, L.; Li, K.; Wang, L. *J. Haz. Mater.* **2010**, *174*, 635-640.

(81) Chiarini, M.; Bunton, C.A. *Colloids Suft., A* **2004**, *245*, 177-182.

(82) Ohara, K.; Kikuchi, K.; Origuchi, T.; Nagaoka, S.-i. *J. Photochem. Photobiol., B* **2009**, *97*, 132-137.

(83) Nishide, N.; Miyoshi, N. *Life Sci.* **2002**, *72*, 321-328.

(84) Ambade, A.V.; Savariar, E.N.; Thayumanavan, S. *Mol. Pharm.* **2005**, *2*, 264-272.

(85) Liu, M.; Frechet, J.M.J. *Polym. Mater. Sci. Eng.* **1999**, *80*, 167-168.

(86) Kaanumalle, L.S.; Nithyanandhan, J.; Pattabiraman, M.; Jayaraman, N.; Ramamurthy, V. *J. Am. Chem. Soc.* **2004**, *126*, 8999-9006.

(87) Chen, Y.; Shen, Z.; Pastor-Perez, L.; Frey, H.; Stiriba, S.-E. *Macromolecules* **2005**, *38*, 227-229.

(88) Hawker, C.J.; Wooley, K.L.; Frechet, J.M.J. *J. Chem. Soc., Perkin Trans. 1* **1993**, 1287-97.

(89) Jain, S.; Bates, F.S. *Macromolecules* **2004**, *37*, 1511-1523.

(90) Arumugam, S.; Vutukuri, D.R.; Thayumanavan, S.; Ramamurthy, V. *J. Am. Chem. Soc.* **2005**, *127*, 13200-13206.

(91) Li, B.; Moriyama, E.H.; Li, F.; Jarvi, M.T.; Allen, C.; Wilson, B.C. *Photochem. Photobiol.* **2007**, *83*, 1505-1512.

(92) Tian, Y.; Chen, C.-Y.; Yip, H.-L.; Wu, W.-C.; Chen, W.-C.; Jen, A.K.Y. *Macromolecules* **2010**, *43*, 282-291.

(93) Bates, F.S.; Brannan, A.K.; Davis, K.P.; Jain, S.; Gong, X.; Scriven, L.E. *Polym. Prepr. (Am. Chem. Soc., Div. Polm Chem.)* **2006**, *47*, 760.

(94) Rodriguez-Hernandez, J.; Checot, F.; Gnanou, Y.; Lecommandoux, S. *Prog. Polym. Sci.* **2005**, *30*, 691-724.

(95) Dong, C.-M.; Chaikof, E.L. *Colloid Polym. Sci.* **2005**, *283*, 1366-1370.

(96) Lodge, T.P.; Bang, J.; Li, Z.; Hillmyer, M.A.; Talmon, Y. *Faraday Discuss.* **2004**, *128*, 1-12.

(97) Ishizu, K.; Tsubaki, K.; Mori, A.; Uchida, S. *Prog. Polym. Sci.* **2002**, *28*, 27-54.

(98) Upadhyay, K.K.; Agrawal, H.G.; Upadhyay, C.; Schatz, C.; Le Meins, J.F.; Misra, A.; Lecommandoux, S. *Crit. Rev. Ther. Drug Carrier Syst.* **2009**, *26*, 157-205.

(99) Gillies, E.R.; Frechet, J.M.J. *Drug Disc. Today* **2005**, *10*, 35-43.

(100) Hackbarth, S.; Horneffer, V.; Wiehe, A.; Hillenkamp, F.; Roder, B. *Chem. Phys.* **2001**, *269*, 339-346.

(101) Nishiyama, N.; Stapert, H.R.; Zhang, G.-D.; Takasu, D.; Jiang, D.-L.; Nagano, T.; Aida, T.; Kataoka, K. *Bioconjugate Chem.* **2003**, *14*, 58-66.

(102) Oar, M.A.; Serin, J.M.; Dichtel, W.R.; Frechet, J.M.J.; Ohulchanskyy, T.Y.; Prasad, P.N. *Chem. Mat.* **2005**, *17*, 2267-2275.

(103) Dichtel, W.R.; Serin, J.M.; Edder, C.; Frechet, J.M.J.; Matuszewski, M.; Tan, L.-S.; Ohulchanskyy, T.Y.; Prasad, P.N. *J. Am. Chem. Soc.* **2004**, *126*, 5380-5381.

(104) Ha, J.-H.; Ko, S.; Lee, C.-H.; Lee, W.-y.; Kim, Y.-R. *Chem. Phys. Lett.* **2001**, *349*, 271-278.

(105) Beverina, L.; Abbotto, A.; Landenna, M.; Cerminara, M.; Tubino, R.; Meinardi, F.; Bradamante, S.; Pagani, G.A. *Org. Lett.* **2005**, *7*, 4257-4260.

Chapter 2

(1) Leifer, A., *The Kinetics of Environmental Aquatic Photochemistry*. ACS Professional Reference Book. 1988: American Chemical Society. 304.

(2) Choudhry, G.G. *Toxicol. Environ. Chem.* **1981**, *4*, 209-60.

(3) Osburn, C.L.; Morris, D.P. *Comp. Ser. Photochem. Photobiol.* **2003**, *1*, 185-217.

(4) Blough, N.V.; Zepp, R.G. *Struct. Energ. React. Chem. Ser.* **1995**, *2*, 280-333.

(5) Larson, R.A.; Weber, E.J., *Reaction Mechanisms Environmental Organic Chemistry*. Carbohydrate Polymers. Vol. 29. 1996. 293-294.

(6) Schwarzenbach, R.P.; Gschwend, P.M.; Imboden, D.M., *Environmental Organic Chemistry*. 1992. 681 pp.

(7) Carlson, D.J.; Mayer, L.M.; Brann, M.L.; Mague, T.H. *Mar. Chem.* **1985**, *16*, 141-53.

(8) De Paolis, F.; Kukkonen, J. *Chemosphere* **1997**, *34*, 1693-1704.

(9) Eriksson, J.; Skyllberg, U. *J. Environ. Qual.* **2001**, *30*, 2053-2061.

(10) Frankki, S.; Skyllberg, U. *Eur. J. Soil Sci.* **2006**, *57*, 655-664.

(11) Hassett, J.P.; Anderson, M.A. *Environ. Sci. Technol.* **1979**, *13*, 1526-9.

(12) Klaus, U.; Oesterreich, T.; Volk, M.; Spiteller, M. *Acta Hydroc. Hydrob.* **1998**, *26*, 311-317.

(13) Kulovaara, M. *Chemosphere* **1993**, *27*, 2333-40.

(14) Li, A.Z.; Marx, K.A.; Walker, J.; Kaplan, D.L. *Environ. Sci. Technol.* **1997**, *31*, 584-589.

(15) McCarthy, J.F.; Roberson, L.E.; Burrus, L.W. *Chemosphere* **1989**, *19*, 1911-20.

(16) Uhle, M.E.; Chin, Y.-P.; Aiken, G.R.; McKnight, D.M. *Environ. Sci. Technol.* **1999**, *33*, 2715-2718.

(17) Stevenson, F.J., *Humus Chemistry: Genesis, Composition, Reactions*. 2nd ed. 1994, New York: John Wiley & Sons, Ltd.

(18) Piccolo, A. *Soil Sci.* **2001**, *166*, 810-832.

(19) Sutton, R.; Sposito, G. *Environ. Sci. Technol.* **2005**, *39*, 9009-9015.

(20) von Wandruszka, R.; Engebretson, R.R.; Yates, L.M., *Humic acid pseudomicelles in dilute aqueous solution: Fluorescence and surface tension measurements.*, in *Understanding Humic Substances: Advance Methods, Properties and Applications*, E.A. Ghabbour and G. Davis, Editors. 1999, Royal Society of Chemistry: Cambridge, U.K. p. 79-85.

(21) Eadie, B.J.; Morehead, N.R.; Val Klump, J.; Landrum, P.F. *J. Great Lakes Res.* **1992**, *18*, 91-7.

(22) Schlautman, M.A.; Morgan, J.J. *Environ. Sci. Technol.* **1993**, *27*, 961-9.

(23) Fang, F.; Kanan, S.; Patterson, H.H.; Cronan, C.S. *Anal. Chim. Acta* **1998**, *373*, 139-151.

(24) Kohn, T.; Grandbois, M.; McNeill, K.; Nelson, K.L. *Environ. Sci. Technol.* **2007**, *41*, 4626-4632.

(25) Latch, D.E.; McNeill, K. *Science* **2006**, *311*, 1743-1747.

(26) Neckers, D.C.; Paczkowski, J. *J. Am. Chem. Soc.* **1986**, *108*, 291-292.

(27) Ter Halle, A.; Richard, C. *Environ. Sci. Technol.* **2006**, *40*, 3842-3847.

(28) Sakkas Vasilios, A.; Lambropoulou Dimitra, A.; Albanis Triantafyllos, A. *Chemosphere* **2002**, *48*, 939-45.

(29) Chin, Y.-P.; Miller, P.L.; Zeng, L.; Cawley, K.; Weavers, L.K. *Environ. Sci. Technol.* **2004**, *38*, 5888-5894.

(30) Graber, E.R.; Borisover, M.D. *Environ. Sci. Technol.* **1998**, *32*, 3286-3292.

(31) Malcolm, R.L.; MacCarthy, P. *Environ. Sci. Technol.* **1986**, *20*, 904-11.

(32) MacManus-Spencer, L.A.; Latch, D.E.; Kroncke, K.M.; McNeill, K. *Anal. Chem.* **2005**, *77*, 1200-1205.

(33) Wu, S.-C.; Gschwend, P.M. *Water Resour. Res.* **1988**, *24*, 1373-1383.

(34) Latch, D.E., *Environmental Photochemistry: Studies on the Degradation of Pharmaceutical Pollutants and the Microheterogeneous Distribution of Singlet Oxygen*, in *Chemistry*. 2005, University of Minnesota: Minneapolis, MN. p. 256.

(35) Hosee, M.; Wilkinson, K.J. *Environ. Sci. Technol.* **2001**, *35*, 4301-4306.

(36) Zandi, I.; Turner, C.D. *Chem. Eng. Sci.* **1970**, *25*, 517-28.

(37) Chin, Y.-P.; Aiken, G.R.; Danielsen, K.M. *Environ. Sci. Technol.* **1997**, *31*, 1630-1635.

(38) Hur, J.; Schlautman, M.A. *Environ. Sci. Technol.* **2003**, *37*, 880-887.

(39) Perminova, I.V.; Grechishcheva, N.Y.; Petrosyan, V.S. *Environ. Sci. Technol.* **1999**, *33*, 3781-3787.

(40) Beckett, R.; Jue, Z.; Giddings, J.C. *Environ. Sci. Technol.* **1987**, *21*, 289-95.

(41) Brown, A.; McKnight, D.M.; Chin, Y.-P.; Roberts, E.C.; Uhle, M. *Mar. Chem.* **2004**, *89*, 327-337.

(42) Dinar, E.; Mentel, T.F.; Rudich, Y. *Atmos. Chem. Phys.* **2007**, *6*, 5213-5224.

(43) Benedetti, M.F.; Van Riemsdijk, W.H.; Koopal, L.K. *Environ. Sci. Technol.* **1996**, *30*, 1805-13.

(44) Buffle, J., *Chapter 6*, in *Metal Ions in Biological Systems*, H. Sigel, Editor. 1984, Marcel Dekker: New York.

(45) de Wit, J.C.M.; van Riemsdijk, W.H.; Koopal, L.K. *Environ. Sci. Technol.* **1993**, *27*, 2005-14.

(46) Poisson, S.-D., *Recherches sur la probabilité des jugements en matières criminelles et matière civile (Research on the Probability of Judgments in Criminal and Civil Matters)*. 1838, Paris: Bachelier.

(47) Burns, S.E.; Hassett, J.P.; Rossi, M.V. *Environ. Sci. Technol.* **1996**, *30*, 2934-2941.

(48) Yue, L.; Wu, F.; Liu, C.; Li, W.; Wang, J.; Mei, Y. *Chin. J. Geochem.* **2004**, *23*, 275-283.

(49) Christl, I.; Knicker, H.; Kogel-Knabner, I.; Kretzschmar, R. *Eur. J. Soil Sci.* **2000**, *51*, 617-625.

(50) Novak, J.; Kozler, J.; Janos, P.; Cezikova, J.; Tokarova, V.; Madronova, L. *React. Funct. Polym.* **2001**, *47*, 101-109.

(51) Baalousha, M.; Motelica-Heino, M.; Galaup, S.; Le Coustumer, P. *Micro. Res. Tech.* **2005**, *66*, 299-306.

(52) Pinheiro, J.P.; Mota, A.M.; d'Oliveira, J.M.R.; Martinho, J.M.G. *Anal. Chim. Acta* **1996**, *329*, 15-24.

(53) Lou, T.; Xie, H. *Chemosphere* **2006**, *65*, 2333-2342.

(54) Lou, T.; Xie, H.; Chen, G.; Gagne, J.-P. *Chemosphere* **2006**, *64*, 1204-1211.

(55) Baalousha, M.; Motelica-Heino, M.; Le Coustumer, P. *Colloids Surf., A* **2006**, *272*, 48-55.

(56) Wagoner, D.B.; Christman, R.F.; Cauchon, G.; Paulson, R. *Environ. Sci. Technol.* **1997**, *31*, 937-941.

(57) Schulze, M. *Berichte des Forschungszentrums Juelich* **1998**, 1-176 pp.

(58) Hefner, K.H.; Fisher, J.M.; Ferry, J.L. *Environ. Sci. Technol.* **2006**, *40*, 3717-3722.

Chapter 3

(1) Sinton, L.W.; Finlay, R.K.; Lynch, P.A. *Appl. Environ. Microbiol.* **1999**, *65*, 3605-3613.

(2) Sinton, L.W.; Hall, C.H.; Lynch, P.A.; Davies-Colley, R.J. *Appl. Environ. Microbiol.* **2002**, *68*, 1122-1131.

(3) Davies-Colley, R.J.; Bell, R.G.; Donnison, A.M. *Appl. Environ. Microbiol.* **1994**, *60*, 2049-2058.

(4) Noble, R.T.; Lee, I.M.; Schiff, K.C. *J. Appl. Microbiol.* **2004**, *96*, 464-472.

(5) Boehm, A.B.; Grant, S.B.; Kim, J.H.; Mowbray, S.L.; McGee, C.D.; Clark, C.D.; Foley, D.M.; Wellman, D.E. *Environ. Sci. Technol.* **2002**, *36*, 3885-3892.

(6) Wegelin, M.; Canonica, S.; Mechsner, K.; Fleischmann, T.; Pesaro, F.; Metzler, A. *J. Water Supply Res. T.* **1994**, *43*, 154-169.

(7) Davies-Colley, R.J.; Donnison, A.M.; Speed, D.J.; Ross, C.M.; Nagels, J.W. *Water Res.* **1999**, *33*, 1220-1230.

(8) Curtis, T.P.; Mara, D.D.; Silva, S.A. *Water Sci. Technol.* **1992**, *26*, 1729-1738.

(9) Davies-Colley, R.J.; Donnison, A.M.; Speed, D.J. *Water Sci. Technol.* **2000**, *42*, 149-158.

(10) Jagger, J., *Solar-UV actions on living cells*. 1985, New York: Praeger Publishers.

(11) Curtis, T.P.; Mara, D.D.; Silva, S.A. *Appl. Environ. Microbiol.* **1992**, *58*, 1335-1343.

(12) Kohn, T.; Nelson, K.L. *Environ. Sci. Technol.* **2007**, *41*, 192-197.

(13) Grandbois, M.; Latch, D.E.; McNeill, K. *Environ. Sci. Technol.* **2008**, *42*, 9184-9190.

(14) Latch, D.E.; McNeill, K. *Science* **2006**, *311*, 1743-1747.

(15) Payment, P.; Morin, E.; Trudel, M. *Can. J. Microbiol.* **1988**, *34*, 907-910.

(16) Hejkal, T.W.; Wellings, F.M.; Lewis, A.L.; LaRock, P.A. *Appl. Environ. Microbiol.* **1981**, *41*,

(17) Bixby, R.L.; O'Brien, D.J. *Appl. Environ. Microbiol.* **1979**, *38*, 840-845.

(18) Schijven, J.F.; Hassanizadeh, S.M. *Crit. Rev. Environ. Sci. Technol.* **2000**, *30*, 49-127.

(19) Havelaar, A.H.; Olphen, M.; Drost, Y.C. *Appl. Environ. Microbiol.* **1993**, *59*, 2956-2962.

(20) MacManus-Spencer, L.A.; Latch, D.E.; Kroncke, K.M.; McNeill, K. *Anal. Chem.* **2005**, *77*, 1200-1205.

(21) APHA; AWWA; WEF, *Standard Methods for the Examination of Water & Wastewater*. 21 ed. 9224 Detection of Coliphages, ed. A.D. Eaton, L.S. Clesceri, and E.W. Rice. 2005, Washington, DC: American Public Health Association, American Water Works Association, and Water Environment Federation.

(22) Voelker, B.M.; Sulzberger, B. *Environmental Science and Technology* **1996**, *30*, 1106-1114.

(23) AWWA, A., *Standard Methods for the Examination of Water & Wastewater*. 21 ed, ed. A.P.H. Association, A.W.W. Association, and W.E. Federation. 2005, Washginton, DC.

(24) Davies, M.J. *Biochem. Bioph. Res. Co.* **2003**, *305*, 761-770.

(25) Matheson, I.B.C.; Etheridge, R.D.; Kratowich, N.R.; Lee, J. *Photochem. Photobiol.* **1975**, *21*, 165-171.

(26) Perdue, E.M., in *Aquatic Humic Substances. Ecology and Biogeochemistry*, D.O. Hessen and L.J. Tranvik, Editors. 1998, Springer Verlag: Berlin Heidelberg: New York.

(27) Gauthier, T.D.; Seltz, W.R.; Grant, C.L. *Environ. Sci. Technol.* **1987**, *21*, 243-248.

(28) Tipping, E. *Geochim. Cosmochim. Ac.* **1981**, *45*, 191-199.

(29) Vermeer, A.W.P.; van Riemsdijk, W.H.; Koopal, L.K. *Langmuir* **1998**, *14*, 2810-2819.

(30) Ochs, M.; Cosovic, B.; Stumm, W. *Geochim. Cosmochim. Ac.* **1994**, *58*, 639-650.

(31) Rodgers, M.A.J.; Snowden, P.T. *J. Am. Chem. Soc.* **1982**, *104*, 5541-5543.

(32) Haag, W.R.; Hoigne, J. *Environ. Sci. Technol.* **1986**, *20*, 341-348.

(33) Gerba, C.P. *Adv. Appl. Microbiol.* **1984**, *30*, 133-168.

(34) Redman, J.A.; Grant, S.B.; Olson, T.M.; Adkins, J.M.; Jackson, J.L.; Castillo, M.S.; Yanko, W.A. *Water Res.* **1999**, *33*, 43-52.

(35) Sobsey, M.D.; Dean, C.H.; Knuckles, M.E.; Wagner, R.A. *Appl. Environ. Microbiol.* **1980**, *40*, 92-101.

(36) Kohn, T.; Grandbois, M.; McNeill, K.; Nelson, K.L. *Environ. Sci. Technol.* **2007**, *41*, 4626-4632.

(37) Clark, M.M.; Lucas, P. *J. Membr. Sci.* **1998**, *143*, 13-25.

(38) Templeton, M.R.; Andrews, R.C.; Hofmann, R. *Water Res.* **2005**, *39*, 3487-3500.

(39) Koizumi, Y.; Taya, M. *Biochem. Eng. J.* **2002**, *12*, 107-116.

Chapter 4

(1) Jones, R. *Nat. Nanotechnol.* **2009**, *4*, 75.

(2) Iden, R.; Kessenich, E.; Wohlleben, W.; Wullkopf, U. *Chem. Ing. Tech.* **2008**, *80*, 1701-1704.

(3) Jayatissa, A.H. *Proc. SPIE-Int. Soc. Opt. Eng.* **2005**, *6008*, 600814/1-600814/6.

(4) Rolison, D.R. *ACS Symp. Ser.* **2005**, *890*, 324-330.

(5) Peet, J.; Heeger, A.J.; Bazan, G.C. *Acc. Chem. Res.* **2009**, *42*, 1700-1708.

(6) Upadhyay, K.K.; Agrawal, H.G.; Upadhyay, C.; Schatz, C.; Le Meins, J.F.; Misra, A.; Lecommandoux, S. *Crit. Rev. Ther. Drug Carrier Syst.* **2009**, *26*, 157-205.

(7) Wang, Y.; Huang, B.; Lu, J.; Liang, X. *Shengwu Wuli Xuebao* **2009**, *25*, 168-174.

(8) Coti, K.K.; Belowich, M.E.; Liong, M.; Ambrogio, M.W.; Lau, Y.A.; Khatib, H.A.; Zink, J.I.; Khashab, N.M.; Stoddart, J.F. *Nanoscale* **2009**, *1*, 16-39.

(9) Divochiy, A.; Marsili, F.; Bitauld, D.; Gaggero, A.; Leoni, R.; Mattioli, F.; Korneev, A.; Seleznev, V.; Kaurova, N.; Minaeva, O.; Gol'tsman, G.; Lagoudakis, K.G.; Benkhaoul, M.; Levy, F.; Fiore, A. *Nat. Photonics* **2008**, *2*, 302-306.

(10) Liu, X.; Ji, B. *Yingyong Huagong* **2008**, *37*, 685-687, 698.

(11) Konishi, K.; Kuwata-Gonokami, M. *Oyo Butsuri* **2009**, *78*, 531-535.

(12) Kobayashi, N.P. *J. Nanophotonics* **2008**, *2*, No pp given.

(13) Dai, D.; He, S. *J. Nanophotonics* **2008**, *2*, No pp given.

(14) Zhang, W.; Zou, L.; Wang, L. *Appl. Catal., A* **2009**, *371*, 1-9.

(15) Lew, C.M.; Cai, R.; Yan, Y. *Acc. Chem. Res. 43*, 210-219.

(16) Pradeep, T.; Anshup *Thin Solid Films* **2009**, *517*, 6441-6478.

(17) Otero, J.A.; Lena, G.; Colina, J.M.; Mazarrasa, O.; Villasante, J.; Silva, V.; Palacio, L.; Pradanos, P.; Hernandez, A. *Recent Res. Dev. Environ. Technol.* **2008**, 31-56.

(18) Lau, W.-J.; Ismail, A.F. *Desalination* **2009**, *245*, 321-348.

(19) Bottino, A.; Capannelli, G.; Comite, A.; Ferrari, F.; Firpo, R.; Venzano, S. *C. R. Chim.* **2009**, *12*, 882-888.

(20) Sharma, Y.C.; Srivastava, V.; Singh, V.K.; Kaul, S.N.; Weng, C.H. *Environ. Technol.* **2009**, *30*, 583-609.

(21) Ritchie, S.M.C. *Nanotechnol. Appl. Clean Water* **2009**, 293-309.

(22) Vernikov, V.M.; Arianova, E.A.; Gmoshinskii, I.V.; Khotimchenko, S.A.; Tutel'yan, V.A. *Vopr. Pitan.* **2009**, *78*, 4-17.

(23) Tseng, A.A.; Li, Z. *J. Nanosci. Nanotechnol.* **2007**, *7*, 2582-2595.

(24) Zinchenko, A.; Baigl, D.; Yoshikawa, K. *Polym. Nanostruct. Their Appl.* **2007**, *1*, 402-442.

(25) Li, M.; Ober, C.K. *Mater. Today* **2006**, *9*, 30-39.

(26) Fisher, F.T.; Dikin, D.A.; Chen, X.; Ruoff, R.S. *Appl. Phys. Carbon Nanotubes* **2005**, 307-337.

(27) Balsara, N.P.; Hahn, H. *Chem. Nanostruct. Mater.* **2003**, 317-327.

(28) Li, Z.; Hillmyer, M.A.; Lodge, T.P. *Langmuir* **2006**, *22*, 9409-9417.

(29) Takai, O. *Ann. N. Y. Acad. Sci.* **2006**, *1093*, 84-97.

(30) Jones, R.A.L. *J. Polym. Sci., Part B: Polym. Phys.* **2005**, *43*, 3367-3368.

(31) Lerner, E.J. *Ind. Phys.* **2004**, *10*, 16-19.

(32) Lena, S.; Masiero, S.; Pieraccini, S.; Spada, G.P. *Chem.--Eur. J.* **2009**, *15*, 7792-7806.

(33) Kuo, S.-W. *Polym. Int.* **2009**, *58*, 455-464.

(34) Lee, B.-C.; Zuckermann, R.N. *Chem. Commun. 46*, 1634-1636.

(35) Liu, G.; Men, P.; Perry, G.; Smith, M.A. *Prog. Brain Res.* **2009**, *180*, 97-108.

(36) Bolognin, S.; Drago, D.; Messori, L.; Zatta, P. *Med. Res. Rev.* **2009**, *29*, 547-570.

(37) Mulder, W.J.M.; Strijkers, G.J.; van Tilborg, G.A.F.; Cormode, D.P.; Fayad, Z.A.; Nicolay, K. *Acc. Chem. Res.* **2009**, *42*, 904-914.

(38) Shiraishi, Y.; Koizumi, H.; Hirai, T. *J. Phys. Chem. B* **2005**, *109*, 8580-8586.

(39) Hecht, S.; Frechet, J.M.J. *J. Am. Chem. Soc.* **2001**, *123*, 6959-6960.

(40) Chen, Y.; Shen, Z.; Pastor-Perez, L.; Frey, H.; Stiriba, S.-E. *Macromolecules* **2005**, *38*, 227-229.

(41) Tian, Y.; Chen, C.-Y.; Yip, H.-L.; Wu, W.-C.; Chen, W.-C.; Jen, A.K.Y. *Macromolecules* **2010**, *43*, 282-291.

(42) Bates, F.S.; Brannan, A.K.; Davis, K.P.; Jain, S.; Gong, X.; Scriven, L.E. *Polym. Prepr. (Am. Chem. Soc., Div. Polm Chem.)* **2006**, *47*, 760.

(43) Figueiredo, T.L.C.; Johnstone, R.A.W.; Sorensen, A.M.P.S.; Burget, D.; Jacques, P. *Photochem. Photobiol.* **1999**, *69*, 517-528.

(44) Li, H.-R.; Wu, H.-Z.; Tung, C.-H. *Tetrahedron* **2000**, *56*, 7437-7442.

(45) Finikova, O.; Galkin, A.; Rozhkov, V.; Cordero, M.; Haegerhaell, C.; Vinogradov, S. *J. Am. Chem. Soc.* **2003**, *125*, 4882-4893.

(46) Schmid, R.; Junge, W. *Biochim. Biophys. Acta Biom.* **1975**, *394*, 76-92.

(47) Dong, C.-M.; Chaikof, E.L. *Colloid Polym. Sci.* **2005**, *283*, 1366-1370.

(48) Ambade, A.V.; Savariar, E.N.; Thayumanavan, S. *Mol. Pharm.* **2005**, *2*, 264-272.

(49) Liu, M.; Frechet, J.M.J. *Polym. Mater. Sci. Eng.* **1999**, *80*, 167-168.

(50) Lodge, T.P.; Rasdal, A.; Li, Z.; Hillmyer, M.A. *J. Am. Chem. Soc.* **2005**, *127*, 17608-17609.

(51) Li, B.; Moriyama, E.H.; Li, F.; Jarvi, M.T.; Allen, C.; Wilson, B.C. *Photochem. Photobiol.* **2007**, *83*, 1505-1512.

(52) O'Reilly, R.K. *Philos. Trans. R. Soc. A* **2007**, *365*, 2863-2878.

(53) Rodriguez-Hernandez, J.; Checot, F.; Gnanou, Y.; Lecommandoux, S. *Prog. Polym. Sci.* **2005**, *30*, 691-724.

(54) Lodge, T.P.; Bang, J.; Li, Z.; Hillmyer, M.A.; Talmon, Y. *Faraday Discuss.* **2004**, *128*, 1-12.

(55) Vermathen, M.; Louie, E.A.; Chodosh, A.B.; Ried, S.; Simonis, U. *Langmuir* **2000**, *16*, 210-221.

(56) Wu, W.; Sun, H.; Wang, L.; Li, K.; Wang, L. *J. Haz. Mater.* **2010**, *174*, 635-640.

(57) Osburn, C.L.; Morris, D.P. *Compr. Ser. Photochem. Photobiol.* **2003**, *1*, 185-217.

(58) Choudhry, G.G. *Toxicol. Environ. Chem.* **1981**, *4*, 209-60.

(59) Choudrhry, G.G., *Humic Substances. Structural, Photophysical, Photochemical and Free Radical Aspects and Interactions with Environmental Chemicals*. Current Topics in Environmental and Toxicological Chemistry. Vol. 7. 1984, London, UK: Gordon and Breach Science Publishers. 185.

(60) Kohn, T.; Grandbois, M.; McNeill, K.; Nelson, K.L. *Environ. Sci. Technol.* **2007**, *41*, 4626-4632.

(61) Blough, N.V.; Zepp, R.G. *Struct. Energ. React. Chem. Ser.* **1995**, *2*, 280-333.

(62) Larson, R.A.; Weber, E.J., *Reaction Mechanisms Environmental Organic Chemistry*. Carbohydrate Polymers. Vol. 29. 1996. 293-294.

(63) Schwarzenbach, R.P.; Gschwend, P.M.; Imboden, D.M., *Environmental Organic Chemistry*. 1992. 681 pp.

(64) Zepp, R.G.; Wolfe, N.L.; Baughman, G.L.; Hollis, R.C. *Nature* **1977**, *267*, 421-3.

(65) Rio, Y.; Accorsi, G.; Nierengarten, H.; Bourgogne, C.; Strub, J.-M.; Van Dorsselaer, A.; Armaroli, N.; Nierengarten, J.-F. *Tetrahedron* **2003**, *59*, 3833-3844.

(66) Ng, A.C.H.; Li, X.-y.; Ng, D.K.P. *Macromolecules* **1999**, *32*, 5292-5298.

(67) Oar, M.A.; Serin, J.M.; Dichtel, W.R.; Frechet, J.M.J.; Ohulchanskyy, T.Y.; Prasad, P.N. *Chem. Mat.* **2005**, *17*, 2267-2275.

(68) Hackbarth, S.; Horneffer, V.; Wiehe, A.; Hillenkamp, F.; Roder, B. *Chem. Phys.* **2001**, *269*, 339-346.

(69) Kaanumalle, L.S.; Nithyanandhan, J.; Pattabiraman, M.; Jayaraman, N.; Ramamurthy, V. *J. Am. Chem. Soc.* **2004**, *126*, 8999-9006.

(70) Grandbois, M.; Latch, D.E.; McNeill, K. *Environ. Sci. Technol.* **2008**, *42*, 9184-9190.

(71) Latch, D.E.; McNeill, K. *Science* **2006**, *311*, 1743-1747.

(72) Li, Z.; Hillmyer, M.A.; Lodge, T.P. *Macromolecules* **2004**, *37*, 8933-8940.

(73) Dougherty, T.J.; Gomer, C.J.; Henderson, B.W.; Jori, G.; Kessel, D.; Korbelik, M.; Moan, J.; Peng, Q. *J. Natl. Cancer Inst.* **1998**, *90*, 889-905.

(74) Blum, A.S.; Soto, C.M.; Vora, G.J.; Sapsford, K.E.; Ratna, B.R. *ACS Symp. Ser.* **2009**, *1016*, 141-154.

(75) Rossello, R.A.; Wang, Z.; Kizana, E.; Krebsbach, P.H.; Kohn, D.H. *Proc. Natl. Acad. Sci. U. S. A.* **2009**, *106*, 13219-13224.

(76) Lee, J.-H.; Kim, K.N.; Kim, J.-W.S.J.; Kim, B.-K.; Lee, H.-W.; Moon, J. *J. Mater. Sci.* **2007**, *42*, 1866-1871.

(77) Aniola, J.; Selman, S.H.; Lilge, L.; Keck, R.; Jankun, J. *Int. J. Mol. Med.* **2003**, *11*, 287-291.

(78) Grundmann-Kollmann, M.; Podda, M.; Braeutigam, L.; Hardt-Weinelt, K.; Ludwig, R.J.; Geisslinger, G.; Kaufmann, R.; Tegeder, I. *Br. J. Clin. Pharmacol.* **2002**, *54*, 535-539.

(79) Bothe, K.; Ramspeck, K.; Hinken, D.; Schinke, C.; Schmidt, J.; Herlufsen, S.; Brendel, R.; Bauer, J.; Wagner, J.M.; Zakharov, N.; Breitenstein, O. *J. Appl. Phys.* **2009**, *106*, 104510/1-104510/8.

(80) Sahoo, S.; Husale, S.; Colwill, B.; Lu, T.-M.; Nayak, S.; Ajayan, P.M. *ACS Nano* **2009**, *3*, 3935-3944.

(81) Wilkinson, F.; Helman, W.P.; Ross, A.B. *J. Phys. Chem. Ref. Data* **1995**, *24*, 663-1021.

(82) MacManus-Spencer, L.A.; McNeill, K. *J. Am. Chem. Soc.* **2005**, *127*, 8954-8955.

(83) MacManus-Spencer, L.A.; Latch, D.E.; Kroncke, K.M.; McNeill, K. *Anal. Chem.* **2005**, *77*, 1200-1205.

(84) Armarego, W.L.F.; Perrin, D.D., eds. *Purification of Laboratory Chemicals*. 4th ed. 1996, Buterworth-Heinemann: Oxford.

(85) Wilkinson, F.; Brummer, J.G. *J. Phys. Chem. Ref. Data* **1981**, *10*, 809-999.

(86) Wu, S.-C.; Gschwend, P.M. *Water Resour. Res.* **1988**, *24*, 1373-1383.

(87) Fetters, L.J.; Lohse, D.J.; Richter, D.; Witten, T.A.; Zirkel, A. *Macromolecules* **1994**, *27*, 4639-4647.

(88) Cantonetti, V.; Monti, D.; Venanzi, M.; Bombelli, C.; Ceccacci, F.; Mancini, G. *Tetrahedron: Assymetry* **2004**, *15*, 1969-1977.

(89) Korinek, M.; Klinger, P.; Dedic, R.; Psencik, J.; Svoboda, A.; Hala, J. *J. Lumin.* **2007**, *122-123*, 247-249.

(90) Poisson, S.-D., *Recherches sur la probabilité des jugements en matières criminelles et matière civile (Research on the Probability of Judgments in Criminal and Civil Matters)*. 1838, Paris: Bachelier.

(91) Fenn, E.E.; Wong, D.B.; Fayer, M.D. *Proc. Nat. Acad. Sci.* **2009**, *106*, 15243-15248.

(92) Jeon, H.K.; Macosko, C.W.; Moon, B.; Hoye, T.R.; Yin, Z. *Macromolecules* **2004**, *37*, 2563-2571.

Chapter 5

(1) Haag, W.R.; Hoigne, J. *Chemosphere* **1985**, *14*, 1659-71.

(2) Cheng, F.-C.; Jen, J.-F.; Tsai, T.-H. *J. Chrom. B.* **2002**, *781*, 481-496.

(3) Xu, M.; Huang, N.; Xiao, Z.; Lu, Z. *Supramol. Sci.* **1998**, *5*, 449-451.

(4) Peralta-Hernandez, J.M.; Manriquez, J.; Meas-Vong, Y.; Rodriguez Francisco, J.; Chapman Thomas, W.; Maldonado Manuel, I.; Godinez Luis, A. *J. Hazard Mater.* **2007**, *147*, 588-93.

(5) Farhataziz; Ross, A.B., *Selected Specific Rate of Reaction of Transients from Water in Aqueous Solutions. III. Hydroxyl radical and perhydroxyl radical and their radical ions*, W. National Bureau of Standards, DC, Editor. 1977.

(6) Atkinson, R. *Chemical Reviews* **1986**, *86*, 69-201.

(7) Larson, R.A.; Weber, E.J., eds. *Reaction Mechanisms in Environmental Organic Chemistry*. 1994, Lewis Publishers: Boca Raton, FL.

(8) Cadet, J.; Delatour, T.; Douki, T.; Gasparutto, D.; Pouget, E.-P.; Ravanat, J.-L.; Sauvaigo, S. *Mutation Res.* **1999**, *424*, 9-21.

(9) Sugioka, K.; Nakano, H.; Tsuchiya, J.; Nakano, M.; Sugioka, Y.; Tero-Kubota, S.; Ikegami, Y. *Biochem. Int.* **1984**, *9*, 237-42.

(10) Ajith, T.A. *Indian J. Clin. Biochem.* **2010**, *25*, 67-73.

(11) Hawkins, C.L.; Davies, M.J. *J. Chem. Soc., Perkin Trans. 2* **1998**, 2617-2622.

(12) Prinsze, C.; Dubbelman, T.M.A.R.; Van Steveninck, J. *Biochim. Biophys. Acta, Protein Struct. Mol. Enzymol.* **1990**, *1038*, 152-7.

(13) Guptasarma, P.; Balasubramanian, D.; Matsugo, S.; Saito, I. *Biochemistry* **1992**, *31*, 4296-303.

(14) Nagy, I.Z. *Annals N.Y. Acad.Sci.* **2001**, *928*, 187-99.

(15) Latch, D.E.; Packer, J.L.; Stender, B.L.; VanOverbeke, J.; Arnold, W.A.; McNeill, K. *Environ. Toxicol. Chem.* **2005**, *24*, 517-525.

(16) Latch Douglas, E.; Stender Brian, L.; Packer Jennifer, L.; Arnold William, A.; McNeill, K. *Environ. Sci. Technol.* **2003**, *37*, 3342-50.

(17) Chin, Y.-P.; Miller, P.L.; Zeng, L.; Cawley, K.; Weavers, L.K. *Environ. Sci. Technol.* **2004**, *38*, 5888-5894.

(18) Shemer, H.; Sharpless, C.M.; Elovitz, M.S.; Linden, K.G. *Environ. Sci. Technol.* **2006**, *40*, 4460-4466.

(19) Sharpless, C.M.; Seibold, D.A.; Linden, K.G. *Aquat. Sci.* **2003**, *65*, 359-366.

(20) Mill, T.; Hendry, D.; Richardson, D. *Science* **1980**, *207*, 886-887.

(21) Zepp, R.G.; Hoigne, J.; Bader, H. *Environ. Sci. Technol.* **1987**, *21*, 443-450.

(22) Zhou, X.; Mopper, K. *Mar. Chem.* **1990**, *30*, 71-88.

(23) Repine, J.E.; Fox, R.B.; Berger, E.M. *J Biol Chem* **1981**, *256*, 7094-6.

(24) Sarma, L.; Devasagayam, T.P.A.; Mohan, H.; Mittal, J.P.; Kesavan, P.C. *Int. J. Radiat. Biol.* **1996**, *69*, 633-643.

(25) Janzen, E.G.; Blackburn, B.J. *J. Amer. Chem. Soc.* **1969**, *91*, 4481-90.

(26) Buettner, G.R.; Oberley, L.W. *Biochem. Biophys. Res. Commun.* **1978**, *83*, 69-74.

(27) Knecht, K.T.; Thurman, R.G.; Mason, R.P. *Arch. Biochem. Biophys.* **1993**, *303*, 339-48.

(28) Biondi, R.; Xia, Y.; Rossi, R.; Paolocci, N.; Ambrosio, G.; Zweier, J.L. *Anal. Biochem.* **2001**, *290*, 138-145.

(29) Iakovlev, A.; Broberg, A.; Stenlid, J. *FEMS Microbiology Ecology* **2003**, *46*, 197-202.

(30) Soh, N. *Anal. Bioanal. Chem.* **2006**, *386*, 532-543.

(31) Barreto, J.C.; Smith, G.S.; Strobel, N.H.P.; McQuillin, P.A.; Miller, T.A. *Life Sci.* **1994**, *56*, PL89-96.

(32) Pi, Y.; Schumacher, J.; Jekel, M. *Ozone: Sci. Eng.* **2005**, *27*, 431-436.

(33) Powell, S.R.; Hall, D. *Free Radical Biol. Med.* **1990**, *9*, 133-41.

(34) Maleknia Simin, D.; Kiselar Janna, G.; Downard Kevin, M. *Rapid Commun. Mass Spectrom.* **2002**, *16*, 53-61.

(35) Soh, N.; Makihara, K.; Ariyoshi, T.; Seto, D.; Maki, T.; Nakajima, H.; Nakano, K.; Imato, T. *Anal. Sci.* **2008**, *24*, 293-296.

(36) King, M.; Kopelman, R. *Sens. Actuators, B* **2003**, *B90*, 76-81.

(37) Manevich, Y.; Held, K.D.; Biaglow, J.E. *Radiat. Res.* **1997**, *148*, 580-591.

(38) Makrigiorgos, G.M.; Baranowska-Kortylewicz, J.; Bump, E.; Sahu, S.K.; Berman, R.M.; Kassis, A.I. *Int. J. Radiat. Biol.* **1993**, *63*, 445-58.

(39) Nakatani, N.; Hashimoto, N.; Shindo, H.; Yamamoto, M.; Kikkawa, M.; Sakugawa, H. *Anal. Chim. Acta* **2007**, *581*, 260-267.

(40) Russi, H.; Kotzias, D.; Korte, F. *Chemosphere* **1982**, *11*, 1041-8.

(41) Page, S.E.; Arnold, W.A.; McNeill, K. *Abstracts of Papers, 239th ACS National Meeting, San Francisco, CA, United States, March 21-25*, **2010**, GEOC-188.

(42) Kwan, W.P.; Voelker, B.M. *Environ. Sci. Technol.* **2004**, *38*, 3425-3431.

(43) Vermilyea, A.W.; Voelker, B.M. *Environ. Sci. Technol.* **2009**, *43*, 6927-6933.

(44) Richmond, R.; Halliwell, B.; Chauhan, J.; Darbre, A. *Anal. Biochem.* **1981**, *118*, 328-35.

(45) Syrychova, I.; Hideg, E. *Funct. Plant Biol.* **2007**, *34*, 1105-1111.

(46) Newton, G.L.; Milligan, J.R. *Radiation Physics and Chemistry* **2006**, *75*, 473-478.

(47) Yan, E.B.; Unthank, J.K.; Castillo-Melendez, M.; Miller, S.L.; Langford, S.J.; Walker, D.W. *J. Appl. Physiol.* **2005**, *98*, 2304-2310.

(48) Neckers, D.C.; Paczkowski, J. *J. Am. Chem. Soc.* **1986**, *108*, 291-292.

(49) Latch, D.E.; McNeill, K. *Science* **2006**, *311*, 1743-1747.

(50) Latch, D.E., *Environmental Photochemistry: Studies on the Degradation of Pharmaceutical Pollutants and the Microheterogeneous Distribution of Singlet Oxygen*, in *Chemistry*. 2005, University of Minnesota: Minneapolis, MN. p. 256.

(51) Grandbois, M.; Latch, D.E.; McNeill, K. *Environ. Sci. Technol.* **2008**, *42*, 9184-9190.

(52) Kohn, T.; Nelson, K.L. *Environ. Sci. Technol.* **2007**, *41*, 192-197.

(53) Harigaya, Y.; Yamaguchi, H.; Onda, M. *Chem. Pharm. Bull.* **1981**, *29*, 1321-7.

(54) Tremblay, M.S.; Sames, D. *Org. Lett.* **2005**, *7*, 2417-2420.

(55) Matsuura, T.; Omura, K. *J. Chem. Soc. Chem. Commun.* **1966**, 127-128.

(56) Armarego, W.L.F.; Perrin, D.D., eds. *Purification of Laboratory Chemicals*. 4th ed. 1996, Buterworth-Heinemann: Oxford.

(57) Berger, S. *Tetrahedron* **1976**, *32*, 2451-2455.

(58) Hattori, T.; Hayashizaka, N.; Miyano, S. *Synthesis* **1995**, 41-43.

(59) Brown, P.M.; Russel, J.; Thomson, R.H.; Wylie, A.G. *J. Chem. Soc. C* **1968**, 842-848.

(60) Huntress, E.H.; Seikel, M.K. *J. Am. Chem. Soc.* **1939**, *61*, 816-822.

(61) McBee, E.T.; Rapkin, E. *J. Am. Chem. Soc.* **1951**, *73*, 2375-2376.

(62) Kaeding, W.W. *J. Org. Chem.* **1964**, *29*, 2556-2559.

(63) Schlegel, D.C.; Tipton, C.D.; Rinehart, K.L. *J. Org. Chem.* **1970**, *35*, 849.

(64) Togo, H.; Muraki, T.; Hoshina, Y.; Yamaguchi, K.; Yokoyama, M. *J. Chem. Soc., Perkin Trans. 1* **1997**, 787-793.

(65) Bunton, C.A.; Kenner, G.W.; Robinson, M.J.T.; Webster, B.R. *Tetrahedron* **1963**, *19*, 1001-1010.

(66) Pandey, J.; Jha, A.K.; Hajela, K. *Bioorg. Med. Chem.* **2004**, *12*, 2239-2249.

(67) Hart, D.J.; Kim, A.; Krishnamurthy, R.; Merriman, G.H.; Waltos, A.-M. *Tetrahedron* **1992**, *48*, 8179-8188.

(68) Korolev, D.N.; Bumagin, N.A. *Tetrahedron Lett.* **2006**, *47*, 4225-4229.

(69) Barton, D.H.R.; Crich, D.; Motherwell, W.B. *Tetrahedron Lett.* **1983**, *24*, 4979-4982.

(70) Barton, D.H.R.; Crich, D.; Motherwell, W.B. *J. Chem. Soc., Chem. Commun.* **1983**, 939-941.

(71) Barton, D.H.R.; Lacher, B.; Zard, S.Z. *Tetrahedron Lett.* **1985**, *26*, 5939-5942.

(72) Barton, D.H.R.; Lacher, B.; Zard, S.Z. *Tetrahedron* **1987**, *43*, 4321-4328.

(73) Barton, D.H.R.; Oxbalik, N.; Vacher, B. *Tetrahedron* **1988**, *44*, 7385-7392.

(74) Jonsson, L.; Wistrand, L.-G. *J. Org. Chem.* **1984**, *49*, 3340-3344.

(75) Davies, D.I.; Waring, C. *J. Chem. Soc.* **1967**, *(C)*, 1639-1642.

(76) An, B.-K.; Gihm, S.H.; Chung, J.W.; Park, C.R.; Kwon, S.-K.; Park, S.Y. *J. Am. Chem. Soc.* **2009**, *131*, 3950-3957.

(77) Ilan, Y.; Luria, M.; Stein, G. *J. Phys. Chem.* **1976**, *80*, 584-7.

(78) Cho, D.W.; Kim, Y.H.; Kang, S.G.; Yoon, M.; Kim, D. *J. Chem. Soc., Faraday Trans.* **1996**, *92*, 29-33.

(79) Lakowicz, J.R., *Principles of Fluorescence Spectroscopy*. 1983, New York: Plenum Press.

(80) Einschlag, F.S.G.; Carlos, L.; Capparelli, A.L. *Chemosphere* **2003**, *53*, 1-7.

(81) Maddigapu, P.R.; Bedini, A.; Minero, C.; Maurino, V.; Vione, D.; Brigante, M.; Mailhot, G.; Sarakha, M. *Photochem. Photobiol. Sci. 9*, 323-330.

(82) Vione, D.; Ponzo, M.; Bagnus, D.; Maurino, V.; Minero, C.; Carlotti, M.E. *Environ. Chem. Lett. 8*, 95-100.

(83) Wang, L.; Zhang, C.; Wu, F.; Deng, N.; Glebov, E.M.; Bazhin, N.M. *React. Kinet. Catal. Lett.* **2006**, *89*, 183-192.

(84) Mack, J.; Bolton, J.R. *J. Photochem. Photobiol., A* **1999**, *128*, 1-14.

(85) Buxton, G.V.; Greenstock, C.L.; Helman, W.P.; Ross, A.B. *J. Phys. Chem. Ref. Data* **1988**, *17*, 513-886.

(86) Arakaki, T.; Faust, B.C. *J. Geophys. Res.* **1998**, *103*, 3487-3504.

(87) Martin, C.; Sanchez, F.; Jimenez, R.; Prado, R.; Perez-Tejeda, P.; Lopez-Cornejo, P. *J. Phys. Chem. B* **2006**, *110*, 12959-12963.

(88) Sneen, R.A.; Carter, J.V. *J. Am. Chem. Soc.* **1972**, *94*, 6990-7.

(89) Neta, P.; Schuler, R.H. *J. Phys. Chem.* **1975**, *79*, 1-6.

(90) Hoigné, J.; Faust, B.C.; Haag, W.R.; Scully, F.E., Jr.; Zepp, R.G., *Aquatic humic substances as sources and sinks of photochemically produced transient reactants*, in *Aquatic Humic Substances: Influence on Fate and Treatment of Pollutants*, I.H. Suffet and P. MacCarthy, Editors. 1989, American Chemical Society: Washington, DC. p. 363-381.

(91) Burnett, R.D. *High Pressure Liq. Chromatogr. Clin. Chem., Proc. Symp.* **1976**, 45-50.

(92) Rice, S.A., *Diffusion-Limited Reactions*. Comprehensive Chemical Kinetics. Vol. 25. 1985, New York: Elsevier.

(93) Hoshino, M.; Akimoto, H.; Okuda, M. *Bull. Chem. Soc. Japan* **1978**, *51*, 718-724.

(94) Skoog, D.A.; Holler, F.J.; Nieman, T.A., *Principles of Instrumental Analysis*. 5th ed. 1997: Brooks Cole.